UNIVERSITÄT BIELEFELD

Phosphazenbasen

und die Darstellung nicht-koordinierter Anionen

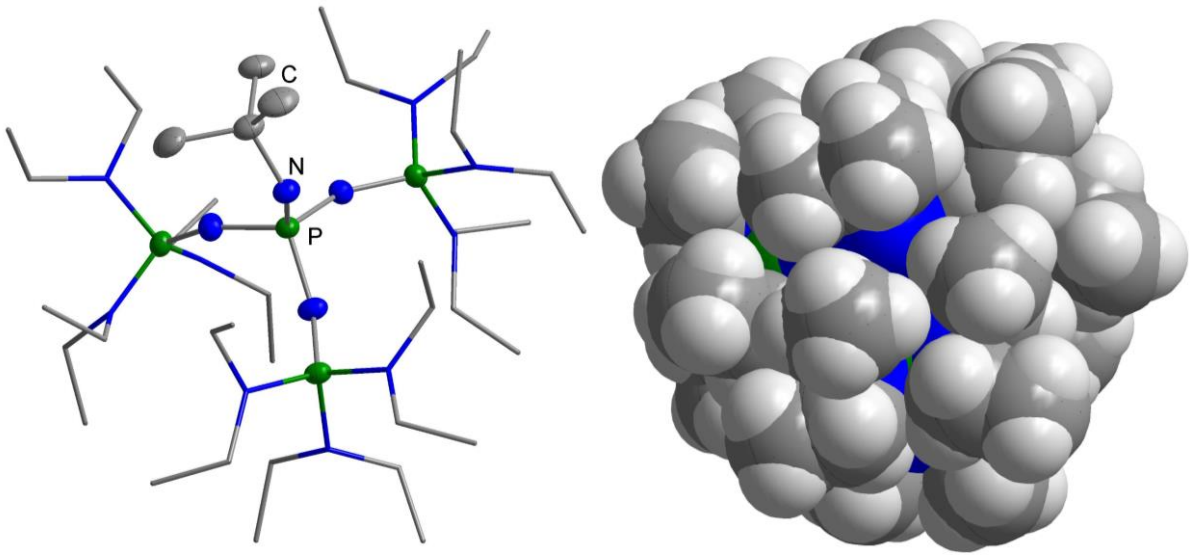

Inaugural-Dissertation

Robin F. Weitkamp

Bielefeld

Februar 2021

UNIVERSITÄT BIELEFELD

Phosphazenbasen

und die Darstellung nicht-koordinierter Anionen

Inaugural-Dissertation

zur Erlangung des Doktorgrades

doctor rerum naturalium

vorgelegt von

Robin F. Weitkamp

aus Spenge

Universität Bielefeld

Fakultät für Chemie

Anorganische Chemie II

Februar 2021

Die vorliegende Dissertationsschrift wurde im Zeitraum von Juni 2018 bis Februar 2021 an der Fakultät für Chemie der Universität Bielefeld im Arbeitskreis Anorganische Chemie II unter der wissenschaftlichen Leitung von Prof. Dr. Berthold Hoge verfasst.

Erster Gutachter	Prof. Dr. Berthold Hoge
Zweiter Gutachter	Prof. Dr. Norbert W. Mitzel
Tag der Disputation	19.03.2021

Für meine Mama

Ich bin Dir sehr dankbar für den Weg, den Du gemeinsam mit mir gegangen bist. Für die vielen schönen und wundervollen Momente, die ich mit Dir erleben durfte. Für den Rückhalt, die Liebe und die stärkenden Worte, die Du mir in schwierigen Zeiten geschenkt hast. Durch Dich bin ich der Mensch geworden, der ich heute sein darf und dafür danke ich Dir von Herzen!

Danksagung

Zunächst möchte ich mich herzlichst bei meinem Doktorvater ***Herrn Prof. Dr. Berthold Hoge*** für die Aufnahme in seinen Arbeitskreis, für das außerordentlich spannende und vielseitige Thema sowie das leidenschaftliche Interesse am Fortgang meiner Arbeit bedanken. Vielen Dank für das große Vertrauen, welches Du mir stets entgegengebracht hast.

Des Weiteren danke ich ***Herrn Prof. Dr. Norbert W. Mitzel*** für die Übernahme der Zweitgutachtertätigkeit.

Herrn Prof. Dr. Lothar Weber danke ich von ganzem Herzen für die zahlreichen Diskussionen, präzisen Korrekturen meiner Arbeiten und die hervorragende Erweiterung meines englischen Wortschatzes.

Ich bedanke mich herzlichst bei den analytischen Abteilungen und den Werkstätten der Fakultät für Chemie. Weiterhin möchte ich mich bei dem Chemikalienlager, allen voran bei meiner ehemaligen Chefin Heike Kosellek bedanken, die in allen Belangen immer außerordentlichen Einsatz gezeigt hat.

Ein besonderer Dank gilt auch Beate Neumann und Dr. Hans-Georg Stammler für die Aufnahme und Lösung zahlreicher Einkristallröntgenstrukturanalysen.

Auch möchte ich mich bei Fridolin Röhs für die Messung von UV/Vis-Spektren und bei Prof. Dr. Volker F. Wendisch für die Bereitstellung des Spektrofluorophotometers bedanken.

Philipp Niewöhner gilt ein besonderer Dank für die Gestaltung der zahlreichen und wunderschönen Cover-Grafiken für meine Publikationen.

Herzlichst möchte ich mich bei dem gesamten ehemaligen und aktuellen Arbeitskreis der ACII für die familiäre Arbeitsatmosphäre, die anregenden Gespräche und die unvergessene gemeinsame Zeit bedanken.

Danke Michaela, dass Du mich bei meiner Phosphazenchemie so tatkräftig unterstützt hast und dass Du auch nie müde wurdest, mit mir das Labor zu teilen und den von mir verdreckten Stinkabzug aufzuräumen.

Vielen Dank Julia, dass Du Dir immer wieder Zeit für meine Belange genommen hast und immer hilfsbereit warst. Ich danke Dir auch für die hervorragende Durchsicht

meiner Publikationen und meiner Arbeit sowie das Design meines ersten Angewandte-Covers.

Danke Mark für die vielen Glasgeräte und die hilfreichen Tipps sowohl im Labor als auch zum Verfassen dieser Arbeit.

Danke Paul für die tollen Spiele, Rätsel, Geschichten und faszinierenden Geschehnisse im Labor, an denen Du mich hast teilhaben lassen.

Danke Markus für die Teilhabe an Deinem riesigen Wissensschatz und die Erheiterung der Mittagspausen und Arbeitsgruppenmeetings mit Deinem humorvollen Wesen.

Danke Natalie, dass Du mir NMR-Tieftemperaturmessungen erklärt hast und immer für meine Fragen und Diskussionen offen warst.

Danke Sven für die vielen lustigen Themen im Kaffeeraum, die Denkanregungen im Laborflur und natürlich Deine Hilfe bei administrativen Problemen.

Danke Mira für die zahlreichen Anmerkungen zu meiner Schnitzel-Pfanne und natürlich auch für die theoretischen Rechnungen für meine Arbeit.

Danke Katha für die Anregungen, Deine Hilfsbereitschaft und auch für den ein oder anderen neckischen Kommentar.

Auch bedanke ich mich bei meinen Praktikantinnen und Praktikanten Oxana Jaroschewski, Katharina Wels, Luisa Koch, Daniel Wegener, Manuel Warkentin und Daniel Heuer für die angenehme Zusammenarbeit und die guten Ergebnisse.

Ich danke meiner Freundin Julia für die stetige Unterstützung sowohl in beflügelten als auch in schwierigen Zeiten, die aufmunternden Worte und die gespendete Kraft. Ich bewundere Dein Durchhaltevermögen, das man als Nichtchemikerin braucht, wenn permanent über Chemie gesprochen wird.

Zum Schluss gilt mein größter Dank meinen Eltern, meiner Familie und meinen Freunden. Danke, dass ihr mich auf meinem Weg begleitet habt, mir immer die Freiheit meiner persönlichen Entfaltung ermöglicht habt und mir in den schwierigsten Zeiten beistandet!

Inhaltsverzeichnis

Abkürzungsverzeichnis

Allgemein

Äq.	Äquivalente
ATR	*attenuated total reflection*
CV	Cyclovoltammetrie
GC-MS	Gaschromatographie mit Massenspektrometrie-Kopplung
HV	Hochvakuum
IR	Infrarot
$K_{BH}+$	Säurekonstante
M	Molar
NMR	*nuclear magnetic resonance*
$pK_{BH}+$	negativer dekadischer Logarithmus der Säurekonstante
RT	Raumtemperatur
Sdp.	Siedepunkt
SET	*single electron transfer*
Smp.	Schmelzpunkt
WCA	weakly coordinating anion
WCC	weakly coordinating cation

NMR-Spektroskopie

d	Dublett
HMBC	*heteronuclear multiple bond correlation*
I	Integral
ppm	parts per million
q	Quartett
quin	Quintett
s	Singulett
t	Triplett
tridec	Tridecett

Substanzen und Restgruppen

Bu	Butyl
D_3	Hexamethlycyclotrisiloxan
D_4	Octamethylcyclotetrasiloxan
D_5	Decamethylcyclopentasiloxan
Et	Ethyl
Et_2O	Diethylether

EtP_4tBu	1-*tert*-Butyl-4,4,4-tris(diethylamino)-2,2-bis[tris(diethylamino)-phosphoranylidenamino]-2λ^5,4λ^5-catenadi(phosphazen)
KHMDS	Kaliumhexamethyldisilazid
LDA	Lithiumdiisopropylamid
Me	Methyl
MeP_1tBu	*N*-*tert*-Butyl-tris(dimethylamino)phosphanimin
MeP_4tBu	1-*tert*-Butyl-4,4,4-tris(dimethylamino)-2,2-bis[tris(dimethylamino)-phosphoranylidenamino]-2λ^5,4λ^5-catenadi(phosphazen)
$[NBu_4]^+$	Tetra-*n*-butylammonium
$[NMe_4]^+$	Tetramethylammonium
$[PBu_4]^+$	Tetra-*n*-butylphosphonium
Ph	Phenyl
*t*Bu	*tert*-Butyl
TCNE	Tetracyanoethylen
TDAE	Tetrakis(dimethylamino)ethylen
THF	Tetrahydrofuran
TMS	Trimethylsilyl

IR-Spektroskopie

br	broad
m	medium
s	strong
vs	very strong
vw	very weak
w	weak

Massenspektrometrie

ESI	Elektronenspray-Ionisation
M	Molekülionenpeak

1. Einleitung

Nicht-koordinierte oder „nackte“ Ionen spielen eine essenzielle Rolle für das tiefe Verständnis von chemischen Prozessen und bilden eine Grundlage für die Weiterentwicklung quantenchemischer Berechnungen und theoretischer Vorhersagen. Während Betrachtungen nackter Ionen ohne jegliche Wechselwirkung nur in verdünnter Gasphase durchgeführt werden können, existieren solche idealisierten Teilchen in chemischer Umgebung nicht.[1,2,3] Durch die Ausbildung von Wechselwirkungen ionischer Art oder durch Wasserstoffbrückenbindungen tendieren die entsprechenden Systeme zur Absenkung ihrer Gesamtenergie. Die Gitterenergie stellt in diesem Bezug eine wichtige Größe dar, denn sie beschreibt die Arbeit, die aufgewendet werden muss, um die Anziehungskräfte zwischen Anion und Kation zu überwinden und die Teilchen unendlich weit voneinander zu entfernen. Dieser Wert wird über den Born-Haber-Kreisprozess ermittelt und ist für Salze mit starken koordinativen Wechselwirkungen deutlich höher als für entsprechende Salze mit schwachen interionischen Wechselwirkungen.[4] Ein Vergleich der Alkalimetallfluoride zeigt eine kontinuierliche Abnahme der Gitterenergie mit zunehmender Größe des Kations, was von Seppelt als „Cäsiumeffekt“[2,3] beschrieben wurde und mit einer gesteigerten Löslichkeit des Salzes sowie Reaktivität des Anions einhergeht.

Schwach koordinierende Anionen (weakly coordinating anions, WCAs) stellen ein breites und aktives Forschungsgebiet dar, denn sie ermöglichen die Isolierung von stark elektrophilen oder oxidierenden Kationen.[5] Dies wird eindrucksvoll an den zahlreichen strukturell charakterisierten Vertretern von Oxonium-Ionen deutlich, beispielsweise den Kationen von Zundel, $[(OH_3)(OH_2)]^+$,[6] und Eigen, $[(OH_3)(OH_2)_3]^+$,[7] deren Existenz stark von der Gegenwart schwach koordinierender Anionen abhängt.[8]

Schwach koordinierende Kationen (weakly coordinating cations, WCCs) stellen das Pendant zu WCAs dar, und sind für die Existenz nicht-koordinierter, hoch nukleophiler und reduzierender Anionen essenziell. Zu ihnen zählen unter anderem Vertreter peralkylierter Ammonium-, Phosphonium- und Phosphazenium-Verbindungen sowie mit Kryptanden oder Kronenethern komplexierte Alkalimetall-Ionen.

Ein Paradebeispiel für die Verwendung von WCCs stellt die Realisierung des nackten Fluorid-Anions dar. Hierbei sind diverse Herausforderungen zu bewältigen, denn

neben der signifikanten Nukleophilie des Teilchens[9,10,11] neigt es aufgrund der enormen Lewis-Basizität zur Ausbildung von extrem starken Wasserstoffbrückenbindungen.[2,3,10,12–14] Dies wird bei der Betrachtung des $[HF_2]^-$-Anions deutlich, welches die stärkste bisher nachgewiesene Wasserstoffbrückenbindung beinhaltet.[13–15] Die Tendenz zur Wasserstoffbrückenbindung erschwert bei der Synthese der Fluorid-Salze vor allem die Entfernung von protischen Solvenz-Molekülen, was infolgedessen in einer verringerten Reaktivität des Fluorid-Anions resultiert.[2,3,10,16] Während heute zahlreiche Fluorid-Salze mit diversen gering CH-aciden und somit schwach koordinierenden Kationen synthetisiert und auf ihre chemischen Eigenschaften untersucht worden sind,[10,11,17–19] existieren bisher nur wenige strukturelle Daten von nicht-koordinierten Fluoriden, unter anderem mit Piperidinium-[17] und Tetramethylphosphonium-Kationen[20] sowie dem Phosphazenium-Kation $[(Me_2N)_3P{=}N{=}P(NMe_2)_3]^+$.[21]

Die Darstellung nicht-koordinierter Hydroxid-Anionen ist aufgrund der im Vergleich zu nicht-koordinierten Fluorid-Anionen nochmals deutlich erhöhten Basizität sowie Nukleophilie problematisch.[22,23] Diese Problematik wird auch in Arbeiten von Schwesinger und Mitarbeitern deutlich, in denen die Deaktivierung von Phosphazeniumfluoriden unter Hydrolyse des Kations durch die Zugabe von geringen Mengen an H_2O beobachtet wird.[18] Ähnlich wie für das nicht-koordinierte Fluorid-Anion erweist sich eine Hydrathülle als wirkungsvoll bei der Deaktivierung des Hydroxid-Anions.[16,22,24] Auch wenn der Generierung nackter Hydroxide unter Verwendung von Phosphazenium-Kationen scheinbar Grenzen gesetzt sind,[25] ergibt sich die Fragestellung, ob das Portfolio neben dem bekannten, jedoch koordinierten Hydroxid-Monohydrat-Anion $[OH(OH_2)]^-$[26] um erste Beispiele isolierter Hydroxid-Hydrat-Anionen $[OH(OH_2)_n]^-$ mittels schwach koordinierender Phosphazenium-Ionen erweitert werden kann.

Besonders elektronenreiche Phosphor-basierte Superbasen wie Phosphine und Phosphazene, deren historische sowie aktuelle Entwicklung bereits detailliert in meinem Mini-Review aufgezeigt wurde, eignen sich hervorragend zur Deprotonierung schwach acider Pronukleophile.

Superbasische Phosphazene, welche nach ihrem Entdecker als „Schwesinger-Basen“ bezeichnet werden, zeichnen sich durch eine hohe Protonenaffinität sowie eine hohe

thermische Stabilität und Resistenz gegenüber Sauerstoff und basischer Hydrolyse aus. Unter dem 1987 erschienenen Konzept der „Homologisierung“ fokussierte sich Schwesinger auf die Implementierung stark π-elektronendonierender Phosphazenyl-Einheiten am zentralen Phosphanimin-Baustein. So wurde die Brønsted-Basizität der erhaltenen Phosphazenbasen signifikant erhöht und gleichzeitig deren Nukleophilie reduziert (Schema 1).[27,28–33]

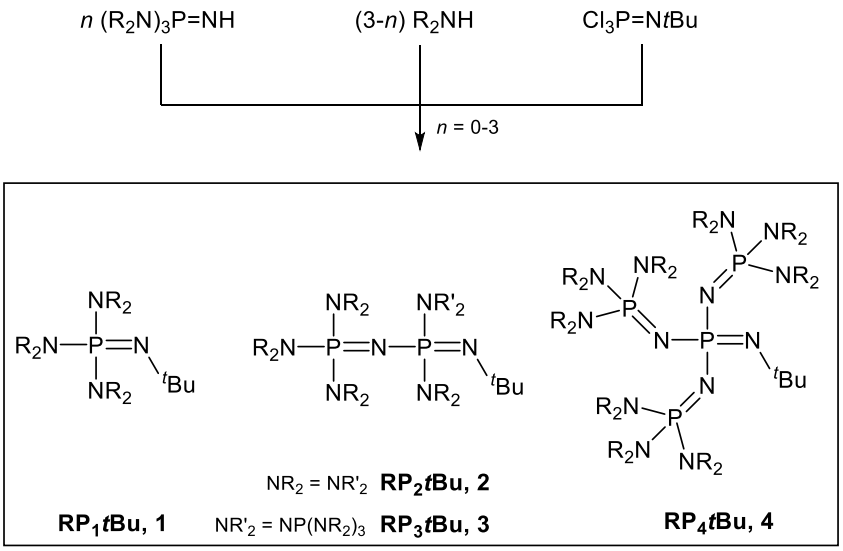

R = R' = Me	**MeP$_1$*t*Bu, 1a**	**MeP$_2$*t*Bu, 2a**	**MeP$_3$*t*Bu, 3a**	**MeP$_4$*t*Bu, 4a**
^{MeCN}pK_{BH^+}	**26.9**	**33.5**	**(38.6)**	**(42.7)**

Schema 1: Beispiele zur Synthese von Schwesingers Phosphazenen mittels Homologisierungskonzept und dargestellte ^{MeCN}pK_{BH^+}-Werte der entsprechenden Säure, bestimmt in Acetonitril bei 25 °C.[28–32] Die Werte in Klammern wurden durch Extrapolation bestimmt.

Eine durch Protonierung auftretende positive Ladung am basischen Imin-Stickstoffatom kann über das gesamte Phosphazen-Gerüst delokalisiert werden. Die Delokalisierung ist stärker ausgeprägt, je höher der Substitutionsgrad ist. Wird das einfachste Methylderivat **MeP$_1$*t*Bu** (**1a**) mit dem höheren Homolog **MeP$_2$*t*Bu** (**2a**) verglichen, so kann ein sprunghafter Anstieg des ^{MeCN}pK_{BH^+}-Wertes von 26.9 zu 33.5 beobachtet werden, welches einer Steigerung der Basizität um einen Faktor von circa 10^7 entspricht. Durch sukzessive Substitution der Dimethylamino-Funktionen mit weiteren Phosphazen-Einheiten kann in Tetraphosphazen **4a** ein ^{MeCN}pK_{BH^+}-Wert von 42.7 erreicht werden, welcher mit dem anorganischer Basen wie Kaliumhexamethyldisilazid (KHMDS) vergleichbar ist.[28,29,32] Die weitere Homologisierung ausgehend von Tetraphosphazen **4a** resultiert in Penta- und

Heptaphosphazen-Derivaten, die zwar einen weiteren geringen Basizitätszuwachs verzeichnen, jedoch macht sich bei letzterem bereits eine signifikante Reduzierung der Stabilität gegenüber Hydrolyse und Sauerstoff bemerkbar.[32,34]

Die sterisch anspruchsvollen Tetraphosphazenbasen **4** vereinen eine extrem hohe Basizität mit einer geringen Nukleophilie und finden deshalb als Hilfsbasen vielseitige Anwendung,[35] wie beispielsweise in Dehydrohalogenierungsreaktionen,[28,29,32] Biarylетherkupplungen[36] und Alkylierungsreaktionen.[37] Die korrespondierende Säure **[4H]$^+$** weist hingegen eine geringe Lewis-Acidität und eine geringe Neigung zur Addition von Nukleophilen auf, wodurch nicht-koordinierte oder „nackte“ Anionen generiert werden.[37,38,39,40]

2. Zielsetzung

Die Zielsetzung der vorliegenden Arbeit liegt in der Verwendung von Tetraphosphazen-Verbindungen **4** als Brønsted-Superbasen zur Deprotonierung von schwach aciden Pronukleophilen und der Generierung der entsprechenden Phosphazenium-Salze mit nicht-koordinierten Anionen. Da bereits gezeigt wurde, dass Pyrrolidinyl-substituierte Tetraphosphazene höhere Basizitäten als ihre entsprechenden Methyl-Vertreter aufweisen, jedoch aufgrund der sterischen Flexibilität der Pyrrolidinyl-Gruppen eine geringere sterische Abschirmung des Basizitätszentrums resultiert,[32] fokussiert sich diese Arbeit auf die Verwendung von elektronendonierenden Diethylamino-Gruppen in **4b** (Schema 2). Die Verwendung der *tert*-Butylgruppe ermöglicht zudem eine hohe sterische Abschirmung der basischen Imin-Funktion.

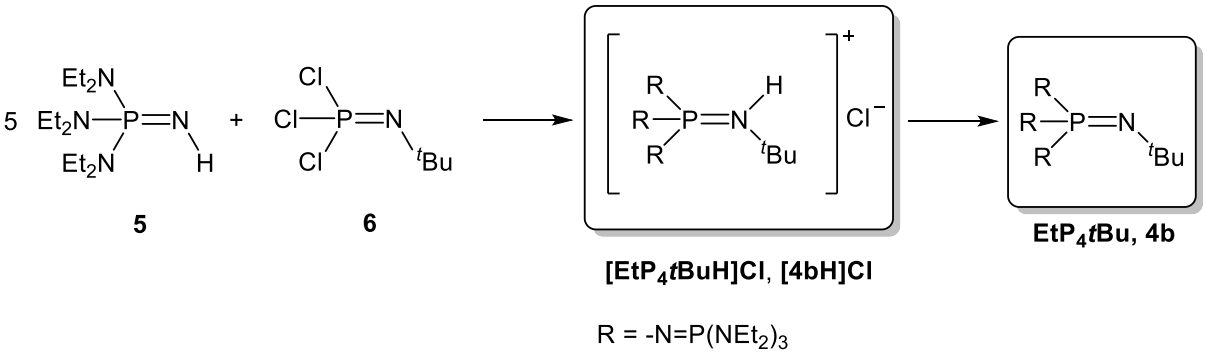

Schema 2: Synthese des Ethyl-Tetraphosphazen-Derivates **EtP$_4$*t*Bu** (**4b**).

Hierzu soll zunächst entsprechend Schema 2 die Synthesestrategie von Schwesinger verfolgt werden.[28–30,32] Durch die Umsetzung des Chlorphosphazens $Cl_3P{=}N$*t*Bu (**6**) mit dem entsprechenden Phosphanimin **5** sollte das Tetraphosphazen **4b** als Hydrochlorid-Salz zugänglich sein. Während die Literatursynthese für die beschriebenen Tetraphosphazen-Derivate zunächst über eine Umsalzung zu den entsprechenden Tetrafluoroborat-Salzen erfolgt, welche anschließend mit Kaliumamid in flüssigem Ammoniak deprotoniert werden, soll im Hinblick auf die Atomökonomie, die Sicherheitsrisiken, die Gesundheitsgefahren und die Umweltaspekte eine alternative Deprotonierungsstrategie entwickelt werden.

Mit Phosphazen **4b** sollen in den folgenden Studien grundlegende Systeme untersucht werden, um ein tieferes Verständnis von der Chemie nicht-koordinierter Anionen zu erlangen. Aus diesem Grund liegt der Fokus auf den drei großen und elementaren

Zielsetzung

Themenbereichen: Wasser und Hydroxide, Silanole und Silanolate sowie Phenole und Phenolate. Die Zielverbindungen sollen entsprechend Schema 3 durch Deprotonierungsreaktionen dargestellt werden und die entsprechenden nicht-koordinierten Anionen in Gegenwart des gering Lewis-aciden und schwach koordinierenden Phosphazenium-Kations **[4bH]$^+$** charakterisiert werden. Des Weiteren werden entsprechende wasserstoffverbrückte Derivate dargestellt, um deren Eigenschaften sowie Reaktivitäten mit denen der nackten Anionen zu vergleichen.

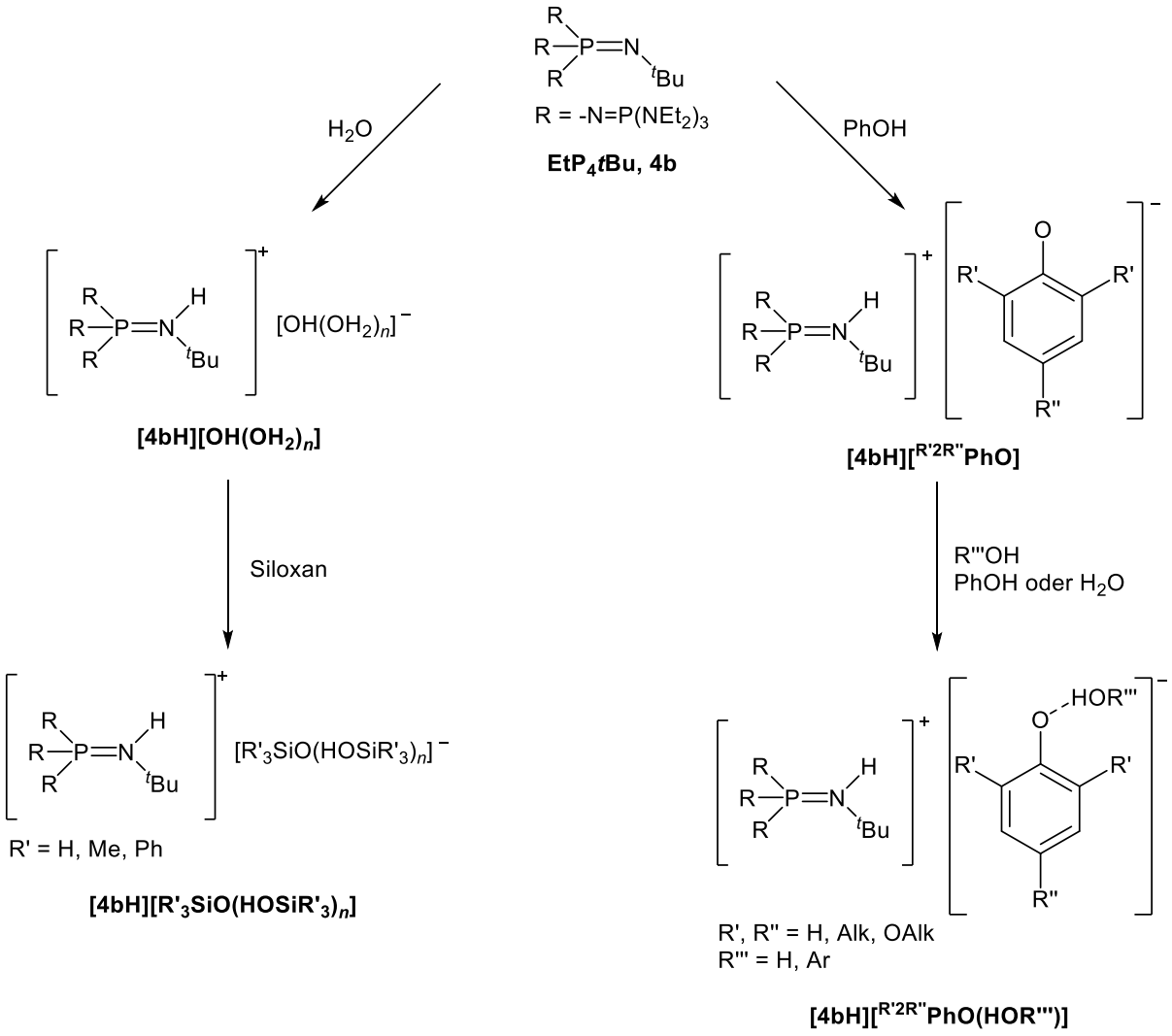

Schema 3: Synthesestrategie für nicht-koordinierte und wasserstoffverbrückte Anionen.

3. Diskussion der Ergebnisse

Die folgende Diskussion fasst die Ergebnisse dieser Dissertation, welche bereits vollständig in den Fachzeitschriften *Angew. Chem.*[41,42] (*Angew. Chem. Int. Ed. Engl.*)[43,44] und *Chem. Eur. J.*[45–47] publiziert wurden und im Anhang aufgeführt sind, prägnant zusammen. Einige Sätze und Textpassagen sind hierfür teilweise oder gänzlich aus den publizierten Manuskripten übernommen worden. Des Weiteren sei an dieser Stelle für detaillierte Informationen über die historische Entwicklung und den aktuellen Stand der Chemie elektronenreicher Phosphazen- und Phosphin-Superbasen noch einmal auf mein Mini-Review in *Chem. Eur. J.* verwiesen.[34]

3.1 Synthese der Phosphazenbase

Die Ethyl-Tetraphosphazenbase **4b** wurde zunächst als Hydrochlorid in einer leicht modifizierten Variante des bereits von Schwesinger *et al.* beschriebenen Syntheseverfahrens dargestellt (Schema 4).[28–30,32,41,43]

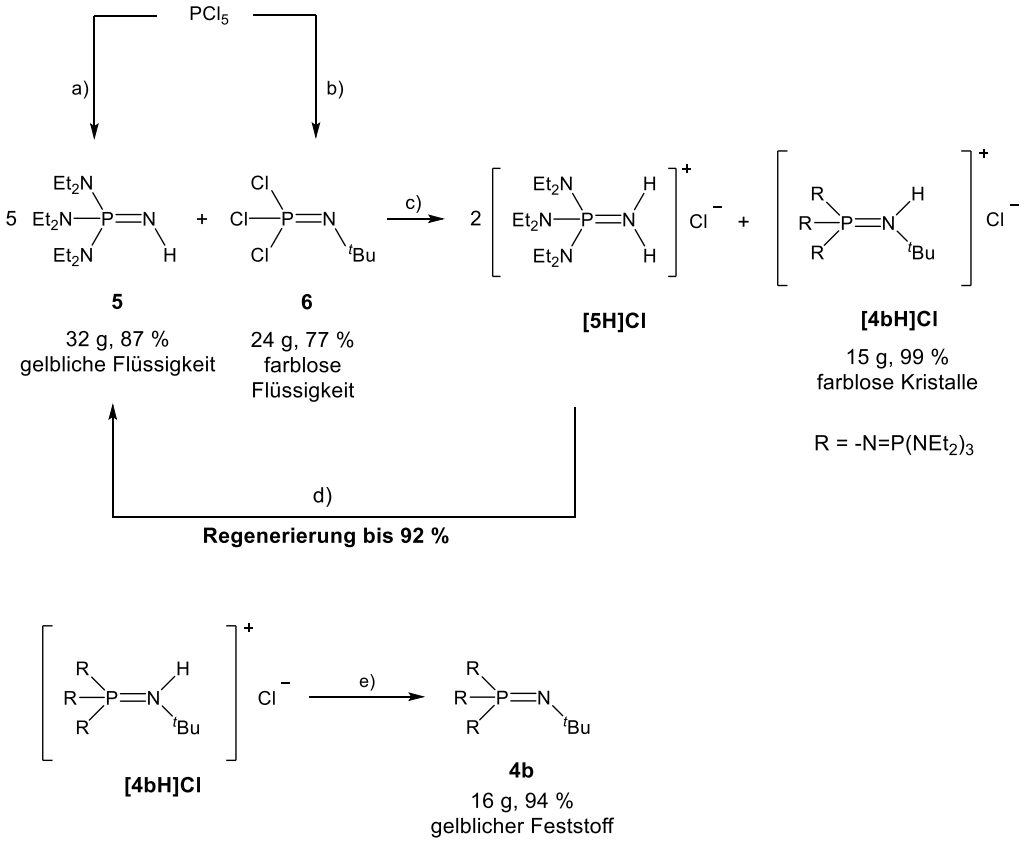

Schema 4: Synthese von **4b**. a) 1. $HNEt_2$ (6 Äq.), CH_2Cl_2, -30 °C, - 3 $[H_2NEt_2]Cl$; 2. NH_3 (2 Äq.), CH_2Cl_2, -20 °C, - $[NH_4]Cl$; 3. KO*t*Bu, MeOH, 0 °C, - KCl, - HO*t*Bu. b) H_2NtBu (3 Äq.), *n*-Pentan, - 2 $[H_3NtBu]Cl$. c) 160 °C, 3 d. d) KO*t*Bu, MeOH, 0 °C, - KCl, - HO*t*Bu. e) $NaNH_2$, NH_3, -70 °C bis RT, -NaCl, $-NH_3$.[41,43]

Hierzu wurde zunächst das Chlorphosphazen $Cl_3P{=}N\textit{t}Bu$ (**6**) in einer Kirsanov-Reaktion aus PCl_5 und *tert*-Butylamin in guten Ausbeuten dargestellt (Schema 4).[28–30,32,41,43,48] Das gewünschte Phosphanimin **5** wurde in Analogie zum entsprechenden literaturbekannten Methyl-Derivat[32] erhalten. Für die Synthese von **[4bH]Cl** wurde Chlorphosphazen **6** lösungsmittelfrei mit fünf Äquivalenten Phosphanimin **5** zur Reaktion gebracht, welches in der Reaktion gleichzeitig als Nukleophil und Base fungiert. Die anschließende wässrige Extraktion ermöglichte eine Rückgewinnung von **[5H]Cl** und ein Recycling von **5** mit einer Ausbeute von über 92 %. Das Produkt **[4bH]Cl** wurde nach Umkristallisation aus Diethylether in nahezu quantitativer Ausbeute im Multigramm-Maßstab erhalten (Schema 4) und vollständig, auch strukturell, charakterisiert (Abb. 1).

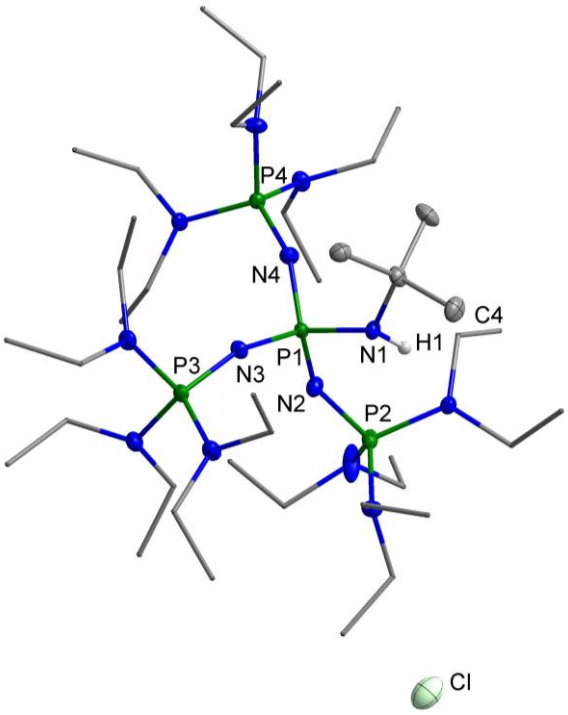

Abbildung 1: Molekülstruktur von **[4bH]Cl** im Festkörper.[41,43] Thermische Ellipsoide sind mit 50 % Aufenthaltswahrscheinlichkeit abgebildet. Die kohlenstoffgebundenen Wasserstoffatome und die gering besetzten fehlgeordneten Ethyl-Gruppen wurden aus Gründen der Übersichtlichkeit nicht abgebildet. Die Diethylamino-Gruppen sind vereinfacht als Stick-Modell gezeigt. Ausgewählte Bindungslängen [pm] und –winkel [°]: P1-N1 167.2(2), P1-N2 160.6(2), P1-N3 158.5(2), P1-N4 158.9(2), P2-N2 155.4(2), N1-C1 148.0(3); C1-N1-P1 128.6(2), N1-P1-N4 109.0(1), P1-N2-P2 140.7(1).

Entgegen der gängigen Deprotonierungsstrategie wurde **[4bH]Cl** aus atomökonomischen Gründen nicht in das entsprechende Tetrafluoroborat überführt, sondern direkt mit Natriumamid in flüssigem Ammoniak deprotoniert, wobei das freie

Tetraphosphazen **4b** als blass-gelber Feststoff in exzellenten Ausbeuten gewonnen wird (> 94 %, Schema 4).

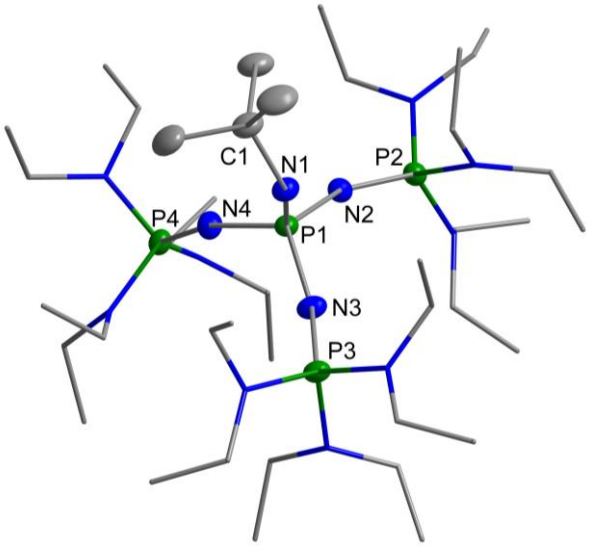

Abbildung 2: Molekülstruktur von **4b** im Festkörper.[41,43] Thermische Ellipsoide sind mit 50 % Aufenthaltswahrscheinlichkeit abgebildet. Die kohlenstoffgebundenen Wasserstoffatome wurden aus Gründen der Übersichtlichkeit nicht abgebildet. Die Diethylamino-Gruppen sind vereinfacht als Stick-Modell gezeigt. Ausgewählte Bindungslängen [pm] und -winkel [°]: P1-N1 157.8(1), P1-N2 163.8(2), P1-N3 163.1(1), P1-N4 163.2(2), P2-N2 153.0(1), N1-C1 145.7(2); C1-N1-P1 126.1(1), N1-P1-N4 113.1(1), P1-N2-P2 150.3(1).

Werden die Molekülstrukturen von **4b** und **[4bH]Cl** hinsichtlich ihrer P1-N1-Bindungslänge miteinander verglichen, so ist zu beobachten, dass diese in der freien Base (157.8(1) pm) relativ zur protonierten Base (167.2(2) pm) signifikant verkürzt ist und Doppelbindungscharakter aufweist.[41,43,49] Während P1-N1 in **[4bH]Cl** einer Einfachbindung entspricht, besitzen die übrigen Bindungen P1-N2, P1-N3 und P1-N4 Mehrfachbindungscharakter (158.5(2) - 160.6(2) pm).

Die Herstellung von **4b** durch Deprotonierung von **[4bH]Cl** mit selbstentzündlichen Metallamiden in flüssigem Ammoniak als Lösungsmittel ist gefährlich und im Hinblick auf die Abfallentsorgung problematisch.[41,43] Eine umfassende Kühlung ist teuer und die Vergrößerung des Ansatzes bleibt eine Herausforderung. Das Methyl-Derivat **4a** ist nicht durch Deprotonierung mit Kalium-*tert*-butanolat freisetzbar, wie zuvor von Schwesinger *et al.* berichtet.[30,32] Weniger basische Phosphazene wie **1a** können jedoch tatsächlich aus den entsprechenden Phosphazenium-Salzen mit Hilfe von Kalium-*tert*-butanolat oder sogar KOH vor der Destillation freigesetzt werden.[33]

^{31}P-NMR-spektroskopisch wurde gezeigt, dass das Ethyl-Phosphazen **4b** in Gegenwart von Wasser vollständig protoniert wird und das Kation des gebildeten Hydroxid-Hydrat-Salzes **[4bH][OH(OH$_2$)$_n$]** sowohl in Lösung als auch im Feststoff unbegrenzte Stabilität aufweist.[50] Durch Anlegen eines Vakuums wurde allerdings eine merkliche Rückbildung der freien Base **4b** nachgewiesen. Diese Beobachtung beweist eine mögliche Freisetzung von **4b** aus dem entsprechenden Hydroxid-Hydrat-Salz und legt eine wässrig-basische Umsalzung ausgehend von **[4bH]Cl** nahe. Die Umsetzungen mit Alkalilaugen, speziell mit 1 M Natronlauge, erwiesen sich zwar als teilweise zielführend, jedoch ergaben sich Probleme bei der vollständigen Umsalzung und der rückstandslosen Entfernung von NaOH im Produkt, was in einer Zersetzung von **[4bH]Cl** resultierte.[50]

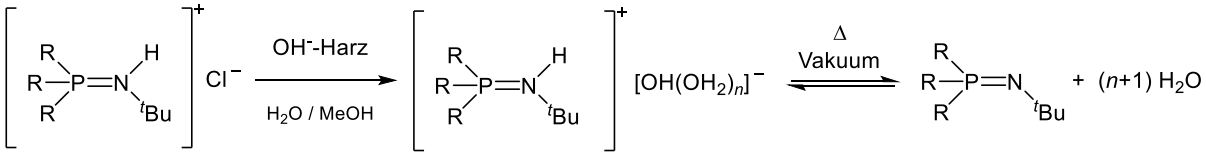

[4bH]Cl **[4bH][OH(OH$_2$)$_n$]** **4b**

R = -N=P(NEt$_2$)$_3$

25 g, 97 % farbloser Feststoff

Schema 5: Synthese von **4b** über eine Umsalzungsreaktion mit einem basischen OH$^-$-Anionenaustauscherharz.[41,43]

Um diese Schwierigkeiten zu umgehen, wurde nach der Vorschrift von Taylor und Hupfield[51] ein basisches OH$^-$-Anionenaustauscherharz verwendet (Schema 5). Die anschließende Thermolyse des isolierten Phosphazeniumhydroxids **[4bH][OH(OH$_2$)$_n$]** bei 70 - 100 °C im Hochvakuum lieferte das gewünschte Phosphazen **4b** als analysenreinen, farblosen Feststoff im großen Maßstab mit exzellenten Ausbeuten (25 g, 97 %).[41,43]

3.2 Darstellung isolierter Anionen ohne Kationen-Wechselwirkung

3.2.1 Das Hydroxid-Trihydrat-Anion

Zur Erzeugung isolierter Hydroxid/Wasser-Cluster wurden Lösungen von Phosphazen **4b** in *n*-Hexan mit unterschiedlichen Mengen an Wasser versetzt.[41,43] Die resultierenden Phosphazeniumhydroxide **[4bH][OH(OH$_2$)$_n$]** sind in Chlorbenzol löslich. Bei Raumtemperatur zersetzen sich solche Lösungen jedoch langsam. Phosphazeniumhydroxide trennen sich als Öl von polaren Lösungsmitteln ab, während amorphe oder kristalline Proben aus unpolaren Lösungsmitteln wie *n*-Hexan gewonnen werden. Dies kann durch die verschiedenen Mengen an Wasser, die in den Niederschlägen enthalten sind, erklärt werden, was die Isolierung einer genau definierten Verbindung erschwert. Nach langsamem Verdampfen einer Methanol/Wasser-Lösung von **4b** bei Raumtemperatur und Normaldruck wurden farblose Kristalle erhalten. Das Ergebnis der Elementaranalyse ließ auf ein mögliches Hydroxid-Hexahydrat-Salz des protonierten Phosphazens, [OH(OH$_2$)$_6$]$^-$, schließen (berechnet: C 47.46, H 11.25, N 17.99, P 12.24, O 11.06; gefunden: C 47.12, H 11.21, N 17.75, P 12.07, O 11.34). Da die Kristalle kein Beugungsmuster zeigten, konnten sie nicht mittels Röntgenbeugung analysiert werden. Jedoch wurde ein Einkristall von **[4bH][OH(OH$_2$)$_3$]** durch langsame Diffusion von Wasser in eine *n*-Hexan-Lösung der Base erhalten.

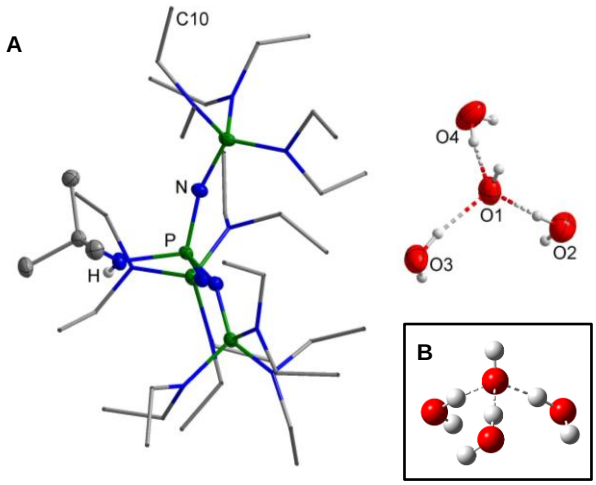

Abbildung 3: A: Molekülstruktur von **[4bH][OH(OH$_2$)$_3$]** im Festkörper.[41,43] Thermische Ellipsoide sind mit 50 % Aufenthaltswahrscheinlichkeit abgebildet. Fehlordnungen wurden aus Gründen der Übersichtlichkeit nicht abgebildet. Die Diethylamino-Gruppen sind vereinfacht als Stick-Modell gezeigt. Ausgewählte Bindungslängen [pm] und -winkel [°]: O1-O2 256.0(3), O1-O3 251.6(3), O1-O4 260.2(3); O2-O1-O4 88.7(1), O3-O1-O4 115.9(1), O2-O1-O3 110.4(1). B: Berechnetes C_3-symmetrisches Hydroxid-Trihydrat (MP2/6-311++G(3df,3pd)).[52]

Die röntgenkristallographische Untersuchung ergab eine Fehlordnung der beiden Ethyl-Gruppen des Kations im Verhältnis 82:18 und eine Fehlordnung des Anions im gleichen Verhältnis (Abb. 3A). Unter Betrachtung des verlässlich modellierten Teils der Fehlordnung mit der höheren Besetzung wird der kürzeste Abstand eines Sauerstoffatoms zur Methyl-Einheit des Kations von O4-C10‘ (Symmetriecode 1-x,1-y,1-z) mit 339.4(3) pm bestimmt. Dieser Abstand liegt deutlich über der Summe der van-der-Waals-Radien und zeigt, dass dies das erste Beispiel für ein isoliertes Hydroxid-Hydrat-Anion ist, das keinen direkten Kontakt zu einem Kation aufweist. Die O-O-Abstände liegen im Bereich von 251.6(1) pm bis 260.2(3) pm. Die berechneten Werte des *C*$_3$-symmetrischen Hydroxids weisen leicht vergrößerte Abstände von 261.2 pm auf (Abb. 3B).[52] Da das Phosphazeniumhydroxid **[4bH][OH(OH$_2$)$_3$]** sehr empfindlich gegenüber einem Verlust von Wasser unter vermindertem Druck ist (vgl. Kap. 3.1), sind zuverlässige Elementaranalysen kaum möglich (Schema 6).

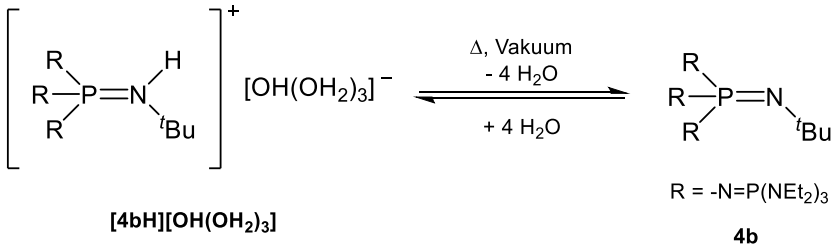

[4bH][OH(OH$_2$)$_3$] **4b**

Schema 6: Zersetzung von **[4bH][OH(OH$_2$)$_3$]** im Vakuum.[41,43]

Im IR-Spektrum des Produkts wird eine sehr breite Bande bei 3411 cm^{-1} für die OH-Streckschwingung des Hydroxid-Anions und der gebundenen Wassermoleküle detektiert. Es sind keine diskreten Banden zu beobachten, was auf einen schnellen Protonenaustausch zwischen den Wassermolekülen und dem Hydroxid-Anion hindeutet.

Die Bildung von **[4bH][OH(OH$_2$)$_3$]** wurde durch Titration einer Chlorbenzollösung von Tetraphosphazen **4b** mit Wasser mittels ^{31}P-NMR-Spektroskopie untersucht (Abb. 4).

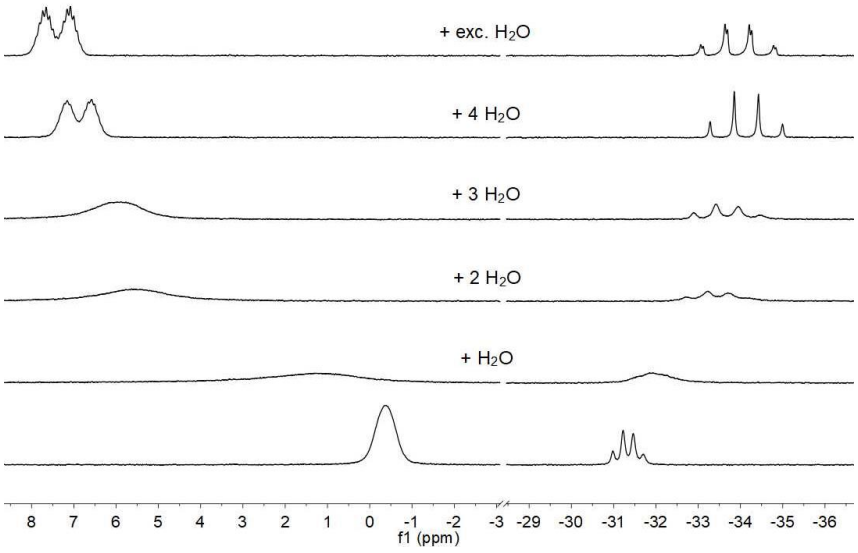

Abbildung 4: ^{31}P-NMR-spektroskopisch analysierte Titration von **4b** mit unterschiedlichen Mengen Wasser in Chlorbenzol. Als Locksubstanz wurde Aceton-d_6 in einer Kapillare verwendet.[41,43]

Normalerweise lassen sich in Mischungen aus freier und protonierter Base **4b** und **[4bH]$^+$** nebeneinander zwei separate Signalsätze im ^{31}P-NMR-Spektrum mit charakteristischen $^2J_{PP}$-Kopplungskonstanten von 29 Hz und 70 Hz beobachten (vgl. Abb. 5).[50] Dieses Phänomen deutet auf eine hohe kinetische Barriere des Protonenaustausches zwischen **4b** und **[4bH]$^+$** hin. Bemerkenswerterweise wird bei der Titration von **4b** mit Wasser nur ein Signalsatz mit einer kontinuierlich steigenden $^2J_{PP}$-Kopplung von 29 zu 70 Hz nachgewiesen. Eine vollständige Protonierung von **4b** wird nur bei Verwendung von vier oder mehr Äquivalenten Wasser beobachtet und die $^2J_{PH}$-Kopplungskonstante von 8 Hz des Kations **[4bH]$^+$** wird nur in Gegenwart eines Wasserüberschusses aufgelöst. Im ^{1}H-NMR-Spektrum der Lösung wird ein breites Signal bei 4.9 ppm für die Protonen von Wasser und dem Hydroxid-Ion beobachtet. Da eine Zersetzung des Hydroxid-Hydrates im Vakuum erfolgt, wird eine Aktivierung oder Orientierung der Wassermoleküle im superbasischen System postuliert. Die geringe Größe eines Wassermoleküls sowie die hohe Basizität des Hydroxid-Anions ermöglichen die Deprotonierung der abgeschirmten Iminium-Einheit. Im Vergleich zu Hydroxiden mit koordinierenden Kationen, wie z. B. Alkalimetall-Kationen, scheint ein nacktes Hydroxid-Anion in Gegenwart von **[4bH]$^+$** instabil und daher nicht realisierbar zu sein. Die stabilisierende Wirkung einer Solvathülle ist notwendig, um die Basizität des Hydroxid-Anions zu senken. Dieses Prinzip scheint für die selektive Freisetzung von **4b** aus seinem Hydroxid verantwortlich zu sein. Durch Entfernen der Solvathülle

im Vakuum steigt die Basizität des entstehenden Anions und ermöglicht eine selektive Deprotonierung des Phosphazenium-Kations.

Die analoge Titration von **4b** mit *tert*-Butanol lieferte die bereits bekannten zwei Signalsätze für **4b** und **[4bH]**$^+$, was im Vergleich zum Hydroxid-Salz auf einen deutlich verlangsamten Protonenaustausch hindeutet (Abb.5).

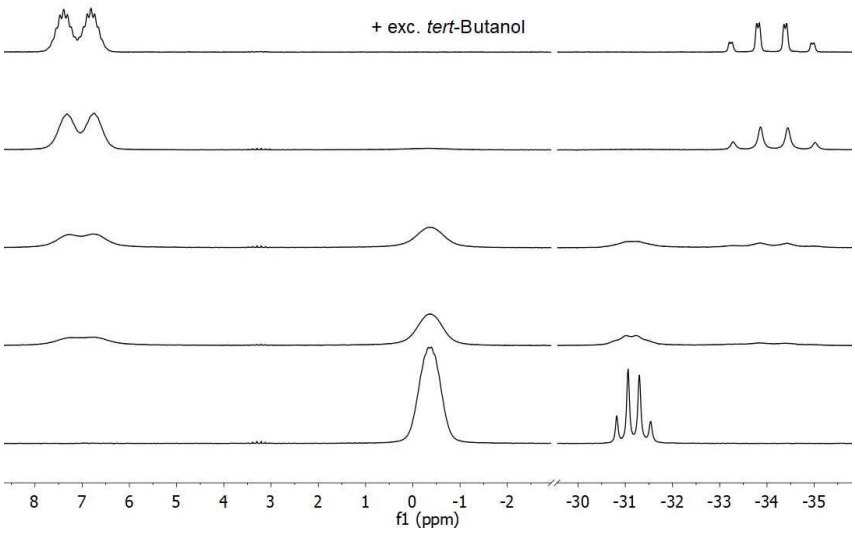

Abbildung 5: ^{31}P-NMR-spektroskopisch untersuchte Titration von **4b** mit unterschiedlichen Mengen *tert*-Butanol in Chlorbenzol. Als Locksubstanz wurde Aceton-d_6 in einer Kapillare verwendet.[34]

Die Zugabe von drei Äquivalenten Alkohol resultierte in der vollständigen Protonierung von **4b**, wohingegen die $^2J_{PH}$-Kopplung in Analogie zum Hydroxid-Hydrat erst in Gegenwart eines Überschusses Alkohol aufgelöst wurde. Isolation und Untersuchung von Einkristallen aus einer gekühlten *n*-Hexanlösung mit entsprechender Stöchiometrie lieferte den Beweis für die Bildung von **[4bH][*t*BuO(HO*t*Bu)$_2$]** (Schema 7).

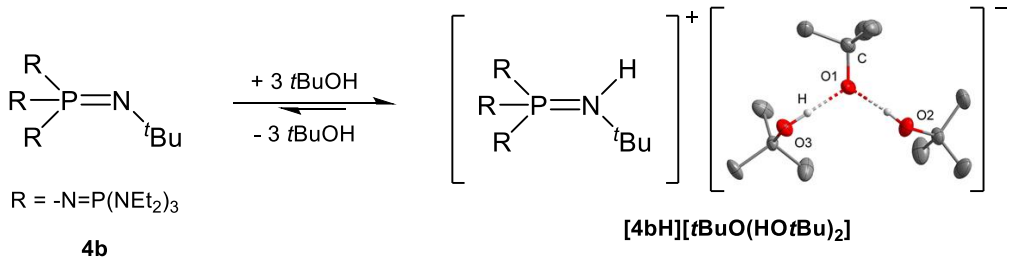

Schema 7: Darstellung von **[4bH][*t*BuO(HO*t*Bu)$_2$]**.[34]

Die Abstände O1-O2 und O1-O3 betragen 258.2(2) und 253.0(2) pm und liegen im Bereich der ermittelten O-O-Abstände des Hydroxid-Hydrat-Anions $[OH(OH_2)_3]^-$.

Das kristalline Salz **[4bH][*t*BuO(HO*t*Bu)$_2$]** zersetzt sich unter Verflüssigung bei Erwärmen auf Raumtemperatur, und die partielle Rückbildung der Base **4b** wurde ^{31}P-NMR-spektroskopisch nachgewiesen.

Für die Realisierung eines nackten Hydroxid-Ions ist ersichtlich, dass die „acide“ Iminium-Funktion in **[4bH]$^+$** geschützt werden muss.[34] Hierfür bietet sich die Verwendung einer Methylgruppe in **[4bMe]$^+$** an, welche über die Reaktion von **4b** mit Alkylhalogeniden eingeführt werden kann (Schema 8). Das Signal des Imin-Phosphor-Atoms in **[4bMe]$^+$** weist durch die zusätzliche Kopplung zur Methylgruppe ein charakteristisches Quartett-von-Quartett-Aufspaltungsmuster auf, resultierend aus $^2J_{PP}$- und $^3J_{PH}$-Kopplungskonstanten von 77 und 14 Hz.

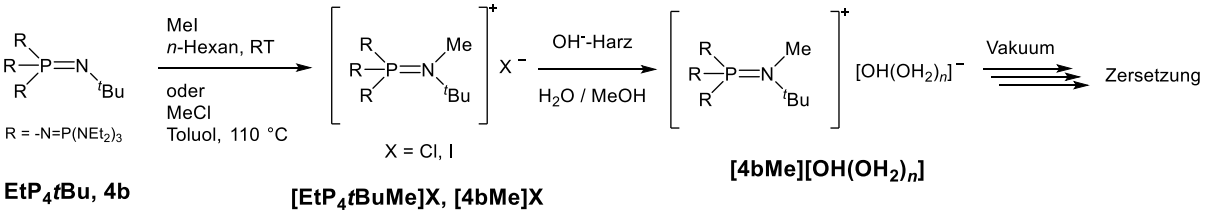

Schema 8: Methylierung von **4b** und Umsalzung zum Hydroxid-Hydrat mit Zersetzung im Vakuum.[34]

Die Umsalzung in das Hydroxid-Solvat mit einem basischen Anionenaustauscherharz und die anschließende Trocknung im Vakuum bei Raumtemperatur führte zur Zersetzung des Kations **[4bMe]$^+$** und zu einer Mischung mehrerer Produkte. Untersuchungen durch multinukleare NMR-Spektroskopie deuten auf eine Zersetzung der *tert*-Butylgruppe als Hauptreaktion hin.

Die Generierung unsolvatisierter Hydroxid-Anionen in Gegenwart von **[4bH]$^+$** und des peralkylierten Phosphazeniumkations **[4bMe]$^+$** scheint somit die Grenzen der Realisierbarkeit zu überschreiten.

3.2.2 Silanol-Silanolat-Anionen

Sowohl Silanole als auch Silandiole sind wertvolle Bausteine in der synthetischen Chemie und zeigen eine ausgeprägte Tendenz zur Bildung von Netzwerken über Wasserstoffbrücken.[53–55] Die Bildung von Addukten von Silanolen mit sauerstoff- und stickstoffhaltigen Basen, die leichter als die entsprechenden Alkohol-Addukte zugänglich sind,[55,56] sowie die Verwendung von Alkoholen und Aminen zur selektiven Wirt-Gast-Komplexierung unterstreicht dieses Verhalten. Ebenso bilden die verwandten *α*,*ω*-Siloxandiole, $HO[SiR_2O]_nH$, inter- und intramolekulare Wasserstoffbrücken, die häufig zur Bildung von Ringstrukturen führen (Schema 9).[57,58]

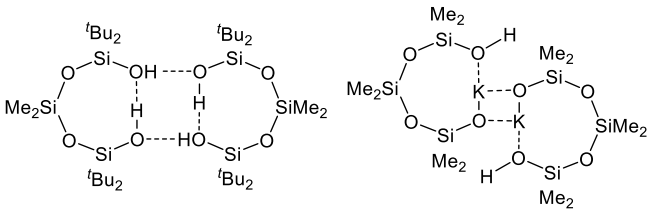

Schema 9: Beispiele für achtgliedrige Siloxanringe.[53,58,59]

Im Falle des Monokaliumsilanolat-Salzes (Schema 9, rechts) ist bemerkenswert, dass die Wechselwirkung von Kalium-Kationen mit dem Silanolat sowie dem Silanol-Sauerstoff im Vergleich zur Bildung einer intramolekularen Wasserstoffbrücke begünstigt ist, was entsprechend zu einem Ring führt, der das Kalium-Ion enthält.

Die Synthese anionischer Silanolate kann durch Spaltung von Siloxanen mit starken Basen erreicht werden. Dieses Konzept stellt die Grundlage für die anionische Ringöffnungspolymerisation ausgehend von cyclischen Siloxanen dar, die es ermöglicht, Silikonpolymere mit einer geringen Polydispersität darzustellen. Neben Initiatoren wie Metallhydroxiden, *n*-Butyllithium oder Metallsilanolaten sind ebenfalls Beispiele für die Kombination von superbasischen Phosphazenen mit protischen Additiven wie Wasser, Alkoholen oder Silanolen beschrieben worden.[60] Der gering Lewis-acide und schwach koordinierende Charakter der Phosphazenium-Kationen ermöglicht die Bildung nicht-koordinierter Anionen, welche eine deutlich gesteigerte Aktivität gegenüber den entsprechenden Metall-Salzen aufweisen. Bis heute sind die Natur und die genauen Strukturen der reaktiven Zwischenprodukte im Wesentlichen unbekannt.

Um die Strukturen hochreaktiver monofunktioneller und difunktioneller Silanolat-Anionen ohne Kontakt zum Gegenion aufzuklären, bietet sich die Verwendung von *in situ* erzeugten Phosphazeniumhydroxiden **[4bH][OH(OH$_2$)$_n$]** an, die im Folgenden mit Siloxanen und Polysiloxanen umgesetzt werden.

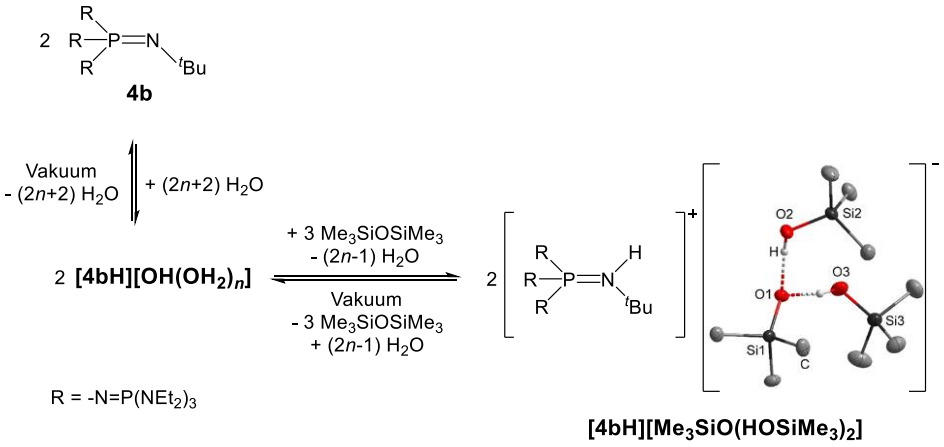

Schema 10: Gleichgewichtsreaktion von Phosphazen **4b**, Hydroxid-Salz **[4bH][OH(OH$_2$)$_n$]** und Silanol-Silanolat-Salz **[4bH][Me$_3$SiO(HOSiMe$_3$)$_2$]**.[42,44]

Die Umsetzung von **[4bH][OH(OH$_2$)$_n$]** mit Hexamethyldisiloxan entsprechend Schema 10 lieferte das Produkt **[4bH][Me$_3$SiO(HOSiMe$_3$)$_2$]**, welches ein Trimethylsilanolat-Anion beinhaltet, das an zwei Silanolmoleküle gebunden ist. Verbindung **[4bH][Me$_3$SiO(HOSiMe$_3$)$_2$]** ist das erste Beispiel für ein isoliertes Silanol-Silanolat-Anion, das nicht in direktem Kontakt zum Gegenion steht. O3 ist an zwei Positionen mit einem Verhältnis von 79:21 fehlgeordnet und zeigt die kürzesten Abstände zu einer CH_2-Gruppe (C37) des Kations mit 331.5(4) und 329.0(1) ppm, beide sind länger als die Summe der van-der-Waals-Radien. Im Vergleich zu den O-O-Abständen der Wasserstoffbrücken im Triphenylsilanol-Pyrrolidin-Komplex von Strohmann *et al.* (249.1 pm, 270.1 pm, 283.3 pm)[61] weisen die Wasserstoffbrücken im Anion von Salz **[4bH][Me$_3$SiO(HOSiMe$_3$)$_2$]** einen O1-O2-Abstand von 258.2(1) pm und einen O1-O3-Abstand von 252.4(5) pm auf.

Wie bereits für die stark basischen Verbindungen **4b** und **[4bH][OH(OH$_2$)$_n$]** angegeben, zersetzt sich das Silanolat-Salz **[4bH][Me$_3$SiO(HOSiMe$_3$)$_2$]** schnell in H- und CH-aciden Lösungsmitteln und erfordert eine Handhabung in Chlorbenzollösung. Die ^{31}P- und ^{29}Si{^{1}H}-NMR-spektroskopische Untersuchung des gelösten Produkts **[4bH][Me$_3$SiO(HOSiMe$_3$)$_2$]** zeigte sowohl das protonierte Phosphazen **[4bH]$^+$** als auch die Rückbildung von $Me_3SiOSiMe_3$, was auf die Gleichgewichtsreaktion in Schema 10

hinweist. Das Signal im $^{29}Si\{^{1}H\}$-NMR-Spektrum bei $\delta = 8.6$ ppm wird den Siliciumatomen in $[Me_3SiO(HOSiMe_3)_2]^-$ zugeordnet. Wie für das Hydroxid-Hydrat-Salz **[4bH][OH(OH$_2$)$_n$]** beobachtet, zersetzt sich das Silanolat-Salz **[4bH][Me$_3$SiO(HOSiMe$_3$)$_2$]** im Vakuum unter Deprotonierung seines Kations **[4bH]$^+$** und Freisetzung von Silanol und Disiloxan. Diese Beobachtung ist ein weiterer Beweis für die Gleichgewichtsreaktion in Schema 10. Diese Situation erschwert eine zuverlässige Elementaranalyse von Salz **[4bH][Me$_3$SiO(HOSiMe$_3$)$_2$]**. Auf diesem Weg ist die Synthese eines unsolvatisierten Trimethylsilanolat-Anions in Gegenwart des Phosphazenium-Ions **[4bH]$^+$** nicht realisierbar.

Die Umsetzung von *in situ* generiertem Salz **[4bH][OH(OH$_2$)$_n$]** mit Hexamethylcyclotrisiloxan (D_3) lieferte ein cyclisches Silanol-Silanolat-Anion vom Typ $[D_3OH]^-$ in **[4bH][D$_3$OH]**, das im festen Zustand eine intramolekulare Wasserstoffbrücke ausbildet (Schema 11).

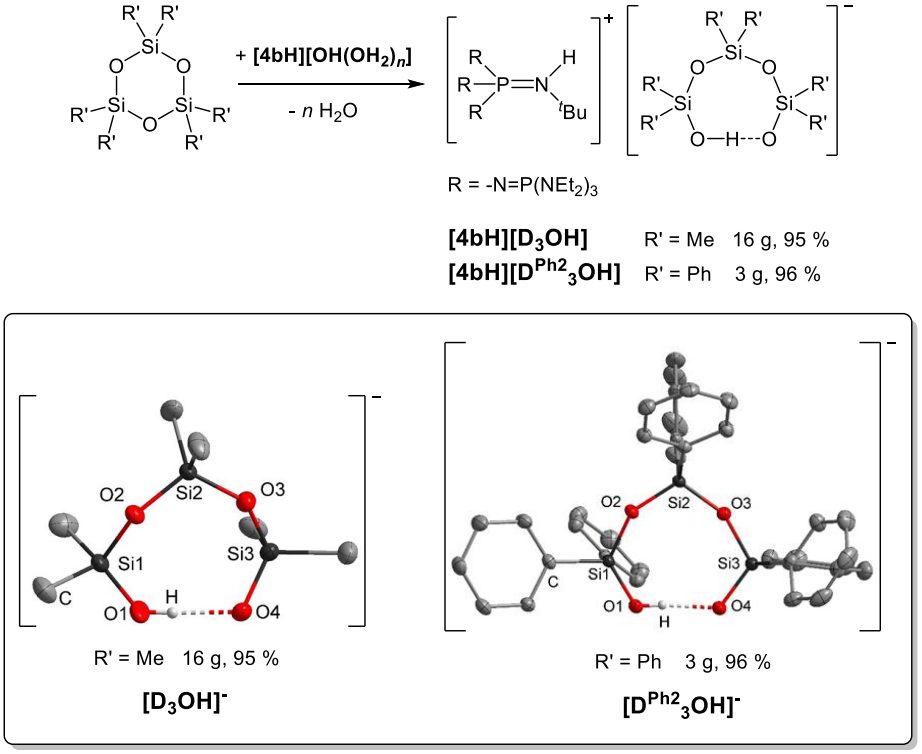

Schema 11: Reaktion von Cyclosiloxanen mit *in situ* generiertem Hydroxid **[4bH][OH(OH$_2$)$_n$]**.[42,44]

Die Sauerstoffatome sind vom Phosphazenium-Kation gut getrennt. Der kürzeste Abstand von 304.4(2) pm liegt zwischen O1 und und einer Methylen-Einheit (C31) vor.

Der O1-O4-Abstand wurde auf 242.8(2) pm bestimmt und deutet auf eine starke Wasserstoffbrückenbindung hin. Die Bindungen O4-Si3 und O1-Si1 reichen von

157.8(2) bis 158.9(1) pm und sind im Vergleich zum achtgliedrigen Siloxanring D_4 leicht verkürzt (Si-O-Abstände von 164 bis 166 pm).[62] Im ^{1}H-NMR-Spektrum in C_6D_6 wird ein breites Singulett bei δ = 14.0 ppm detektiert, das dem an der Wasserstoffbrückenbindung beteiligten Proton zugeordnet wird. Im ^{29}Si{^{1}H}-NMR-Spektrum von **[4bH][D$_3$OH]** wurde das Signal für die der Wasserstoffbrücke benachbarten Siliciumatome bei δ = 23.9 ppm beobachtet. Es konnte keine O-H-O-Streckschwingung von **[4bH][D$_3$OH]** im IR-Spektrum nachgewiesen werden.

Das Silanolat-Salz **[4bH][D$_3$OH]** beginnt sich im Vakuum bei 90 °C langsam und oberhalb von 100 °C schnell zu zersetzen. Die flüchtigen Produkte wurden durch Gaschromatographie-Massenspektrometrie als Wasser und cyclische Siloxane, mit D_4 als Hauptkomponente, identifiziert. Eine ^{31}P-NMR-spektroskopische Untersuchung des Rückstands ergab das freie Phosphazen **4b**, ähnlich der Zersetzung von Hydroxid-Hydrat **[4bH][OH(OH$_2$)$_n$]**.

Die Reaktion von *in situ* generiertem Phosphazenium-Hydroxid mit Hexaphenylcyclotrisiloxan führte zur selektiven Bildung des analogen [D$^{Ph2}{}_3$OH]$^-$-Anions in Salz **[4bH][D$^{Ph2}{}_3$OH]**, das in hervorragender Ausbeute isoliert wurde (> 96 %, Schema 11). Mit einem O1-O4-Abstand von 242.9(2) ppm weist die Länge der Wasserstoffbrückenbindung einen identischen Wert zu **[4bH][D$_3$OH]** auf. Analog zu Verbindung **[4bH][D$_3$OH]** wurde die O-H-O-Streckschwingung von Salz **[4bH][D$^{Ph2}{}_3$OH]** nicht in der IR-Analyse beobachtet.

3.2.2.1 Der Einfluss des Kations auf Silanol-Silanolat-Anionen

Die Untersuchung isolierter Wasserstoffbrücken in Silanol-Silanolat-Anionen gelang erstmalig unter Verwendung des schwach koordinierenden Phosphazenium-Kations **[4bH]$^+$**. Im Folgenden wird gezeigt, dass zusätzlich zu der geringen Koordinationsfähigkeit der Kationen ebenfalls deren Größe eine entscheidende Rolle für die Konstruktion der beobachteten Strukturmotive darstellt.

Für diese Studie wurden zunächst nach Schema 12 aus den entsprechenden Hydroxid-Salzen mit cyclischen Siloxanen die Silanolat-Anionen des Typs $[D_3OH]^-$ mit den kleineren Kationen $[PBu_4]^+$, $[NBu_4]^+$ und $[NMe_4]^+$ sowie dem Kation der Monophosphazenbase $[(Me_2N)_2C{=}N]_3P{=}N\textit{t}Bu$ (**1c**) dargestellt und mit Silanolat **[4bH][D$_3$OH]** verglichen.

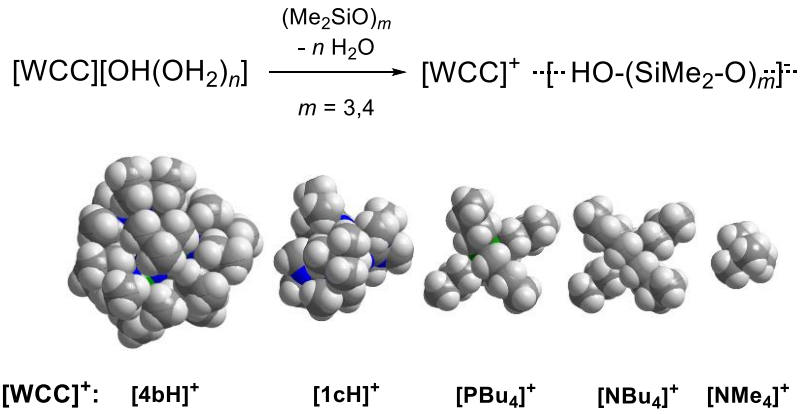

Schema 12: Reaktion von Hydroxid-Hydraten von schwach koordinierenden Kationen mit cyclischen Siloxanen (oben) und Darstellung der Kalottenmodelle verwendeter Kationen (unten).[46]

Während das Kation in **[4bH][OH(OH$_2$)$_n$]** resistent gegenüber Hydroxid-Ionen ist, unterliegt das Kation in **[1cH][OH(OH$_2$)$_n$]** einer basischen Hydrolyse unter Ausbildung des cyclischen Amids **7** (Schema 13).

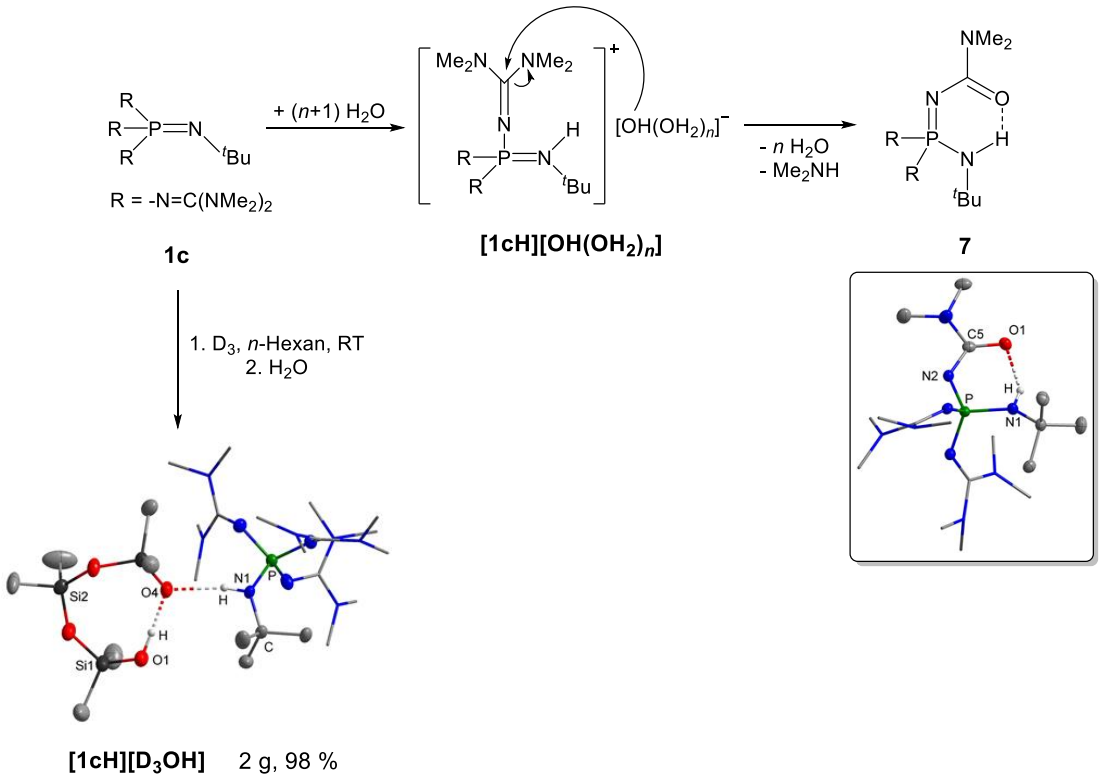

Schema 13: Basische Hydrolyse von **1c** und Synthese von **[1cH][D$_3$OH]**.[46]

Die Hydrolyse von **[1cH]$^+$** kann temporär unterdrückt werden, wenn cyclische Siloxane wie D$_3$ vor der Zugabe von Wasser in der Reaktionslösung vorhanden sind. So wurde das korrespondierende Silanolat **[1cH][D$_3$OH]** in exzellenter Ausbeute von 98 % isoliert und röntgenkristallographisch charakterisiert (Schema 13). Die O1-O4-Separation von 250.8(2) pm ist im Vergleich zu **[4bH][D$_3$OH]** (242.8(2) pm) deutlich aufgeweitet, welches auf die zusätzliche Interaktion des Kations über eine N1-O4-Wasserstoffbrückenbindung von 285.2(2) pm zurückzuführen ist. Verlässliche Elementaranalysen sind nicht möglich, da in Gegenwart von [D$_3$OH]$^-$ innerhalb weniger Tage bei Raumtemperatur eine Hydrolyse von **[1cH]$^+$** zu **7** beobachtet wird.

Die Silanolate **[NBu$_4$][D$_3$OH]** und **[PBu$_4$][D$_3$OH]** wurden in guten Ausbeuten von 92 % und 73 % als extrem hygroskopische, farblose Kristalle isoliert. Aus Röntgenstrukturanalysen konnten für beide Verbindungen cyclische [D$_3$OH]$^-$-Anionen nachgewiesen werden. Die intramolekularen Wasserstoffbrückenbindungen werden durch O1-O4-Abstände von 245.1(1) pm in **[NBu$_4$][D$_3$OH]** und 244.3(1) pm in **[PBu$_4$][D$_3$OH]** charakterisiert.

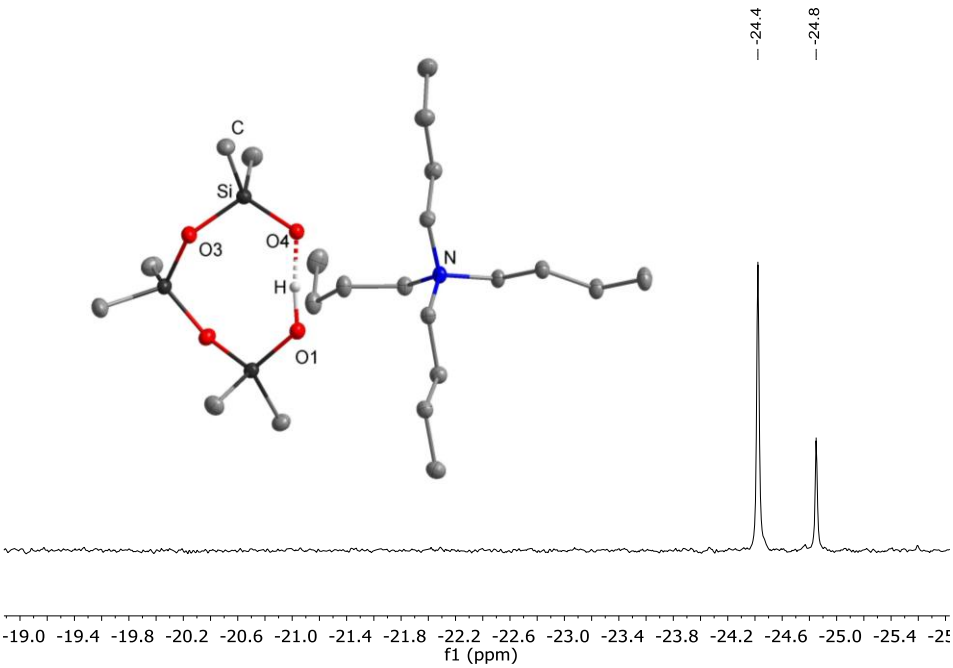

Abbildung 6: Molekülstruktur im Festkörper und $^{29}Si\{^{1}H\}$-IG-NMR-Spektrum von **[NBu$_4$][D$_3$OH]** in Et_2O (Lock mit Aceton-d_6 in einer Kapillare).[46]

Die Molekülstruktur von **[NBu$_4$][D$_3$OH]** ist exemplarisch in Abbildung 6 dargestellt. Die Resonanz im $^{29}Si\{^{1}H\}$-IG-NMR-Spektrum bei δ = -24.4 ppm resultiert von den Siliciumatomen in Nachbarschaft zur Wasserstoffbrückenbindung.

Während **[NBu$_4$][D$_3$OH]** als Feststoff bei Raumtemperatur über Monate ohne Zersetzung lagerbar ist und sich erst oberhalb von 80 °C unter Hofmann-Abbau zersetzt, hydrolysiert festes **[PBu$_4$][D$_3$OH]** innerhalb weniger Tage und in Lösung innerhalb weniger Stunden zu Tributylphosphanoxid.

Die analoge Reaktion von D_3 mit [NMe$_4$]OH lieferte ein klebriges Öl, aus welchem durch Überschichten mit Diethylether farblose Kristalle von **[NMe$_4$][D$_3$OH]$_{1/\infty}$** isoliert wurden. Im starken Gegensatz zu den cyclischen Silanol-Silanolaten des Typs $[D_3OH]^-$, welche in Gegenwart von sperrigen Gegenionen erhalten worden sind, sind mit dem kleinen Tetramethylammonium-Ion intermolekulare Wasserstoffbrücken bevorzugt, was in der Ausbildung polyanionischer Ketten von $[D_3OH]^-$-Ionen resultiert (Abb. 7).

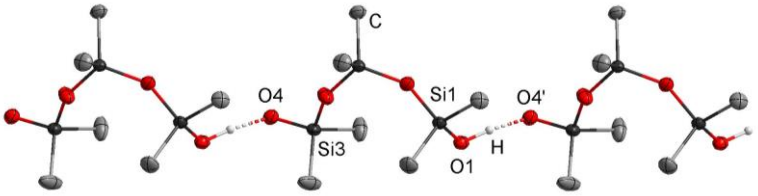

Abbildung 7: Ansicht des polyanionischen Strangs von $[D_3OH]^-$-Ionen aufgespannt über Wasserstoffbrücken in **$[NMe_4][D_3OH]_{1/\infty}$**.[46]

Die intermolekulare O1-O4‘-Distanz wurde auf 247.0(1) pm bestimmt und ist somit im Gegensatz zu der intramolekularen Bindung in **[4bH][D₃OH]** (242.8(2) pm) und **[NBu₄][D₃OH]** (245.1(1) pm) leicht vergrößert.

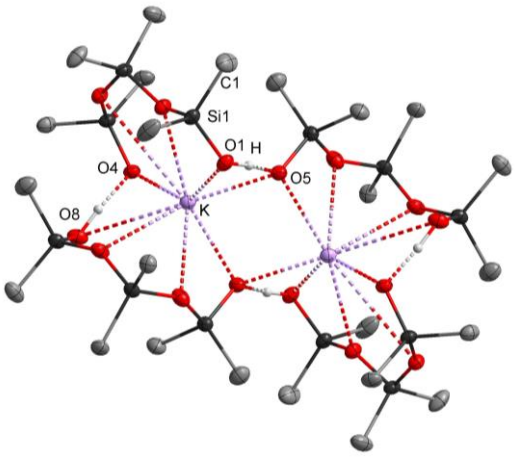

Abbildung 8: Molekülstruktur des dianionischen Dimers von **$[NMe_4][K(D_3OH)_2]$**. Die Ammonium-Kationen sind nicht dargestellt.[46]

Die Notwendigkeit für die Präsenz von schwach koordinierenden Ionen zur Untersuchung isolierter Silanol-Silanolat-Wasserstoffbrücken wird eindrucksvoll durch Betrachtung des Salzes **$[NMe_4][K(D_3OH)_2]$** deutlich, welches durch Rückstände von Kaliumhydroxid in einer Reaktionslösung aus $[NMe_4]OH$ und cyclischen Siloxanen gebildet wurde. Die Kalium-Ionen sind in einem monoanionischen Komplex von zwei $[D_3OH]^-$-Anionen umgeben und weisen starke Kalium-Silanolat- (d(K-O4) = 269.1(2) pm) und Silanol-Silanolat-Wechselwirkungen (d(O4-O8‘) = 249.6(2) pm) auf. Dieser Komplex liegt im Feststoff als dianionisches Dimer vor, welches über eine K-O5-Wechselwirkung (274.4(1) pm) und zusätzliche O1-O5-Wasserstoffbrücken (244.5(2) pm) verbunden ist. Das Strukturmerkmal von drei $SiMe_2O$-Einheiten ist ebenfalls in **$[NMe_4][K(D_3OH)_2]$** favorisiert.

3.2.2.2 Silikonrecycling

In Bezug auf die chemische Robustheit von Silikonen in der Natur verursacht ihre Multitonnenproduktion ernsthafte Entsorgungsprobleme. Der Abbau von Siloxanen unter Bildung cyclischer Derivate ist von allgemeinem Interesse, da dieser die Grundlage für ein mögliches Recycling weit verbreiteter Silikonkunststoffe bildet.

Die Depolymerisation von Silikonen kann unter sauren, basischen und fluoridierenden Bedingungen erreicht werden, was zu niedermolekularen cyclischen Siloxanen oder Organosilylfluoriden führt, die anschließend in neue Silikonkunststoffe umgewandelt werden können.[63,64]

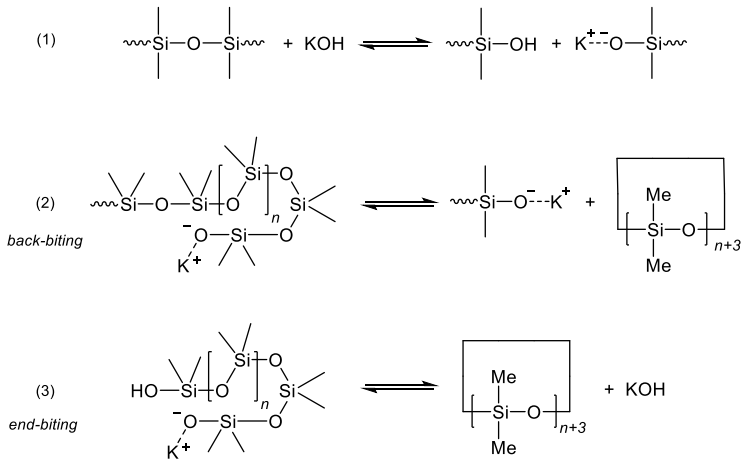

Schema 14: Gleichgewichtsreaktionen von linearen und cyclischen Siloxanen in Gegenwart von KOH.[63]

Bekannte Verfahren zur Depolymerisation von Silikonen verwenden Metallhydroxide wie KOH (Schema 14), erfordern jedoch erhöhte Temperaturen. Die niedrige Umsatzrate ist möglicherweise auf eine verminderte Nukleophilie zurückzuführen, welche durch die ausgeprägte Wechselwirkung des Kalium-Kations mit dem Silanolat-Anion resultiert.

Aufgrund des schwach koordinierenden Verhaltens des Phosphazenium-Gegenions weisen das Hydroxid-Trihydrat-Anion in **[4bH][OH(OH$_2$)$_3$]** sowie die Silanolat-Anionen in **[4bH][Me$_3$SiO(HOSiMe$_3$)$_2$]**, **[4bH][D$_3$OH]** und **[4bH][D$^{Ph2}_3$OH]** erhöhte Nukleophilie auf. Dies wurde beispielhaft für das Silanolat-Salz **[4bH][D$_3$OH]** in der Depolymerisations-Reaktion von Polydimethylsiloxan mit terminalen Trimethylsilyl-Gruppen gezeigt (Schema 15).

Die gesteigerte Nukleophilie des Silanolat-Sauerstoffatoms geht mit einer schnellen Gleichgewichtsreaktion einher, die sich durch *back-biting* und *end-biting* Prozesse auszeichnet (Schema 14).[63]

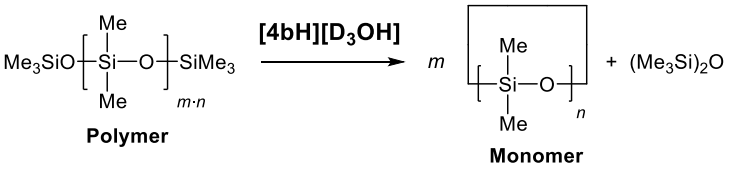

T / °C	p / mbar	Destillations-geschwindigkeit / mL h^{-1}	Zusammensetzung des Destillats / %			
			$(Me_3Si)_2O$	D_3	D_4	D_5
RT	0.001	3.1(2)	8	2	82	8
90	7	24.7(19)	6	6	79	9

Schema 15: Depolymerisation von Polydimethylsiloxan mit terminalen Trimethylsilyl-Gruppen unter Verwendung von Silanolat-Salz **[4bH][D$_3$OH]**.[42,44]

Die Äquilibrierungsaktivität kann durch die zeitliche Menge an cyclischen Siloxan-Spezies bestimmt werden, die durch Destillation aus dem Siloxangemisch entfernt werden. Das Silanolat-Salz **[4bH][D$_3$OH]** wurde in einer Konzentration von 0.1 Mol-% bei Raumtemperatur verwendet, zeigte jedoch eine schlechte Löslichkeit und verblieb als Suspension feiner farbloser Partikel. Trotzdem wurden cyclische Siloxan-Spezies und Hexamethyldisiloxan gebildet und im Vakuum (0.001 mbar) mit einer durchschnittlichen Geschwindigkeit von 3.1(2) mL/h vollständig entfernt. Anschließend wurde der Katalysator **[4bH][D$_3$OH]** als farbloser Feststoff ohne Spuren von Zersetzung isoliert. Das erhaltene Destillat bestand hauptsächlich aus D_4 (82 %) und D_5 (8 %) sowie Spuren von D_3 (2 %). Außerdem wurde Hexamethyldisiloxan isoliert (8 %).

Da industrielle Prozesse verglichen mit den bereits gewählten Reaktionsbedingungen vorzugsweise bei höheren Temperaturen und höheren Drücken durchgeführt werden, wurde versucht, diese Bedingungen durch Anlegen eines Membranpumpenvakuums (7 mbar) und einer Temperatur von 90 °C nachzuahmen. Hierbei bildete sich eine klare Lösung von **[4bH][D$_3$OH]** in Silikonöl und die gemittelte Destillationsgeschwindigkeit der flüchtigen Bestandteile wurde auf 24.7(19) mL/h bestimmt. Die durchschnittliche Zusammensetzung des Destillats unterscheidet sich nicht signifikant von der Reaktion bei Raumtemperatur (Schema 15). Im Vergleich zu den Ergebnissen der Depolymerisation unter Verwendung von Natrium- (0 mL/h) oder Kaliumhydroxid

(< 1 ml/h) mit Konzentrationen von 11 Mol-%, die bei 90 °C durchgeführt wurden, zeigte Verbindung **[4bH][D$_3$OH]** eine signifikant erhöhte Äquilibrierungsaktivität.

Die Empfindlichkeit des Katalysators **[4bH][D$_3$OH]** gegenüber Feuchtigkeit wurde durch die Zugabe eines Überschusses an Wasser zum System untersucht. Hierbei fiel ein farbloser Feststoff aus und die Destillation von cyclischen Siloxanen brach ab. Nach Entfernen des Wassers im Vakuum über einen Zeitraum von zwei Stunden sprang die Destillation von Cyclosiloxanen erneut an und erreichte die zuvor bestimmte Destillationsrate (24.7(19) mL/h).

Der Katalysator **[4bH][D$_3$OH]** wurde auch durch Verwendung eines Überschusses an Trimethylchlorsilan (Me$_3$SiCl) deaktiviert und so die weitere Umsetzung unterbunden. Die katalytische Aktivität wurde durch die Zugabe einer wässrigen 0.5 M Natriumhydroxid-Lösung wieder regeneriert. Durch das Entfernen von überschüssigem Wasser im Vakuum wurde in der Silikonphase gebildetes Natriumchlorid als feiner Niederschlag beobachtet. Die Umsatzgeschwindigkeit des reaktivierten Katalysators ist mit den zuvor durchgeführten Depolymerisationsreaktionen identisch.

3.2.3 Phenolat-Anionen

Phenol stellt den einfachsten aromatischen Alkohol dar und dient deshalb als Modell für zahlreiche theoretische Berechnungen.[65,66,67,68] Praktische Anwendungen[69,70] betreffen etwa die großindustrielle Synthese von Salicylsäure im Kolbe-Schmitt-Prozess.[71,72] Des Weiteren sind fundamentale Prozesse in der Biosphäre von den Eigenschaften des Phenol-Moleküls abhängig. Die Aminosäure Tyrosin (*p*-Hydroxyphenylalanin) ist für den Erfolg der Photosynthese essenziell, da Tyrosin im Sauerstoff-bildenden Komplex (oxygen evolving complex, OEC) des Photosystems II in einem protonengekoppelten Elektronentransfer (proton coupled electron transfer, PCET) mit einem wasserstoffgebundenen Histidin photooxidiert wird.[73,74] Aus diesem Grund ist die Phenol-Wasserstoffbrückenbindung für die Aufklärung des PCET-Mechanismus‘ von fundamentalem Interesse.[74,75,76] Für viele biologische und chemische Systeme wurde bereits der Einfluss von Wasserstoffbrücken auf die Acidität der phenolischen OH-Funktion nachgewiesen.[67–69,75,77,78]

Während das schwach acide Phenol (pK_S = 9.98)[65,79] von Metall-Hydroxiden oder -Hydriden leicht deprotoniert wird[69,71,80] und auch entsprechende Kronenether-Komplexe von Natrium- und Kaliumphenolaten bekannt sind,[81] existiert bisher kein Beispiel für das nicht-koordinierte $[H_5C_6\text{-}O]^-$-Anion. Ähnlich wie Fluorid- und Hydroxid-Ionen ist auch das Phenolat-Anion stark basisch und zeigt eine starke Tendenz zur Ausbildung von Wasserstoffbrückenbindungen,[82] was die Isolierung des nicht-koordinierten Anions erschwert und zu Phenol-Phenolat-Addukten[78] oder zu Kontaktionenpaaren führt.[83]

Neutrale Phosphazenbasen bieten die Möglichkeit des selektiven Designs von sowohl nicht-koordinierten als auch wasserstoffverbrückten Phenolat-Addukten und erlauben somit das Studium dieser Wechselwirkung im Hinblick auf Reaktivität, Reduktionsvermögen sowie Absorptions- und Fluoreszenzeigenschaften von Phenolat-Anionen.[45,47] Für diesen Zweck wird im Folgenden ein breites Spektrum an unsubstituierten und 2,6-di-*tert*-butylsubstituierten Phenolderivaten sowie 2-Naphthol untersucht. Das Pyrrolidin-Monophosphazen **pyrrP$_1$*t*Bu** (**1b**) und das Tetraphosphazen **EtP$_4$*t*Bu** (**4b**) dienen hierbei als zu vergleichende Protonenakzeptoren.

3.2.3.1 Synthese nicht-koordinierter Phenolate

Die Durchführung der Reaktionen in Diethylether als schwach polarem und schwach CH-acidem Solvens erwies sich bezüglich der guten Präzipitation der ionischen Produkte als besonders wertvoll.

Die äquimolare Umsetzung von Monophosphazen **1b** mit Phenol liefert entgegen der Erwartung nicht das gewünschte nicht-koordinierte Anion. Stattdessen fiel das Salz **[1bH][(PhO)$_2$H]** als Kontaktionenpaare aus der überstehenden Phosphazen-Lösung aus (Schema 16).[45] Die Untersuchung mittels Röntgendiffraktometrie zeigte neben einer Phenol-Phenolat-Wasserstoffbrücke mit einem O1-O2-Abstand von 249.1(2) pm einen weiteren N1-O1-Kontakt von 279.2(1) pm. Hier ist besonders hervorzuheben, dass die Basizität von **1b** für eine vollständige Deprotonierung von Phenol nicht ausreichend zu sein scheint, obwohl der Vergleich der pK_{BH^+}-Werte dieses vermuten lässt.

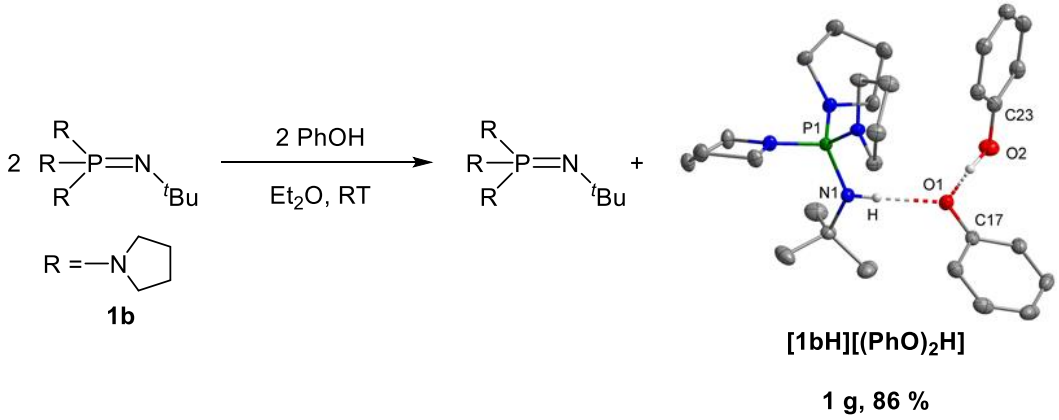

Schema 16: Deprotonierung von Phenol mit Monophosphazen **1b**.[45]

Im Gegensatz dazu wurden unter Verwendung von Tetraphosphazen **4b** Phenol (H_5C_6-OH) und alle substituierten Phenolderivate vollständig deprotoniert (Schema 17). Während die Salze **[4bH][PhO]**, **[4bH][^{Met}Bu^{2}PhO]** und **[4bH][^{t}Bu^{3}PhO]** farblos sind, ist **[4bH][^{MeO}tBu^{2}PhO]** tiefgelb. Die Deprotonierung von 2-Naphthol ($C_{10}H_7OH$, Schema 17) lieferte das Salz **[4bH][$C_{10}H_7O$]** als fluoreszierende, grüne Kristalle. Alle Verbindungen sind luftempfindlich und wechseln ihre Farbe durch Oxidation zu gelb, violett, braun oder rostrot, wohingegen **[4bH][$C_{10}H_7O$]** komplett entfärbt wird. Die Salze zersetzen sich in Brønsted-Säuren und Lösungsmitteln wie Chloroform, Dichlormethan oder Acetonitril und müssen in THF oder Diethylether gehandhabt werden.

Erstmalig wurde das nicht-koordinierte $[H_5C_6\text{-}O]^-$-Anion in **[4bH]PhO]** isoliert und vollständig charakterisiert.[45] Als der kürzeste Kationen-Anionen-Abstand der hauptbesetzten Fehlordnung wurde ein O1B-C33*-Abstand zur Methyl-Gruppe einer Diethylamino-Funktion mit 352.4(2) pm ermittelt, was die Summe der van-der-Waals-Radien übersteigt, jedoch im Bereich von C-H···O$^-$-Wasserstoffbrücken liegt (Symmetriecode C33*: ½ + X, ½ - Y, -½ + Z).[84] Die O1B-C3-Bindung mit 128.7(2) pm ist im Vergleich zu koordinierten Phenolaten wie in NaOPh (133(1) pm) deutlich verkürzt.[45,47,85]

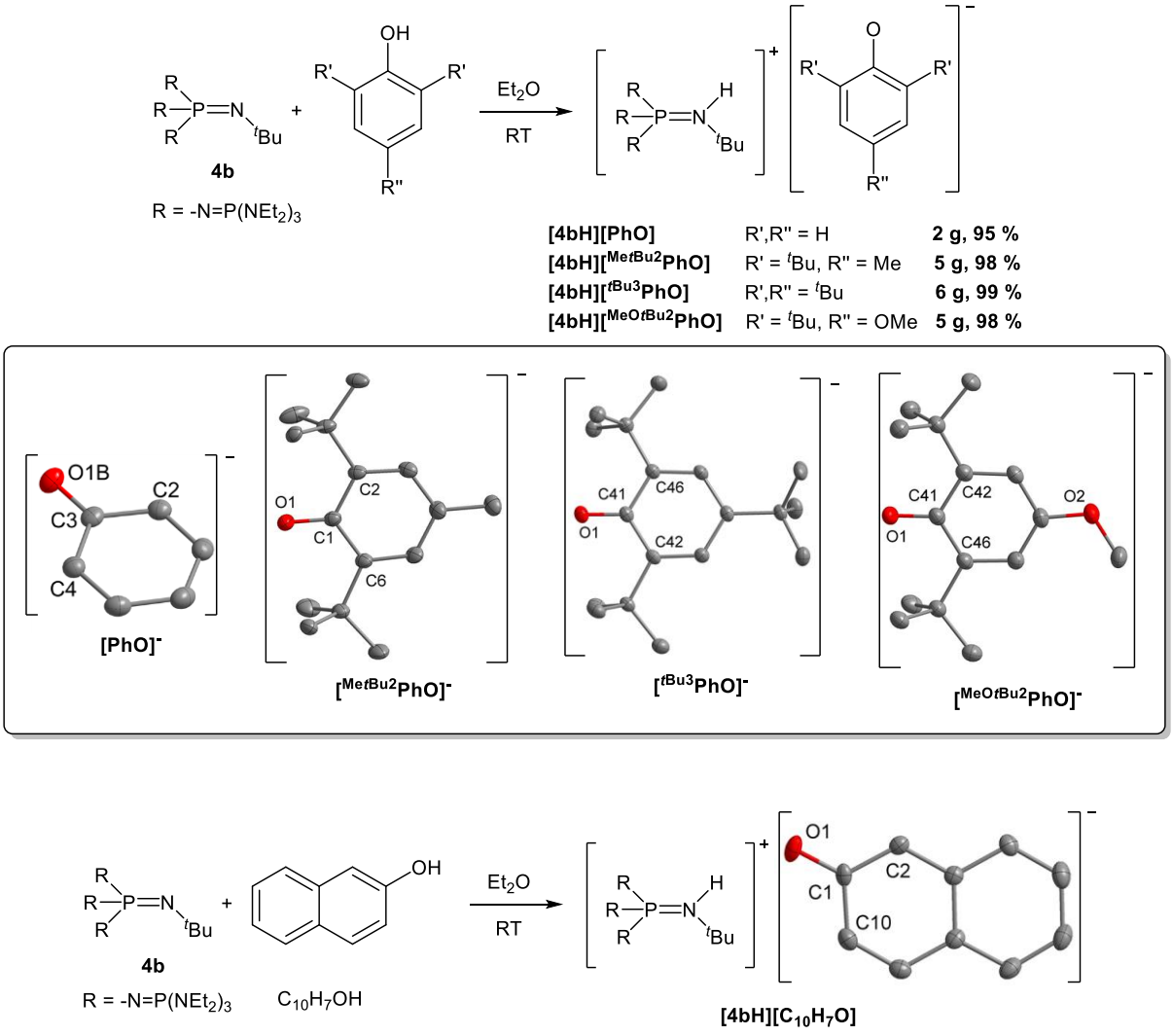

Schema 17: Synthese nicht-koordinierter Phenolat-Anionen mit Tetraphosphazen **4b**.[45,47]

Die ^{13}C-NMR-Resonanz des O1B-C3-Kohlenstoffatoms in $[PhO]^-$ (δ = 175.0 ppm) ist im Vergleich zu den Anionen $[C_{10}H_7O]^-$ (δ = 173.7 ppm), $[^{Me}t^{Bu2}PhO]^-$ (δ = 170.2 ppm), $[^{t}Bu^{3}PhO]^-$ (δ = 170.3 ppm) und $[^{MeO}tBu^{2}PhO]^-$ (δ = 168.0 ppm) deutlich entschirmt.[45,47]

Die entsprechenden C-O^--Abstände der substituierten Phenolate von 128.4(2) pm bis 129.8(2) pm variieren jedoch nicht signifikant.

3.2.3.2 Synthese wasserstoffverbrückter Phenolat-Addukte

Die selektive und nahezu quantitative Darstellung der Phenol-Phenolat-Salze **[4bH][(PhO)$_2$H]**, **[4bH][(C$_{10}$H$_7$O)$_2$H]** und **[4bH][(**$^{\mathbf{MeO}t\mathbf{Bu}2}$**PhO)$_2$H]** erfolgt über die Deprotonierung der Phenol-Derivate mit einem halben Äquivalent Base **4b** oder im Fall von **[4bH][PhO(H$_2$O)]** durch Deprotonieren von Phenol vor der Zugabe eines Äquivalents an Wasser (Schema 18). Alle Versuche, Hemi-, Di- oder Trihydrate [PhO(H$_2$O)$_n$]$^-$ durch Zugabe von Wasser zu **[4bH][PhO]** zu isolieren und röntgendiffraktometrisch zu untersuchen, führten zur Bildung amorpher Feststoffe, wobei enthaltene kristalline Fragmente als **[4bH][PhO(H$_2$O)]** identifiziert wurden.

Das Salz **[4bH][(PhO)$_2$H]** beinhaltet das Phenol-Phenolat mit einer asymmetrischen, starken Wasserstoffbrücke, charakterisiert durch einen O-O-Abstand von 243.7(2) pm. Das Phenolat-Hydrat [PhO(H$_2$O)]$^-$ bildet im Festkörper dimere Strukturen mit einem linearen Zickzack-Motiv aus (Schema 18). Die Phenolat-Wasserstoffbrücken mit O1-O2- und O1*-O2B-Abständen von 260.8(7) pm und 265.2(7) pm sind im Vergleich zu [(PhO)$_2$H]$^-$ deutlich verlängert. Auffällig ist die besonders lange O2-O2B-Distanz von 293.1(5) pm.

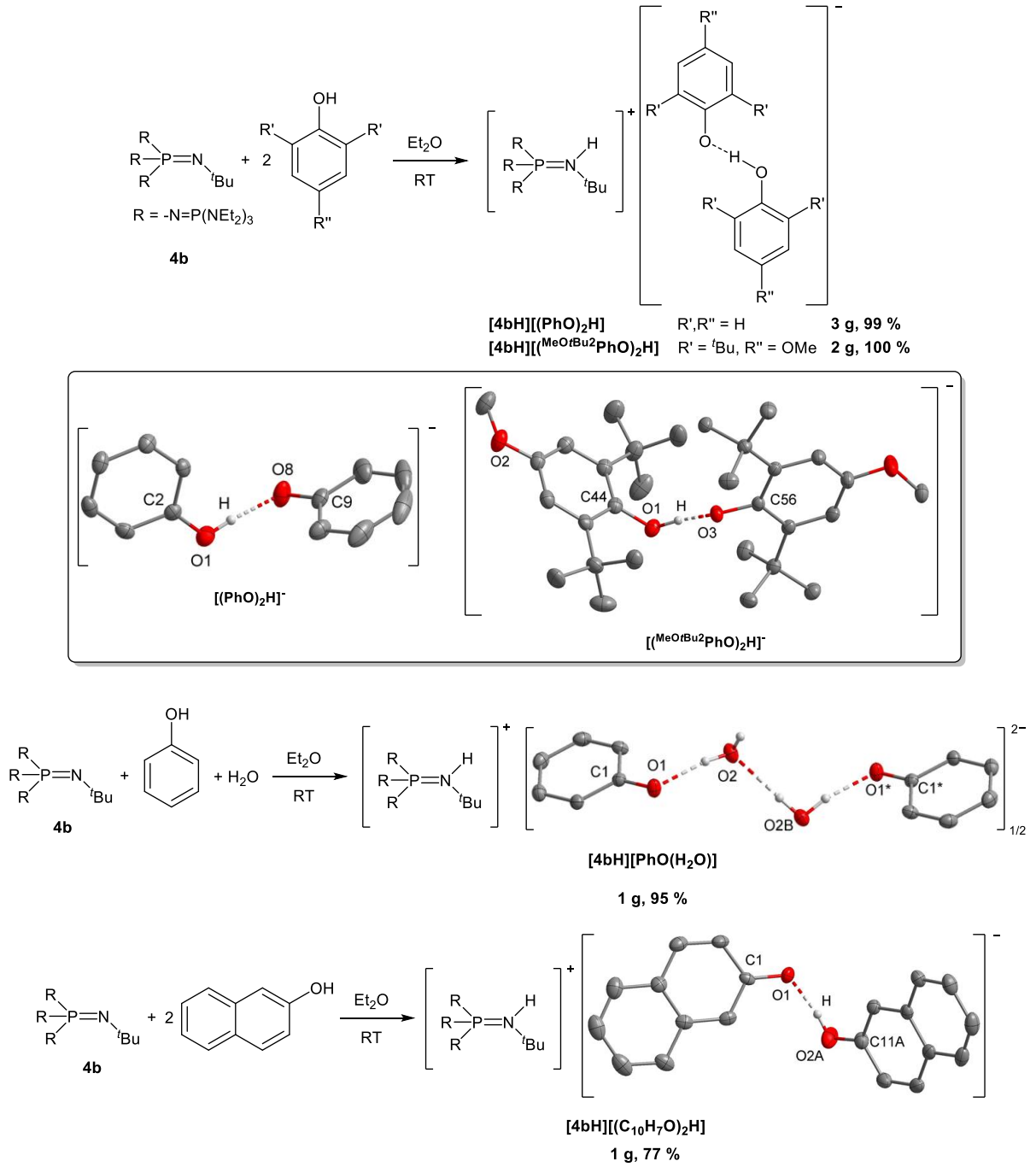

Schema 18: Synthese von Phenol-Phenolat- und Phenolat-Hydrat-Salzen.[45,47]

In Abbildung 9 sind die aromatischen Bereiche der ^{1}H-NMR-Spektren von $[PhO]^-$, $[PhO(H_2O)]^-$ und $[(PhO)_2H]^-$ dargestellt. Die Ausbildung einer Wasserstoffbrückenbindung von $[PhO]^-$ mit Wasser und Phenol geht mit einer signifikanten Tieffeldverschiebung der Signale und einer verbesserten Auflösung der Kopplungen einher. Letzteres kann durch eine verringerte Delokalisierung der negativen Ladung über das aromatische System erklärt werden, welches durch die ladungsentziehende Wasserstoffbrücke hervorgerufen wird. Im Einklang dazu treten

die entsprechenden ^{13}C-NMR-Resonanzen der C-O-Funktionen relativ zu $[PhO]^-$ (δ = 175.0 ppm) bei deutlich höherem Feld auf ($[PhO(H_2O)]^-$ δ = 173.6 ppm; $[(PhO)_2H]^-$ δ = 167.2 ppm).

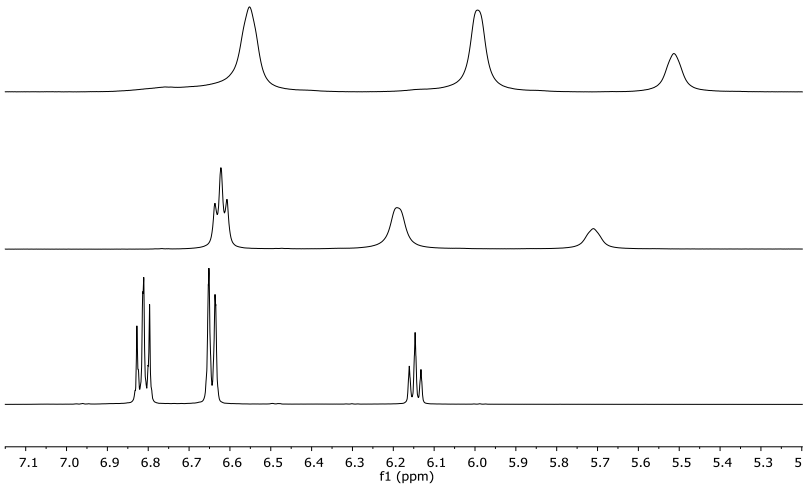

Abbildung 9: Aromatische Region der ^{1}H-NMR-Spektren von $[PhO]^-$ (oben), $[PhO(H_2O)]^-$ (Mitte) und $[(PhO)_2H]^-$ (unten) in THF-d_8.[45,47]

Das Anion in **[4bH][(C$_{10}$H$_7$O)$_2$H]** weist die stärkste Wasserstoffbrücke aller untersuchten Phenolat-Addukte mit einem O1-O2A-Abstand von 238.5(4) pm auf. Interessanterweise wird dieses Salz als farbloser Feststoff isoliert, während **[4bH][C$_{10}$H$_7$O]** intensiv grün fluoresziert. UV/Vis-Spektren der Salze in trockenem THF lassen eine bathochrome Absorptionsverschiebung für $[C_{10}H_7O]^-$ mit zwei lokalen Maxima bei 412 und 439 nm erkennen (Abbildung 10). Die Absorption des Anions $[(C_{10}H_7O)_2H]^-$ ist hingegen hypsochrom verschoben und wird erst unterhalb von 400 nm beobachtet, was eine Erklärung für die fehlende Farbigkeit liefert. Der Einfluss der Wasserstoffbrücke wurde ebenfalls mit Hilfe von Fluoreszenz-Emissions-Spektren bei einer Anregungswellenlänge von λ_{ex} = 320 nm nachgewiesen. Die Fluoreszenz des nicht-koordinierten Anions in **[4bH][C$_{10}$H$_7$O]** ist intensiv und besitzt ein Fluoreszenzmaximum bei λ_{em} = 462 nm mit einer Stokes-Verschiebung von 9605 cm^{-1}. Das Addukt **[4bH][(C$_{10}$H$_7$O)$_2$H]** besitzt hingegen eine nur schwach ausgeprägte Fluoreszenz mit vier Maxima bei λ_{em} = 344 nm, 360 nm, 427 nm und 458 nm (Stokes-Verschiebungen von 2181, 3472, 7831 und 9416 cm^{-1}).

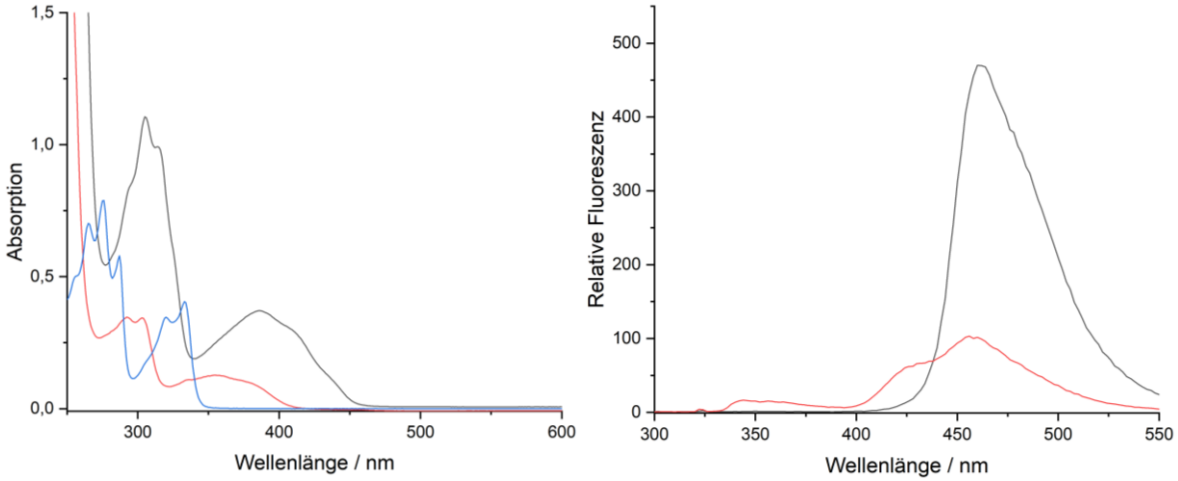

Abbildung 10: UV/Vis-Absorptionsspektrum (links, 32 µM) von 2-Naphthol ($C_{10}H_7OH$, blau), **[4bH][$C_{10}H_7O$]** (schwarz) und **[4bH][$(C_{10}H_7O)_2H$]** (rot) und Fluoreszenz-Emissionsspektren (rechts, 200 µM, λ_{ex} = 320 nm) von **[4bH][$C_{10}H_7O$]** (schwarz) und **[4bH][$(C_{10}H_7O)_2H$]** (rot).[47]

Auch sterisch anspruchsvolle *tert*-Butylsubstituenten in 2- und 6-Position des Phenols verhindern nicht die Ausbildung einer Wasserstoffbrücke, wie für **[4bH][(^{MeOtBu2}PhO)$_2$H]** gezeigt wurde (Schema 18). Auffällig ist die Vergrößerung des O1-O3-Kontaktes von 247.0(1) pm verglichen mit jenem in den Derivaten $[PhO(HOPh)]^-$ (243.7(2) pm) und $[(C_{10}H_7O)_2H]^-$ (238.5(4) pm), welche möglichweise durch sterische Repulsion resultiert.

3.2.3.3 Redoxpotentiale von Phenolat-Anionen

Mehrere Arbeiten haben sich der Redoxpotentiale diverser Phenole[86] und Phenolate[87,88] mittels (Cyclo-) Voltammetrie, bevorzugt in Acetonitril-Lösung, gewidmet. Die Anionen wurden hierbei meist *in situ* durch Deprotonierung mit Tetraalkylammoniumhydroxiden erzeugt. Die erfolglose Darstellung des freien Phenolat-Anions durch Deprotonierung mit Ammoniumhydroxiden[78] sowie die schnelle Zersetzung koordinierter Phenolate wie **[4bH][PhO]** in Acetonitril lassen jedoch Zweifel an den berichteten Redoxpotentialen aufkommen.

Durch die selektiven Darstellungsmöglichkeiten für nicht-koordinierte und wasserstoffverbrückte Phenolat-Anionen können nunmehr die Einflüsse der Wasserstoffbrückenbindungen auf die Redox-Eigenschaften der Anionen mit Hilfe der Cyclovoltammetrie (CV) detailliert untersucht werden. Für diesen Zweck wurde getrocknetes THF als nicht CH-acides Lösungsmittel verwendet.

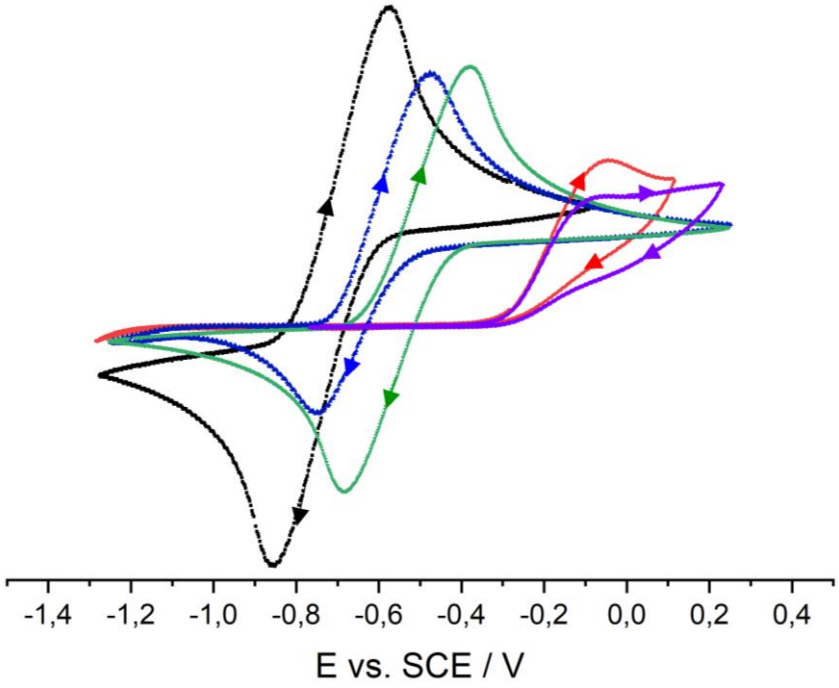

Abbildung 11: Cyclovoltammogramme von nicht-koordinierten Phenolaten.[45,47] **[1H][PhO]** (rot), **[1H][$C_{10}H_7O$]** (violett), **[1H][^{tBu3}PhO]** (grün), **[1H][^{MetBu2}PhO]** (blau) und **[1H][^{MeOtBu2}PhO]** (schwarz). Voltammogramme aufgenommen in 0.1 m [NBu_4][PF_6]-THF-Lösung bei 100 mV/s unter inerter Atmosphäre mit einer Glassy-Carbon-Arbeitselektrode (2.0(1) mm), einer Gegenelektrode (Stahl 18/8, 2.0(1) mm) und einer Ag/AgCl-Referenzelektrode. Alle Potentiale wurde gegen Fc/Fc^+ referenziert (+0.405 V vs. SCE).

Während die sterisch gehinderten Anionen [^{MeO}*t*^{Bu2}PhO]$^-$ und [^{t}^{Bu3}PhO]$^-$ reversibel oxidiert werden, resultieren bei geringerer sterischer Abschirmung irreversible Oxidationsprozesse, weshalb für [PhO]$^-$ und [$C_{10}H_7O$]$^-$ nur das Oxidationspotential E_{Ox} gemessen werden kann. Das Anion [^{Me}*t*^{Bu2}PhO]$^-$ wird ebenfalls irreversibel oxidiert. Die Redoxpotentiale E^0 der nicht-koordinierten substituierten Phenolate in Abbildung 11 liegen bei -0.52(1) V vs. SCE für [^{t}^{Bu3}PhO]$^-$ und -0.72(1) V vs. SCE für [^{MeO}*t*^{Bu2}PhO]$^-$ und übersteigen somit die Literaturdaten in Acetonitril um 0.3 V.[88] Das Anion [^{MeO}*t*^{Bu2}PhO]$^-$ besitzt ein ähnliches Reduktionsvermögen wie metallisches Zink.[89]

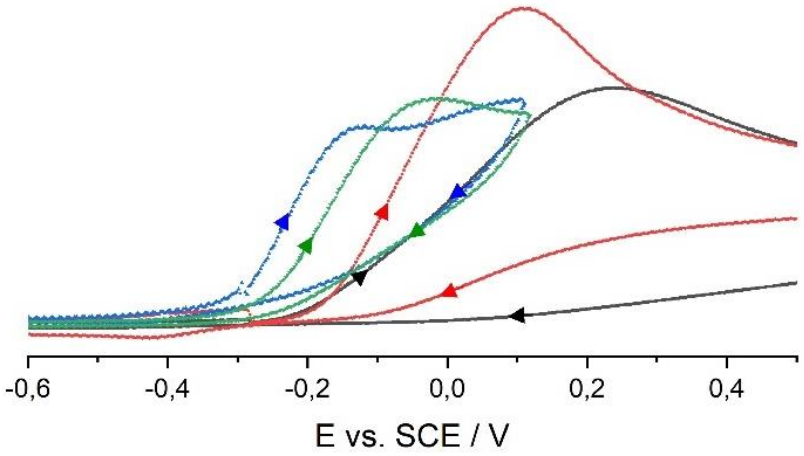

Abbildung 12: Cyclovoltammogramme von **[4bH][PhO]** (blau), **[4bH][PhO(H_2O)]** (grün), **[4bH][$(PhO)_2H$]** (schwarz) und **[4bH][$(PhO)_2H$]** + Überschuss H_2O (Konzentration von 0.1 M H_2O in der Elektrolytlösung, rot).[45,47] Voltammogramme aufgenommen in 0.1 m [NBu_4][PF_6] THF Lösung bei 100 mV/s unter inerter Atmosphäre mit einer Glassy-Carbon-Arbeitselektrode (2.0(1) mm), eine Gegenelektrode (Stahl 18/8, 2.0(1) mm) und einer Ag/AgCl Referenzelektrode. Alle Potentiale wurde gegen Fc/Fc^+ referenziert (+0.405 V vs. SCE).

Im Vergleich der Oxidationspotentiale von $[PhO]^-$ (E_{Ox} = -0.12(1) V vs. SCE), $[PhO(H_2O)]^-$ (E_{Ox} = -0.04(1) V vs. SCE) und $[(PhO)_2H]^-$ (E_{Ox} = +0.22(1) V vs. SCE) wird in Korrelation zur Stärke der ausgebildeten Wasserstoffbrückenbindung eine signifikante anodische Verschiebung des Oxidationspotentials beobachtet (Abbildung 12). Durch die Zugabe von Wasser wurde in der Elektrolytlösung von **[4bH][$(PhO)_2H$]** eine Konzentration von 0.1 M H_2O erzeugt, wodurch das Oxidationspotential eine kathodische Verschiebung von +0.22(1) V zu +0.10(1) V vs. SCE erfuhr.

Berechnete Ionisationspotentiale auf dem BP86/6-311+g(3df,2p)-Niveau bestätigen die experimentellen Erkenntnisse und belegen einen deutlichen Einfluss von Wasserstoffbrücken auf das nicht-koordinierte Anion $[PhO]^-$ (E_i = 228.69(1) kJ/mol).[45,47] Die Steigerung des Ionisationspotentials ist im Hydrat $[PhO(H_2O)]^-$ (E_i = 267.42(1) kJ/mol) deutlich geringer ausgeprägt als im Phenol-Addukt $[(PhO)_2H]^-$ (E_i = 314.90(1) kJ/mol).

Die gesammelten Beobachtungen lassen sich durch eine reduzierte Ladungsdichte am Phenolat-Sauerstoffatom erklären, welche durch die Stärke der ausgebildeten Wasserstoffbrückenbindung beeinflusst wird. Diese Wasserstoffbrücke bestimmt weiterhin die Dissoziation der Addukte in Lösung. Unter der Annahme, dass in der Gleichgewichtsreaktion ein Überschuss an Wasser das Phenol-Molekül im Addukt

$[(PhO)_2H]^-$ substituiert, deutet das erhöhte Oxidationspotential auf die Bildung von Phenolat-Hydraten hin.

Die Untersuchungen der 2-Naphthol-Salze **[4bH][$C_{10}H_7O$]** und **[4bH][$(C_{10}H_7O)_2H$]** liefern analoge Ergebnisse. Das Oxidationspotential von **[4bH][$C_{10}H_7O$]** (E_{Ox} = -0.15(1) V vs. SCE) ist verglichen mit dem verbrückten Addukt **[4bH][$(C_{10}H_7O)_2H$]** (E_{Ox} = +0.08(1) V vs. SCE) ebenfalls signifikant anodisch verschoben.

Interessanterweise kann aus der CV-Untersuchung des Adduktes in **[4bH][($^{MeOtBu2}PhO)_2H$]** mit einem Redoxpotential von E^0 = -0.70(1) V vs. SCE ein sehr ähnlicher Wert zu dem nicht-koordinierten Anion $[^{MeOtBu2}PhO]^-$ (-0.72(1) V vs. SCE) nachgewiesen werden. Im Vergleich zu freiem $[PhO]^-$ und $[(PhO)_2H]^-$ ist die geringe Verschiebung möglicherweise durch eine schwächere Wasserstoffbrücke in $[(^{MeOtBu2}PhO)_2H]^-$ relativ zu $[(PhO)_2H]^-$ zu erklären. Diese Tatsache könnte zu einer ausgeprägteren Dissoziation von $[(^{MeOtBu2}PhO)_2H]^-$ in Lösung führen und somit in einer geringeren Redox-Verschiebung des koordiniertem relativ zum nicht-koordinierten Anion resultieren.

3.2.3.4 Phenolate als Reduktionsmittel

Radikal-Ionen spielen eine wichtige Rolle als Intermediate in Oxidations- und Reduktionsprozessen. Ein Zugang zu Radikal-Anionen ist im Allgemeinen über elektrochemische Reduktions- oder single-electron-transfer-Prozesse (SET) möglich. Besonders organische Vertreter mit konjugierten π-Systemen besitzen energetisch tief liegende π*-Orbitale und ermöglichen die Ausbildung stabiler Radikal-Anionen. Das bekannte und vielfach untersuchte Tetracyanoethylen (TCNE)[90] weist hervorragende Elektronenakzeptoreigenschaften auf und dient als interessantes Ausgangsmaterial für organische Halbleitermaterialien und organische Magneten.

Eine potentielle Anwendungsmöglichkeit für Phosphazeniumphenolat-Salze als Reduktionsmittel findet sich bei der Darstellung reaktiver Radikal-Anionen durch SET-Reaktionen. Sterisch anspruchsvolle Gruppen in den Positionen 2, 4 und 6 sind notwendig für die Stabilisierung der gebildeten Phenoxyl-Radikale, da ihre Nukleophilie reduziert und ihre Dimerisierung verhindert wird.

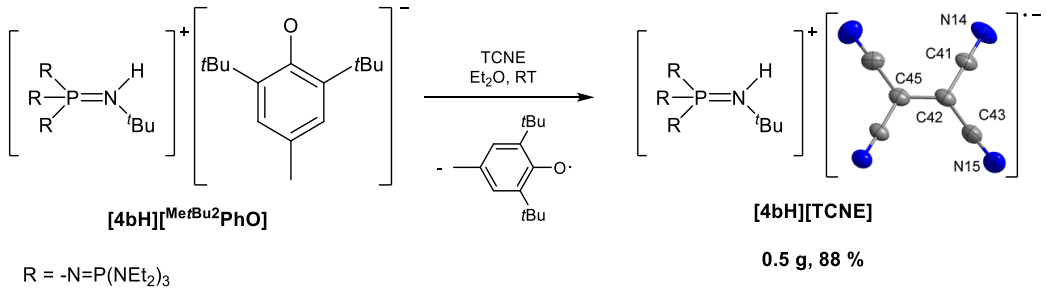

Schema 19: Synthese von **[4bH][TCNE]** durch Ein-Elektronen-Reduktion von TCNE mit **[4bH][^{MetBu2}PhO]**.[47]

Für diesen Zweck wurde **[4bH][^{MetBu2}PhO]** in etherischer Lösung mit TCNE umgesetzt (Schema 19). Die schnelle SET-Reaktion wurde von einer unmittelbaren Farbänderung von farblos zu gelb-grün begleitet. Vorteilhafterweise schied sich das Produkt **[4bH][TCNE]** als kristalliner orangefarbener Feststoff aus der überstehenden Phenoxyl-Radikallösung ab und wurde durch Waschen mit Diethylether analysenrein erhalten. Obwohl die Bildung von dimeren $[TCNE]_2^{2-}$-Dianionen[91] bekannt ist, ist das $[TCNE]^{\cdot-}$-Radikal-Anion in **[4bH][TCNE]** strikt monomer und mit dem kürzesten Kation-Anion-Abstand von 326.6(1) pm deutlich vom Gegenion separiert. Die Bindung C42-C45 mit 141.7(1) pm ist mit berechneten und experimentellen Literaturdaten vergleichbar.[92]

Mit der Verwendung von TCNE als Elektronentranfer-Reagenz wurde das Konzept zur Darstellung von Radikal-Anionen mittels Phosphazeniumphenolaten bestätigt und ist derzeit Gegenstand aktueller Forschung.

Im Hinblick auf die beträchtliche Umweltverschmutzung, die durch unsere Wirtschaft verursacht wird und entscheidend die Klimaerwärmung auf unserem Planeten vorantreibt, wurde versucht, diesbezüglich praktische Anwendungen für die neu synthetisierten Phenolate zu finden.

Schwefelhexafluorid (SF_6) ist das stärkste bekannte Treibhausgas. Dessen extreme chemische Robustheit hat einen dramatischen Einfluss auf das Klima.[93] Aus diesem Grund werden effiziente Methoden zum selektiven Abbau von SF_6 dringend benötigt. Zahlreiche Publikationen untersuchen die SF_6-Aktivierung mit Übergangsmetallkomplexen von Titan, Rhodium, Platin, Chrom und Vanadium sowie Nickel.[47] In allen Fällen werden die entsprechenden Sulfido- und Fluorokomplexe erhalten. SF_6 kann außerdem elektrochemisch oder über SET-Reaktionen aktiviert werden, wie durch die Umsetzung mit Alkalimetallen in flüssigem Ammoniak

demonstriert wurde. Außerdem wurden SET-Reaktionen von SF_6 mit organischen Elektronendonoren, TEMPOLi und photo-aktivierten Systemen beschrieben. Der Mechanismus für den SF_6-Abbau ist nicht vollständig geklärt. Während einige Publikationen die Aktivierung über einen SET-Prozess mit anschließender Zersetzung des entsprechenden Radikal-Anions $[SF_6]^{-\cdot}$ beschreiben, postulieren Dielmann und Mitarbeiter eine nukleophile Aktivierung unter Verwendung elektronenreicher Phosphine.

In diesem Kontext wurden alle nicht-koordinierten Phenolate in der Reaktion mit SF_6 untersucht (Schema 20).

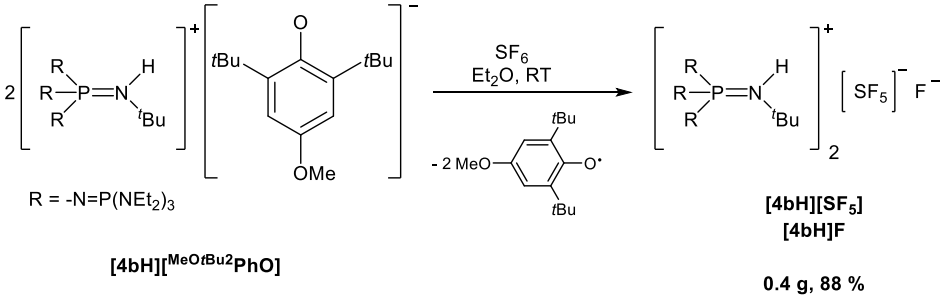

Schema 20: Aktivierung von SF_6 mit Phosphazeniumphenolat-Salzen.[45,47]

Die Umsetzung des stärksten Reduktionsmittels **[4bH][^{MeOtBu2}PhO]** mit SF_6 in etherischer Lösung resultierte in der spontanen Bildung des Pentafluorosulfanid-Anions $[SF_5]^-$ und einer Farbänderung von gelb zu tiefrot, wofür die entsprechenden Phenoxyl-Radikale verantwortlich zu sein scheinen (Schema 20). Das $[SF_5]^-$-Anion ist im ^{19}F-NMR-Spektrum der Lösung als charakteristisches Quintett (δ = 88.7 ppm) und Dublett (δ = 59.5 ppm) mit einer $^2J_{FF}$-Kopplungskonstante von 45 Hz zu beobachten. Für die Bildung des Pentafluorosulfanid-Anions ausgehend von SF_6 wurde ein zweifacher SET-Mechanismus postuliert (Schema 21).[94,95]

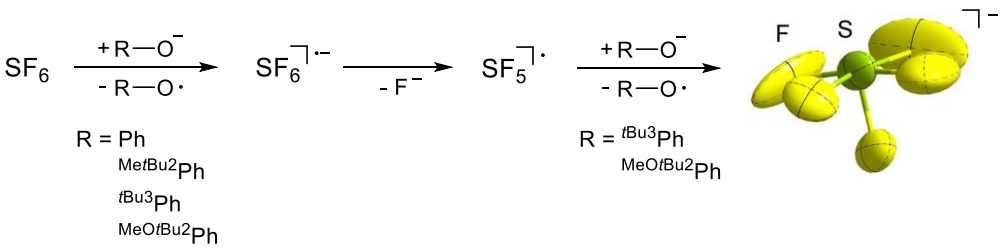

Schema 21: Postulierter Mechanismus der SF_6-Aktivierung mit nicht-koordinierten Phenolat-Anionen und Darstellung des Anions aus der Molekülstruktur von **[4bH][SF_5]**.[45,47]

In Anlehnung an den als favorisiert beschriebenen Prozess zerfällt das intermediär gebildete $[SF_6]^{\cdot-}$-Radikal-Anion in ein Fluorid-Anion (F^-) und ein $(SF_5)^{\cdot}$-Radikal. Letzteres wird durch ein weiteres Phenolat zum $[SF_5]^-$-Anion reduziert. Das thermisch stabile Salzgemisch aus **[4bH][SF$_5$]** und **[4bH]F** (dec. > 123 °C) fällt als farbloser Feststoff an. Die Reaktion von F^- mit der Borosilikat-Glasoberfläche führte im zeitlichen Verlauf zur Bildung unterschiedliche Fluoride, hauptsächlich $[HF_2]^-$, wie ^{19}F-NMR-spektroskopisch nachgewiesen wurde. Die Untersuchung von Einkristallen, welche durch langsame Kristallisation von **[4bH][SF$_5$]** aus der Reaktionslösung isoliert wurden, bestätigen die Existenz des $[SF_5]^-$-Anions mit seiner bekannten verzerrten pseudo-quadratisch-pyramidalen Geometrie.[96]

Die Umsetzung von SF_6 mit **[4bH][^{t}Bu^{3}PhO]** führte ebenfalls zur Bildung von $[SF_5]^-$ und Fluoriden (hauptsächlich $[HF_2]^-$), wie durch das ^{19}F-NMR-Spektrum bewiesen wurde. Im zeitlichen Verlauf färbte sich die farblose Reaktionslösung tiefblau, was mit der Farbe des freien Phenoxyl-Radikals übereinstimmt.[97] Die ^{19}F-NMR-spektroskopische Untersuchung der über mehrere Wochen bei Raumtemperatur gelagerten Reaktionslösung belegt die Stabilität von $[SF_5]^-$ in Gegenwart des Phenoxyl-Radikals.

Die Phenolate **[4bH][^{Met}Bu^{2}PhO]** und **[4bH][PhO]** sind ebenfalls in der Lage, SF_6 zu aktivieren (Schema 21). Im starken Gegensatz zu den sterisch anspruchsvollen 2,4,6-tri-*tert*-butyl- und 2,6-di-*tert*-butyl-4-methoxy-substituierten Phenolaten führten die Reaktionen mit **[4bH][^{Met}Bu^{2}PhO]** und **[4bH][PhO]** nicht zur Bildung von Pentafluorosulfanid-Anionen, sondern lieferten ausschließlich Fluoride. Da in CV-Untersuchungen von [^{Met}Bu^{2}PhO]$^-$ und $[PhO]^-$ irreversible Oxidationen nachgewiesen wurden, liegt die Vermutung nahe, dass gebildete Phenoxyl-Radikale mit Intermediaten reagieren, bevor das $[SF_5]^-$-Anion generiert wird.

Ebenfalls ist das wasserstoffverbrückte Addukt in **[4bH][(^{MeO}^{t}Bu^{2}PhO)$_2$H]** fähig, SF_6 zu aktivieren. In Analogie zum nicht-koordinierten Anion [^{MeO}^{t}Bu^{2}PhO]$^-$ wurde die Bildung von $[SF_5]^-$ und eine tiefrote Färbung der Lösung beobachtet. Neben einer deutlich verlangsamten Bildungsrate von $[SF_5]^-$ mit [(^{MeO}^{t}Bu^{2}PhO)$_2$H]$^-$ wurde ebenfalls die Bildung mehrerer unspezifizierter Fluorverbindungen nachgewiesen. Möglicherweise ist dies auf Reaktionen mit phenolischen OH-Funktionen zurückzuführen.

Es wurde berichtet, dass Tetrakis(dimethylamino)ethylen (TDAE) trotz eines Redoxpotentials (E^0 = -0.78 V vs. SCE), welches das aller präsentierten Phenolate

übersteigt, nicht in der Lage ist, SF_6 zu reduzieren.[95] Diese Beobachtung legt die Vermutung nahe, dass das Redoxpotential nicht den einzigen Faktor für einen erfolgreichen Abbau von SF_6 darstellt. In Analogie zu Dielmann wäre eine nukleophile Wechselwirkung des Phenolat-Sauerstoffatoms mit einem Fluoratom von SF_6 eine mögliche Erklärung, welches die anschließende Aktivierung in einem SET-Prozess unterstützt.

3.2.4 Perfluoralkylierungsreaktionen

Aufgrund der mit KHMDS vergleichbaren enormen Basizität von Tetraphosphazenbasen[28,29] eröffnet sich ein breites Spektrum an möglichen Deprotonierungsreaktionen und Nukleophil-Übertragungsreaktionen. Während starke anorganische Basen wie *n*-Butyllithium (*n*-BuLi), Lithiumdiisopropylamid (LDA) oder KHMDS bei einer Deprotonierung die entsprechenden Metall-Salze liefern, können unter Verwendung von Phosphazenbasen nicht-koordinierte Nukleophile erzeugt und übertragen werden.

Der enorme Vorteil von Phosphazenbasen lässt sich anschaulich am Beispiel der Trifluormethylierung verdeutlichen.[41,43] Fluoroform (HCF_3) stellt als Abfallprodukt der Teflonherstellung eine ausgezeichnete und kostengünstige Quelle für den Trifluormethylbaustein dar.[98] Die Deprotonierung von HCF_3 kann unter Verwendung von *n*-Butyllithium oder Kalium-*tert*-butanolat durchgeführt werden. Die hohe Fluorophilie von Alkalimetallkationen führt jedoch zu einer carbenoiden Bindungssituation und einer schnellen Difluorcarben-Eliminierung bei niedrigen Temperaturen.[99]

Schwach koordinierende Phosphazenium-Kationen verhindern die Difluorcarben-Eliminierung (Schema 22), wie von Shibata *et al.* und Zhang *et al.* für die Trifluormethylierung elektrophiler Carbonylverbindungen,[40] Sulfonylfluoride[39] sowie verschiedener Epoxide, Kohlendioxid und Ester[100] in guten bis hervorragenden Ausbeuten mit **4a** und Fluoroform gezeigt werden konnte.

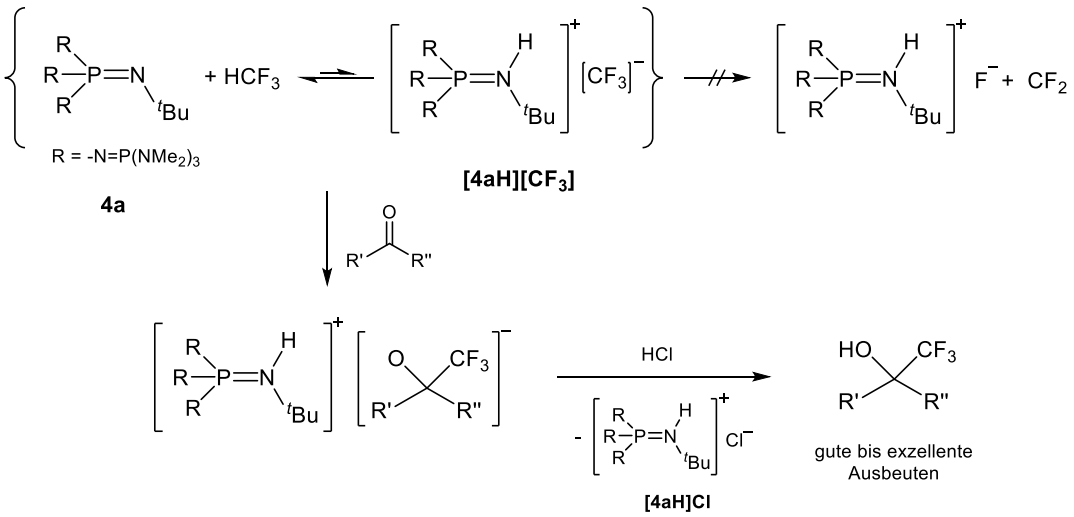

Schema 22: Trifluormethylierung von Carbonyl-Verbindungen mit Tetraphosphazen **4a**.

Die ^{19}F- und ^{31}P-NMR-spektroskopische Untersuchung einer Mischung aus **4b** und Fluoroform zeigte keine Reaktion, wie Zhang *et al.* ebenfalls für das Methylderivat **4a** berichteten. Die Zugabe von Elektrophilen führt zu einer schnellen Trifluormethylierung bei Raumtemperatur (Schema 22).

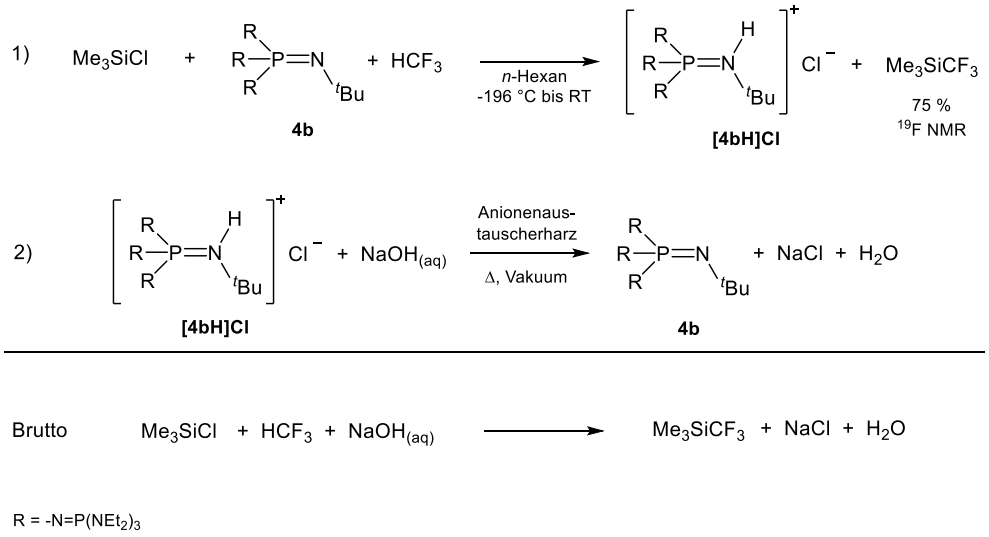

Schema 23: Bruttoreaktion der Synthese des Ruppert-Prakash-Reagenzes mit Tetraphosphazen **4b**.[41,43]

Phosphazen **4b** reagiert schnell mit Me_3SiCF_3 unter Bildung von Me_3SiF und einer Vielzahl von Nebenprodukten aufgrund einer Difluorcarben-Eliminierung. Die Zersetzungsreaktion von Me_3SiCF_3 mit Fluorid-Salzen wurde bereits von Tyrra und Naumann *et al.* untersucht und resultierte in der Bildung von perfluoralkylierten Polyanionen.[101] Mit einem Überschuss an Me_3SiCl kann die Reaktion von **4b** und HCF_3 kinetisch gesteuert werden, was zur selektiven Bildung von Me_3SiCF_3

(-67.7 ppm im ^{19}F-NMR-Spektrum) mit Ausbeuten von bis zu 75 % führte (Schema 23).[41,43]

Die Verwendung von Kohlenwasserstoffen als Lösungsmittel ist entscheidend, da die hohe Basizität von Phosphazen **4b** in Gegenwart von Lewis-aciden Komponenten wie Me_3SiCl zu einer Deprotonierung des Lösungsmittels führt.

Das hohe Molekulargewicht und die hohen Kosten der Phosphazene **4a** und **4b** machen die Trifluormethylierung in größeren Mengen unrentabel. Aus diesem Grund schlugen Zhang und Shibata die Verwendung von Additiven wie Bis(trimethylsilyl)amin zur Verwendung von **4a** in katalytischen Mengen von etwa 20 Mol-% vor.[39] Die Verwendung von Additiven führt trotzdem zu einem Verlust großer Mengen der Schwesinger-Base bei der Umsetzung im multimolaren Maßstab. In unserem Fall wurde das in der Trifluormethylierungsreaktion ausgefällte Phosphazeniumhydrochlorid **[4bH]Cl** (Schema 23) nach jedem Reaktionsschritt unter Verwendung eines Anionenaustauscherharzes in hervorragenden Ausbeuten von etwa 98 bis 100% regeneriert. Kleine Mengen von **4b** wurden nach jedem Schritt für ^{31}P-NMR-spektroskopische Untersuchungen verwendet.

So wurde die Rückgewinnung belegt und die Möglichkeit aufgezeigt, Phosphazen **4b** in weiteren Trifluormethylierungsreaktionen ohne jeglichen Reaktivitätsverlust einzusetzen.

In der Bruttoreaktion zur Synthese des Ruppert-Prakash-Reagenzes, wie in Schema 23 gezeigt, wird die Trifluormethylierungsreaktion unter Verwendung von Natriumhydroxid als Base durchgeführt.

Die Pentafluorethylierung von Me_3SiCl mit Pentafluorethan und **4b** führt ebenfalls zur Bildung von Trimethylpentafluorethylsilan in Ausbeuten von etwa 61 %. Auch bei dieser Reaktion wird keine Zersetzung von **4b** beobachtet. Dies befürwortet die Verwendung von Phosphazen **4b** für weitere Fluor- und Perfluoralkylierungsreaktionen.

4. Zusammenfassung

Zusammenfassend wurde über das erste strukturell charakterisierte metastabile Hydroxid-Trihydrat $[OH(OH_2)_3]^-$ berichtet, das unter Verwendung der neu dargestellten Tetraphosphazenbase **4b** generiert wurde. Das Hydroxid verliert im Vakuum die Solvathülle, was zur selektiven Deprotonierung des Phosphazenium-Kations **[4bH]$^+$** führt. So gelang die selektive Bildung von **4b** aus seinem Hydrochlorid mit Hilfe eines basischen Anionenaustauscherharzes in exzellenten Ausbeuten von über 97 %. Diese Strategie umgeht die Verwendung gefährlicher Metallamide in flüssigem Ammoniak und ermöglicht eine Herstellung von **4b** im größeren Maßstab (> 25 g).

Die Synthese des Ruppert-Prakash-Reagenzes Me_3SiCF_3 wurde in Ausbeuten von etwa 75 % unter Verwendung von Fluoroform (HCF_3), Me_3SiCl und der Schwesinger-Base **4b** vorgestellt. Die freie Base **4b** wurde mit einem Anionenaustauscherharz aus gefälltem Phosphazeniumchlorid **[4bH]Cl** in exzellenten Ausbeuten von über 98 % regeneriert und ohne Reaktivitätsverlust für weitere Trifluormethylierungsreaktionen verwendet. Da das Austauscherharz mit wässriger Natronlauge regeneriert werden kann, wird in der Gesamtreaktion die Trifluormethylierung mit Natronlauge als Base durchgeführt.

Außerdem wurden die ersten Silanol-Silanolat-Anionen in kondensierter Phase durch die Reaktion von **[4bH][OH(OH$_2$)$_n$]** mit Siloxanen synthetisiert. Aufgrund des schwach koordinierenden Phosphazenium-Kations **[4bH]$^+$** bilden die Anionen der Salze **[4bH][D$_3$OH]** und **[4bH][D$^{Ph2}_3$OH]** starke intramolekulare Wasserstoffbrückenbindungen aus. Das solvatisierte Anion in **[4bH][Me$_3$SiO(HOSiMe$_3$)$_2$]** zersetzt sich im Vakuum, ähnlich wie das Hydroxid-Hydrat-Salz **[4bH][OH(OH$_2$)$_3$]**. Die entsprechenden Monophosphazenium-, Tetra-*n*-butylammonium- und -phosphonium-Salze **[1cH][D$_3$OH]**, **[NBu$_4$][D$_3$OH]** und **[PBu$_4$][D$_3$OH]** wurden analog unter Verwendung ihrer Hydroxide hergestellt. Alle cyclischen $[D_3OH]^-$-Anionen zeigen intramolekulare Wasserstoffbrückenbindungen, wobei die O-O-Abstände von der Größe und dem Koordinationsvermögen des eingesetzten Kations abhängen. Während eine Vergrößerung der nicht-koordinierenden Kationen von $[NBu_4]^+$ zu **[4bH]$^+$** mit einer Verkürzung der intramolekularen Wasserstoffbrückenbindung von 245.1(1) pm zu 242.8(2) pm einhergeht, begünstigen wasserstoffbrückendonierende Kationen wie **[1cH]$^+$** eine Bindungsaufweitung (250.8(2) pm). Eine Verringerung der Kationengröße zu $[NMe_4]^+$

in **[NMe$_4$][D$_3$OH]$_{1/\infty}$** begünstigt die Anordnung der [D$_3$OH]$^-$-Einheiten in einem polyanionischen Strang. Im Gegensatz zu cyclischen [D$_3$OH]$^-$-Anionen überwiegt in Gegenwart weniger sperriger Gegenionen eine intermolekulare Wasserstoffbrückenbindung (247.0(1) pm).

Der erhöhte nukleophile Charakter des Silanolat-Anions in Salz **[4bH][D$_3$OH]** wurde genutzt, um eine schnelle lösungsmittelfreie Depolymerisation von Polydimethylsiloxanen zu cyclischen Siloxanen durchzuführen. Unter identischen Reaktionsbedingungen wurde eine signifikant erhöhte katalytische Aktivität von Silanolat **[4bH][D$_3$OH]** im Vergleich zu Natrium- und Kaliumhydroxid beobachtet.

Die Synthesen einer Reihe nicht-koordinierter Phenolat-Anionen sowie wasserstoffgebundener Phenol-Phenolate und Phenolat-Hydrate wurden durch Deprotonierung der entsprechenden Alkohole mit der Tetraphosphazenbase **4b** in hervorragenden Ausbeuten beschrieben. Wasserstoffgebundene Addukte sind durch die Deprotonierung von Phenol in Gegenwart von einem Äquivalent Phenol oder Wasser zugänglich. Die C-O$^-$-Bindungen nicht-koordinierter Phenolate sind im Vergleich zu ihren wasserstoffgebundenen Addukten oder koordinierten Phenolaten, wie in NaOPh, verkürzt.

Der Einfluss der Wasserstoffbrückenbindungen wurde außerdem durch signifikante Änderungen der Oxidationspotentiale der nicht-koordinierten Phenolate **[4bH][PhO]** und **[4bH][C$_{10}$H$_7$O]** im Vergleich zu ihren Addukten in **[4bH][PhO(H$_2$O)]**, **[4bH][(PhO)$_2$H]** und **[4bH][(C$_{10}$H$_7$O)$_2$H]** gezeigt. Darüber hinaus werden ebenfalls die Absorptions- und Fluoreszenzemissionseigenschaften der 2-Naphtholat-Anionen [C$_{10}$H$_7$O]$^-$ und [(C$_{10}$H$_7$O)$_2$H]$^-$ stark durch diese Wechselwirkung beeinflusst. Das Addukt **[4bH][(MeO*t*Bu2PhO)$_2$H]** weist eine leicht verlängerte Wasserstoffbrücke im Vergleich zu [(PhO)$_2$H]$^-$ auf. Folglich wird das Redoxpotential des freien Phenolats [MeO*t*Bu2PhO]$^-$ nur geringfügig durch die Wasserstoffbrückenbindung zum Phenol beeinflusst.

Zusätzlich wurde das Potential nicht-koordinierter Phenolate als Ein-Elektronen-Reduktionsmittel untersucht. Die Möglichkeit zur Darstellung von Radikal-Anionen-Salzen ausgehend von Phosphazeniumphenolaten wurde durch deren Reaktion mit TCNE und der Isolierung des entsprechenden Salzes **[4bH][TCNE]** in hoher Ausbeute (88 %) gezeigt. Weiterhin wurde die Reduktion des chemisch extrem inerten

Zusammenfassung

Schwefelhexafluorids mit Phosphazeniumphenolaten beschrieben, die im Falle der Phenolate [^{MeO}*t*Bu^{2}PhO]$^{-}$ und [^{t}Bu^{3}PhO]$^{-}$ mit sterisch anspruchvollen Gruppen zur Bildung von Pentafluorosulfanid-Anionen führte. Auch andere nicht-koordinierte Phenolate sind in der Lage, SF_6 zu reduzieren. In diesen Fällen bilden sich Fluoride als Produkte.

5. Summary

In conclusion, the first structurally characterized metastable hydroxide trihydrate $[OH(OH_2)_3]^-$ was reported, generated by use of the newly prepared tetraphosphazene base **4b**. The hydroxide loses water in vacuum, which results in the selective deprotonation of the phosphazenium cation **[4bH]$^+$**. This protocol was useful for the selective formation of **4b** from its hydrochloride by means of a basic anion exchange resin in excellent yields of over 97 % and circumvents the use of hazardous metal amides in liquid ammonia which allows the production on a larger scale (> 25 g).

The synthesis of the Ruppert-Prakash reagent Me_3SiCF_3 was disclosed in yields of about 75 % by using fluoroform (HCF_3), Me_3SiCl and Schwesinger base **4b**. The free base **4b** was regenerated by an anion exchange resin from precipitated phosphazenium chloride **[4bH]Cl** in excellent yields of over 98 % and reutilized for the trifluoromethylation reaction without any loss of reactivity. Since the exchange resin can be regenerated with aqueous sodium hydroxide solution, in the overall reaction the trifluoromethylation is carried out using sodium hydroxide as the base.

The first silanol-silanolate anions in the condensed phase are synthesized by the reaction of **[4bH][OH(OH$_2$)$_n$]** with siloxanes. Due to the weakly coordinating phosphazenium cation **[4bH]$^+$**, the anions of salts **[4bH][D$_3$OH]** and **[4bH][D$^{Ph2}_3$OH]** feature strong intramolecular hydrogen-bonding. The solvated anion in **[4bH][Me$_3$SiO(HOSiMe$_3$)$_2$]** decomposes in vacuum, similar to the hydroxide hydrate salt **[4bH][OH(OH$_2$)$_3$]**. The corresponding monophosphazenium-, tetra-*n*-butylammonium- and -phosphonium salts **[1cH][D$_3$OH]**, **[NBu$_4$][D$_3$OH]** and **[PBu$_4$][D$_3$OH]** were prepared analogously by use of their hydroxides. All cyclic $[D_3OH]^-$ anions show intramolecular hydrogen bonding, with O-O distances depending on the size and the coordination capability of the applied cation. While an enlargement of non-coordinating cations from $[NBu_4]^+$ to **[4bH]$^+$** results in a shortening of the intramolecular hydrogen bond from 245.1(1) pm to 242.8(2) pm, hydrogen bond donating cations like **[1cH]$^+$** favor an extension of the formed bond (250.8(2) pm). Downsizing the cation to $[NMe_4]^+$ in **[NMe$_4$][D$_3$OH]$_{1/\infty}$** benefits the organization of the $[D_3OH]^-$ moieties in a polyanionic strand. In contrast to cyclic $[D_3OH]^-$ anions, an intermolecular hydrogen bond (247.0(1) pm) is predominant in the presence of less bulky counterions.

Summary

The increased nucleophilic character of the silanolate anion in salt **[4bH][D$_3$OH]** was applied to perform the fast solvent-free depolymerization of polydimethylsiloxanes into cyclic siloxanes. Under identical reaction conditions a significantly enhanced catalytic activity of silanolate **[4bH][D$_3$OH]** in comparison to sodium and potassium hydroxide was observed.

High-yield syntheses of a series of non-coordinated phenolates anions as well as hydrogen bonded phenol-phenolates and phenolate-hydrates were presented by deprotonation of the corresponding alcohols with tetraphosphazene base **4b**. Hydrogen-bonded adducts are accessible by the deprotonation of phenol in the presence of one equivalent of phenol or water, respectively. The C-O$^-$ bonds of non-coordinated phenolates are shortened compared to their hydrogen-bonded adducts or coordinated phenolates like in NaOPh.

The influence of hydrogen bonding was further demonstrated by significant changes of the oxidation potentials of non-coordinated phenolates **[4bH][PhO]** and **[4bH][C$_{10}$H$_7$O]** relative to their adducts in **[4bH][PhO(H$_2$O)]**, **[4bH][(PhO)$_2$H]** and **[4bH][(C$_{10}$H$_7$O)$_2$H]**. Moreover, the light absorption and fluorescence emission properties of 2-naphtholate anions [C$_{10}$H$_7$O]$^-$ and [(C$_{10}$H$_7$O)$_2$H]$^-$ are strongly affected by hydrogen bond interactions. The adduct **[4bH][(**$^{\mathbf{MeO}t\mathbf{Bu2}}$**PhO)$_2$H]** features a slightly elongated hydrogen bond relative to [(PhO)$_2$H]$^-$. Consequently, the redox potential of the free phenolate [$^{MeO}t^{Bu2}$PhO]$^-$ is only minor influenced by hydrogen bonding to phenol.

Additionally, the potential of non-coordinated phenolates as one-electron reducing agents was disclosed. The possibility of the preparation of radical anion salts from phosphazenium phenolates was demonstrated by the reaction with TCNE and isolation of the corresponding salt **[4bH][TCNE]** in high yield (88 %). The reduction of the chemically extremely inert sulfur hexafluoride with phosphazenium phenolates was described, which in case of the sterically encumbered phenolates [^{MeOtBu2}PhO]$^-$ and [^{tBu3}PhO]$^-$ resulted in the formation of the pentafluorosulfanide anion. Other non-coordinated phenolates are also capable in SF_6 reduction, and lead to the formation of fluorides.

6. Literaturverzeichnis

[1] a) I. Krossing, I. Raabe, *Angew. Chem. Int. Ed.* **2004**, *43*, 2066; b) I. Krossing, I. Raabe, *Angew. Chem.* **2004**, *116*, 2116.

[2] K. Seppelt, *Angew. Chem. Int. Ed. Engl.* **1992**, *31*, 292.

[3] K. Seppelt, *Angew. Chem.* **1992**, *104*, 299.

[4] a) D. F. C. Morris, E. L. Short, *Nature* **1969**, *224*, 950; b) M. Born, *Verh. Dtsch. Phys. Ges.* **1919**, *21*, 679; c) F. Haber, *Verh. Dtsch. Phys. Ges.* **1919**, *21*, 750; d) K. Fajans, *Verh. Dtsch. Phys. Ges.* **1919**, *21*, 714; e) P. W. Atkins, T. Overton, J. Rourke, M. Weller, F. Armstrong, *Shriver & Atkins' Inorganic Chemistry*, Oxford University Press, **2010**.

[5] a) I. M. Riddlestone, A. Kraft, J. Schaefer, I. Krossing, *Angew. Chem. Int. Ed.* **2018**, *57*, 13982; b) I. M. Riddlestone, A. Kraft, J. Schaefer, I. Krossing, *Angew. Chem.* **2018**, *130*, 14178.

[6] G. Zundel, H. Metzger, *Z. Phys. Chem.* **1968**, *58*, 225.

[7] a) M. Eigen, *Angew. Chem.* **1963**, *75*, 489-508; b) M. Eigen, *Angew. Chem. Int. Ed.* **1964**, *3*, 1.

[8] a) N. Schwarze, S. Steinhauer, B. Neumann, H.-G. Stammler, B. Hoge, *Angew. Chem. Int. Ed.* **2016**, *55*, 15528; b) N. Schwarze, S. Steinhauer, B. Neumann, H.-G. Stammler, B. Hoge, *Angew. Chem.* **2016**, 15756; c) M. Niemann, B. Neumann, H.-G. Stammler, B. Hoge, *Angew. Chem. Int. Ed. Engl.* **2019**, *58*, 8938; d) M. Niemann, B. Neumann, H.-G. Stammler, B. Hoge, *Angew. Chem.* **2019**, *131*, 9033; e) Z. Xie, R. Bau, C. A. Reed, *Inorg. Chem.* **1995**, *34*, 5403; f) D. Steinborn, O. Gravenhorst, H. Hartung, U. Baumeister, *Inorg. Chem.* **1997**, 2195; g) B. Krebs, S. Bonmann, K. Erpenstein, *Z. Naturforsch., B: Chem. Sci.* **1991**, 919; h) E. S. Stoyanov, S. P. Hoffmann, K.-C. Kim, F. S. Tham, C. A. Reed, *J. Am. Chem. Soc.* **2005**, *127*, 7664.

[9] a) C. Bolli, J. Gellhaar, C. Jenne, M. Keßler, H. Scherer, H. Seeger, R. Uzun, *Dalton Trans.* **2014**, *43*, 4326; b) D. Albanese, D. Landini, M. Penso, *J. Org. Chem.* **1998**, *63*, 9587; c) B. Mathiessen, A. T. I. Jensen, F. Zhuravlev, *Chem. Eur. J.* **2011**, *17*, 7796.

[10] K. O. Christe, W. W. Wilson, R. D. Wilson, R. Bau, J. an Feng, *J. Am. Chem. Soc.* **1990**, *112*, 7619.

[11] H. Sun, S. G. DiMagno, *J. Am. Chem. Soc.* **2005**, *127*, 2050.

[12] Z. Chen, Y. Tonouchi, K. Matsumoto, M. Saimura, R. Atkin, T. Nagata, M. Katahira, R. Hagiwara, *J. Phys. Chem. Lett.* **2018**, *9*, 6662.

[13] S. Grabowski, *Crystals* **2016**, *6*, 3.

[14] B. Dereka, Q. Yu, N. H. C. Lewis, W. B. Carpenter, J. M. Bowman, A. Tokmakoff, *Science* **2021**, *371*, 160.

[15] J. Emsley, *Chem. Soc. Rev.* **1980**, *9*, 91.

[16] D. Landini, A. Maia, A. Rampoldi, *J. Org. Chem.* **1989**, *54*, 328.

[17] A. R. Mahjoub, X. Zhang, K. Seppelt, *Chem. Eur. J.* **1995**, *1*, 261.

[18] R. Schwesinger, R. Link, P. Wenzl, S. Kossek, *Chem. Eur. J.* **2006**, *12*, 438.

[19] R. Z. Gnann, R. I. Wagner, K. O. Christe, R. Bau, G. A. Olah, W. W. Wilson, *J. Am. Chem. Soc.* **1997**, *119*, 112.

[20] A. Kornath, F. Neumann, H. Oberhammer, *Inorg. Chem.* **2003**, *42*, 2894.

[21] a) R. Schwesinger, R. Link, G. Thiele, H. Rotter, D. Honert, H.-H. Limbach, F. Männle, *Angew. Chem. Int. Ed. Engl.* **1991**, *30*, 1372; b) R. Schwesinger, R. Link, G. Thiele, H. Rotter, D. Honert, H.-H. Limbach, F. Männle, *Angew. Chem.* **1991**, *103*, 1376.

[22] D. Landini, A. Maia, *J. Chem. Soc., Chem. Commun.* **1984**, 1041.

[23] D. Landini, A. Maia, A. Rampoldi, *J. Org. Chem.* **1986**, *51*, 5476.

[24] P. Spanel, D. Smith, *J. Phys. Chem.* **1995**, 15551.

[25] F. Hartmann, D. Mootz, R. Schwesinger, *Z. Naturforsch., B: Chem. Sci.* **1996**, *51*, 1369.

[26] K. Abu-Dari, K. N. Raymond, D. P. Freyberg, *J. Am. Chem. Soc.* **1979**, 3688.

[27] a) R. Schwesinger, *Chimia* **1985**, *39*, 269; b) R. Schwesinger, *Nachr. Chem. Tech. Lab.* **1990**, *38*, 1214; c) R. Schwesinger, R. Link, P. Wenzl, S. Kossek, M. Keller, *Chem. Eur. J.* **2005**, *12*, 429.

[28] R. Schwesinger, H. Schlemper, *Angew. Chem.* **1987**, *99*, 1212.

[29] R. Schwesinger, H. Schlemper, *Angew. Chem. Int. Ed. Engl.* **1987**, *26*, 1167-1169.

[30] R. Schwesinger, C. Hasenfratz, H. Schlemper, L. Walz, E.-M. Peters, K. Peters, H.-G. von Schnering, *Angew. Chem. Int. Ed. Engl.* **1993**, *32*, 1361.

[31] R. Schwesinger, C. Hasenfratz, H. Schlemper, L. Walz, E.-M. Peters, K. Peters, H. G. von Schnering, *Angew. Chem.* **1993**, *105*, 1420.

[32] R. Schwesinger, H. Schlemper, C. Hasenfratz, J. Willaredt, T. Dambacher, T. Breuer, C. Ottaway, M. Fletschinger, J. Boele, H. Fritz, D. Putzas, H. W. Rotter, F. G. Bordwell, A. V. Satish, G.-Z. Ji, E.-M. Peters, K. Peters, H. G. von Schnering, L. Walz, *Liebigs Ann.* **1996**, *1996*, 1055.

[33] R. Schwesinger, J. Willaredt, H. Schlemper, M. Keller, D. Schmitt, H. Fritz, *Chem. Ber.* **1994**, *127*, 2435.

[34] R. F. Weitkamp, B. Neumann, H.-G. Stammler, B. Hoge, *Chem. Eur. J.* **2021**, *[prepared manuscript]*.

[35] a) J. G. Verkade in *Topics in current chemistry*, *Vol. 223* (Eds.: A. de Meijere, H. Kessler, S. V. Ley, J. Thiem, F. Vögtle, K. N. Houk, J.-M. Lehn, S. L. Schreiber, B. M. Trost, H. Yamamoto et al.), Springer Berlin Heidelberg, Berlin, Heidelberg, **2003**, pp. 1–44; b) T. Pietzonka, D. Seebach, *Chem. Ber.* **1991**, *124*, 1837; c) M.-A. Courtemanche, M.-A. Légaré, É. Rochette, F.-G. Fontaine, *Chem. Commun.* **2015**, *51*, 6858.

[36] C. Palomo, M. Oiarbide, R. López, E. Gómez-Bengoa, *Chem. Commun.* **1998**, 2091.

[37] T. Ishikawa, *Superbases for Organic Synthesis*. *Guanidines, amidines and phosphazenes and related organocatalysts*, John Wiley & Sons, Ltd, Chichester, UK, **2009**.

[38] a) J. Braun, C. Hasenfratz, R. Schwesinger, H.-H. Limbach, *Angew. Chem.* **1994**, *106*, 2302; b) J. Braun, C. Hasenfratz, R. Schwesinger, H.-H. Limbach, *Angew. Chem. Int. Ed. Engl.* **1994**, *33*, 2215.

[39] S. Okusu, K. Hirano, E. Tokunaga, N. Shibata, *Chemistry Open* **2015**, *4*, 581.

[40] H. Kawai, Z. Yuan, E. Tokunaga, N. Shibata, *Org. Biomol. Chem.* **2013**, *11*, 1446.

[41] R. F. Weitkamp, B. Neumann, H.-G. Stammler, B. Hoge, *Angew. Chem.* **2019**, *131*, 14775.

[42] R. F. Weitkamp, B. Neumann, H.-G. Stammler, B. Hoge, *Angew. Chem.* **2020**, *132*, 5536.

[43] R. F. Weitkamp, B. Neumann, H.-G. Stammler, B. Hoge, *Angew. Chem. Int. Ed. Engl.* **2019**, *58*, 14633.

[44] R. F. Weitkamp, B. Neumann, H.-G. Stammler, B. Hoge, *Angew. Chem. Int. Ed. Engl.* **2020**, *59*, 5494.

[45] R. F. Weitkamp, B. Neumann, H.-G. Stammler, B. Hoge, *Chem. Eur. J.* **2020**, DOI: 10.1002/chem.202003504.

[46] R. F. Weitkamp, B. Neumann, H.-G. Stammler, B. Hoge, *Chem. Eur. J.* **2021**, *27*, 915.

[47] R. F. Weitkamp, B. Neumann, H.-G. Stammler, B. Hoge, *Chem. Eur. J.* **2021**, DOI: 10.1002/chem.202005123.

[48] a) A. V. Kirsanov, *Zh. Obshch. Khim.* **1952**, *88*; b) C. Glidewell, *Angew. Chem. Int. Ed. Engl.* **1975**, *14*, 826; c) C. Glidewell, *Angew. Chem.* **1975**, *87*, 875.

[49] F. H. Allen, O. Kennard, D. G. Watson, L. Brammer, A. G. Orpen, R. Taylor, *J. Chem. Soc. Perkin Trans. II* **1987**, *194*.

[50] Robin Weitkamp, *Masterarbeit*, Universität Bielefeld, Bielefeld, **2018**.

[51] P. C. Hupfield, R. G. Taylor, *J. Inorg. Organomet. Polym.* **1999**, *9*, 17.

[52] M. Morita, K. Takahashi, *Phys. Chem. Chem. Phys.* **2013**, *15*, 114.

[53] P. Jutzi, U. Schubert, *Silicon chemistry*. *From the atom to extended systems*, Wiley-VCH, Weinheim, Cambridge, **2003**.

[54] W. Clegg, G. M. Sheldrick, U. Klingebiel, D. Bentmann, *Acta Cryst* **1984**, *C40*, 819.

[55] R. West, R. H. Baney, *J. Am. Chem. Soc.* **1959**, *81*, 6145.

[56] H. Schmidbaur, *Chem. Ber.* **1964**, *97*, 830.

[57] a) H. Behbehani, B. J. Brisdon, M. F. Mahon, K. C. Molloy, M. Mazhar, *J. Organomet. Chem.* **1993**, *463*, 41; b) S. T. Malinovskii, A. Tesuro Vallina, H. Stoeckli-Evans, *J. Struct. Chem.* **2006**, *47*, 1127.

[58] O. Graalmann, U. Klingebiel, W. Clegg, M. Haase, G. M. Sheldrick, *Chem. Ber.* **1984**, *117*, 2988.

[59] B. Laermann, M. Lazell, M. Motevalli, A. C. Sullivan, *J. Chem. Soc., Dalton Trans.* **1997**, *1997*, 1263.

[60] R. G. Jones, W. Ando, J. Chojnowski (Eds.) *Silicon-Containing Polymers*. *The Science and Technology of Their Synthesis and Applications*, Springer Netherlands, Dordrecht, **2000**.

[61] J. O. Bauer, C. Strohmann, *J. Organomet. Chem.* **2015**, *797*, 52.

[62] H. Steinfink, B. Post, I. Fankuchen, *Acta Cryst.* **1955**, *8*, 420.

[63] A. Oku, W. Huang, Y. Ikeda, *Polymer* **2002**, *43*, 7289.

[64] a) T. W. Greenlee, US005110972A, **1991**; b) Y. Ikeda, W. Huang, A. Oku, *Green Chem.* **2003**, *5*, 508.

[65] K. C. Gross, P. G. Seybold, *Int. J. Quantum Chem.* **2001**, *85*, 569.

[66] a) Z. Pawlak, J. Magonski, *J. Chem. Soc., Faraday Trans.* **1985**, *1*, 2021; b) R. J. Mayer, M. Breugst, N. Hampel, A. R. Ofial, H. Mayr, *J. Org. Chem.* **2019**, *84*, 8837.

[67] A. M. Buytendyk, J. D. Graham, K. D. Collins, K. H. Bowen, C.-H. Wu, J. I. Wu, *Phys. Chem. Chem. Phys.* **2015**, *17*, 25109.

[68] T. M. Krygowski, H. Szatyłowicz, *J. Phys. Chem. A* **2006**, *110*, 7232.

[69] N. Kornblum, P. J. Berrigan, W. J. Le Noble, *J. Am. Chem. Soc.* **1963**, *85*, 1141.

[70] A. Kütt, V. Movchun, T. Rodima, T. Dansauer, E. B. Rusanov, I. Leito, I. Kaljurand, J. Koppel, V. Pihl, I. Koppel, G. Ovsjannikov, L. Toom, M. Mishima, M. Medebielle, E. Lork, G.-V. Röschenthaler, I. A. Koppel, A. A. Kolomeitsev, *J. Org. Chem.* **2008**, *73*, 2607.

[71] H. Kolbe, *J. Prakt. Chem.* **1874**, *10*, 89.

[72] Z. Marković, S. Marković, N. Manojlović, J. Predojević-Simović, *J. Chem. Inf. Model* **2007**, *47*, 1520.

[73] a) A. Zouni, H. T. Witt, J. Kern, P. Fromme, N. Krauss, W. Saenger, P. Orth, *Nature* **2001**, *409*, 739; b) Y. Umena, K. Kawakami, J.-R. Shen, N. Kamiya, *Nature* **2011**, *473*, 55.

[74] J. D. Megiatto, D. D. Méndez-Hernández, M. E. Tejeda-Ferrari, A.-L. Teillout, M. J. Llansola-Portolés, G. Kodis, O. G. Poluektov, T. Rajh, V. Mujica, T. L. Groy, D. Gust, T. A. Moore, A. L. Moore, *Nat. Chem.* **2014**, *6*, 423.

[75] A. Sirjoosingh, S. Hammes-Schiffer, *J. Phys. Chem. A* **2011**, *115*, 2367.

[76] a) C. Costentin, M. Robert, J.-M. Savéant, *Phys. Chem. Chem. Phys.* **2010**, *12*, 11179; b) L. Benisvy, R. Bittl, E. Bothe, C. D. Garner, J. McMaster, S. Ross, C. Teutloff, F. Neese, *Angew. Chem. Int. Ed.* **2005**, *44*, 5314; c) L. Benisvy, R. Bittl, E. Bothe, C. D. Garner, J. McMaster, S. Ross, C. Teutloff, F. Neese, *Angew. Chem.* **2005**, *117*, 5448; d) Y. Fang, L. Liu, Y. Feng, X.-S. Li, Q.-X. Guo, *J. Phys. Chem. A* **2002**, *106*, 4669; e) D. L. Jenson, B. A. Barry, *J. Am. Chem. Soc.* **2009**, *131*, 10567; f) I. J. Rhile, T. F. Markle, H. Nagao, A. G. DiPasquale, O. P. Lam, M. A. Lockwood, K. Rotter, J. M. Mayer, *J. Am. Chem. Soc.* **2006**, *128*, 6075; g) I. J. Rhile, J. M. Mayer, *J. Am. Chem. Soc.* **2004**, *126*, 12718; h) M. Sjödin, T. Irebo, J. E. Utas, J. Lind, G. Merényi, B. Akermark, L. Hammarström, *J. Am. Chem. Soc.* **2006**, *128*, 13076.

[77] a) T. Steiner, I. Majerz, C. C. Wilson, *Angew. Chem. Int. Ed.* **2001**, *40*, 2651; b) T. Steiner, I. Majerz, C. C. Wilson, *Angew. Chem.* **2001**, *113*, 2728; c) A. Chandra, T. Uchimaru, *Int. J. Mol. Sci.* **2002**, *3*, 407; d) M. Kołaski, A. Kumar, N. J. Singh, K. S. Kim, *Phys. Chem. Chem. Phys.* **2011**, *13*, 991; e) D. Kanamori, A. Furukawa, T.-a. Okamura, H. Yamamoto, N. Ueyama, *Org. Biomol. Chem.* **2005**, *3*, 1453.

[78] R. Goddard, H. M. Herzog, M. T. Reetz, *Tetrahedron* **2002**, *58*, 7847.

[79] A. Albert, E. P. Serjeant, *Ionization Constants of Acids and Bases*, Methuen, London, **1962**.

[80] R. E. Dinnebier, M. Pink, J. Sieler, P. W. Stephens, *Inorg. Chem.* **1997**, *36*, 3398.

[81] M. E. Fraser, S. Fortier, A. Rodrigue, J. W. Bovenkamp, *Can. J. Chem.* **1986**, *64*, 816.

[82] M. E. Fraser, S. Fortier, M. K. Markiewicz, A. Rodrigue, J. W. Bovenkamp, *Can. J. Chem.* **1987**, *65*, 2558.

[83] a) J. A. Cowan, J. A. C. Clyburne, M. G. Davidson, R. L. W. Harris, J. A. K. Howard, P. Küpper, M. A. Leech, S. P. Richards, *Angew. Chem. Int. Ed.* **2002**, *41*, 1432-1434; b) J. A. Cowan, J. A. C. Clyburne, M. G. Davidson, R. L. W. Harris, J. A. K. Howard, P. Küpper, M. A. Leech, S. P. Richards, *Angew. Chem.* **2002**, *114*, 1490; c) J. P. Canal, T. Ramnial, D. A. Dickie, J. A. C. Clyburne, *Chem. Commun.* **2006**, 1809; d) J. K. W. Chui, T. Ramnial, J. A. C. Clyburne, *Comments Inorg. Chem.* **2003**, *24*, 165; e) N. Kuhn, C. Maichle-Mößmer, M. Steimann, *Z. Naturforsch., B: Chem. Sci.* **2009**, *64*, 835.

[84] a) R. Taylor, O. Kennard, *J. Am. Chem. Soc.* **1982**, *104*, 5063; b) G. R. Desiraju, *Acc. Chem. Res.* **1991**, *24*, 290; c) T. Steiner, *Cryst. Rev.* **2006**, *6*, 1; d) M. G. Davidson, A. E. Goeta, J. A. K. Howard, S. Lamb, S. A. Mason, *New J. Chem.* **2000**, *24*, 477.

[85] M. Kunert, E. Dinjus, M. Nauck, J. Sieler, *Chem. Ber.* **1997**, *130*, 1461.

[86] a) J. A. Richards, P. E. Whitson, D. H. Evans, *J. Electroanal. Chem. Interfacial Electrochem.* **1975**, *63*, 311; b) L. Kiss, D. Bősz, F. Kovács, H. Li, G. Nagy, S. Kunsági-Máté, *Polym. Bull.* **2019**, *76*, 5849; c) N. L. Zabik, C. N. Virca, T. M. McCormick, S. Martic-Milne, *J. Phys. Chem. B* **2016**, *120*, 8914; d) A. S. Pavitt, E. J. Bylaska, P. G. Tratnyek, *Environ. Sci. Processes Impacts* **2017**, *19*, 339.

[87] L. L. Williams, R. D. Webster, *J. Am. Chem. Soc.* **2004**, *126*, 12441.

[88] P. Hapiot, J. Pinson, N. Yousfi, *New J. Chem.* **1992**, *16*, 877.

[89] W. M. Haynes, *CRC Handbook of Chemistry and Physics*, CRC Press, London, **2016**.

[90] D. N. Dhar, *Chem. Rev.* **1967**, *67*, 611.

[91] a) J. J. Novoa, P. Lafuente, R. E. Del Sesto, J. S. Miller, *Angew. Chem. Int. Ed.* **2001**, *40*, 2540; b) J. J. Novoa, P. Lafuente, R. E. Del Sesto, J. S. Miller, *Angew. Chem.* **2001**, *113*, 2608; c) R. E. Del Sesto, J. S. Miller, P. Lafuente, J. J. Novoa, *Chem. Eur. J.* **2002**, *8*, 4894; d) J. S. Miller, J. J. Novoa, *Acc. Chem. Res.* **2007**, *40*, 189; e) J. Casado, P. M. Burrezo, F. J. Ramírez, J. T. L. Navarrete, S. H. Lapidus, P. W. Stephens, H.-L. Vo, J. S. Miller, F. Mota, J. J. Novoa, *Angew. Chem.* **2013**, *125*, 6549; f) J. Casado, P. Mayorga Burrezo, F. J. Ramírez, J. T. López Navarrete, S. H. Lapidus, P. W. Stephens, H.-L. Vo, J. S. Miller, F. Mota, J. J. Novoa, *Angew. Chem. Int. Ed. Engl.* **2013**, *52*, 6421; g) A. G. Graham, F. Mota, E. Shurdha, A. L. Rheingold, J. J. Novoa, J. S. Miller, *Chem. Eur. J.* **2015**, *21*, 13240; h) A. G. Graham, M. V. Fedin, J. S. Miller, *Chem. Eur. J.* **2017**, *23*, 12620; i) M. Capdevila-Cortada, J. Ribas-Arino, A. Chaumont, G. Wipff, J. J. Novoa, *Chem. Eur. J.* **2016**, *22*, 17037.

[92] a) J. S. Miller, J. C. Calabrese, H. Rommelmann, S. R. Chittipeddi, J. H. Zhang, W. M. Reiff, A. J. Epstein, *J. Am. Chem. Soc.* **1987**, *109*, 769; b) J.-M. Lü, S. V. Rosokha, J. K. Kochi, *J. Am. Chem. Soc.* **2003**, *125*, 12161; c) J. S. Miller, *Angew. Chem. Int. Ed.* **2006**, *45*, 2508; d) J. S. Miller, *Angew. Chem.* **2006**, *118*, 2570; e) B. Milián, R. Pou-Amérigo, M. Merchán, E. Ortí, *ChemPhysChem* **2005**, *6*, 503; f) S. Flandrois, K. Ludolf, H. J. Keller, D. Nöthe, S. R. Bondeson, Z. G. Soos, D. Wehe, *Mol. Cryst. Liq. Cryst.* **2011**, *95*, 149; g) Z.-H. Cui, H. Lischka, T. Mueller, F. Plasser, M. Kertesz, *ChemPhysChem* **2014**, *15*, 165.

[93] a) P. Forster, V. Ramaswamy, P. Artaxo, T. Berntsen, R. Betts, D. W. Fahey, J. Haywood, J. Lean, D. C. Lowe, G. Myhre, J. Nganga, R. Prinn, G. Raga, M. Schulz, R. Van Dorland, *Changes in Atmospheric Constituents and in Radiative Forcing, in: Climate Change 2007: The Physical Science Basis. Contribution of Working Group I to the Fourth Assessment Report of the IPCC, Cambridge University Press, 2007*; b) K. Seppelt, *Chem. Rev.* **2015**, *115*, 1296; c) L. Zámostná, T. Braun, *Nachr. Chem.* **2016**, *64*, 829.

[94] G. Iakobson, M. Pošta, P. Beier, *J. Fluorine Chem.* **2018**, *213*, 51.

[95] M. Rueping, P. Nikolaienko, Y. Lebedev, A. Adams, *Green Chem.* **2017**, *19*, 2571.

[96] a) F. Buß, C. Mück-Lichtenfeld, P. Mehlmann, F. Dielmann, *Angew. Chem.* **2018**, *130*, 5045; b) F. Buß, C. Mück-Lichtenfeld, P. Mehlmann, F. Dielmann, *Angew. Chem. Int. Ed. Engl.* **2018**, *57*,

4951; c) K. Matsumoto, Y. Haruki, S. Sawada, S. Yamada, T. Konno, R. Hagiwara, *Inorg. Chem.* **2018**, *57*, 14882.

[97] a) E. R. Altwicker, *Chem. Rev.* **1967**, *67*, 475; b) E. Müller, K. Ley, W. Kiedaisch, *Chem. Ber.* **1954**, *87*, 1605; c) V. W. Manner, T. F. Markle, J. H. Freudenthal, J. P. Roth, J. M. Mayer, *Chem. Commun.* **2008**, 256.

[98] a) G. K. S. Prakash, P. V. Jog, P. T. D. Batamack, G. A. Olah, *Science* **2012**, *338*, 1324; b) V. V. Grushin, *Chim. Oggi - Chem. Today* **2014**, *32*, 81-88.

[99] a) R. D. Chambers, *Fluorine in Organic Chemistry*, Wiley, New York, **1973**; b) B. Waerder, S. Steinhauer, B. Neumann, H.-G. Stammler, A. Mix, Y. V. Vishnevskiy, B. Hoge, N. W. Mitzel, *Angew. Chem. Int. Ed.* **2014**, *53*, 11640; c) B. Waerder, S. Steinhauer, B. Neumann, H.-G. Stammler, A. Mix, Y. V. Vishnevskiy, B. Hoge, N. W. Mitzel, *Angew. Chem.* **2014**, *126*, 11824.

[100] Y. Zhang, M. Fujiu, H. Serizawa, K. Mikami, *J. Fluorine Chem.* **2013**, *156*, 367.

[101] W. Tyrra, M. M. Kremlev, D. Naumann, H. Scherer, H. Schmidt, B. Hoge, I. Pantenburg, Y. L. Yagupolskii, *Chem. Eur. J.* **2005**, *11*, 6514.

Erklärung

Hiermit versichere ich, dass ich die vorliegende Arbeit selbstständig verfasst und keine anderen als die angegebenen Quellen und Hilfsmittel benutzt habe, dass alle Stellen der Arbeit, die wörtlich oder sinngemäß aus anderen Quellen übernommen wurden, als solche kenntlich gemacht sind und dass die Arbeit in gleicher oder ähnlicher Form noch keiner Prüfungsbehörde vorgelegt wurde.

Die Bestimmungen der Rahmenpromotionsordnung der Universität Bielefeld vom 15. Juni 2010 und die Promotionsordnung der Fakultät für Chemie vom 1. Juli 2011 sind mir bekannt.

Bielefeld, den 15.02.2021

_____

Unterschrift: Robin Weitkamp

Anhang

Manuskripte

1. Generation and Applications of the Hydroxide Trihydrate Anion, $[OH(OH_2)_3]^-$, Stabilized by a Weakly Coordinating Cation
   R. F. Weitkamp, B. Neumann, H.-G. Stammler, B. Hoge, *Angew. Chem.* **2019**, *131*, 14775; *Angew. Chem. Int. Ed.* **2019**, *58*, 14633.

2. Synthesis and Reactivity of the First Isolated Hydrogen-Bridged Silanol-Silanolate Anions
   R. F. Weitkamp, B. Neumann, H.-G. Stammler, B. Hoge, *Angew. Chem.* **2020**, *132*, 5536; *Angew. Chem. Int. Ed. Engl.* **2020**, *59*, 5494.

3. Non-Coordinated Phenolate Anions and Their Application in SF_6 Activation
   R. F. Weitkamp, B. Neumann, H.-G. Stammler, B. Hoge, *Chem. Eur. J.* **2020**, *[accepted]*. DOI: 10.1002/chem.202003504.

4. The Influence of Weakly Coordinating Cations on the O-H···O^- Hydrogen Bond of Silanol-Silanolate Anions
   R. F. Weitkamp, B. Neumann, H.-G. Stammler, B. Hoge, *Chem. Eur. J.* **2021**, *27*, 915.

5. Non-Coordinated and Hydrogen Bonded Phenolate Anions as One-Electron Reducing Agents
   R. F. Weitkamp, B. Neumann, H.-G. Stammler, B. Hoge, *Chem. Eur. J.* **2021**, *[accepted]*. DOI: 10.1002/chem.202005123.

6. Phosphorus Containing Superbases: Recent Progress in the Chemistry of Electron Abundant Phosphines and Phosphazenes
   R. F. Weitkamp, B. Neumann, H.-G. Stammler, B. Hoge, *Chem. Eur. J.* **2021**, *[prepared manuscript]*.

Anhang 1

Generation and Applications of the Hydroxide Trihydrate Anion, $[OH(OH_2)_3]^-$, Stabilized by a Weakly Coordinating Cation

Robin F. Weitkamp, Beate Neumann, Hans-Georg Stammler and Berthold Hoge

Angew. Chem. **2019**, *131*, 14775; *Angew. Chem. Int. Ed.* **2019**, *58*, 14633.

Anhang

A Journal of the German Chemical Society

Angewandte International Edition Chemie

GDCh

www.angewandte.org

2019–58/41

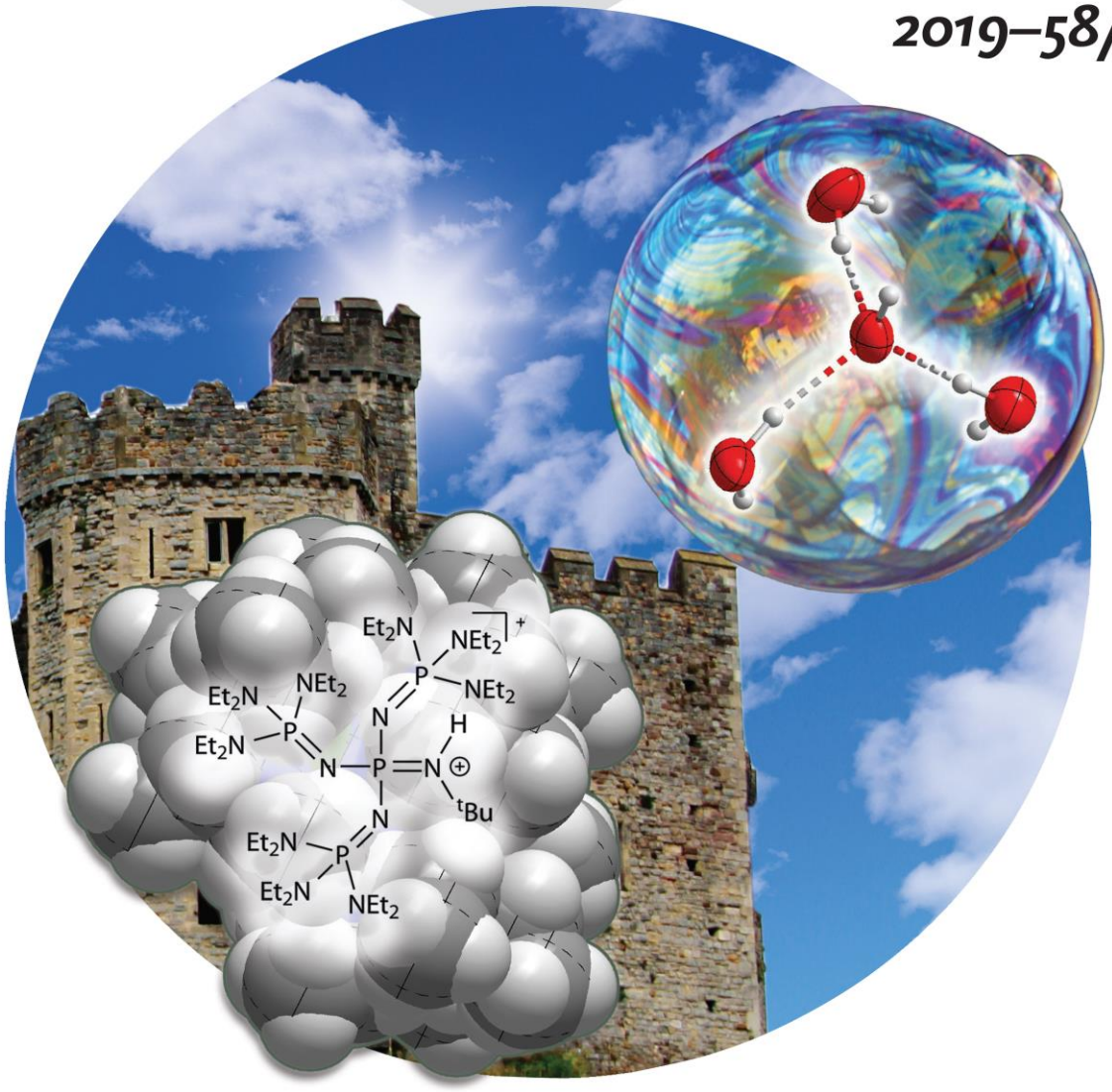

The hydroxide trihydrate anion ...

... was generated for the first time and structurally characterized thanks to the use of a weakly coordinating phosphazenium counterion. As B. Hoge et al. describe in their Communication on page 14633 ff., the space-filling phosphazenium cation represents an impregnable castle wall in protecting and stabilizing this rare anion. Under vacuum, the salt decomposes like a fragile aqueous "hydroxide soap bubble".

WILEY-VCH

GDCh Communications Angewandte International Edition Chemie

VIP Hydroxide Hydrate Very Important Paper

International Edition: DOI: 10.1002/anie.201908589
German Edition: DOI: 10.1002/ange.201908589

Generation and Applications of the Hydroxide Trihydrate Anion, $[OH(OH_2)_3]^-$, Stabilized by a Weakly Coordinating Cation

*Robin F. Weitkamp, Beate Neumann, Hans-Georg Stammler, and Berthold Hoge**

Abstract: *The reaction of a strongly basic phosphazene (Schwesinger base) with water afforded the corresponding metastable hydroxide trihydrate $[OH(OH_2)_3]^-$ salt. This is the first hydroxide solvate that is not in contact with a cation and furthermore one of rare known water-stabilized hydroxide anions. Thermolysis in vacuum results in the decomposition of the hydroxide salt and quantitative liberation of the free phosphazene base. This approach was used to synthesize the Schwesinger base from its hydrochloride salt after anion exchange in excellent yields of over 97 %. This deprotonation method can also be used for the phosphazene-base-catalyzed preparation of the Ruppert–Prakash reagent Me_3SiCF_3 using fluoroform (HCF_3) as the trifluoromethyl building block and sodium hydroxide as the formal deprotonation agent.*

Oxonium and hydroxide ions play major roles in aqueous chemistry, and they serve as key subjects of numerous quantum-chemical calculations. Thus, currently a considerable number of reports focus on oxonium ions of the general formula $[(OH_3)_n(OH_2)_m)]^{n+}$ such as, for example, the "Zundel cation" $[(OH_3)(OH_2)]^+$[1] and the "Eigen cation" $[(OH_3)(OH_2)_3]^+$.[2] Their existence is closely related to the presence of weakly coordinating anions.[3]

Considering the many variations of hydrated oxonium salts in the liquid or solid state, information on isolated hydrates of the hydroxide anion is rare.[4] In contrast to the gas phase where different anions are evidenced by theoretical calculation, for example, the local mode calculations on MP2 level,[5] isolated hydrated hydroxides have not been unambiguously documented.[5,6] In 1978 Raymond et al. reported the geometrical structure of the anion $[OH(OH_2)]^-$.[7] This anion, however, is packed in a network of 18 water molecules and also has significant contacts to the sodium counterions. Clearly, such a species does not fulfil the requirements of an isolated hydrated OH^- anion. Thus, it is obvious that the presence of weakly Lewis acidic cations is a prerequisite for the observation of well-separated hydroxide ions solvated by a shell of water molecules.

Phosphazene superbases, introduced by Schwesinger et al. in 1987,[8–10] exhibit extremely high $^{MeCN}pK_{BH^+}$ values, such as 26.9[11] for monophosphazene **1** up to 42.7[9] for tetraphosphazene **2** (Figure 1). The Schwesinger base **2** has found many applications in, for example, the anti-Markovnikov addition of alcohols to aryl alkenes,[12] Ullmann couplings,[13] as well as ether deprotonation processes.[14]

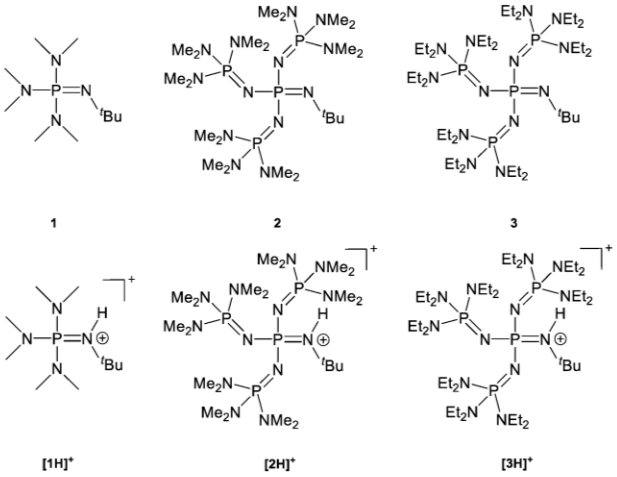

Figure 1. Overview of free and protonated mono- (**1**) and tetraphosphazene (**2**) bases, published by Schwesinger et al.,[10] and the more weakly coordinating phosphazenium cation **[3H]**$^+$ of this work.

For the preparation of naked and highly reactive anions like the fluoride anion,[15] phosphazenium counterions are particularly beneficial due to their low electrophilicity. For our investigation of hydroxide-based water clusters, we envisaged ion separations as large as possible. For this purpose Schwesinger bases like **2** (Figure 1) seem promising. A compound having an increased volume should also have a lower tendency to add nucleophiles. Moreover, deprotonation processes at the iminium functionality of the corresponding acid should be considerably impeded. An obvious route to this objective should be the replacement of the dimethylamino substituents in **2** by bulkier diethylamino groups, as in **3**. The synthesis of this derivative was realized by a slight modification of the published procedure as depicted in Scheme 1.[8–10]

Compound Cl_3PNtBu (**5**) was prepared from phosphorus pentachloride and *tert*-butylamine in a Kirsanov-type reaction.[10,11,16] Compound $(Et_2N)_3PNH$ (**4**) is accessible in

[*] M. Sc. R. F. Weitkamp, B. Neumann, Dr. H.-G. Stammler, Prof. Dr. B. Hoge
Centrum für Molekulare Materialien, Fakultät für Chemie
Universität Bielefeld
Universitätsstraße 25, 33615 Bielefeld (Germany)
E-mail: b.hoge@uni-bielefeld.de

Supporting information and the ORCID identification number(s) for the author(s) of this article can be found under: https://doi.org/10.1002/anie.201908589.

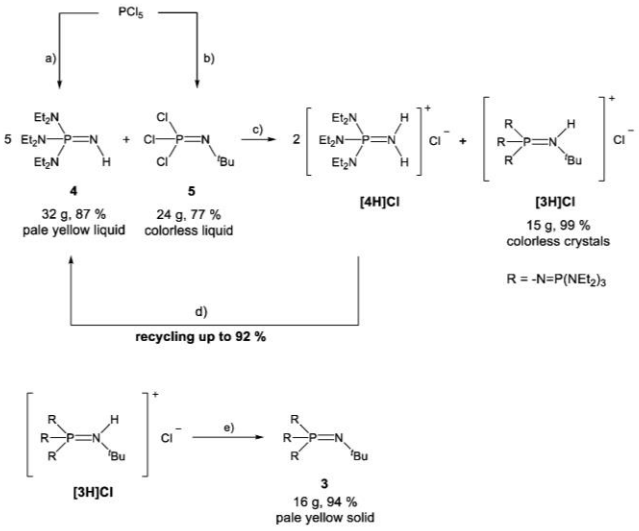

Scheme 1. Synthesis of **3**. a) 1. $HNEt_2$ (6 equiv.), CH_2Cl_2, −30 °C, −3 $[H_2NEt_2]Cl$; 2. NH_3 (2 equiv.), CH_2Cl_2, −20 °C, −$[NH_4]Cl$; 3. KO*t*Bu, MeOH, 0 °C, −KCl, −HO*t*Bu. b) H_2NtBu (3 equiv.), *n*-pentane, −2 $[H_3NtBu]Cl$. c) 160 °C, 3 days. d) KO*t*Bu, MeOH, 0 °C, −KCl, −HO*t*Bu. e) $NaNH_2$, NH_3, −70 °C to rt, −NaCl, $-NH_3$.

analogy to the synthesis of $(Me_2N)_3PNH$ as previously devised by Schwesinger et al.[9] Combination of neat **4** and **5** resulted in a nucleophilic substitution with the formation of phosphazenium chloride $[\{Et_2N)_3P{=}N\}_3P{=}NH(t\text{Bu})]Cl$ (**[3H]Cl**) in high yield. In the ^{31}P NMR spectrum of salt **[3H]Cl** the central phosphorus atom was observed as a quartet of doublets at $\delta = -33.9$ ppm with coupling constants of $^2J_{PP} = 70$ Hz and $^2J_{PH} = 8$ Hz. The phosphorus atoms of the three peripheral phosphazenyl substituents gave rise to a signal at $\delta = 7.4$ ppm, which is split into a doublet of tridecets with a $^2J_{PP}$ coupling constant of 70 Hz and a $^3J_{PH}$ coupling constant of 10 Hz to the 12 methylene protons of the ethyl units.[17]

The crystal structure[18] of **[3H]Cl** was elucidated by X-ray crystallography. Suitable single crystals were grown from a saturated ethereal solution at −28 °C (Figure 2). The hydrogen atom bonded to N1 could be refined isotropically. The nitrogen atom N1 of the iminium group is slightly pyramidalized (sum of angles 350.6°). The bond length P1−N1 of 167.2(2) pm is significantly longer than the bonds P1−N2, P1−N3 and P1−N4, which range from 158.5(2) to 160.6(2) pm.

The byproduct **[4H]Cl** can be isolated by aqueous extraction from the reaction mixture. Deprotonation results in the regeneration of **4** in high yields of about 92 %, which improves the waste-to-product ratio. Deprotonation of **[3H]Cl** to the free base **3** was achieved in 94 % yield by treatment with sodium amide in liquid ammonia (Scheme 1).[17] The molecular structure[18] of **3** was ascertained by X-ray diffractometry utilizing single crystals grown in a saturated solution of the compound in *n*-hexane at −28 °C (Figure 3). Phosphazene **3** crystallizes in the orthorhombic space group *Pbca*. In comparison to its corresponding acid, the atomic distance P1−N1 is shortened to 157.8(1) pm, representing a double bond. The bonds P1−N2, P1−N3, and P1−N4 range from 163.2(2) to 163.8(2) pm and also point to some degree of multiple bonding.[19]

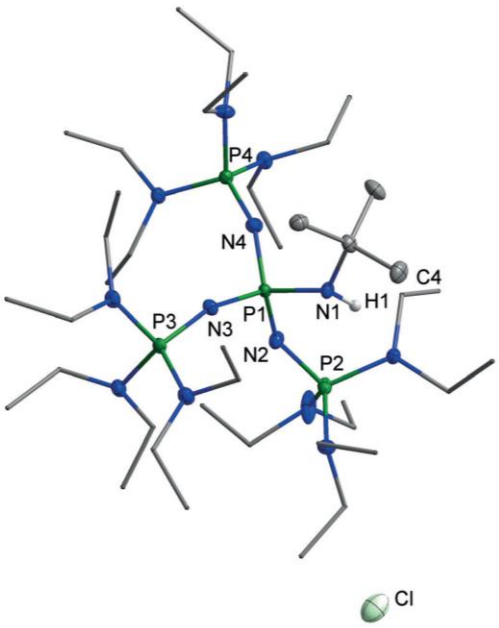

Figure 2. Molecular structure of the salt **[3H]Cl**. Thermal ellipsoids are shown at 50 % probability. Hydrogen atoms bonded at carbon and one minor occupied disordered ethyl group are omitted for clarity. Diethylamino groups are shown simplified as stick model. Selected bond lengths [pm] and angles [°]: P1−N1 167.2(2), P1−N2 160.6(2), P1−N3 158.5(2), P1−N4 158.9(2), P2−N2 155.4(2), N1−C1 148.0(3); C1−N1−P1 128.6(2), N1−P1−N4 109.0(1), P1−N2−P2 140.7(1).

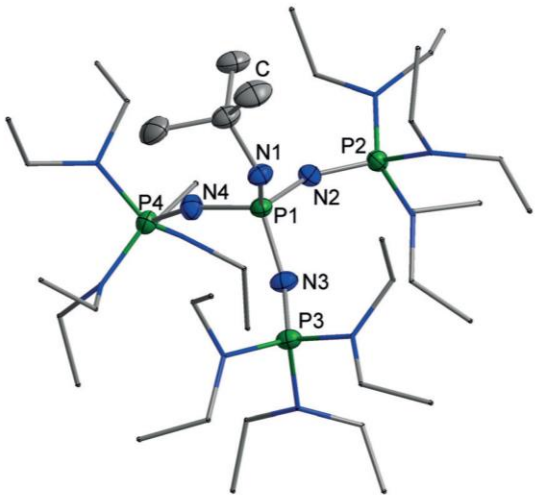

Figure 3. Molecular structure of **3**. Thermal ellipsoids are shown at 50 % probability. Hydrogen atoms are omitted for clarity. Diethylamino groups are shown simplified as a stick model. Selected bond lengths [pm] and angles [°]: P1−N1 157.8(1), P1−N2 163.8(2), P1−N3 163.1(1), P1−N4 163.2(2), P2−N2 153.0(1), N1−C1 145.7(2); C1−N1−P1 126.1-(1), N1−P1−N4 113.1(1), P1−N2−P2 150.3(1).

For the generation of isolated hydroxide/water clusters, different quantities of water were added to solutions of phosphazene **3** in *n*-hexane. The resulting phosphazenium hydroxides are soluble in chlorobenzene. At room temperature, however, such solutions slowly decompose. This

product separates from polar solvents as an oil, whereas amorphous or crystalline samples are obtained from apolar solvents like *n*-hexane. This finding may be rationalized by the various amounts of water incorporated in the precipitates, which hampered the isolation of a well-defined bulk material. However, colorless crystals were obtained after slow evaporation of a methanol/water solution of **3** at room temperature and atmospheric pressure. The result of the elemental analysis revealed a possible hydroxide hexahydrate salt of the protonated phosphazene, $[OH(OH_2)_6]^-$ (calcd: C 47.46, H 11.25, N 17.99, P 12.24, O 11.06; found: C 47.12, H 11.21, N 17.75, P 12.07, O 11.34). Since the crystals did not show any diffraction pattern, they could not be analyzed by X-ray diffraction. Nevertheless, a single crystal of **[3H][OH(OH$_2$)$_3$]** was isolated by slow diffusion of water into an *n*-hexane solution of the base.[17] The X-ray crystallographic analysis[18] revealed a disorder of two ethyl groups of the cation with a ratio of 82:18 and a disorder of the anion with the same ratio (Figure 4 A). The hydrogen atoms of the protonated nitrogen atom N4 and the major occupied part of the disordered anion could be refined isotropically, the latter with fixed O–H distances and angles. Looking at the ions of the reliably modelled major part, the shortest separation between an oxygen atom and the cation can be measured for O4–C10′ (symmetry code $1-x,1-y,1-z$) with 339.4(3) pm. This distance is clearly greater than the van der Waals radii and shows that this is the first example of an isolated hydroxide hydrate anion that is not in direct contact to a cation. The O–O distances are in the range of 251.6(1) pm to 260.2(3) pm. The calculated value of the C_3-symmetrical hydroxide shows a slightly longer distance of 261.2 pm (Figure 4 B).[5] The experimental O–O–O angles range from 88.7(1)° to 115.9(1)° and include the calculated angle of 102.4°.

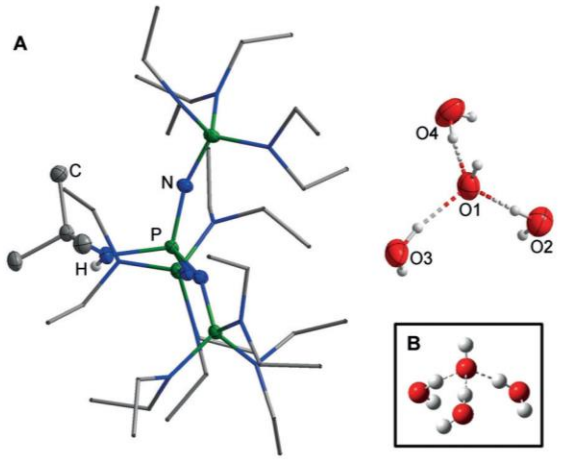

Figure 4. A) Molecular structure of **[3H][OH(OH$_2$)$_3$]**. Thermal ellipsoids are shown at 50% probability. Hydrogen atoms and minor occupied disordered parts are omitted for clarity. Diethylamino groups are shown simplified as a stick model. The anion is disordered (82:18). The hydrogens of the disordered water molecules could not be located reliably. Disorder of two ethyl groups (C33, C34, C35, C36) over two sites (82:18). Selected bond lengths [pm] and angles [°]: O1–O2 256.0(3), O1–O3 251.6(3), O1–O4 260.2(3); O2–O1–O4 88.7(1), O3–O1–O4 115.9(1), O2–O1–O3 110.4(1). B) Calculated C_3-symmetrical hydroxide trihydrate (MP2/6-311++G(3df,3pd)).[5]

Since the phosphazenium hydroxide **[3H][OH(OH$_2$)$_3$]** is highly sensitive towards loss of water under reduced pressure, reliable elemental analyses are nearly impossible to obtain (Scheme 2). An IR spectrum of the product displays a very broad band at 3411 cm^{-1} for the OH stretching vibration of the hydroxide anion and the bonded water molecules. No discrete bands are indicated, which points to a fast proton exchange between the water molecules and the hydroxide anion.

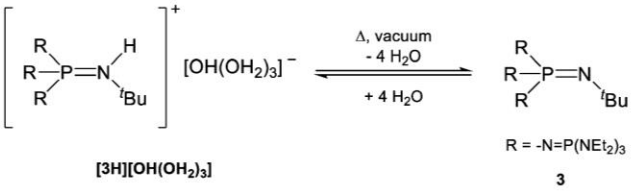

Scheme 2. Equilibrium reaction of **3** and H_2O.

To prove the existence of **[3H][OH(OH$_2$)$_3$]**, a chlorobenzene solution of **3** was titrated with water and analyzed by ^{31}P NMR spectroscopy (Figure 5). Complete protonation of **3** is observed only when four equivalents of water or more are employed, and was evidenced by the characteristic $^2J_{PP}$ coupling constant of 70 Hz. The $^2J_{PH}$ coupling constant of 8 Hz for the protonated phosphazenium **[3H]**$^+$ could only be resolved when an excess of water was used. This phenomenon is probably due to a dynamic proton exchange (Scheme 2). Addition of less than four equivalents of water leads to an upfield shift of the signal for the central phosphorus atom from −31.3 ppm to −34.2 ppm with an increase in the $^2J_{PP}$ coupling constant from 29 Hz to 70 Hz (Figure 5). In the ^{1}H NMR spectrum a broad signal at 4.9 ppm is observed for the protons of water and the hydroxide ion. The hydroxide hydrate decomposes at ambient temperature under vacuum, leading to the liberation of the free base **3**. Based on the collected data we suggest that the water molecules are activated or oriented in the superbasic system. The small size of a water molecule as well as the high basicity of the

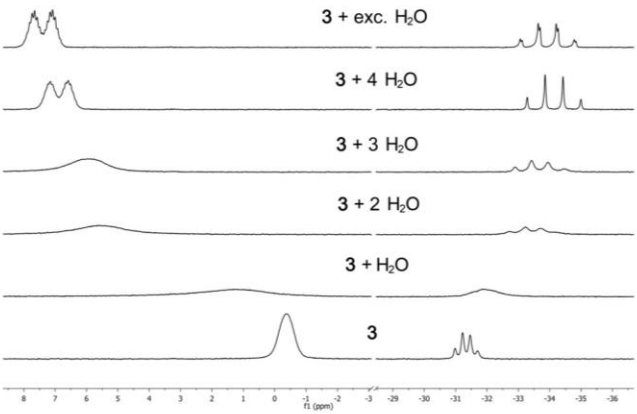

Figure 5. ^{31}P NMR spectroscopic titration of **3** with different amounts of water in chlorobenzene. Lock with [D$_6$]acetone in a capillary.

hydroxide anion render the deprotonation of the shielded iminium unit possible. In comparison to hydroxides with coordinating cations like alkali metal cations, a naked hydroxide anion in the presence of **[3H]**$^+$ seems to be unstable and therefore not preparable. The stabilizing effect of hydrogen-bonding water molecules is necessary to lower the basicity of the hydroxide anion. This principle seems to be responsible for the selective generation of **3** from its hydroxide. Following the removal of stabilizing water molecules in vacuum, the basicity of the resulting anion is high enough for a selective deprotonation of the phosphazenium cation.

The preparation of **3** by deprotonation of **[3H]Cl** with self-igniting metal amides in liquid ammonia as a solvent is hazardous and problematic in view of waste disposal. Extensive cooling is expensive and upscaling to obtain base **3** in larger quantities remains a challenge. Reaction with potassium *tert*-butanolate does not provide base **3** free of alcohol as claimed earlier by Schwesinger et al.[9,10] Less basic phosphazenes like **1**, indeed, could be liberated from the corresponding phosphazenium salts with the aid of potassium *tert*-butanolate or even KOH, prior to distillation.[11]

A viable and elegant conversion of **[3H]Cl** into free **3** on a larger scale makes use of the intermediacy of reactive hydroxide hydrate **[3H][OH(OH$_2$)$_3$]**. Following a procedure by Taylor and Hupfield[20] for the conversion of phosphazenium chlorides into their hydroxide by means of anion-exchange resins, we succeeded in the clean formation of the hydroxide trihydrate **[3H][OH(OH$_2$)$_3$]** by exposing solutions of **[3H]Cl** to a strongly basic OH^- ion-exchange resin (Scheme 3). The free, anhydrous base **3** was isolated after thermolysis of **[3H][OH(OH$_2$)$_3$]** in high vacuum at 70–100 °C (yield > 97 %). Following a protocol disclosed in the literature, the anion-exchange resin was regenerated with 1 M aqueous sodium hydroxide solution.[20] In conclusion, our sequence represents a straightforward and selective route for the deprotonation of **[3H]Cl**.

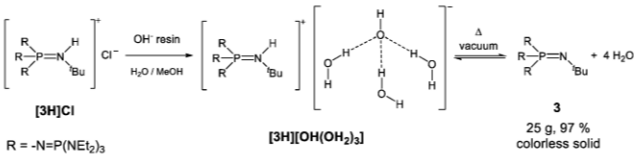

Scheme 3. Synthesis of **3** using a salt-exchange reaction to generate the metastable hydroxide hydrate **[3H][OH(OH$_2$)$_3$]**.

We used this method for the phosphazene-base-catalyzed trifluoromethylation reaction of Me_3SiCl to generate the Ruppert–Prakash reagent, as shown in Scheme 4. The Ruppert–Prakash reagent Me_3SiCF_3 is the most commonly used trifluoromethylation agent in laboratory and industry,[21–23] especially in medicinal chemistry for the preparation of trifluoromethyl-substituted arenes, trifluoromethyl ethers, and trifluoromethyl ketones.[24]

Fluoroform (HCF_3) is an excellent and cheap source of the trifluoromethyl building block, since it is a waste product

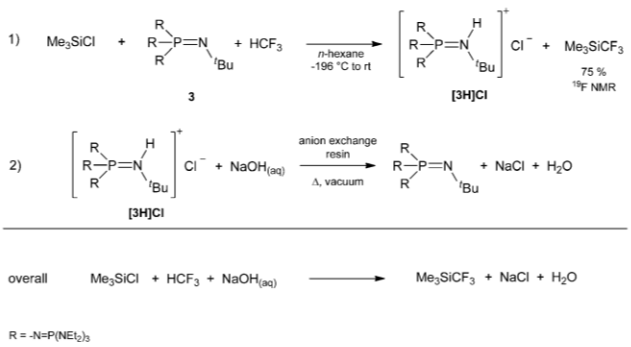

Scheme 4. Overall reaction for the preparation of the Ruppert–Prakash reagent.

of Teflon production.[22,25] The deprotonation of HCF_3 can be performed by using *n*-butyllithium or potassium *tert*-butanolate; however, the high fluorophilicity of alkali cations leads to a carbenoidic bond situation and rapid difluorocarbene elimination at low temperatures.[26] Therefore the preparative trifluoromethylation reaction is accomplished via the detour of Me_3SiCF_3. Prakash et al. managed the synthesis of Me_3SiCF_3 in high yields from Me_3SiCl, HCF_3, and potassium bis(trimethylsilyl)amide (KHMDS) in toluene at low temperatures.[22] Shibata et al. recently presented the possibility to lower the fluorophilicity of the potassium cation of trifluoromethyl potassium by the use of glyme as a coordinating solvent.[27] Weakly coordinating phosphazenium cations also prevent the difluorocarbene elimination (Scheme 5) as presented by Shibata et al. and Zhang et al. for the trifluoromethylation of electrophilic carbonyl compounds[28] and sulfonyl fluorides,[29] as well as for different epoxides, carbon dioxide, and esters[30] in good to excellent yields using **2** and fluoroform.

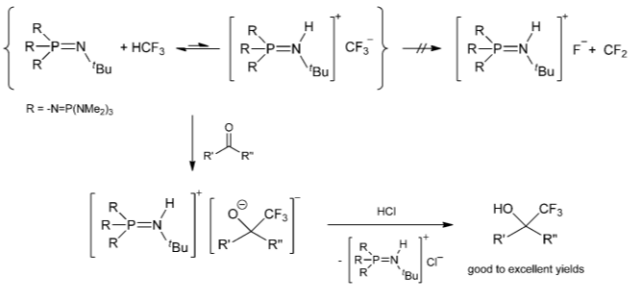

Scheme 5. Trifluoromethylation of carbonyl compounds.[28]

The ^{19}F and ^{31}P NMR spectroscopic investigation of a mixture of **3** and fluoroform does not show any reaction, as reported by Zhang for the methyl derivative **2**.[30] The addition of electrophiles leads to a rapid trifluoromethylation at ambient temperature (Scheme 5). Phosphazene **3** reacts rapidly with Me_3SiCF_3, forming Me_3SiF and a wide range of byproducts due to a difluorocarbene elimination. The decomposition reaction of Me_3SiCF_3 with fluoride salts was already studied by Tyrra and Naumann et al. and resulted in

perfluoroalkylated polyanions.[31] By using an excess of Me_3SiCl, the reaction of **3** and HCF_3 can be controlled kinetically leading to the selective formation of Me_3SiCF_3 (−67.7 ppm in the ^{19}F NMR spectrum) with yields of up to 75% (Scheme 4).[17]

The use of a hydrocarbon solvent is crucial, because the high basicity of phosphazene **3** causes solvent deprotonation in the presence of Lewis acidic components like Me_3SiCl. The high molecular weight and high cost of phosphazenes **2** and **3** make trifluoromethylation unprofitable on a larger scale. For this reason, Zhang and Shibata suggested the use of additives such as bis(trimethylsilyl)amine and use of **2** in catalytic amounts of about 20 mol%.[29,30] The use of additives leads to a loss of high amounts of the Schwesinger base during the conversion on multimolar scales. In our case the precipitated phosphazenium hydrochloride **[3H]Cl** in the trifluoromethylation reaction (Scheme 4) was regenerated in excellent yields of about 98 to 100% after every reaction step through the use of an anion-exchange resin, as shown in Table 1 in the Supporting Information,[17] whereas small amounts of **3** are used for ^{31}P NMR spectroscopic investigations after every step. Thus we showed the recovery and the possibility to use phosphazene **3** in further trifluoromethylation reactions without any loss of reactivity.

In the overall reaction for the synthesis of the Ruppert–Prakash reagent, as shown in Scheme 4, the trifluoromethylation reaction is accomplished by the use of sodium hydroxide as a base. The pentafluoroethylation of Me_3SiCl with pentafluoroethane and **3** results in the formation of trimethylpentafluoroethylsilane in yields of about 61%.[17] In this reaction decomposition of **3** is not observed. This recommends the use of phosphazene **3** for further fluoro- and perfluoroalkylation reactions.

In conclusion, we have reported the first structurally characterized metastable hydroxide trihydrate $\mathbf{[OH(OH_2)_3]^-}$, generated via the newly prepared phosphazene base **3**. The hydroxide shows the tendency to lose water under vacuum, which effects selective deprotonation of the phosphazenium cation $\mathbf{[3H]^+}$. This protocol is used for the selective formation of **3** from its hydrochloride by means of a basic anion-exchange resin in excellent yields of over 97% and circumvents the use of hazardous metal amides in liquid ammonia which allows the production on a larger scale (>25 g). We also described the synthesis of the Ruppert–Prakash reagent Me_3SiCF_3 in yields of about 75% by using fluoroform (HCF_3), Me_3SiCl, and Schwesinger base **3**. The free base **3** was regenerated by an anion-exchange resin from precipitated phosphazenium chloride **[3H]Cl** in excellent yields of over 98% and reused for the trifluoromethylation reaction without a loss of reactivity. Since the exchange resin can be regenerated with aqueous sodium hydroxide solution, in the overall reaction the trifluoromethylation is carried out using sodium hydroxide as base.

Acknowledgements

We acknowledge the financial support by Merck KGaA and Solvay. We thank Prof. Dr. Lothar Weber and Dr. Julia Bader for helpful discussions. We thank Michaela Schimmel, Rafael Methling, and Katharina Wels for assistance in laboratory.

Conflict of interest

The authors declare no conflict of interest.

Keywords: hydroxide hydrate · phosphazene base · Ruppert–Prakash reagent · trifluoromethylation · weakly coordinating cations

How to cite: *Angew. Chem. Int. Ed.* **2019**, *58*, 14633–14638
Angew. Chem. **2019**, *131*, 14775–14780

[1] H. M. G. Zundel, *Z. Phys. Chem.* **1968**, 225.
[2] M. Eigen, *Angew. Chem. Int. Ed. Engl.* **1964**, *3*, 1–19; *Angew. Chem.* **1963**, *75*, 489–508.
[3] a) N. Schwarze, S. Steinhauer, B. Neumann, H.-G. Stammler, B. Hoge, *Angew. Chem. Int. Ed.* **2016**, *55*, 15528; *Angew. Chem.* **2016**, *128*, 15756; b) Z. Xie, R. Bau, C. A. Reed, *Inorg. Chem.* **1995**, *34*, 5403; c) M. Niemann, B. Neumann, H.-G. Stammler, B. Hoge, *Angew. Chem. Int. Ed.* **2019**, *58*, 8938; *Angew. Chem.* **2019**, *131*, 9033; d) D. Steinborn, O. Gravenhorst, H. Hartung, U. Baumeister, *Inorg. Chem.* **1997**, *36*, 2195; e) B. Krebs, S. Bonmann, K. Erpenstein, *Z. Naturforsch. B* **1991**, *46*, 919; f) E. S. Stoyanov, S. P. Hoffmann, K.-C. Kim, F. S. Tham, C. A. Reed, *J. Am. Chem. Soc.* **2005**, *127*, 7664.
[4] R. Ludwig, *Angew. Chem. Int. Ed.* **2003**, *42*, 258; *Angew. Chem.* **2003**, *115*, 268.
[5] M. Morita, K. Takahashi, *Phys. Chem. Chem. Phys.* **2013**, *15*, 114.
[6] a) W. H. Robertson, E. G. Diken, E. A. Price, J.-W. Shin, M. A. Johnson, *Science* **2003**, *299*, 1367; b) D. Zanuttini, B. Gervais, *J. Phys. Chem. A* **2015**, *119*, 8188; c) A. Mandal, K. Ramasesha, L. de Marco, A. Tokmakoff, *J. Chem. Phys.* **2014**, *140*, 204508; d) E. E. Dahlke, M. A. Orthmeyer, D. G. Truhlar, *J. Phys. Chem. B* **2008**, *112*, 2372; e) F. C. Pickard, E. K. Pokon, M. D. Liptak, G. C. Shields, *J. Chem. Phys.* **2005**, *122*, 024302; f) J. J. Novoa, F. Mota, C. Perez del Valle, M. Planas, *J. Phys. Chem. A* **1997**, *101*, 7842; g) P. Spanel, D. Smith, *J. Phys. Chem.* **1995**, *99*, 15551; h) H. D. Lutz, *Struct. Bonding (Berlin)* **1995**, *82*, 85–103.
[7] K. Abu-Dari, K. N. Raymond, D. P. Freyberg, *J. Am. Chem. Soc.* **1979**, *101*, 3688.
[8] R. Schwesinger, H. Schlemper, *Angew. Chem. Int. Ed. Engl.* **1987**, *26*, 1167–1169; *Angew. Chem.* **1987**, *99*, 1212–1214.
[9] R. Schwesinger, H. Schlemper, C. Hasenfratz, J. Willaredt, T. Dambacher, T. Breuer, C. Ottaway, M. Fletschinger, J. Boele, H. Fritz, et al., *Liebigs Ann.* **1996**, 1055.
[10] R. Schwesinger, C. Hasenfratz, H. Schlemper, L. Walz, E.-M. Peters, K. Peters, H. G. von Schnering, *Angew. Chem. Int. Ed. Engl.* **1993**, *32*, 1361; *Angew. Chem.* **1993**, *105*, 1420.
[11] R. Schwesinger, J. Willaredt, H. Schlemper, M. Keller, D. Schmitt, H. Fritz, *Chem. Ber.* **1994**, *127*, 2435.
[12] C. Luo, J. S. Bandar, *J. Am. Chem. Soc.* **2018**, *140*, 3547–3550.
[13] C. Palomo, M. Oiarbide, R. López, E. Gómez-Bengoa, *Chem. Commun.* **1998**, 2091.
[14] G. A. Kraus, N. Zhang, J. G. Verkade, M. Nagarajan, P. B. Kisanga, *Org. Lett.* **2000**, *2*, 2409.
[15] R. Schwesinger, R. Link, G. Thiele, H. Rotter, D. Honert, H.-H. Limbach, F. Männle, *Angew. Chem. Int. Ed. Engl.* **1991**, *30*, 1372–1375; *Angew. Chem.* **1991**, *103*, 1376.
[16] a) A. V. Kirsanov, *Zh. Obshch. Khim.* **1952**, *22*, 88; b) C. Glidewell, *Angew. Chem. Int. Ed. Engl.* **1975**, *14*, 826; *Angew. Chem.* **1975**, *87*, 875.
[17] Details are given in the Supporting Information for this paper.

[18] Details of the X-ray investigation are given in Table 2 in the Supporting Information. CCDC 1938109, 1938110, and 1938111 contain the supplementary crystallographic data for this paper. These data can be obtained free of charge from The Cambridge Crystallographic Data Centre.
[19] F. H. Allen, O. Kennard, D. G. Watson, L. Brammer, A. G. Orpen, R. Taylor, *J. Chem. Soc. Perkin Trans. 2* **1987**, 194.
[20] P. C. Hupfield, R. G. Taylor, *J. Inorg. Organomet. Polym.* **1999**, *9*, 17 – 34.
[21] G. K. S. Prakash, A. K. Yudin, *Chem. Rev.* **1997**, *97*, 757.
[22] G. K. S. Prakash, P. V. Jog, P. T. D. Batamack, G. A. Olah, *Science* **2012**, *338*, 1324.
[23] a) M. Schlosser, *Angew. Chem. Int. Ed.* **2006**, *45*, 5432; *Angew. Chem.* **2006**, *118*, 5558.
[24] S. Swallow, *Prog. Med. Chem.* **2015**, *54*, 65.
[25] V. V. Grushin, *Chim. Oggi – Chem. Today* **2014**, *32*, 81 – 88.
[26] a) R. D. Chambers, *Fluorine in Organic Chemistry*, Wiley, New York, **1973**; b) B. Waerder, S. Steinhauer, B. Neumann, H.-G. Stammler, A. Mix, Y. V. Vishnevskiy, B. Hoge, N. W. Mitzel, *Angew. Chem. Int. Ed.* **2014**, *53*, 11640; *Angew. Chem.* **2014**, *126*, 11824.
[27] T. Saito, J. Wang, E. Tokunaga, S. Tsuzuki, N. Shibata, *Sci. Rep.* **2018**, *8*, 11501.
[28] H. Kawai, Z. Yuan, E. Tokunaga, N. Shibata, *Org. Biomol. Chem.* **2013**, *11*, 1446.
[29] S. Okusu, K. Hirano, E. Tokunaga, N. Shibata, *ChemistryOpen* **2015**, *4*, 581.
[30] Y. Zhang, M. Fujiu, H. Serizawa, K. Mikami, *J. Fluorine Chem.* **2013**, *156*, 367.
[31] W. Tyrra, M. M. Kremlev, D. Naumann, H. Scherer, H. Schmidt, B. Hoge, I. Pantenburg, Y. L. Yagupolskii, *Chem. Eur. J.* **2005**, *11*, 6514.

Manuscript received: July 10, 2019
Accepted manuscript online: August 1, 2019
Version of record online: September 9, 2019

Angewandte Chemie
Eine Zeitschrift der Gesellschaft Deutscher Chemiker

Supporting Information

Generation and Applications of the Hydroxide Trihydrate Anion, $[OH(OH_2)_3]^-$, Stabilized by a Weakly Coordinating Cation

*Robin F. Weitkamp, Beate Neumann, Hans-Georg Stammler, and Berthold Hoge**

anie_201908589_sm_miscellaneous_information.pdf

1. Experimental Section

1.1 General Part

All chemicals were obtained from commercial sources and used without further purification. Standard high-vacuum techniques were employed throughout all preparative procedures, except aqueous workups. Non-volatile compounds were handled in a dry N_2 atmosphere using Schlenk techniques.

1.2 Analysis Methods

1.2.1 NMR Spectroscopy

NMR spectra were recorded on a Bruker Model Avance III 300 spectrometer (^{1}H 300.13 MHz; ^{13}C 75.47 MHz; ^{19}F 282.40 MHz; ^{31}P 121.49 MHz). Positive shifts are downfield from the external standards TMS (^{1}H, ^{13}C), CCl_3F (^{19}F) and H_3PO_4 (^{31}P). The NMR spectra were recorded in the indicated deuterated solvent or in relation to acetone-d_6-filled capillaries.

1.2.2 IR Spectroscopy

IR spectra were recorded on an ALPHA-FT-IR spectrometer (Bruker) using an ATR unit with a diamond crystal for liquids and solids.

1.2.3 Elemental Analyses

Elemental analyses were performed by Mikroanalytisches Laboratorium Kolbe (Oberhausen, Germany).

1.2.4 Melting Point

Melting points were measured on a Mettler Toledo Mp70 Melting Point System.

1.3 Syntheses

1.3.1 Synthesis of $(Et_2N)_3PNH$ (4)

Phosphorus pentachloride (29.62 g, 142.2 mmol) is suspended in 250 mL of dichloromethane at -78 °C. A solution of diethylamine (6.6 eq, 98.0 mL, 944 mmol) in 50 mL of dichloromethane is added dropwise, so that the inner temperature is kept below -30 °C. After the addition, the orange slurry is allowed to warm to room temperature. After an additional hour of stirring, the mixture is cooled to -20 °C and gaseous ammonia is bubbled into the reaction mixture via a syringe over a period of 50 minutes. After positive ^{31}P NMR control, the suspension is filtrated over a Schlenk frit and the colorless solid is washed with dichloromethane (3 x 25 mL). The solvent is removed under reduced pressure, leading to a hygroscopic orange solid (60.78 g), containing diethylammonium chloride. The product is dissolved in 60 mL of methanol at -20 °C and a solution of potassium-*tert*-butanolate (65.85 g, 586.9 mmol) in 150 mL of methanol is added dropwise to the orange solution. After addition, the mixture is allowed to warm to room temperature and stirred overnight. The precipitate is filtered off and washed with methanol (3 x 20 mL). The filtrate is freed from solvent under reduced pressure. All volatile components are condensed into a second Schlenk flask (110 °C, 10^{-3} mbar). The yellow solution is distilled in vacuo, leading to a pale yellow liquid (32.39 g, 123.5 mmol, 87 % based on PCl_5, 10^{-3} mbar, 60-82 °C).

^1H NMR ($CDCl_3$, rt): δ [ppm] = 1.1 (t, d, $^3J_{HH}$ = 7 Hz, $^4J_{PH}$ = 1 Hz, 18 H, CH_3), 3.0 (d, q, $^3J_{PH}$ = 10 Hz, $^3J_{HH}$ = 7 Hz, 12 H, CH_2).
^{31}P NMR ($CDCl_3$, rt): δ [ppm] = 42.7 (tridec, $^3J_{PH}$ = 10 Hz).
IR (ATR): ν [cm^{-1}] = 3403 (vw), 2967 (w), 2930 (w), 2867 (w), 1460 (w), 1376 (m), 1348 (w), 1296 (vw), 1201 (m), 1184 (s), 1096 (m), 1057 (w), 1015 (vs), 933 (s), 837 (w), 790 (m), 692 (s), 630 (w), 531 (w, br).
elemental analysis for $C_{12}H_{31}N_4P$ (262.4 g/mol): calcd.: C 54.93, H 11.91, N 21.35, P 11.81; found: C 54.61, H 11.91, N 21.48, P 11.68.

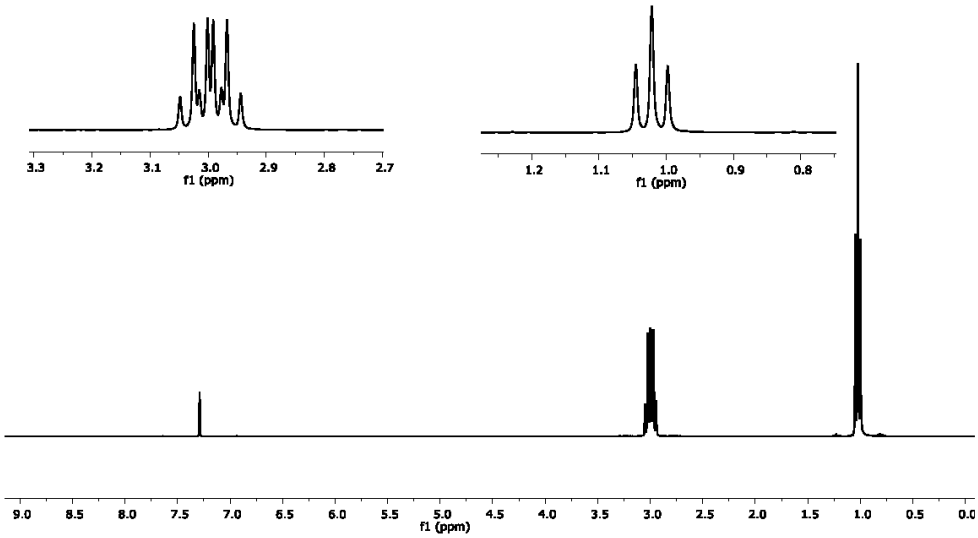

Figure 1. ^{1}H NMR spectrum of **4** in chloroform-d_1.

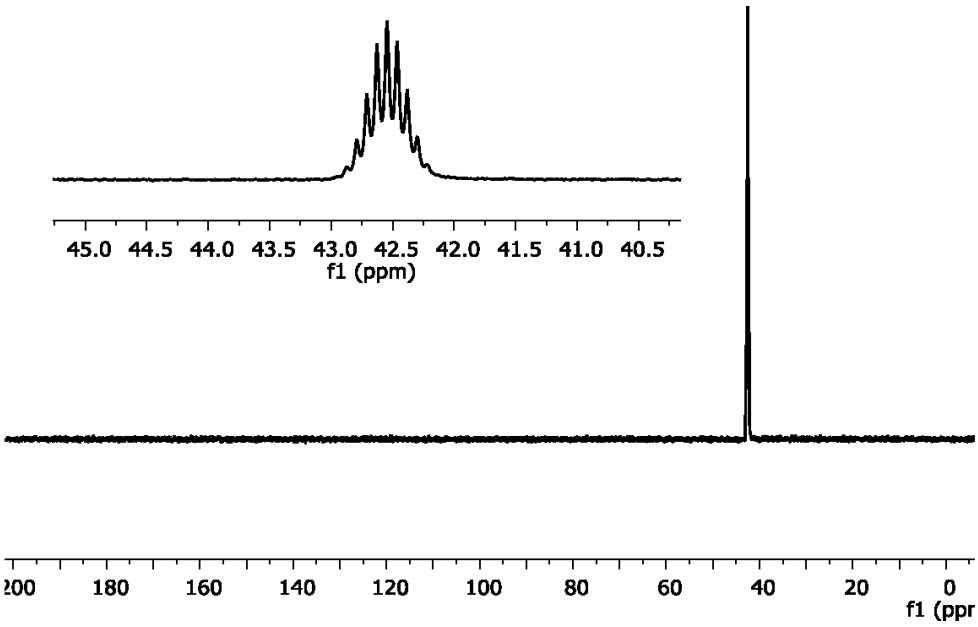

Figure 2. ^{31}P NMR spectrum of **4** in chloroform-d_1.

1.3.2 Synthesis of Cl_3PNtBu (5)

Phosphorus pentachloride (31.53 g, 151.5 mmol) is suspended in 750 mL of *n*-pentane before a solution of *tert*-butylamine (3.1 eq, 34.34 g, 469.5 mmol) in 150 mL of *n*-pentane is added dropwise under ice bath cooling. Thereafter the suspension is refluxed for 1.5 h and then stirred overnight at room temperature. The precipitate is filtered off and washed with *n*-pentane (3 x 50 mL). After removing the solvent under reduced pressure, the colorless liquid residue is distilled in vacuo (25 mbar, 55 °C) leading to the product (24.21 g, 116.1 mmol, 77 % based on PCl_5) as a colorless liquid.

^{1}H NMR ($CDCl_3$, rt): δ [ppm] = 1.4 (d, $^4J_{PH}$ = 3 Hz).
^{31}P NMR ($CDCl_3$, rt): δ [ppm] = -78.3 (s).

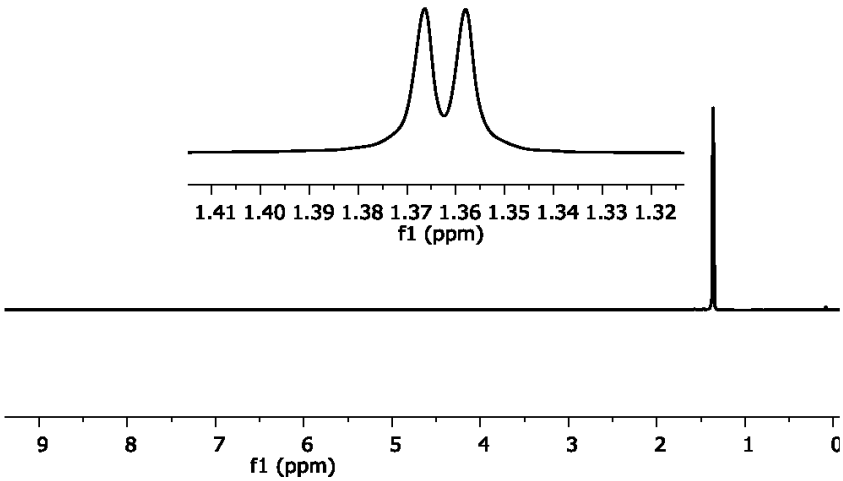

Figure 3. ^{1}H NMR spectrum of **5** in chloroform-d_1.

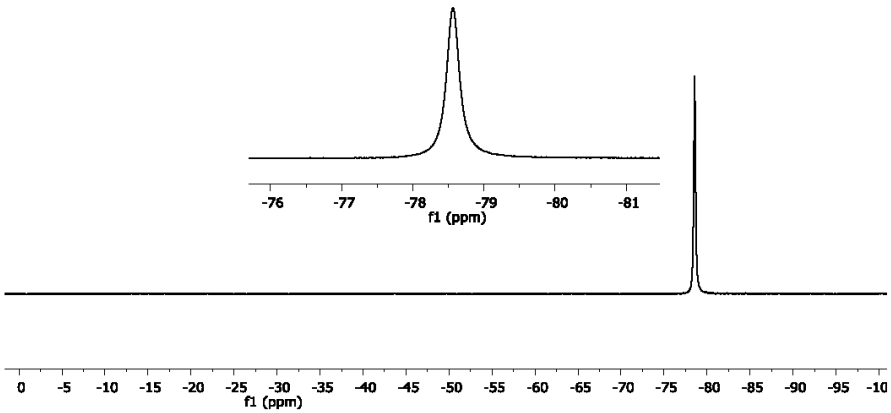

Figure 4. ^{31}P NMR spectrum of **5** in chloroform-d_1.

1.3.3 Synthesis of [{$(Et_2N)_3PN$}$_3$PN(H)*t*Bu]Cl ([3H]Cl)

At 0 °C a sample of **5** (3.40 g, 16.27 mmol) is added dropwise with a syringe to neat **4** (6 eq, 25.62 g, 97.64 mmol). The suspension is heated for three days at 160 °C in an evacuated Young-flask and afterwards extracted with boiling water (2 x 75 mL). The residue is dried in high vacuum prior to recrystallization from diethyl ether (30 mL) at -28 °C. The product (14.92 g, 16.17 mmol, 99 % based on Cl_3PNtBu) is collected as a colorless solid (m.p. > 185 °C (dec.)).

^{1}H NMR ($CDCl_3$, rt): δ [ppm] = 1.1 (t, $^3J_{HH}$ = 7 Hz, 54 H, CH_3), 1.3 (s, 9 H, $C(CH_3)_3$), 2.0 (d, $^2J_{PH}$ = 8 Hz, 1 H, NH), 3.1 (d,q, $^3J_{PH}$ = 10 Hz, $^3J_{HH}$ = 7 Hz, 36 H, CH_2).
^{13}C{^{1}H}APT NMR ($CDCl_3$, rt): δ [ppm] = 13.5 (d, $^3J_{PC}$ = 4 Hz, CH_3), 31.4 (d, $^3J_{PC}$ = 5 Hz, $C(\mathbf{C}H_3)_3$), 39.0 (d, $^2J_{PC}$ = 6 Hz, CH_2), 50.6 (d, $^2J_{PC}$ = 4 Hz, $\mathbf{C}(CH_3)_3$).
^{31}P NMR ($CDCl_3$, rt): δ [ppm] = -33.9 (q, d, $^2J_{PP}$ = 70 Hz, $^2J_{PH}$ = 8 Hz, 1 P, P=NH), 7.4 (d, tridec, $^2J_{PP}$ = 70 Hz, $^3J_{PH}$ = 10 Hz, 3 P, $(Et_2N)_3P$).
IR (ATR): ν [cm^{-1}] = 3387 (vw, vbr), 2967 (vw), 2931 (vw), 2870 (vw), 1633 (vw, br), 1463 (vw), 1379 (w), 1350 (w), 1265 (m, br), 1201 (m), 1173 (vs), 1107 (vw), 1054 (vw), 1016 (vs), 941 (s), 845 (vw), 792 (m), 740 (vw), 700 (m), 613 (w), 507 (s), 439 (m).
elemental analysis for $C_{40}H_{100}N_{13}P_4Cl$ (922.7 g/mol): calcd.: C 52.07, H 10.92, N 19.74, P 13.43; found: C 51.31, H 10.78, N 19.67, P 13.13.

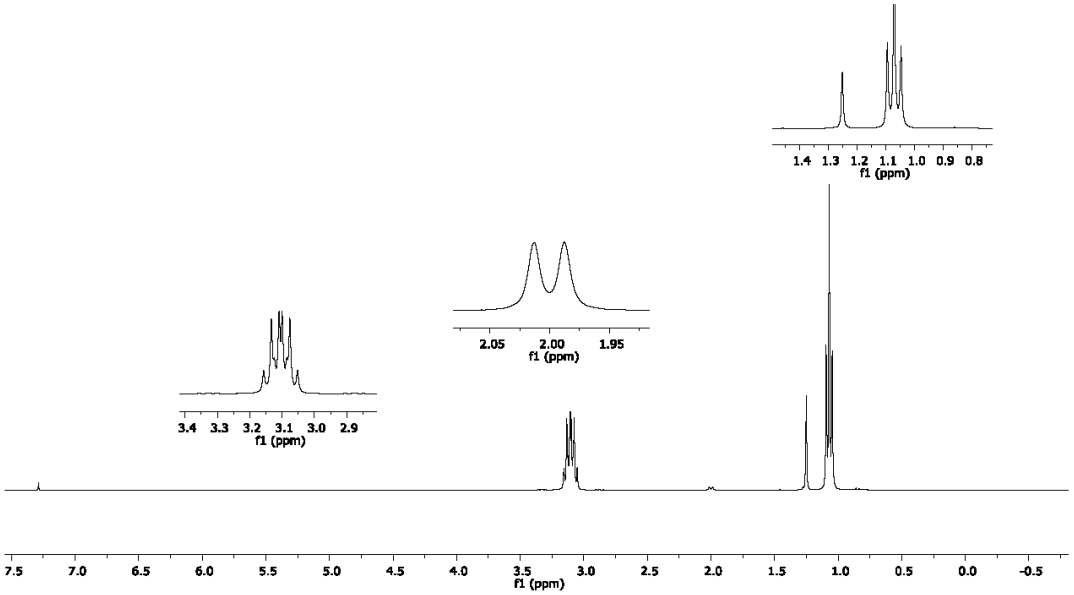

Figure 5. ^{1}H NMR spectrum of **[3H]Cl** in chloroform-d_1.

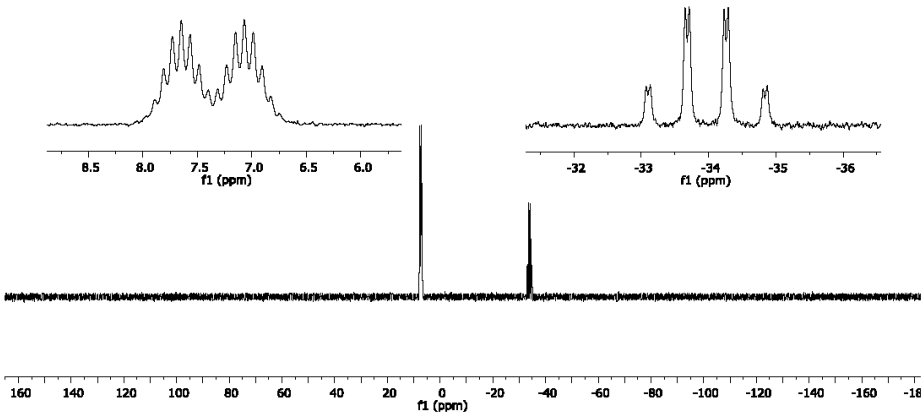

Figure 6. ^{31}P NMR spectrum of **[3H]Cl** in chloroform-d_1.

1.3.4 Synthesis of $[(Et_2N)_3PN]_3PN$*t*Bu (3)

a) Deprotonation via anion exchange resin

Hydrochloride **[3H]Cl** (26.33 g, 28.53 mmol) is dissolved in 60 mL of a methanol / water mixture (7 : 3) and passed three times through a strongly basic anion exchange resin (110 mL resin in 110 mL of MeOH / H_2O, Ion Exchanger III, 0.9 mol/L, Merck KGaA). The column is washed two times with 30 mL of a methanol / water mixture (7 : 3). The combined colorless solutions are evaporated in vacuo (10^{-3} mbar) at room temperature and the resulting solid is dried at 70 °C until no further solvent signal in the ^{1}H NMR spectrum is detectable. The product (24.55 g, 27.70 mmol, 97 %) is isolated as a bright yellowish solid (m.p. 230-240 °C (dec.)).

^{1}H NMR (C_6D_6, rt): δ [ppm] = 1.1 (t, $^3J_{HH}$ = 7 Hz, 54 H, CH_3), 1.7 (s, 9 H, $C(CH_3)_3$), 3.3 (d,q, $^3J_{PH}$ = 9 Hz, $^3J_{HH}$ = 7 Hz, 36 H, CH_2).
$^{13}C\{^1H\}$ NMR (C_6D_6, rt): δ [ppm] = 13.9 (d, $^3J_{PC}$ = 4 Hz, CH_3), 35.2 (d, $^3J_{PC}$ = 15 Hz, $C(\mathbf{C}H_3)_3$), 39.4 (d, $^2J_{PC}$ = 5 Hz, CH_2), 51.0 (d, $^2J_{PC}$ = 5 Hz, $\mathbf{C}(CH_3)_3$).
^{31}P NMR (C_6D_6, rt): δ [ppm] = -31.3 (q, $^2J_{PP}$ = 29 Hz, 1 P, P=N), 0.3 (m, 3 P, $(Et_2N)_3P$).
IR (ATR): ν [cm^{-1}] = 2968 (w), 2930 (vw), 2865 (w), 1462 (vw, br), 1374 (w), 1349 (w), 1267 (m), 1229 (m), 1181 (vs), 1104 (w), 1054 (w), 1015 (vs), 932 (s), 838 (w), 782 (m), 752 (w), 729 (w), 694 (s), 609 (w), 505 (s, br).
elemental analysis for $C_{40}H_{99}N_{13}P_4$ (886.2 g/mol): calcd.: C 54.21, H 11.26, N 20.55, P 13.98; found: C 53.31, H 11.07, N 20.21, P 14.34.

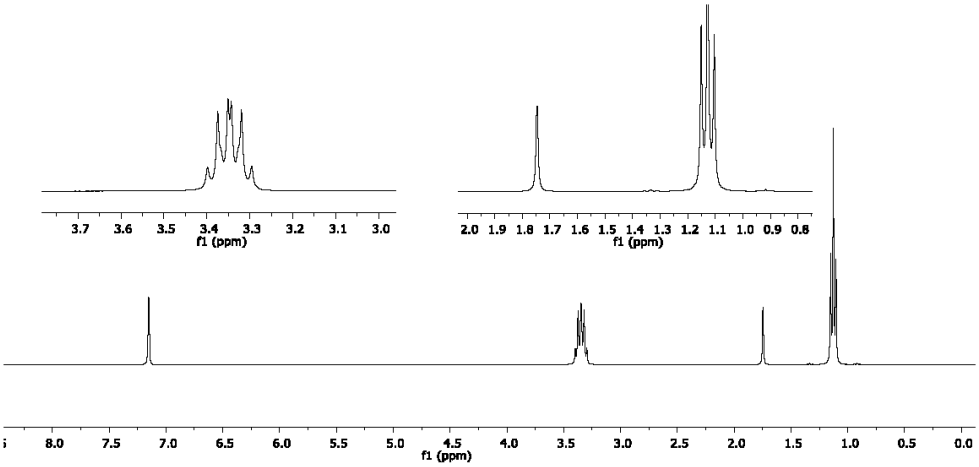

Figure 7. ^{1}H NMR spectrum of **3** in benzene-d_6.

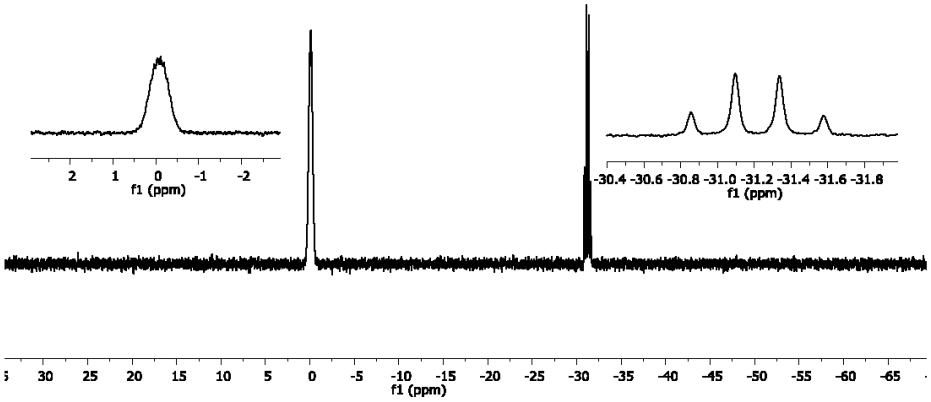

Figure 8. ^{31}P NMR spectrum of **3** in benzene-d_6.

b) Deprotonation via sodium amide

Ammonia (120 mL) is condensed onto sodium metal (1.13 g, 49.2 mmol) at -196 °C. In a cooling bath the suspension is allowed to warm to -70 °C and then a catalytic amount of iron(III)nitrate nonahydrate is added. The blue suspension is stirred for 2.5 h, until the suspension changed color from deep blue to brown. Then **[3H]Cl** (18.45 g, 20.0 mmol) is added and the suspension is allowed to warm to room temperature in the cooling bath overnight. The solid is suspended in 60 mL of *n*-hexane and the slurry is filtrated over a Schlenk-frit (P4). The residue is washed two times with 10 mL of *n*-hexane. The solvent is removed from the combined filtrates to give **3** (16.19 g, 18.7 mmol, 94 %) as a bright yellowish solid.

1.3.5 Generation of [{$(Et_2N)_3PN\}_3PN(H)tBu][OH(OH_2)_3]$ ([3H][$OH(OH_2)_3$])

a) Generation in chlorobenzene solution

To a solution of **3** (556 mg, 0.63 mmol) in 4 mL of chlorobenzene, water (4 eq, 45 mg, 2.50 mmol) is added. ^{31}P NMR spectroscopic analysis shows complete protonation.

^{1}H NMR (C_6H_5Cl, rt): δ [ppm] = 0.7 (t, $^{3}J_{HH}$ = 7 Hz, 54 H, CH_3), 1.0 (s, 9 H, $C(CH_3)_3$), 2.7 (m, 36 H, CH_2), 4.9 (s, 8 H, OH).

^{31}P NMR (C_6H_5Cl, rt): δ [ppm] = -34.2 (q, $^{2}J_{PP}$ = 70 Hz, 1 P, P=NH), 6.9 (d, tridec, $^{2}J_{PP}$ = 70 Hz, $^{2}J_{PH}$ = 8 Hz, 3 P, $(Et_2N)_3P$).

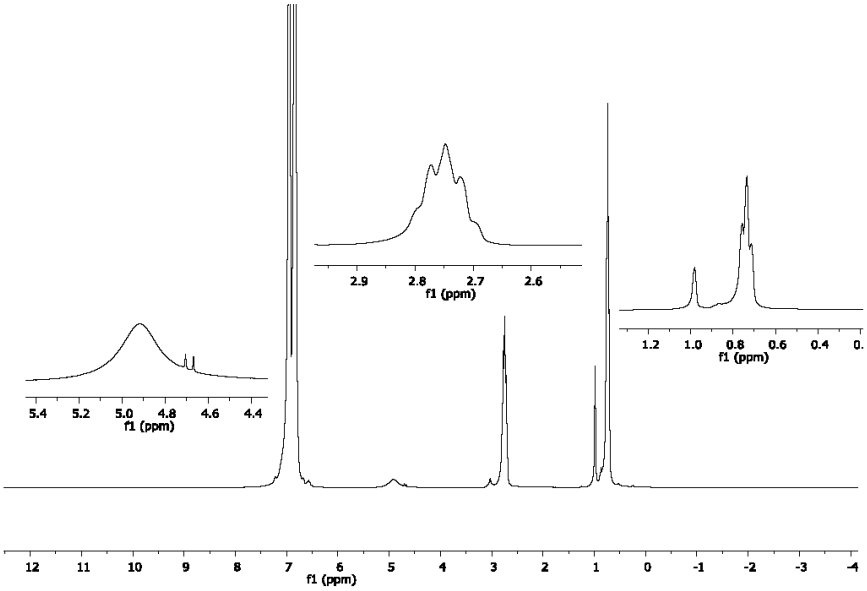

Figure 10. ^{1}H NMR spectrum of **[3H][$OH(OH_2)_3$]** generated in chlorobenzene (lock with acetone-d_6 in a capillary).

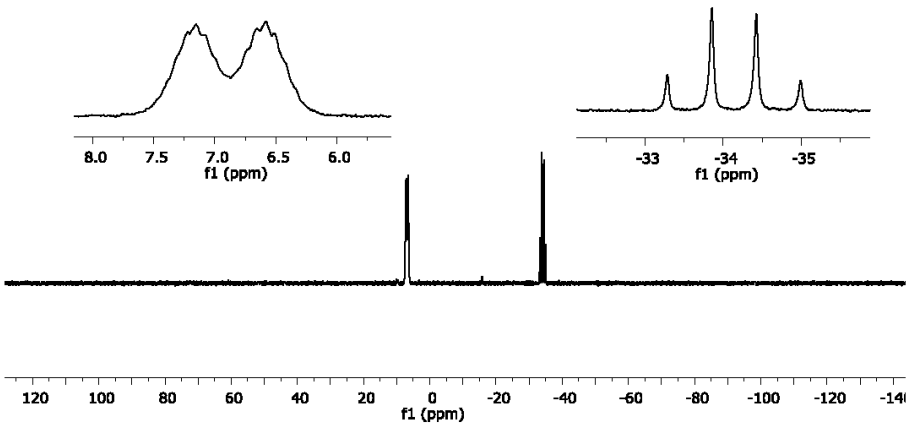

Figure 10. ^{31}P NMR spectrum of **[3H][OH(OH$_2$)$_3$]** generated in chlorobenzene (lock with acetone-d$_6$ in a capillary).

b) Generation from *n*-hexane solution

By slow diffusion of water into a solution of **3** (240 mg) in 4 mL of *n*-hexane a colorless solid is obtained.

IR (ATR): $\tilde{\nu}$ [cm^{-1}] = 3411 (vw, vbr), 2969 (w), 2932 (w), 2871 (w), 1653 (w, br), 1464 (w), 1411 (w), 1379 (m), 1351 (w), 1271 (s, br), 1227 (w), 1202 (s), 1174 (vs), 1107 (w), 1055 (w), 1017 (vs), 942 (s), 921 (w), 845 (w), 792 (m), 740 (w), 699 (s), 612 (m), 507 (vs), 439 (s).

1.3.6 Synthesis of Me_3SiCF_3 and exemplary regeneration of 3

In a flame-dried flask equipped with a Young valve a sample of **3** (5.39 g, 6.08 mmol) is dissolved in 20 mL of *n*-hexane. The solution is degassed three times. Fluoroform (30 mmol) is condensed onto the solution at -196 °C and the mixture is allowed to melt for mixing. Me_3SiCl (7.11 mmol, 772 mg) is condensed onto the solution at -196 °C and the obtained emulsion is warmed to room temperature over a period of two hours. All volatile compounds are condensed into a second flask. The yield of Me_3SiCF_3 (69 %) is determined using ^{19}F NMR spectroscopy by adding 1,3-bis(trifluoromethyl)benzene (247 mg, 1.15 mmol). The precipitated solid **[3H]Cl** is dissolved in 20 mL of a methanol / water mixture (7 : 3) and passed three times through a strongly basic anion exchange resin (50 mL resin in 50 mL of MeOH / H_2O, Ion Exchanger III, 0.9 mol/L, Merck KGaA), after every run, the column is washed with additional 10 mL of MeOH / H_2O (7 : 3). The solvent of the combined fractions is removed under reduced pressure. The resulting solid residue is dried in high vacuum at 70 to 100 °C. Phosphazene **3** (5.30 g, 5.98 mmol, 98 %) is regenerated as a colorless solid. The purity is confirmed by ^1H and ^{31}P NMR spectroscopy (C_6D_6 as a solvent).

^{19}F NMR (*n*-hexane, rt): δ [ppm] = -67.7 (s, $^1J_{CF}$ = 320 Hz, $^2J_{SiF}$ = 40 Hz, CF_3).

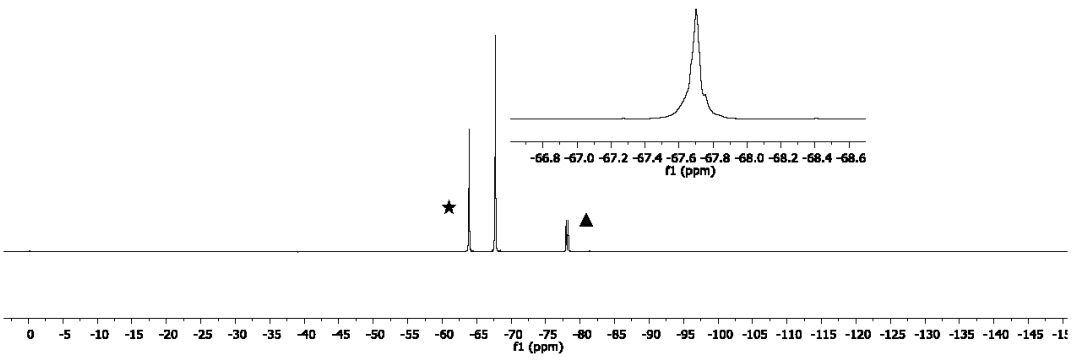

Figure 10. ^{19}F NMR spectrum of Me_3SiCF_3 generated in *n*-hexane (lock with acetone-d_6 in a capillary, 1,3-bis(trifluoromethyl)benzene as a standard). ★ 1,3-bis(trifluoromethyl)benzene, ▲ HCF_3.

Table 1. Regeneration of **3** with basic anion exchange resin.

Reaction[a]	**3**[b]	Me_3SiCF_3[c]	Recovery of **3**
1	6.08 mmol	69 %	98 %
2	5.79 mmol	74 %	98 %
3	5.57 mmol	75 %	100 %

[a] *n*-hexane, -196 °C to rt, 2 h. [b] Used quantity of **3**. [c] Yield determined via ^{19}F NMR spectroscopy using 1,3-bis(trifluoromethyl)benzene as standard, lock with acetone-d_6 in a capillary.

1.3.7 Synthesis of $Me_3SiC_2F_5$

In a flame-dried flask equipped with a Young valve a sample of **3** (4.84 g, 5.46 mmol) is dissolved in 25 mL of *n*-hexane and the solution is degassed three times. Pentafluoroethane (27.3 mmol) is condensed onto the solution at -196 °C and the mixture is allowed to melt for mixing. Me_3SiCl (5.82 mmol, 632 mg) is condensed onto the solution at -196 °C and the formed emulsion is allowed to warm to room temperature over a period of two hours. All volatile compounds are condensed into a second flask. The yield of $Me_3SiC_2F_5$ (61 %) is determined using ^{19}F NMR spectroscopy by adding 1,3-bis(trifluoromethyl)benzene (176 mg, 0.82 mmol).
^{19}F NMR (*n*-hexane, rt): δ [ppm] = -131.9 (s, $^1J_{CF}$ = 271 Hz, $^2J_{SiF}$ = 26 Hz, CF_2), -82.4 (s, $^1J_{CF}$ = 284 Hz, $^3J_{SiF}$ = 40 Hz, CF_3).

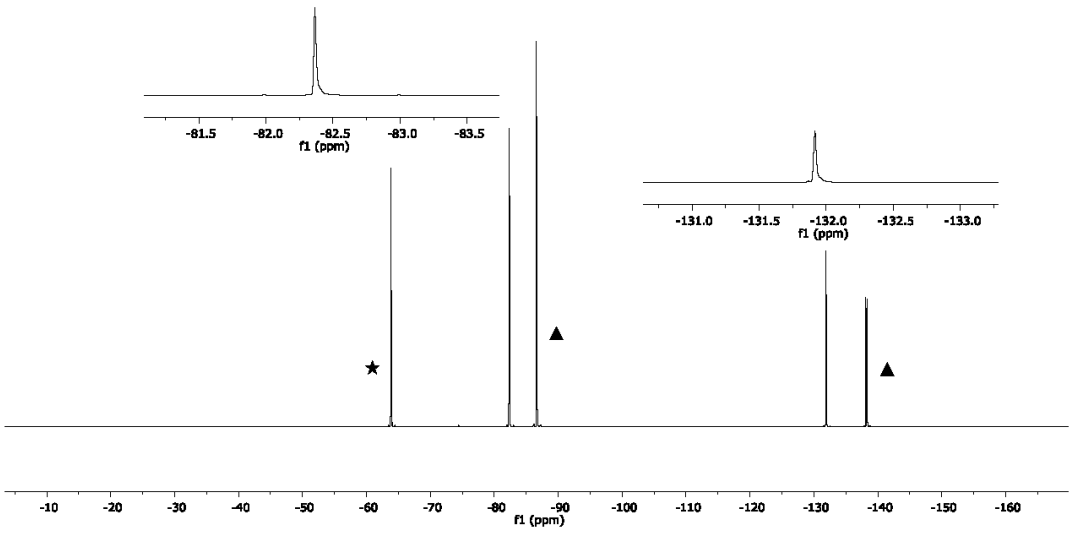

Figure 11. ^{19}F NMR spectrum of $Me_3SiC_2F_5$ generated in *n*-hexane (lock with acetone-d_6 in a capillary, 1,3-bis(trifluoromethyl)benzene as a standard). ★ 1,3-bis(trifluoromethyl)benzene, ▲ HC_2F_5.

1.4 Details on the X-Ray Diffraction

The crystal data were collected on a Rigaku Supernova diffractometer using graphite-monochromated Mo-K_α radiation (λ = 71.073 pm) or Cu-K_α radiation (λ = 154.184 pm) at 100.0(2) K.

Using Olex2[2], the structures were solved with the ShelXS[3] structure solution program using direct methods and refined with the ShelXL[4] refinement package using least squares minimization.

[3H]Cl showed a disorder of one ethyl group (C11/C12) over two sites (55:45)

[3H][OH(OH$_2$)$_3$] showed a disorder of two ethyl-groups (C33, C34, C35, C36) over two sites (82:18). The anion is disordered with the same ratio. N4 is protonated. All hydrogen atoms bonded at nitrogen or oxygen were refined isotropically, the ones in the major occupied part of the disordered anion with fixed O-H distances and H…H distances inside the water molecules. The hydrogen atoms of the minor part were neglected, but they were included in the sum formula for further calculations. An additional 1:1 disorder of one oxygen atom of the minor occupied part was modelled having in mind that the complete minor occupied part of the anion is most unreliable. The positions of the hydrogen atoms of the major occupied disorder of the anion can not be refined freely because some of the positions are disturbed by electron density of the minor occupied part. The small Uiso value of the hydrogen atom of the hydroxide reflects the high electron density inside this anion. Because of the separating of the hydroxide trihydrate anions by the weak coordinating cation only the half of the hydrogen atoms of the solvent water molecules are involved in hydrogen bonds. Details of the X-ray investigation are given in Table 2. CCDC 1938109 – 1938111 contain the supplementary crystallographic data for this paper. These data can be obtained free of charge via http://www.ccdc.cam.ac.uk/conts/retrieving.html.

Table 2. Structure refinement data of **[3H]Cl**, **3** and **[3H][OH(OH$_2$)$_3$]**.

compound	**[3H]Cl**	**3**	**[3H][OH(OH$_2$)$_3$]**
Crystallographic Section			
empirical formula	$C_{40}H_{100}ClN_{13}P_4$	$C_{40}H_{99}N_{13}P_4$	$C_{40}H_{107}N_{13}O_4P_4$
a / pm	1260.86(2)	2231.95(4)	1103.99(3)
b / pm	2370.47(5)	1930.14(3)	2582.00(7)
c / pm	1767.13(3)	2437.55(4)	1969.22(7)
β	98.4343(17)	90	98.631(3)
V / 10^6 pm^3	5224.54(16)	10500.9(3)	5549.7(3)
Z	4	8	4
ρ_{calc} / mg·mm^{-3}	1.173	1.121	1.147
crystal system	Monoclinic	orthorhombic	monoclinic
space group	*Cc*	*Pbca*	*P*2$_1$/*n*
color shape	Colorless prisms	Colorless block	Colorless block
crystal size / mm^{-3}	0.23 × 0.14 × 0.05	0.37 × 0.18 × 0.06	0.44 × 0.19 × 0.13
Data collection			
μ / mm^{-1}	0.237	1.633	0.184
F(000)	2032.0	3920.0	2120
2θ range for data col. / °	3.4 to 60.1°	7.1 to 144.3°	3.2 to 60.3
index ranges	-17 ≤ *h* ≤ 17 -33 ≤ *k* ≤ 33 -24 ≤ *l* ≤ 24	-27 ≤ *h* ≤ 25 -23 ≤ *k* ≤ 16 -30 ≤ *l* ≤ 29	-14 ≤ *h* ≤ 15 -28 ≤ *k* ≤ 35 -26 ≤ *l* ≤ 26
reflections col.	37747	30476	51246
independent refl.	14863	10324	14683
R(int)	0.0376	0.0282	0.0367
data/restraints/ parameter	14863/2/568	10324/0/535	14683/7/637
goodness-of-fit on F^2	1.025	1.034	1.061
R_1 / wR_2 [I>2σ(I)]	0.0384/0.0802	0.0435/0.1170	0.0465/0.1093
R_1 / wR_2 (all data)	0.0458/0.0834	0.0494/0.1226	0.0676/0.1205
$\Delta\rho_{max/min}$ / e Å^{-3}	0.38/-0.36	0.78/-0.36	0.63/-0.45
Flack parameter	0.02(2)	n/a	n/a
CCDC number	1938109	1938110	1938111

2 References

[1] Matthew Monroe, *Molecular Weight Calculator*, **2012**.

[2] O. V. Dolomanov, L. J. Bourhis, R. J. Gildea, J. A. K. Howard, H. Puschmann, *J. Appl. Cryst.* **2009**, *42*, 339.

[3] G. M. Sheldrick, *Acta Cryst. A* **2015**, *71*, 3.

[4] G. M. Sheldrick, *Acta Cryst. C* **2015**, *71*, 3.

Anhang 2

Synthesis and Reactivity of the First Isolated Hydrogen Bridged Silanol-Silanolate Anions

Robin F. Weitkamp, Beate Neumann, Hans-Georg Stammler and Berthold Hoge

Angew. Chem. **2020**, *132*, 5536; *Angew. Chem. Int. Ed. Engl.* **2020**, *59*, 5494.

Anhang

Silicon Compounds

International Edition: DOI: 10.1002/anie.201914339
German Edition: DOI: 10.1002/ange.201914339

Synthesis and Reactivity of the First Isolated Hydrogen-Bridged Silanol–Silanolate Anions

*Robin F. Weitkamp, Beate Neumann, Hans-Georg Stammler, and Berthold Hoge**

Dedicated to Prof. Dr. Reinhold Tacke on the occasion of his 70th birthday

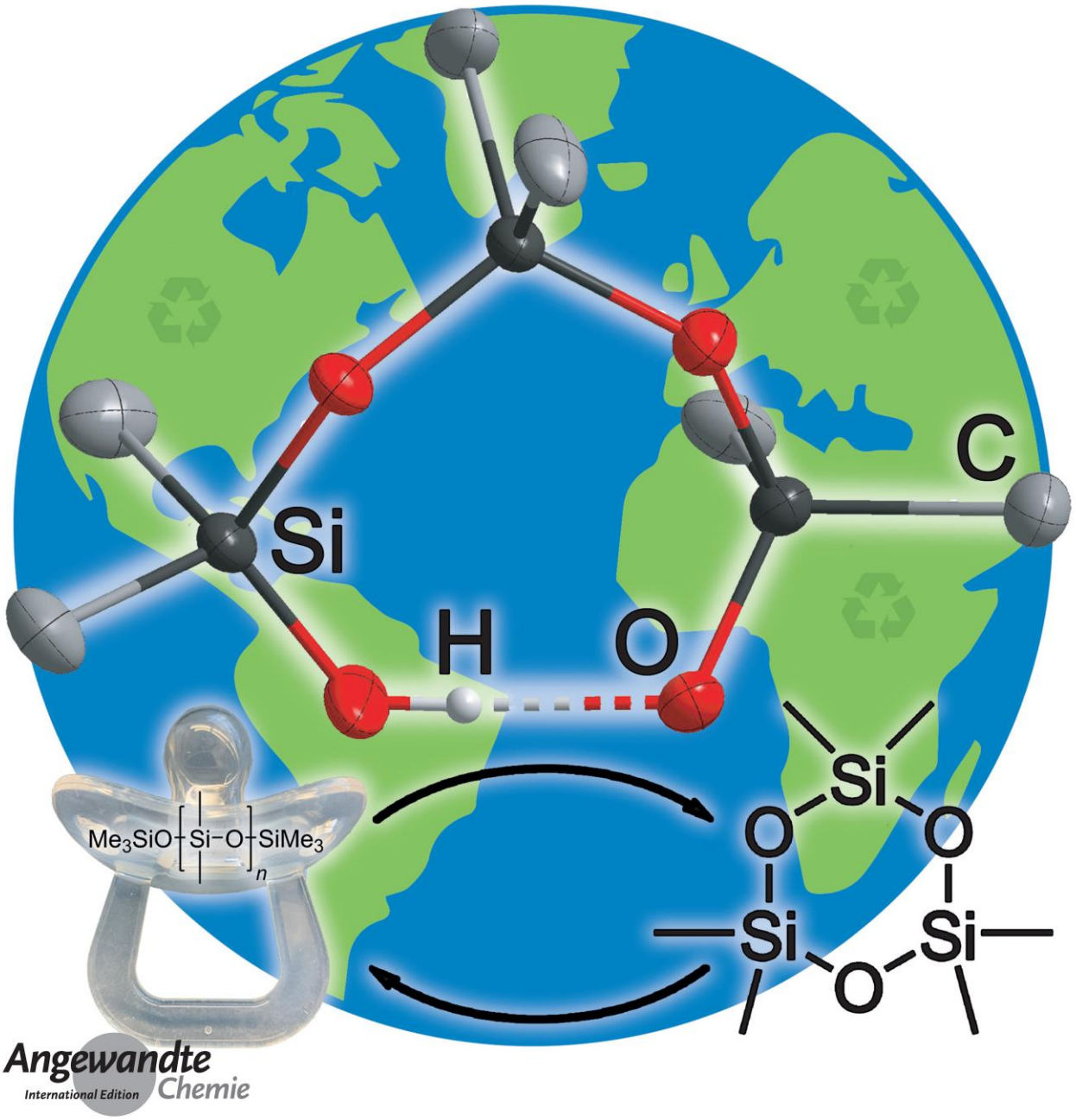

Abstract: *We report on the first examples of isolated silanol–silanolate anions, obtained by utilizing weakly coordinating phosphazenium counterions. The silanolate anions were synthesized from the recently published phosphazenium hydroxide hydrate salt with siloxanes. The silanol–silanolate anions are postulated intermediates in the hydroxide-mediated polymerization of aryl and alkyl siloxanes. The silanolate anions are strong nucleophiles because of the weakly coordinating character of the phosphazenium cation, which is perceptible in their activity in polysiloxane depolymerization.*

Silicones constitute the passage between organic and inorganic polymers with outstanding chemical and physical properties and are of broad scientific and industrial interest.[1,2] Linear polydimethylsiloxanes with repeating difunctional (D) units are mostly employed as materials in the modern silicone industry and are largely synthesized by hydrolysis of dimethylchlorosilanes from the Müller–Rochow process (Scheme 1).[2–5]

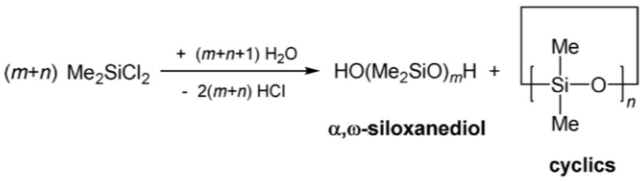

Scheme 1. Industrial synthesis of silicones.[4]

The intermediately formed α,ω-siloxanediols eliminate water under formation of the final silicones or cyclic siloxanes like octamethylcyclotetrasiloxane (D_4). The latter can be converted into linear polysiloxanes by ionic ring-opening polymerization reactions.[2–6]

Silanols as well as silanediols are valuable building blocks in synthetical chemistry and exhibit a distinct tendency to form hydrogen-bridge networks.[7–15] The formation of coordination adducts of silanols with oxygen- and nitrogen-containing bases, which form more readily than the corresponding alcohol adducts,[8,11] and their utilization for selective guest–host complexation of alcohols and amines emphasize this behavior.[9,12,16] In the same way, the related α,ω-siloxanediols, $HO[SiR_2O]_nH$, form inter- and intramolecular hydrogen bonds that often result in the formation of ring structures (Scheme 2).[13–15]

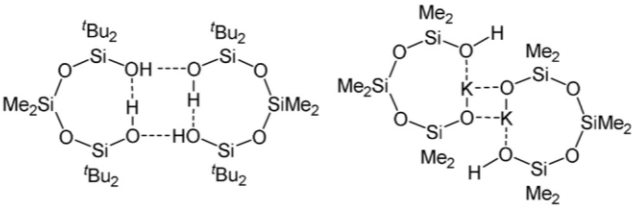

Scheme 2. Examples of eight-membered siloxane rings.[10,14,17]

In the case of the monopotassium silanolate salt (Scheme 2, right), it is noteworthy that the potassium cation interaction with the silanolate as well as the silanol oxygen atom is favored with respect to the formation of an intramolecular hydrogen bond, which correspondingly leads to a ring containing the potassium ion.

Anionic silanolates can be synthesized by cleavage of siloxanes with strong bases.[18] A subsequent treatment of α,ω-siloxanediolates with metal halides or alkoxides leads to a broad class of cyclic metallacyclosiloxanes, in which a ring expansion is commonly observed.[19] Sullivan et al. investigated this ring expansion in more detail and treated salts of the tetraphenyldisiloxanediolate anion, $[O(SiPh_2O)_2]^{2-}$, with metal halides under several reaction conditions, which resulted in the formation of six- and eight-membered metallacyclosiloxanes.[20] Although the reaction mechanism has not been completely elucidated, the formation of eight-membered siloxane rings via repeated rearrangements of Si–O bonds seems thermodynamically favorable.

Regarding the chemical robustness of silicones in nature, their multi-ton production causes serious waste disposal problems. The degradation of siloxanes under formation of cyclic derivatives is of general interest because it forms the basis of a possible recycling of widely used silicone plastics.

The depolymerization of silicones can be achieved under acidic, basic, and fluorinating conditions, leading to low-molecular cyclic siloxanes or organosilyl fluorides, which can be converted into new silicone plastics afterwards.[21,22] Known processes for the depolymerization of silicones utilize metal hydroxides such as KOH but require elevated temperatures. A pronounced interaction between the potassium cation and the silanolate anion and therefore a reduced nucleophilicity may be considered as a reasonable explanation for the relatively low conversion rate.

Recently, we reported the synthesis of the phosphazenium hydroxide salt [**1**H][$OH(OH_2)_n$] (**2**; Scheme 3), which exhibits pronounced reactivity due to the weakly coordinating character of the phosphazenium ion.[23]

In the following work, the reaction of the hydroxide salt **2** with siloxanes and polysiloxanes was in the focus of our interest in order to examine the nature of silanolate anions that do not show direct contact to the counterion and to investigate their application as a depolymerization catalyst for polysiloxanes.

[*] M. Sc. R. F. Weitkamp, B. Neumann, Dr. H.-G. Stammler, Prof. Dr. B. Hoge
Centrum für Molekulare Materialien
Fakultät für Chemie, Universität Bielefeld
Universitätsstraße 25, 33615 Bielefeld (Germany)
E-mail: b.hoge@uni-bielefeld.de

Supporting information and the ORCID identification number(s) for the author(s) of this article can be found under: https://doi.org/10.1002/anie.201914339.

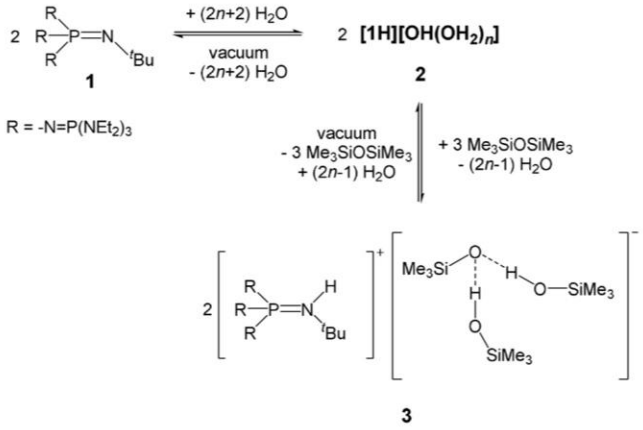

Scheme 3. Equilibrium reaction of phosphazene **1**, hydroxide salt **2**, and silanol–silanolate salt **3**.

The reactions of **2** with siloxane species were carried out in *n*-hexane as a nonpolar solvent, which was chosen because of the fast decomposition of **1** and **2** in H-acidic, even C–H-acidic, solvents and the beneficial precipitation of ionic products.[24]

A mixture of equimolar quantities of phosphazene **1** and hexamethyldisiloxane showed no reaction. The hydroxide salt **2** was generated by the addition of one equivalent of water to the mixture. Hydroxide salt **2** precipitates as an amorphous colorless solid, which is rapidly consumed to yield a slightly yellowish second phase. The obtained crystalline product **3**, which was isolated from the cooled reaction mixture and analyzed by single-crystal X-ray diffraction (Figure 1), features a silanolate anion that is bonded to two silanol molecules.[25] To increase the yield of **3**, the run was repeated accordingly with the appropriate stoichiometry of the reactants (Scheme 3).[24]

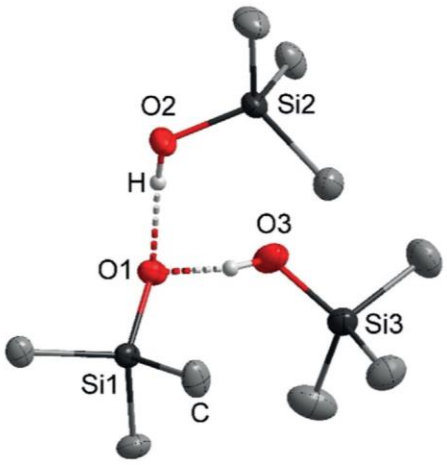

Figure 1. Molecular structure of the silanolate anion in **3**. The phosphazenium cation and minor occupied disordered atoms are not shown. Thermal ellipsoids set at 50% probability. The hydrogen atoms of the methyl groups are omitted for clarity. Selected bond lengths [pm] and angles [°]: O1–O2 258.2(1), O1–O3 252.4(5), O1–Si1 159.9(1), O2–Si2 162.4(1), O3–Si3 161.8(3); Si1-O1-O2 118.0(1), Si1-O1-O3 124.6(1), O2-O1-O3 102.7(2).[25]

Compound **3** is the first example of an isolated silanol–silanolate anion that is not in direct contact with any counterion. O3 is disordered at two positions with a ratio of 79:21 and shows the shortest distances to C37 with 331.5(4) and 329.0(1) ppm; both distances are longer than the sum of the van der Waals radii. The donor hydrogen atom is disordered as well, and bonded to O1 or O3. Both positions were refined isotropically, but restrained to have the same O–H distances.

Compared to the O–O distances of the hydrogen bridges in the triphenylsilanol pyrrolidine complex of Strohmann and co-workers (249.1, 270.1, 283.3 pm),[12] the hydrogen bridges in the anion of salt **3** exhibit an O1–O2 distance of 258.2(1) pm and an O1–O3 distance of 252.4(5) pm.

As already stated for the strongly basic compounds **1** and **2**, silanolate salt **3** undergoes rapid decomposition in H- and C–H-acidic solvents and requires handling in chlorobenzene solution. A ^{31}P and $^{29}Si\{^1H\}$ NMR spectroscopic investigation of the dissolved product **3** indicated the presence of the protonated phosphazene **[1H]**$^+$ and also a reformation of $Me_3SiOSiMe_3$, which points to the equilibrium reaction shown in Scheme 3. The signal in the $^{29}Si\{^1H\}$ NMR spectrum at $\delta = -8.6$ ppm was attributed to the silicon atoms of the silanolate anion in **3**. As observed for the hydroxide hydrate salt **2**, silanolate salt **3** decomposes in vacuum by the deprotonation of its cation **[1H]**$^+$ and liberation of silanol and disiloxane.[23] This observation is further evidence for the equilibrium reaction between hydroxide **2** and the silanolate anion in **3** (Scheme 3). This situation hampers a reliable elemental analysis of salt **3**. By this route, the synthesis of a "naked" trimethylsilanolate anion in the presence of the phosphazenium ion **[1H]**$^+$ is not possible.

In the following, phosphazene **1** was combined with a small excess of hexamethylcyclotrisiloxane (D_3). After the addition of water, the reaction with the in situ generated hydroxide produced a second phase. In the upper phase, a mixture of cyclic compounds, mainly D_4 and D_5 and traces of D_3, were detected by ^1H–^{29}Si HMBC NMR spectroscopy. This result clearly underlines the existence of a fast equilibrium between cyclic species, whose interconversion is catalyzed by **2**. The initial ring-opening reaction is presented in Scheme 4. ^{31}P NMR spectroscopic analysis confirmed that there are no phosphorus species in the upper phase.

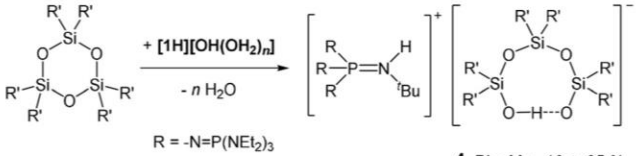

4 R' = Me 16 g, 95 %
5 R' = Ph 3 g, 96 %

Scheme 4. Reaction of cyclotrisiloxanes with in situ generated phosphazenium hydroxide.

Upon cooling the reaction mixture to −28 °C, colorless crystals of silanolate salt **4** were obtained in an excellent yield of 95 %. X-ray crystallographic analysis[25] revealed a cyclic silanol–silanolate anion of the type $[D_3OH]^-$ in **4**, which forms

an intramolecular hydrogen bridge in the solid state (Figure 2). An elemental analysis underlined the selective formation of compound **4** in high yields (Scheme 4; calcd: C 49.04, H 10.65, N 16.16, P 11.00, Si 7.48; found: C 48.61, H 10.64, N 15.89, P 10.98, Si 7.59).

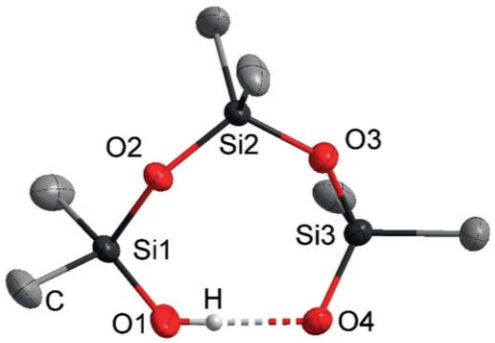

Figure 2. Molecular structure of the $[D_3OH]^-$ anion in **4**. The phosphazenium cation is not shown. Thermal ellipsoids set at 50% probability. The donor hydrogen atom is disordered in a ratio of 1:1, bonded to O1 or O4, but only one is shown. The hydrogen atoms of the methyl groups are omitted for clarity. Selected bond lengths [pm] and angles [°]: O1–O4 242.8(2), O1–Si1 157.9(2), O4–Si3 158.9(1), O2–Si2 161.8(1), O2–Si1 165.8(1); O4-O1-Si1 124.4(1), O1-O4-Si3 113.2(1), O2-Si2-O3 112.7(1).[25]

The oxygen atoms are well separated from the phosphazenium cation. The shortest distance of 304.4(2) pm is observed between O1 and C31. The disordered donor hydrogen atom was refined isotropically at two positions with a ratio of 1:1; both were restrained to have the same distances to oxygen atoms O1 and O4, respectively.

Based on potentiometric titrations of siloxanes, the thermodynamically favored eight-membered-ring structure was already proposed by Baney and Atkari in 1967.[26] The O1–O4 distance was determined to be 242.8(2) pm and points to strong hydrogen bonding.[27] The O4–Si3 and O1–Si1 bond lengths range from 157.8(2) to 158.9(1) pm and are slightly shortened in comparison to the eight-membered siloxane ring D_4 (Si-O distances from 164 to 166 pm).[28]

The O-H-O vibration mode of **4** could not be determined in the IR analysis. The ^{1}H NMR spectrum in C_6D_6 displayed a broad singlet at $\delta = 14.0$ ppm, which was assigned to the proton involved in the hydrogen bridging. In the ^{29}Si-{^{1}H} NMR spectrum of **4** the signal for the silicon atoms adjacent to the hydrogen bridge was observed at $\delta = -23.9$ ppm.

Compound **4** is also accessible from the treatment of D_4 or D_5 with the phosphazenium hydroxide, as evident by NMR and X-ray analysis. The reaction of **2** with equimolar quantities of D_5 afforded compound **4** in a 85% yield. A plausible reaction pathway mirrors a series of equilibria and confirms the high thermodynamic stability of the hydrogen-bridged eight-membered ring.

Silanolate salt **4** begins to decompose slowly at 90 °C in vacuo, with fast decomposition above 100 °C. The volatile products were identified by GC-MS analysis as water and cyclic siloxanes, with D_4 as the main component. A ^{31}P NMR spectroscopic investigation of the residue revealed the free phosphazene **1**, and the decomposition route is thus similar to that of hydroxide hydrate **2**.

The reaction of in situ generated phosphazenium hydroxide with hexaphenylcyclotrisiloxane in diethyl ether as a solvent results in the clean formation of the analogous $[D^{Ph2}{}_3OH]^-$ anion in salt **5**, which was isolated in excellent yield (> 96%; Scheme 4). Single crystals of **5** were obtained from a cooled reaction mixture (−28 °C) and were subjected to X-ray crystallography (Figure 3).[25]

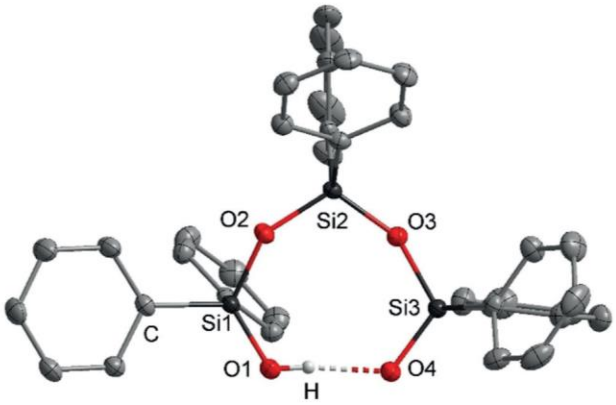

Figure 3. Molecular structure of the $[D^{Ph2}{}_3OH]^-$ anion in **5**. The phosphazenium cation is not shown. Thermal ellipsoids set at 50% probability. The donor hydrogen atom is disordered in a ratio of 1:1, bonded to O1 or O4, but only one is shown. The hydrogen atoms of the phenyl groups are omitted for clarity. Selected bond lengths [pm] and angles [°]: O1–O4 242.9(2), O1–Si1 158.4(1), O4–Si3 157.8(1), O2–Si1 164.9(1), O2–Si2 162.1(1); O1-O4-Si3 125.1(1), O4-O1-Si1 119.0(1), O2-Si2-O3 112.3(1).[25]

The disordered donor hydrogen atom was refined isotropically at two positions with a ratio of 1:1; both were restrained to have the same distances to the oxygen atoms O1 and O4, respectively. The O1–O4 distance of 242.9(2) ppm shows the same value as in **4**. Analogously to compound **4**, the O-H-O vibration mode of salt **5** could not be determined by IR analysis.

Because of the weakly coordinating nature of the phosphazenium counterion, the hydroxide hydrate anion in **2**, as well as the silanolate anions in **3**, **4**, and **5** exhibit increased nucleophilicity. This was exemplary shown for silanolate salt **4** in the depolymerization reaction of a polydimethylsiloxane with terminal trimethylsilyl groups (Scheme 5).

The increased nucleophilicity of the silanolate oxygen atom is accompanied by a fast equilibrium reaction, which is distinguished by back-biting and end-biting processes.[22]

The equilibrium activity can be determined by the temporal quantity of cyclic siloxane species, which are removed from the siloxane mixture by distillation. The silanolate salt **4** was applied in a concentration of 0.1 mol%. Salt **4** showed poor solubility at room temperature and remained present as fine colorless particles. Nevertheless,

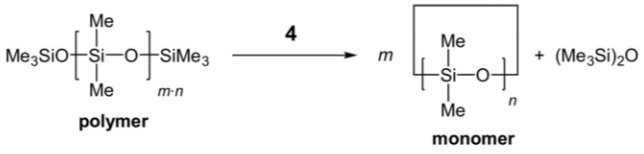

T / °C	p / mbar	distillation speed / mLh^{-1}	composition of the crude distillate / %			
			$(Me_3Si)_2O$	D_3	D_4	D_5
rt	0.001	3.1(2)	8	2	82	8
90	7	24.7(19)	6	6	79	9

Scheme 5. Depolymerization of trimethylsilyl-end-blocked polydimethylsiloxanes employing silanolate salt **4** (see also Tables S1–S3).[24]

cyclic siloxane species and hexamethyldisiloxane were formed and entirely removed in vacuum (0.001 mbar) with an average rate of 3.1(2) mL h^{-1}.[24] After completion of this process, catalyst **4** was regained as a colorless solid devoid of any traces of decomposition. The obtained distillate consisted mainly of D_4 (82 %) as well as D_5 (8 %) and traces of D_3 (2 %; see the Supporting Information, Table S2).[24] Trimethylsiloxane species (8 %) were isolated as well.

As industrial processes are preferably run at higher temperatures and higher pressures, we also mimicked these conditions by applying a membrane pump vacuum (7 mbar) and a temperature of 90 °C. Under these conditions, a clear solution of **4** in silicone oil was formed, whereby the averaged distillation rate of volatiles was determined to be 24.7(19) mL h^{-1}. The average composition of the distillate does not significantly differ from that of the run at room temperature (Scheme 5). In comparison to the results in sodium (0 mL h^{-1}) or potassium hydroxide (< 1 mL h^{-1}) mediated depolymerizations with concentrations of 11 mol % carried out at 90 °C, compound **4** showed a significantly enhanced equilibrium activity (Table S1 in the Supporting Information).[24]

In conclusion, we have reported on the first three silanol–silanolate anions in the condensed phase, which were synthesized by the reaction of the in situ generated hydroxide hydrate anion $[OH(OH_2)_n]^-$ in **2** in the presence of the weakly coordinating phosphazenium cation **[1H]**$^+$. The silanolate anions are not in contact with the counterion, and the $[D_3OH]^-$ salt **4** and the $[D^{Ph2}{}_3OH]^-$ salt **5** show only intramolecular hydrogen bonding. Similar to the hydroxide hydrate salt **2**, trimethylsilanolate salt **3** decomposes in vacuum. An NMR spectroscopic investigation provided evidence for an equilibrium reaction of hydroxide salt **2** and silanolate salt **3**. The salts [**1**H][D_3OH] (**4**) and [**1**H][$D^{Ph2}{}_3$OH] (**5**) were synthesized in excellent yields of over 95 % and structurally characterized.

The increased nucleophilicity of the silanolate anion in salt **4** was used to perform a fast solvent-free depolymerization of polydimethylsiloxanes into cyclic siloxanes. Under identical reaction conditions, the catalytic activity of silanolate **4** was significantly higher than that of sodium and potassium hydroxide.

Acknowledgements

We acknowledge Prof. Dr. Lothar Weber, Dr. Julia Bader, and Dr. Markus Wiesemann for helpful discussions.

Conflict of interest

The authors declare no conflict of interest.

Keywords: phosphazene · silanolates · silicone · siloxanes · weakly coordinating cations

How to cite: *Angew. Chem. Int. Ed.* **2020**, *59*, 5494–5499
Angew. Chem. **2020**, *132*, 5536–5541

[1] a) W. Noll, *Angew. Chem.* **1954**, *66*, 41; b) S. J. Clarson, *ACS Symp. Ser.* **2003**, *838*, 1.
[2] S. J. Clarson, J. A. Semlyen, *Siloxane polymers*, Prentice Hall, Englewood Cliffs, NJ, **1993**.
[3] a) J. Ackermann, V. Damrath, *Chem. Unserer Zeit* **1989**, *23*, 86; b) A. J. O'Lenick, Jr., *Silicone Spectator* **2009**, 1; c) *ACS Symposium Series* (Eds.: S. J. Clarson, J. J. Fitzgerald, M. J. Owen, S. D. Smith, M. E. van Dyke), American Chemical Society, Washington, DC, **2003**; d) R. Schliebs, J. Ackermann, *Chem. Unserer Zeit* **1987**, *21*, 121–127.
[4] *Silicon-Containing Polymers. The Science and Technology of Their Synthesis and Applications* (Eds.: R. G. Jones, W. Ando, J. Chojnowski), Springer, Dordrecht, **2000**.
[5] R. Corriu, P. Jutzi, *Tailor-made silicon-oxygen compounds. From molecules to materials*, Vieweg, Braunschweig/Wiesbaden, **1996**.
[6] a) D. T. Hurd, R. C. Osthoff, M. L. Corrin, *J. Am. Chem. Soc.* **1954**, *76*, 249; b) A. Purkayastha, J. B. Baruah, *Appl. Organomet. Chem.* **2004**, *18*, 166; c) A. Molenberg, M. Möller, *Macromol. Rapid Commun.* **1995**, *16*, 449; d) P. C. Hupfield, R. G. Taylor, *J. Inorg. Organomet. Polym.* **1999**, *9*, 17–34; e) T. Pietzonka, D. Seebach, *Angew. Chem. Int. Ed. Engl.* **1993**, *32*, 716–717; *Angew. Chem.* **1993**, *105*, 741–742.
[7] a) H. Kriegsmann, *Z. Anorg. Allg. Chem.* **1958**, *294*, 6145; b) S. Grabowsky, M. F. Hesse, C. Paulmann, P. Luger, J. Beckmann, *Inorg. Chem.* **2009**, *48*, 4384; c) L. King, A. C. Sullivan, *Coord. Chem. Rev.* **1999**, *189*, 19; d) U. Klingebiel, *Angew. Chem. Int. Ed. Engl.* **1981**, *20*, 678; *Angew. Chem.* **1981**, *93*, 696; e) A. Bleiber, J. Sauer, *Chem. Phys. Lett.* **1995**, *238*, 243; f) V. Chandrasekhar, R. Boomishankar, S. Nagendran, *Chem. Rev.* **2004**, *104*, 5847; g) C. Reiche, S. Kliem, U. Klingebiel, M. Noltemeyer, C. Voit, R. Herbst-Irmer, S. Schmatz, *J. Organomet. Chem.* **2003**, *667*, 24; h) U. Klingebiel, P. Neugebauer, I. Müller, M. Noltemeyer, I. Usón, *Eur. J. Inorg. Chem.* **2002**, 717; i) K. Durka, M. Urban, M. Czub, M. Dąbrowski, P. Tomaszewski, S. Luliński, *Dalton Trans.* **2018**, *47*, 3705; j) J. Beckmann, A. Duthie, G. Reeske, M. Schürmann, *Organometallics* **2004**, *23*, 4630.
[8] R. West, R. H. Baney, *J. Am. Chem. Soc.* **1959**, *81*, 6145.
[9] W. Clegg, G. M. Sheldrick, U. Klingebiel, D. Bentmann, *Acta Crystallogr. Sect. C* **1984**, *40*, 819.
[10] P. Jutzi, U. Schubert, *Silicon chemistry. From the atom to extended systems*, Wiley-VCH, Weinheim, **2003**.
[11] H. Schmidbaur, *Chem. Ber.* **1964**, *97*, 830.
[12] J. O. Bauer, C. Strohmann, *J. Organomet. Chem.* **2015**, *797*, 52.
[13] H. Behbehani, B. J. Brisdon, M. F. Mahon, K. C. Molloy, M. Mazhar, *J. Organomet. Chem.* **1993**, *463*, 41.
[14] O. Graalmann, U. Klingebiel, W. Clegg, M. Haase, G. M. Sheldrick, *Chem. Ber.* **1984**, *117*, 2988.

[15] S. T. Malinovskii, A. Tesuro Vallina, H. Stoeckli-Evans, *J. Struct. Chem.* **2006**, *47*, 1127.
[16] a) S. A. Bourne, L. R. Nassimbeni, K. Skobridis, E. Weber, *J. Chem. Soc. Chem. Commun.* **1991**, 282; b) S. A. Bourne, L. Johnson, C. Marais, L. R. Nassimbeni, E. Weber, K. Skobridis, F. Toda, *J. Chem. Soc. Perkin Trans. 2* **1991**, 1707; c) A. E. Goeta, S. E. Lawrence, M. M. Meehan, A. O'Dowd, T. R. Spalding, *Polyhedron* **2002**, *21*, 1689; d) E. Weber, W. Seichter, K. Skobridis, D. Alivertis, V. Theodorou, P. Bombicz, I. Csöregh, *J. Inclusion Phenom. Macrocyclic Chem.* **2006**, *55*, 131; e) C. R. Hilliard, S. Kharel, K. J. Cluff, N. Bhuvanesh, J. A. Gladysz, J. Blümel, *Chem. Eur. J.* **2014**, *20*, 17292; f) D. Marappan, M. Palanisamy, K. Velappan, N. Muthukumaran, P. Ganesan, *Inorg. Chem. Commun.* **2018**, *92*, 101.
[17] B. Laermann, M. Lazell, M. Motevalli, A. C. Sullivan, *J. Chem. Soc. Dalton Trans.* **1997**, 1263.
[18] S. M. Sieburth, W. Mu, *J. Org. Chem.* **1993**, *58*, 7584.
[19] a) V. Lorenz, A. Fischer, K. Jacob, W. Brüser, T. Gelbrich, P. G. Jones, F. T. Edelmann, *Chem. Commun.* **1998**, 2217; b) D. Hoebbel, M. Nacken, H. Schmidt, V. Huch, M. Veith, *J. Mater. Chem.* **1998**, *8*, 171; c) B. J. Brisdon, M. F. Mahon, C. C. Rainford, *J. Chem. Soc. Dalton Trans.* **1998**, 3295; d) R. Murugavel, V. S. Shete, K. Baheti, P. Davis, *J. Organomet. Chem.* **2001**, *625*, 195; e) Y. K. Gun′ko, R. Reilly, V. G. Kessler, *New J. Chem.* **2001**, *25*, 528; f) R. N. Kapoor, F. Cervantes-Lee, C. F. Campana, C. Haltiwanger, K. Abney, K. H. Pannell, *Inorg. Chem.* **2006**, *45*, 2203; g) M. Veith, H. Vogelgesang, V. Huch, *Organometallics* **2002**, *21*, 380.
[20] a) M. A. Hossain, M. B. Hursthouse, A. Ibrahim, M. Mazid, A. C. Sullivan, *J. Chem. Soc. Dalton Trans.* **1989**, 2347; b) I. Abrahams, M. Motevalli, S. A. A. Shah, A. C. Sullivan, *J. Organomet. Chem.* **1995**, *492*, 99; c) M. Lazell, M. Motevalli, S. A. A. Shah, C. K. S. Simon, A. C. Sullivan, *J. Chem. Soc. Dalton Trans.* **1996**, 1449; d) M. Motevalli, D. Shah, S. A. A. Shah, A. C. Sullivan, *J. Chem. Soc. Chem. Commun.* **1994**, 2427.
[21] a) T. W. Greenlee, US005110972A, **1991**; b) Y. Ikeda, W. Huang, A. Oku, *Green Chem.* **2003**, *5*, 508; c) M. R. Alexander, F. S. Mair, R. G. Pritchard, J. E. Warren, *Appl. Organomet. Chem.* **2003**, *17*, 730; d) P. Döhlert, S. Enthaler, *J. Appl. Polym. Sci.* **2015**, *132*, 1–7; e) P. Döhlert, S. Enthaler, *Catal. Lett.* **2016**, *146*, 345; f) O. Farooq, *J. Organomet. Chem.* **2000**, *613*, 239; g) M. Okamoto, S. Suzuki, E. Suzuki, *Appl. Catal. A* **2004**, *261*, 239.
[22] A. Oku, W. Huang, Y. Ikeda, *Polymer* **2002**, *43*, 7289.
[23] R. F. Weitkamp, B. Neumann, H.-G. Stammler, B. Hoge, *Angew. Chem. Int. Ed.* **2019**, *58*, 14633; *Angew. Chem.* **2019**, *131*, 14775.
[24] Details are given in the Supporting Information.
[25] Details of the X-ray investigation are given in Table S4 of the Supporting Information. CCDC 1952715, 1952716, 1952717 contain the supplementary crystallographic data for this paper. These data can be obtained free of charge from The Cambridge Crystallographic Data Centre.
[26] R. H. Baney, F. S. Atkari, *J. Organomet. Chem.* **1967**, *9*, 183.
[27] A. Bondi, *J. Phys. Chem.* **1964**, *68*, 441.
[28] H. Steinfink, B. Post, I. Fankuchen, *Acta Crystallogr.* **1955**, *8*, 420.

Manuscript received: November 10, 2019
Revised manuscript received: November 29, 2019
Accepted manuscript online: December 13, 2019
Version of record online: February 11, 2020

Angewandte Chemie
Eine Zeitschrift der Gesellschaft Deutscher Chemiker

Supporting Information

Synthesis and Reactivity of the First Isolated Hydrogen-Bridged Silanol–Silanolate Anions

*Robin F. Weitkamp, Beate Neumann, Hans-Georg Stammler, and Berthold Hoge**

anie_201914339_sm_miscellaneous_information.pdf

1. Experimental Section

1.1 General Part

All chemicals were obtained from commercial sources and used without further purification. Standard high-vacuum techniques were employed throughout all experiments. Non-volatile compounds were handled in a dry N_2 atmosphere using Schlenk techniques.

1.2 Analysis Methods

1.2.1 NMR Spectroscopy

NMR spectra were recorded on a Bruker Model Avance III 300 spectrometer (^{1}H 300.13 MHz; ^{13}C 75.47 MHz; ^{29}Si 59.63 MHz; ^{31}P 121.49 MHz) or on a Bruker Avance III 500 HD spectrometer (^{1}H 500.20 MHz; ^{13}C 125.79 MHz; ^{29}Si 99.38 MHz; ^{31}P 202.48 MHz). Positive shifts are downfield from the external standards TMS (^{1}H, ^{13}C, ^{29}Si) and H_3PO_4 (^{31}P). The NMR spectra were recorded in the indicated deuterated solvent or in relation to acetone-d_6 filled capillaries.

1.2.2 IR Spectroscopy

IR spectra were recorded on an ALPHA-FT-IR spectrometer (Bruker) using an ATR unit with a diamond crystal for liquids and solids.

1.2.3 Elemental Analyses

Elemental analyses were performed by Mikroanalytisches Laboratorium Kolbe (Oberhausen, Germany). The elemental analysis of [1H][$D^{Ph2}{}_3$OH] (**5**) was accomplished in the element-analytical laboratory of the Universität Bielefeld using the EURO EA Element Analyzer 2010 (HEKAtech GmbH).

1.2.4 Melting Point

Melting points were measured on a Mettler Toledo Mp70 Melting Point System.

1.3 Syntheses

1.3.1 Generation of [1H][$Me_3SiO(HOSiMe_3)_2$] (3)

Phosphazene **1** (2.50 g, 2.82 mmol) and hexamethyldisiloxane (0.69 g, 4.24 mmol) are diluted in 10 mL of *n*-hexane, and water (80 mg, 4.44 mmol) is added to form a two-phase system. The reaction mixture is stirred for 9 hours and then cooled in a fridge overnight. The supernatant is removed via a syringe. By adding *n*-pentane (10 mL) and cooling of the resulting emulsion in a fridge, small yellowish crystals were obtained.

^{1}H NMR (C_6H_5Cl, rt): δ [ppm] = -0.3 (s, hexamethyldisiloxane), 0.1 (s, Me_3SiO/OH), 0.6 (t, $^3J_{HH}$ = 7 Hz, 54 H, CH_3), 0.8 (s, 9 H, $C(CH_3)_3$), 1.5 (d, $^2J_{PH}$ = 8 Hz, 1 H, NH), 2.5 (dq, $^3J_{PH}$ = 10 Hz, $^3J_{HH}$ = 7 Hz, 36 H, CH_2), 8.5 (s, 1 H, OH).
$^{13}C\{^1H\}$ NMR (C_6H_5Cl, rt): δ [ppm] = 4.1 (s, Me_3SiO-/OH), 12.8 (d, $^3J_{PC}$ = 4 Hz, CH_3), 30.9 (d, $^3J_{PC}$ = 5 Hz, $C(\mathbf{C}H_3)_3$), 38.5 (d, $^2J_{PC}$ = 6 Hz, CH_2), 50.0 (d, $^2J_{PC}$ = 4 Hz, $\mathbf{C}(CH_3)_3$).
$^{29}Si\{^1H\}$IG NMR (C_6H_5Cl, rt): δ [ppm] = -8.6 (Me_3SiO/OH).
^{31}P NMR (C_6H_5Cl, rt): δ [ppm] = -34.4 (q, d, $^2J_{PP}$ = 70 Hz, $^2J_{PH}$ = 8 Hz, 1 P, P=NH), 6.8 (d, tridec, $^2J_{PP}$ = 70 Hz, $^3J_{PH}$ = 10 Hz, 3 P, $(Et_2N)_3P$).
IR (ATR): $\tilde{\nu}$ [cm^{-1}] = 3383 (vw), 2966 (w), 2935 (vw), 2872 (vw), 1641 (vw), 1463 (vw), 1378 (w), 1351 (w), 1270 (m), 1202 (m), 1174 (vs), 1107 (w), 1054 (w), 1017 (vs), 940 (s), 844 (w), 784 (s), 740 (w), 700 (m), 614 (w), 508 (s), 440 (m).

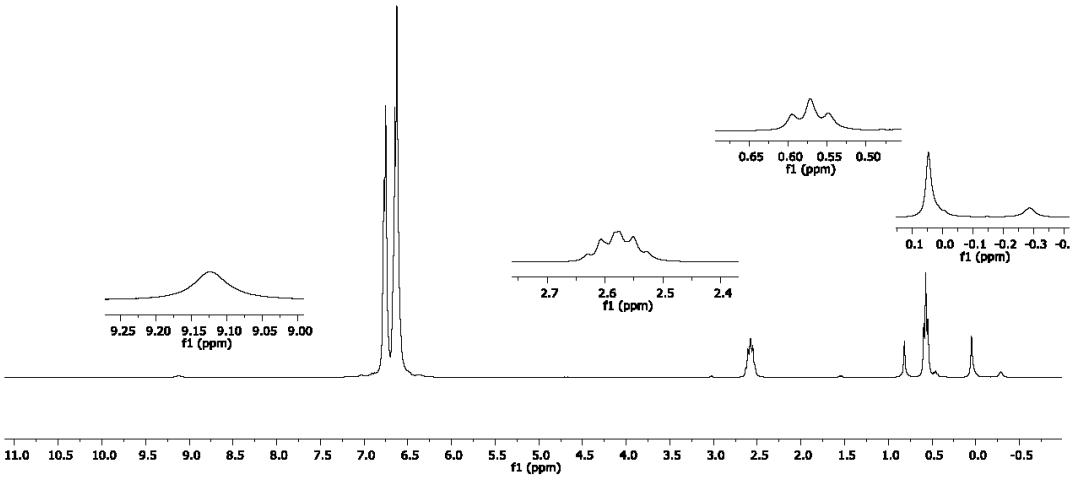

Figure 1. ^{1}H NMR spectrum of **3** in chlorobenzene (lock with acetone-d_6 in a capillary) (300 MHz).

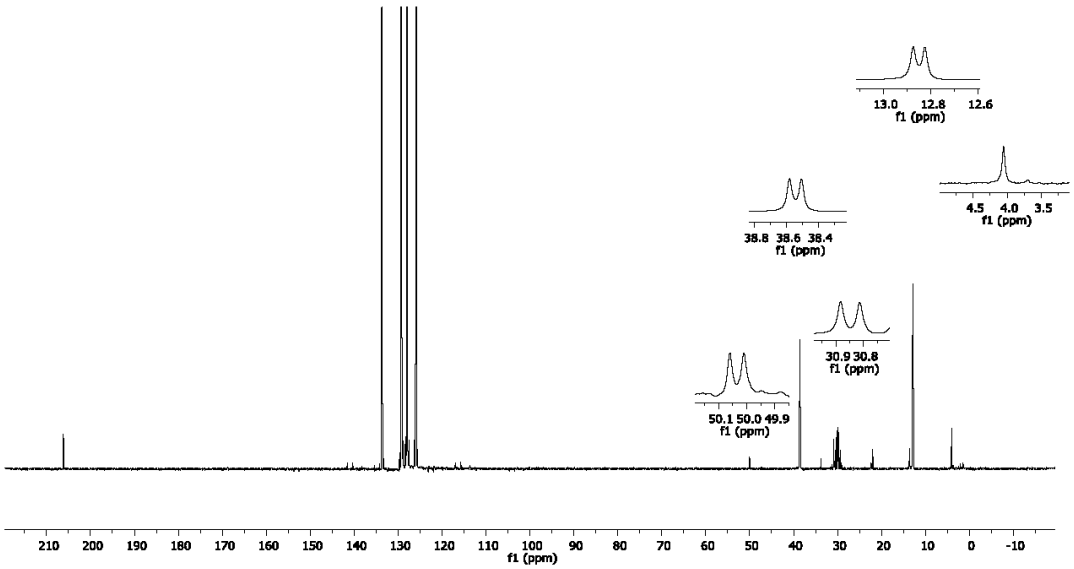

Figure 2. $^{13}C\{^{1}H\}$ NMR spectrum of **3** in chlorobenzene (lock with acetone-d_6 in a capillary) (300 MHz).

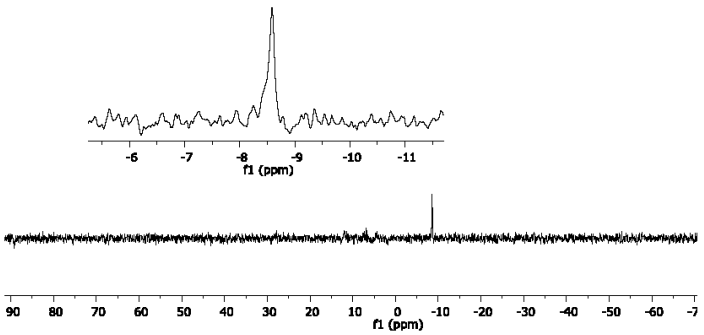

Figure 3. $^{29}Si\{^{1}H\}IG$ NMR spectrum of **3** in chlorobenzene (lock with acetone-d_6 in a capillary) (300 MHz).

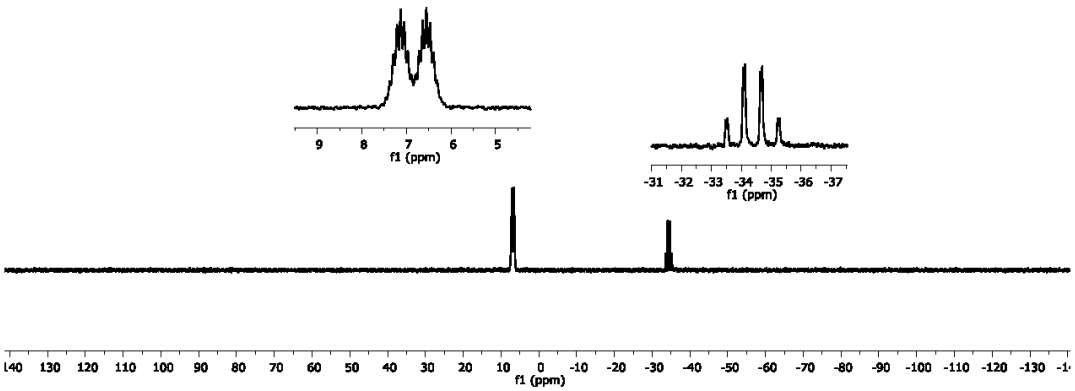

Figure 4. ^{31}P NMR spectrum of **3** in chlorobenzene (lock with acetone-d_6 in a capillary) (300 MHz).

1.3.2 Synthesis of [1H][D$_3$OH] (4)

Phosphazene **1** (13.69 g, 15.45 mmol) is dissolved in 45 mL of *n*-hexane before hexamethylcyclotrisiloxane (3.44 g, 15.45 mmol) is added. After addition of water (0.29 g, 15.45 mmol) two phases separated. After stirring at room temperature overnight, a pale yellow solid precipitates. The supernatant solution is removed via a syringe and the solid is dried in high vacuum (10^{-3} mbar). The product (16.46 g, 14.61 mmol, 95 % based on **3**) is obtained as a colorless crystalline solid (m.p. 99-101 °C).

^{1}H NMR (C_6D_6, rt): δ [ppm] = 0.6 (s, 7 H, SiO(H_3C)$_2$SiOSi), 0.7 (s, 11 H, (H_3C)$_2$SiO), 1.0 (t, $^{3}J_{HH}$ = 7 Hz, 54 H, CH_3), 1.3 (s, 9 H, C(CH_3)$_3$), 2.1 (d, $^{2}J_{PH}$ = 8 Hz, 1 H, NH), 3.0 (d, q, $^{3}J_{PH}$ = 10 Hz, $^{3}J_{HH}$ = 7 Hz, 36 H, CH_2), 14.0 (s, OH).
^{13}C{^{1}H} NMR (C_6D_6, rt): δ [ppm] = 2.3 (s, SiO(H_3C)$_2$SiOSi), 3.6 (s, (H_3C)$_2$SiOH-OSi(CH_3)$_2$), 13.4 (d, $^{3}J_{PC}$ = 4 Hz, CH_3), 31.3 (d, $^{3}J_{PC}$ = 5 Hz, C(**C**H_3)$_3$), 39.0 (d, $^{2}J_{PC}$ = 6 Hz, CH_2), 50.4 (d, $^{2}J_{PC}$ = 4 Hz, **C**(CH_3)$_3$).
^{29}Si{^{1}H}dept30 NMR (C_6D_6, rt): δ [ppm] = -24.1 (s, SiO(H_3C)$_2$**Si**OSi), -23.9 (s, (H_3C)$_2$SiOH-OSi(CH_3)$_2$).
^{31}P NMR (C_6D_6, rt): δ [ppm] = -33.7 (q, d, $^{2}J_{PP}$ = 70 Hz, $^{2}J_{PH}$ = 8 Hz, 1 P, P=NH), 7.6 (d, tridec, $^{2}J_{PP}$ = 70 Hz, $^{3}J_{PH}$ = 10 Hz, 3 P, (Et_2N)$_3$P).
IR (ATR): $\tilde{\nu}$ [cm^{-1}] = 2966 (vw), 2872 (vw), 1627 (vw, vbr), 1464 (vw), 1379 (w), 1351 (w), 1273 (m, br), 1247 (m), 1202 (m), 1175 (s), 1053 (w), 1016 (vs), 940 (vs), 847 (w), 784 (vs), 700 (m), 614 (w), 508 (m), 440 (m).
elemental analysis of $C_{46}H_{119}N_{13}O_4P_4Si_3$ (M = 1126.7 g/mol): calcd.: C 49.04, H 10.65, N 16.16, P 11.00, Si 7.48; found: C 48.61, H 10.64, N 15.89, P 10.98, Si 7.59.

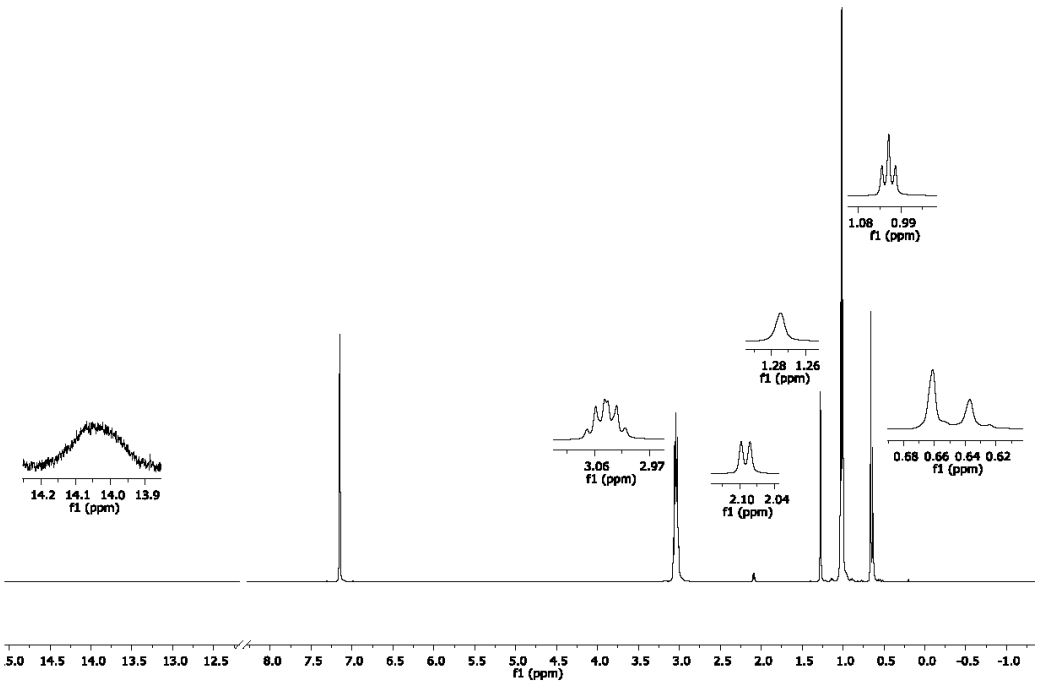

Figure 5. ^{1}H NMR spectrum of **4** in benzene-d_6 (500 MHz).

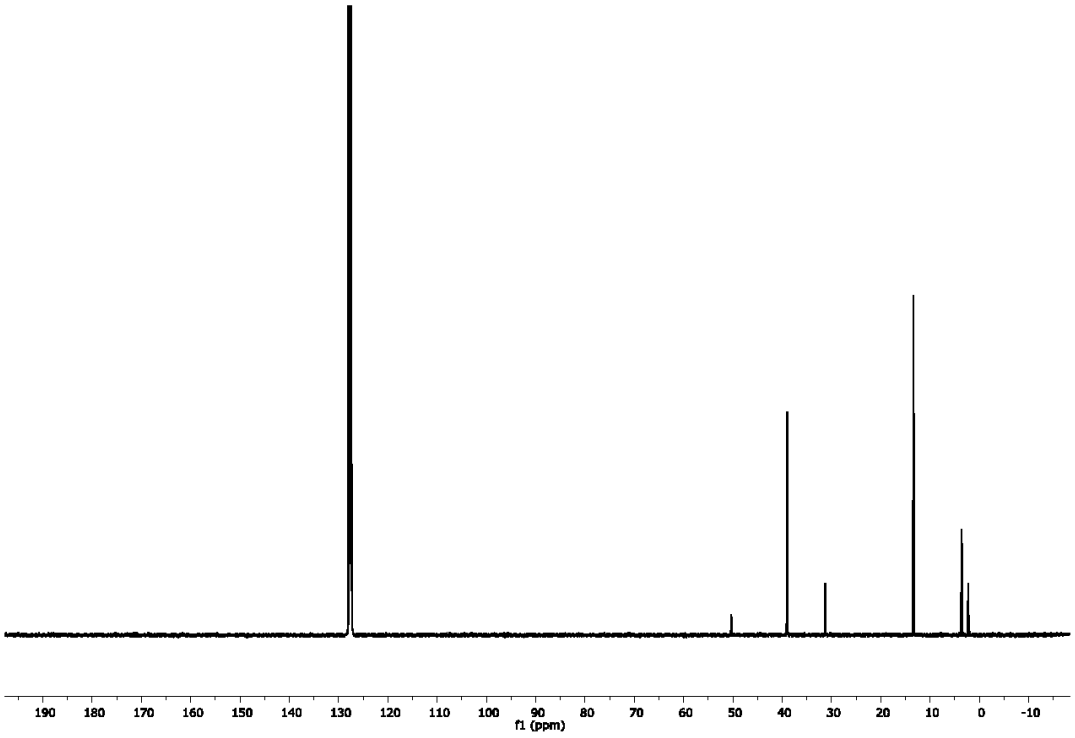

Figure 6. $^{13}C\{^{1}H\}$ NMR spectrum of **4** in benzene-d_6 (500 MHz).

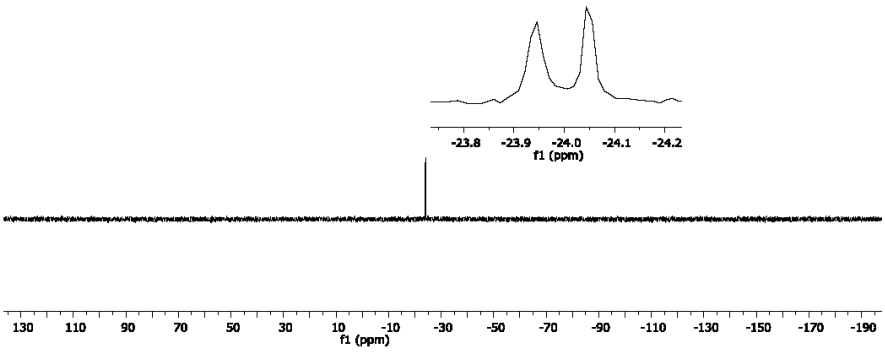

Figure 7. $^{29}Si\{^{1}H\}$dept30 NMR spectrum of **4** in benzene-d_6 (500 MHz).

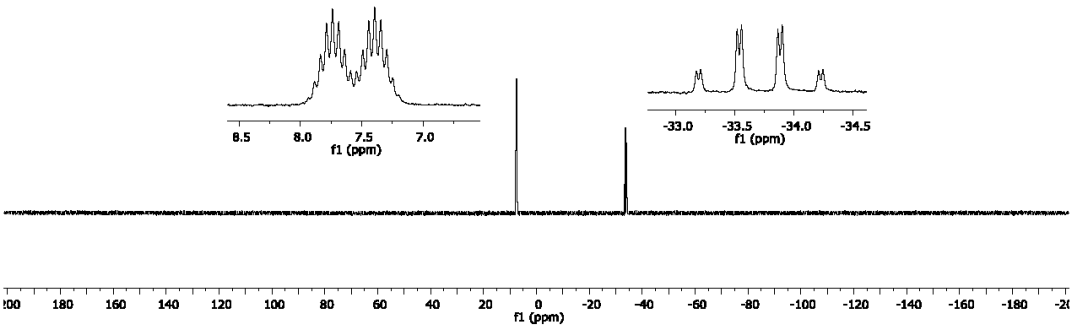

Figure 8. ^{31}P NMR spectrum of **4** in benzene-d_6 (500 MHz).

1.3.3 Synthesis of [1H][D^{Ph2}$_3$OH] (5)

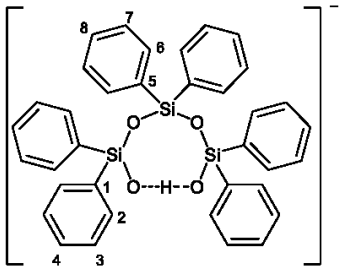

To a solution of **1** (1.69 g, 1.90 mmol) in 10 mL of diethylether hexaphenylcyclotrisiloxane (1.13 g, 1.90 mmol) and water (46 mg, 2.55 mmol) are added. After one hour of stirring, the solution was kept at -28 °C overnight. The solvent is removed and the product (2.74 g, 1.82 mmol, 96 % based on **3**) is isolated as a colorless crystalline solid (m.p. 113-115 °C).

^{1}H NMR (C_6D_6, rt): δ [ppm] = 0.9 (t, $^{3}J_{HH}$ = 7 Hz, 54 H, CH_3), 1.2 (s, 9 H, $C(CH_3)_3$), 2.0 (d, $^{2}J_{PH}$ = 8 Hz, 1 H, NH), 3.0 (d,q, $^{3}J_{PH}$ = 10 Hz, $^{3}J_{HH}$ = 7 Hz, 36 H, CH_2), 7.1 (m), 7.3 (m), 8.1 (m), 8.3 (m), 16.1 (s, br, SiOH).

^{13}C{^{1}H} NMR (C_6D_6, rt): δ [ppm] = 13.3 (d, $^{3}J_{PC}$ = 4 Hz, CH_3), 31.2 (d, $^{3}J_{PC}$ = 5 Hz, $C(\mathbf{C}H_3)_3$), 38.9 (d, $^{2}J_{PC}$ = 5 Hz, CH_2), 50.3 (d, $^{2}J_{PC}$ = 4 Hz, $\mathbf{C}(CH_3)_3$), 126.7 (s, C3), 127.0 (s, C7), 128.2 (s, C4/C8), 128.3 (s, C4/C8), 135.2 (s, C6), 135.5 (s, C2), 139.3 (s, C5), 143.8 (s, C1).

^{29}Si{^{1}H}IG NMR (C_6D_6, rt): δ [ppm] = -46.1 (s, 1 Si, $SiOPh_2\mathbf{Si}OSi$), -43.8 (s, 2 Si, $Ph_2\mathbf{Si}OH\text{-}O\mathbf{Si}Ph_2$).

^{31}P NMR (C_6D_6, rt): δ [ppm] = -34.2 (q, d, $^{2}J_{PP}$ = 70 Hz, $^{2}J_{PH}$ = 8 Hz, 1 P, P=NH), 6.9 (d, tridec, $^{2}J_{PP}$ = 70 Hz, $^{3}J_{PH}$ = 10 Hz, 3 P, $(Et_2N)_3P$).

IR (ATR): $\tilde{\nu}$ [cm^{-1}] = 2969 (vw), 2926 (vw), 2863 (vw), 1464 (vw), 1425 (w), 1379 (w), 1348 (w), 1288 (w), 1264 (m), 1226 (w), 1202 (m), 1173 (s), 1114 (m), 1101 (m), 1074 (m), 1058 (m), 1019 (s), 942 (m), 919 (w), 845 (w), 793 (m), 740 (m), 697 (vs), 657 (m), 613 (m), 590 (w), 579 (w), 523 (vs), 493 (vs), 462 (s), 442 (vs), 434 (vs), 406 (vs).

elemental analysis of $C_{76}H_{131}N_{13}O_4P_4Si_3$ (M = 1499.1 g/mol): calcd.: C 60.89, H 8.81, N 12.15; found: C 60.23, H 8.93, N 12.06.

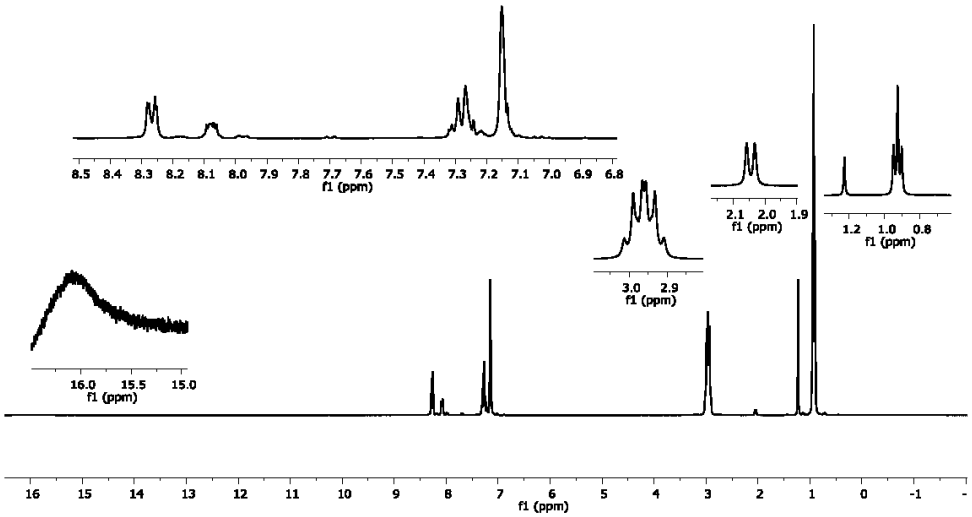

Figure 9. ^{1}H NMR spectrum of **5** in benzene-d_6 (300 MHz).

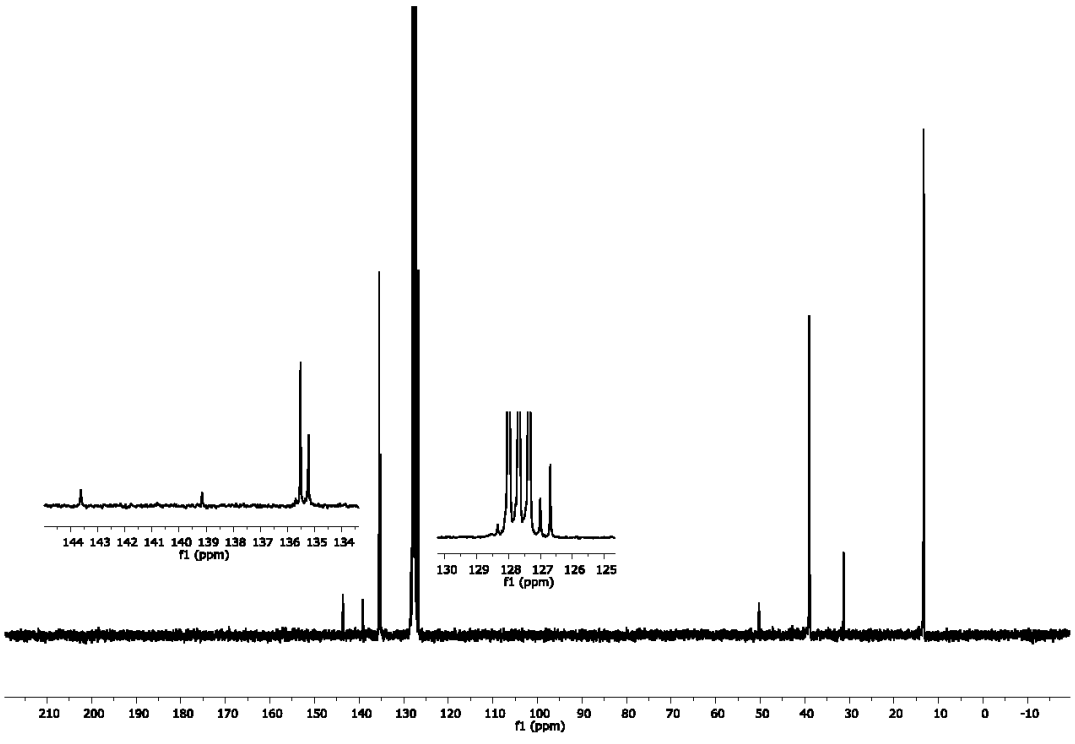

Figure 10. $^{13}C\{^{1}H\}$ NMR spectrum of **5** in benzene-d_6 (300 MHz).

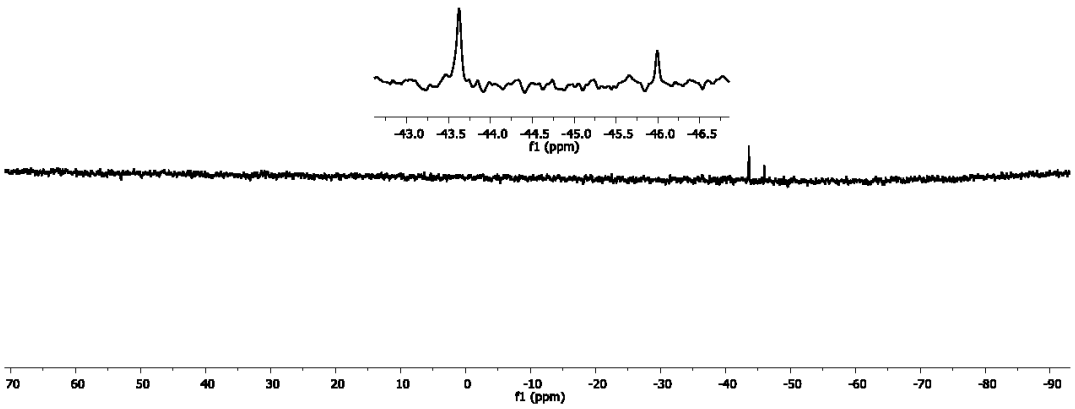

Figure 11. $^{29}Si\{^{1}H\}IG$ NMR spectrum of **5** in benzene-d_6 (300 MHz).

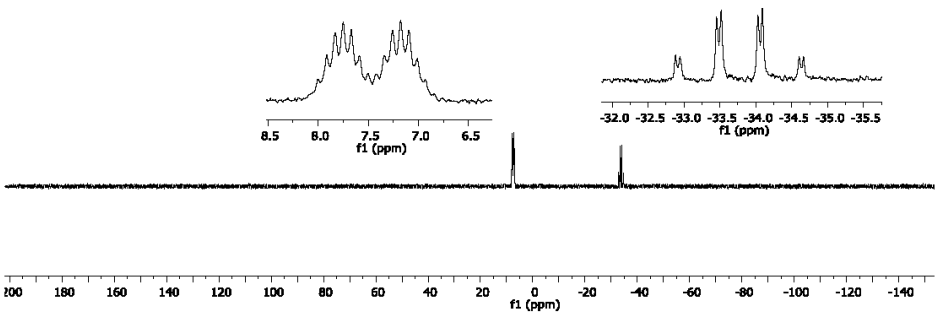

Figure 12. ^{31}P NMR spectrum of **5** in benzene-d_6 (300 MHz).

1.4 Depolymerization reactions of polydimethylsiloxane

In a 250 mL Young flask pure silicon oil (110 g, 1.48 mol, polydimethylsiloxane, Roth Siliconöl M 200, Art.-Nr. 4030.1) is charged with catalyst **4** (1.68 g, 1.49 mmol, 0.1 mol%). Under stirring at room temperature the vessel is evacuated to 0.001 mbar. Thereby generated cyclic products are collected in a cold trap. The distillation speed was determined by weighing the amount of the crude distillate in dependence of time (Figure 13). After complete removal of volatile compounds, catalyst **4** remains as residue.

Afterwards the flask with catalyst **4** is refilled with silicone oil. The temperature is raised to 90 °C and the pressure is raised to 7 mbar. The cooling trap is exchanged by a graduated flask and the distillation speed (Figure 13) is volumetrically determined, by using the first distillation flashover as starting point. The catalyst was reused by adding further amounts of silicone oil after complete turnover. A small amount of silicone oil is kept in the flask to prevent the slow thermolysis of pure catalyst **4**, which is not observed at room temperature. The results are graphically shown in Figure 13.

The collected data were confirmed by an additional depolymerization run at room temperature (0.001 mbar) and two additional runs at 90 °C (7 mbar) with a given amount of polydimethylsiloxane and load of catalyst **4** (results in Tables 1 - 3).

For the comparison with alkali hydroxides as a catalyst, potassium and sodium hydroxide were used as a catalyst for the depolymerization reactions, as shown in Table 1, using identical conditions (90 °C, 7 mbar) for the comparison with catalyst **4**.

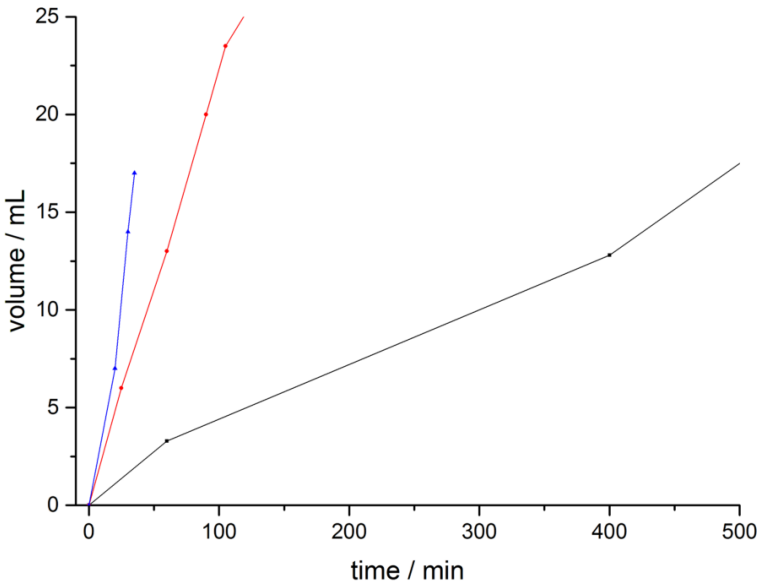

Figure 13. Depolymerization of silicone oil and distillation of cyclic species using **4** as a catalyst. Black: first run, 0.001 mbar, rt. Red: second run, 90 °C, 7 mbar. Blue: third run, 90 °C, 7 mbar.

Table 1. Silanolate salt **[1H][D$_3$OH]** (**4**) as a catalyst for the depolymerisation of trimethylsilyl endblocked polydimethylsiloxane.

catalyst	**molar ratio / mol% [cat./(Si-O)-unit]**	**T / °C**	**p / mbar**	**distillation speed / mLh^{-1}[c]**
4[a]	0.1	rt	0.001	3.1(2)
	0.1	90	7	24.7(19)
KOH[1][a]	13	90	7	< 1
KOH[1][b]	2	90	7	0
NaOH[b]	13	90	7	0

[a] Used as solid. [b] Used as aqueous solution. [c] Averaged distillation speed.

Table 2. Composition of the collected volatile compounds of two depolymerisations of polydimethylsiloxane (Roth Siliconöl M 200, Art.-Nr. 4030.1) at room temperature and a pressure of 0.001 mbar employing **[1H][D$_3$OH]** (**4**) as a catalyst. D_3, D_4 and D_5 mean hexamethylcyclotrisiloxane, octamethylcyclotetrasiloxane and decamethylcyclopentasiloxane.

Silicon compound	Yield / %[a]	Yield / %[a]	Average yield / %
Me_3SiOH / $(Me_3Si)_2O$	11	6	8
D_3	2	2	2
D_4	80	83	82
D_5	7	9	8

[a] Determined via $^{29}Si\{^1H\}IG$ NMR spectroscopy.

Table 3. Composition of the collected volatile compounds of two depolymerisations of polydimethylsiloxane (Roth Siliconöl M 200, Art.-Nr. 4030.1) at 90 °C and a pressure of 7 mbar employing **[1H][D$_3$OH]** (**4**) as a catalyst. D_3, D_4 and D_5 mean hexamethylcyclotrisiloxane, octamethylcyclotetrasiloxane and decamethylcyclopentasiloxane.

Silicon compound	Yield / %[a]	Yield / %[a]	Average yield / %
Me_3SiOH / $(Me_3Si)_2O$	5	6	6
D_3	7	6	6
D_4	79	79	79
D_5	9	9	9

[a] Determined via $^{29}Si\{^{1}H\}IG$ NMR spectroscopy.

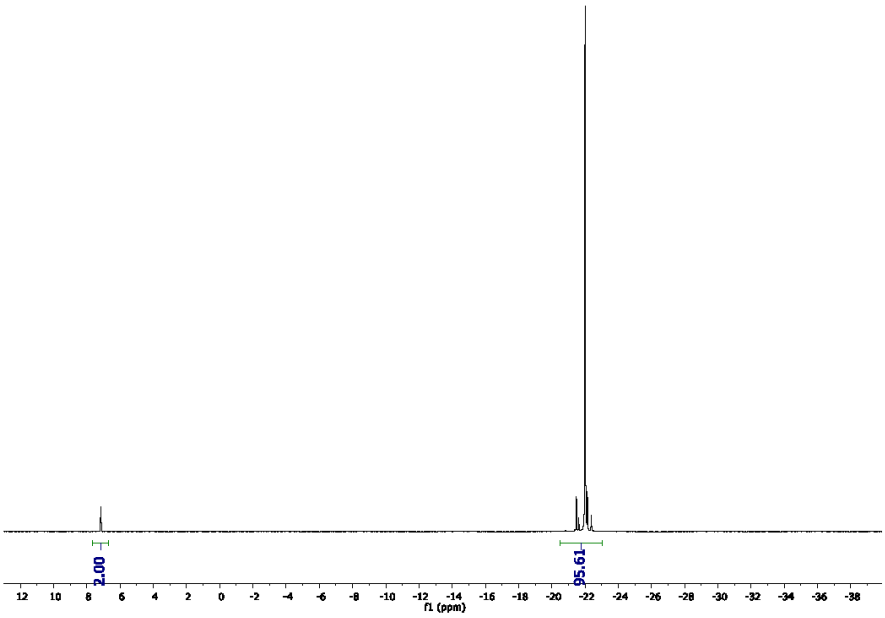

Figure 14. $^{29}Si\{^{1}H\}$dept30 NMR spectrum of trimethylsilyl endblocked polydimethylsiloxane (Roth Siliconöl M 200, Art.-Nr. 4030.1) in chloroform-d_1 (500 MHz).

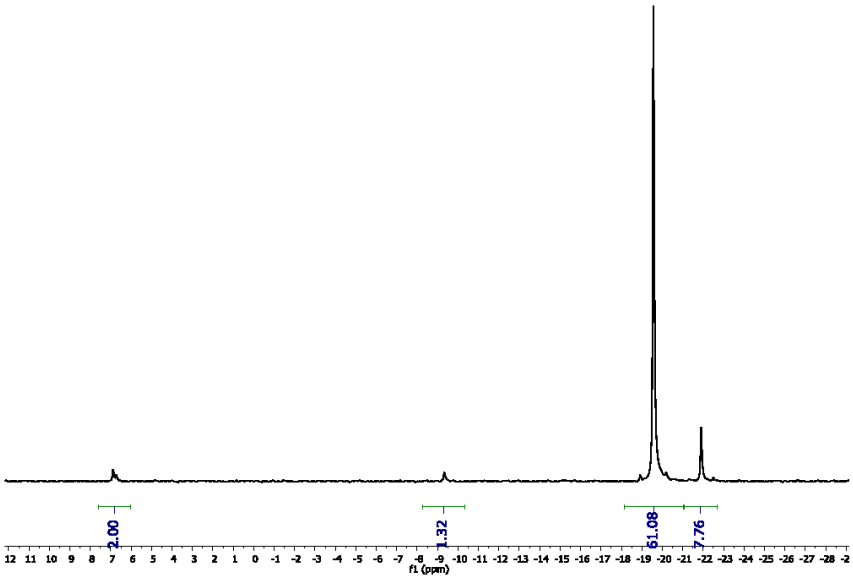

Figure 15. $^{29}Si\{^{1}H\}IG$ NMR spectrum of the crude distillate of a depolymerization reaction at room temperature and 0.001 mbar using trimethylsilyl endblocked polydimethylsiloxane and **4** as a catalyst (lock with acetone-d_6 in a capillary) (300 MHz).

1.5 Details on the X-Ray Diffraction

The crystal data were collected on a Rigaku Supernova diffractometer (Cu-K_α radiation (λ = 154.184 pm) at 100.0(2) K).

Using Olex2[2], the structures were solved with the ShelXS[3] structure solution program using direct methods and refined with the ShelXL[4] refinement package using least squares minimization.

In **3** the ratio of disorder of O3A-HA and O3B...HB was refined to 79(2):21(2).

The distances O3A-HA and O1-HB were restrained to be same.

The adp's of O3A and O3B were constrained to be same.

In **4** N13, C35-C38 are disordered in a ratio of 94:6, the minor occupied atoms were restrained using "ISOR 0.001 0.002". The P4-N13 and P4-N13B distances were restrained to be same as well as the distances O1-HA and O4-HB. The ratio of HA:HB was refined to 506(6):494(6). Using a model without this disorder, the U_{eq} value of this hydrogen atom becomes unreasonably large and the R-values increase slightly.

The crystal of **5** was a non-merohedrical twin, with component 2 rotated by 180.0° [0.02 1.00 -0.05] (reciprocal) or [0.01 1.00 -0.04] (direct). Three ethyl groups (C63, C64, C65, C66 and C68) were disordered with a ratio of 78:22. Hydrogen atoms were taken into account using a riding model; only donor hydrogen atoms, i.e. HA, HB and H1, were refined isotropically. HA and HB were disordered, a ratio of 1:1 was assumed. The distances O1-HA and O4-HB were restrained to be same.

Details of the X-ray investigation are given in Table 3. CCDC 1952715 – 1952717 contain the supplementary crystallographic data for this paper. These data can be obtained free of charge via http://www.ccdc.cam.ac.uk/conts/retrieving.html.

Table 4. Structure refinement data of **[1H][$Me_3SiO(HOSiMe_3)_2$]** (**3**), **[1H][D_3OH]** (**4**) and **[1H][$D^{Ph2}{}_3OH$]** (**5**).

compound	**3**	**4**	**5**
Crystallographic Section			
empirical formula	$C_{49}H_{129}N_{13}O_3P_4Si_3$	$C_{46}H_{119}N_{13}O_4P_4Si_3$	$C_{76}H_{131}N_{13}O_4P_4Si_3$
a / pm	1365.42(2)	1101.915(13)	1663.91(12)
b / pm	1519.23(3)	2358.13(3)	2276.99(7)
c / pm	1715.28(2)	2495.13(3)	2312.88(13)
α / °	91.7566(13)	90	90
β / °	90.5974(12)	93.5860(11)	108.284(7)
γ / °	98.9787(14)	90	90
V / 10^6 pm^3	3512.49(10)	6470.81(13)	8320.4(9)
Z	2	4	4
ρ_{calc} / mg·mm^{-3}	1.094	1.157	1.197
crystal system	triclinic	monoclinic	monoclinic
space group	*P*-1	$P2_1/c$	$P2_1/n$
color shape	yellowish prisms	colorless needles	colorless prisms
crystal size / mm^{-3}	0.29 × 0.13 × 0.07	0.29 × 0.09 × 0.05	0.33 × 0.30 × 0.17
Data collection			
μ / mm^{-1}	1.827	1.985	1.674
F(000)	1280.0	2480.0	3248
2θ range for data col. / °	5.2 to 151.3°	5.2 to 144.3°	5.6 to 153.0°
index ranges	$-16 \le h \le 15$ $-18 \le k \le 18$ $-12 \le l \le 21$	$-13 \le h \le 13$ $-28 \le k \le 28$ $-30 \le l \le 30$	$-20 \le h \le 20$ $-24 \le k \le 28$ $-28 \le l \le 28$
reflections col.	31246	74329	40620

independent refl.	14332	12607	21342
R(int)	0.0199	0.0321	0.0151
data/restraints/ parameter	14332/0/1169	12607/32/719	21342/13/978
goodness-of-fit on F^2	1.044	1.025	1.063
R_1 / wR_2 [I>2σ(I)]	0.0291/0.0758	0.0339/0.0832	0.0321/0.0875
R_1 / wR_2 (all data)	0.0324/0.0780	0.0430/0.0882	0.0361/0.0894
$\Delta\rho_{max/min}$ / e Å^{-3}	0.41/-0.34	0.34/-0.36	0.46/-0.34
CCDC number	1952715	1952716	1952717

References

[1] A. Oku, W. Huang, Y. Ikeda, *Polymer* **2002**, *43*, 7289.

[2] O. V. Dolomanov, L. J. Bourhis, R. J. Gildea, J. A. K. Howard, H. Puschmann, *J. Appl. Cryst.* **2009**, *42*, 339.

[3] G. M. Sheldrick, *Acta Cryst. A* **2015**, *71*, 3.

[4] G. M. Sheldrick, *Acta Cryst. C* **2015**, *71*, 3.

Anhang 3

Non-Coordinated Phenolate Anions and Their Application in SF_6 Activation

Robin F. Weitkamp, Beate Neumann, Hans-Georg Stammler and Berthold Hoge

Chem. Eur. J. **2020**, *[accepted]*.
DOI: 10.1002/chem.202003504.

Anhang

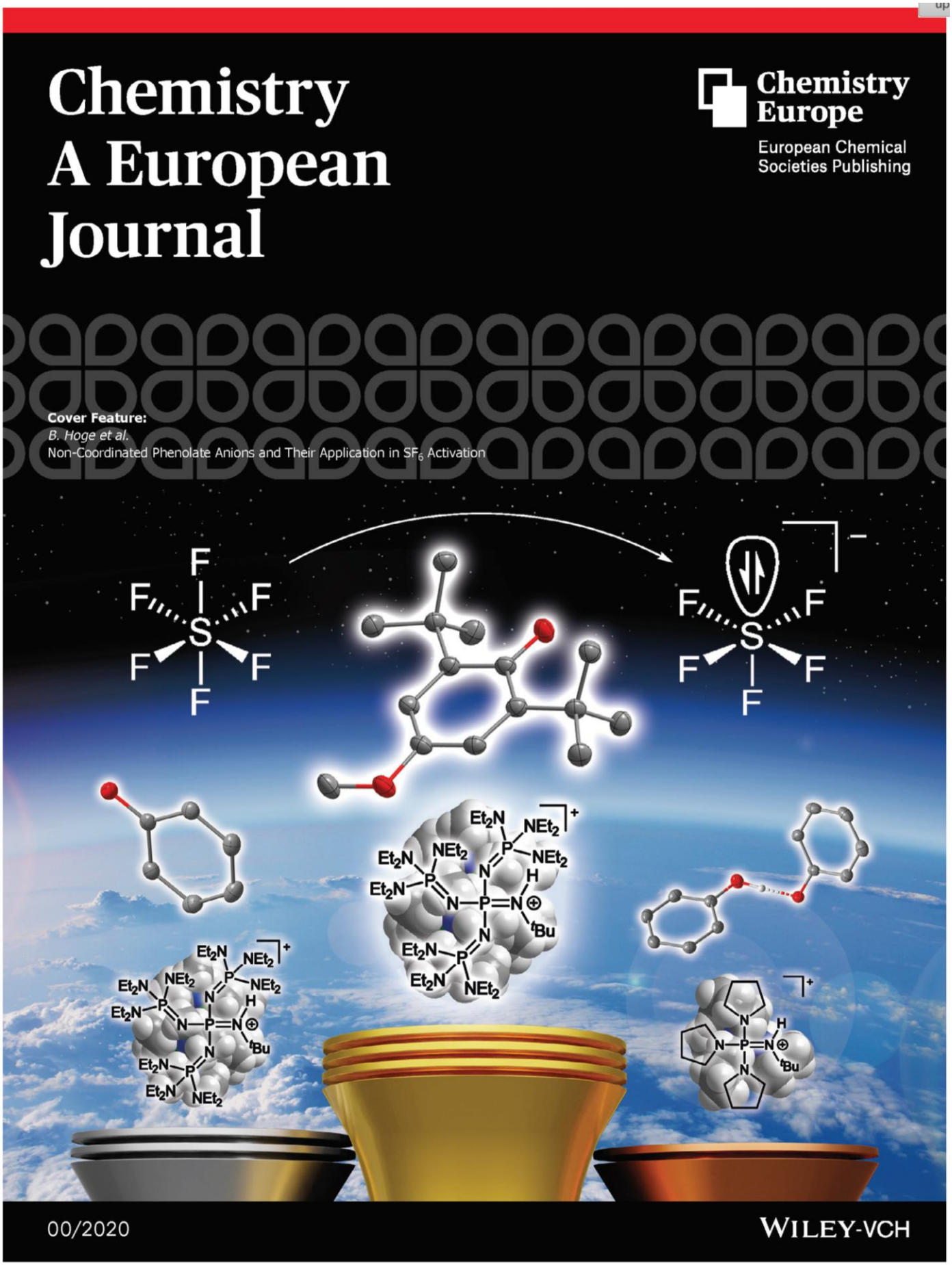
Chemistry
A European
Journal
Chemistry
Europe
European Chemical
Societies Publishing
Cover Feature:
B. Hoge et al.
Non-Coordinated Phenolate Anions and Their Application in SF6 Activation
00/2020
WILEY-VCH

Chemistry–A European Journal | Communication
doi.org/10.1002/chem.202003504

Reduction |Hot Paper|

Non-Coordinated Phenolate Anions and Their Application in SF_6 Activation

Robin F. Weitkamp, Beate Neumann, Hans-Georg Stammler, and Berthold Hoge*[a]

Abstract: The reaction of the strong monophosphazene base with the weakly acidic phenol leads to the formation of a phenol–phenolate anion with a moderately strong hydrogen bond. Application of the more powerful tetraphosphazene base (Schwesinger base) renders the isolation of the corresponding salt with a free phenolate anion possible. This compound represents the first species featuring the free phenolate anion $[H_5C_6\text{-}O]^-$. The deprotonation of phenol derivatives with tetraphosphazene bases represents a great way for the clean preparation of salts featuring free phenolate anions and in addition allows the selective syntheses of hydrogen bonded phenol-phenolate salts. This work presents a phosphazenium phenolate salt with a redox potential of −0.72 V and its capability for the selective activation of the chemically inert greenhouse gas SF_6. The performed two-electron reduction of SF_6 leads to phosphazenium pentafluorosulfanide ($[SF_5]^-$) and fluoride salts.

Phenol represents the simplest aromatic alcohol, and thus has been in the focus of numerous theoretical calculations[1,2,3,4] as well as practical applications.[5,6] Especially sodium phenolate has emerged as a highly important bulk chemical for the industrial production of salicylic acid in the Kolbe–Schmitt process.[7,8]

Fundamental reactions in the biosphere are strongly dependent on phenolic species. The amino acid tyrosine (*p*-hydroxyphenylalanine) is crucial for the success of photosynthesis, as tyrosine is photo-oxidized in the oxygen evolving complex (OEC) of the photosystem II via a proton coupled electron transfer (PCET) reaction with a hydrogen bonded histidine.[9] Hydrogen bonds of phenol are strongly governing the acidity of OH functions, which turned out to be crucial in several biological and chemical systems.[3–5,10,11]

[a] R. F. Weitkamp, B. Neumann, Dr. H.-G. Stammler, Prof. Dr. B. Hoge
Centrum für Molekulare Materialien
Fakultät für Chemie, Universität Bielefeld,
Universitätsstraße 25, 33615 Bielefeld (Germany)
E-mail: b.hoge@uni-bielefeld.de

Supporting information and the ORCID identification number(s) for the author(s) of this article can be found under:
https://doi.org/10.1002/chem.202003504.

With regard to the great importance of phenol, it is surprising that the molecular structure and the characteristics of the non-coordinated phenolate anion have not been unambiguously documented.

Phenol with a pK_{BH^+} value of 9.98[1,12] is weakly acidic and is easily deprotonated by alkali hydroxides or hydrides to yield the corresponding metal phenolates.[5,7,13]

Fraser et al. reported on the separation of sodium and potassium cations from phenolates[15] and phenol-phenolate salts[16] by means of crown ethers. For the latter they reported short hydrogen bonds with O–O distances of 247.1(3) pm to 248(1) pm. The strong tendency of hydrogen bonding is also observed in the imidazolium salt of Clyburne and co-workers (Figure 1, right), which exhibits strong cation-anion interactions.[14]

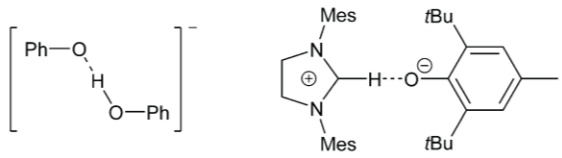

Figure 1. Structures of the phenol-phenolate anion[11] and an NHC adduct of a phenol derivative.[14]

Reetz et al. used tetra-*n*-butylammonium hydroxide for the deprotonation of phenol to generate a free $[H_5C_6\text{-}O]^-$ anion without cation-anion interactions. All attempts to isolate the phenolate anion were thwarted by the selective formation of the phenol-phenolate adduct (Figure 1, left).[11] Davidson applied phosphonium ylides for the deprotonation of phenols resulting in salts featuring short cation-anion C–H···O^- hydrogen bonds.[17,18] In addition to that, numerous substituted phenol derivatives containing electron-withdrawing groups, thus featuring an increased acidity, were investigated.[6,19]

However, no example of the non-coordinated phenolate anion $[H_5C_6\text{-}O]^-$ was reported so far. The structural characteristics of mono- and tetraphosphazene bases like **1** and **2**,[20] presented in Scheme 1 and Scheme 2, seem promising for the design of systems featuring the free phenolate anion, as well as phenolate derivatives containing electron-donating groups.

The deprotonation of phenol with equimolar quantities of the commercially available pyrrolidino phosphazene **1** in diethyl ether leads to the precipitation of a light brown oil.[21] The ^{31}P NMR spectrum of the supernatant shows the signal of the free base at $\delta = -10.3$ ppm. Thus, the basicity of the pyrrolidino phosphazene **1** is not sufficient for the complete deproto-

Chemistry–A European Journal | Communication doi.org/10.1002/chem.202003504 | Chemistry Europe European Chemical Societies Publishing

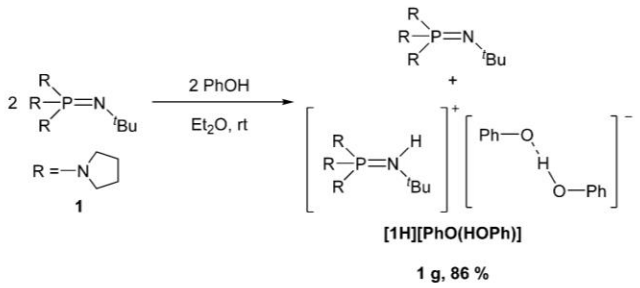

Scheme 1. Synthesis of **[1H][PhO(HOPh)]**.

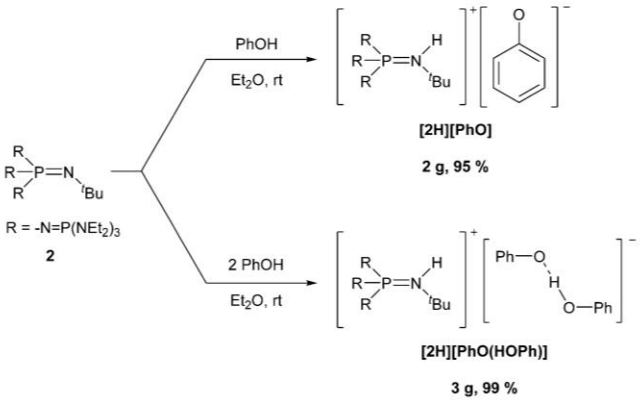

Scheme 2. Synthesis of phenolate salts using phosphazene **2**.

nation of phenol and solely affords a phenol-phenolate adduct (Scheme 1, Figure 2).[22]

Salt **[1H][PhO(HOPh)]** crystallizes from the reaction mixture at −28 °C in an 84% yield.[21] In the ^{31}P NMR spectrum of the product a signal at $\delta = 22.2$ ppm is observed, which is due to the protonated phosphazene **[1H]**$^+$.

With regard to familiar O–O distances in $[OH(OH_2)]^-$ (229 pm),[24] $[H_3O(H_2O)]^+$ (249 pm)[25] and water aggregates (283 pm),[25] the phenolate anion exhibits moderately strong hydrogen bonding to the phenol molecule with an O1–O2 distance of 249.1(2) pm, which is well comparable with the literature data.[11,16] Furthermore, an additional interaction of the phenolate anion with the iminium proton (N1–O1 279.2(1) pm) is observed.

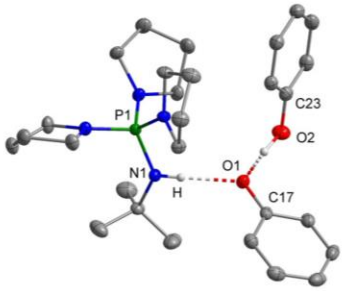

Figure 2. Molecular structure of **[1H][PhO(HOPh)]**.[23] Selected bond lengths [pm] and angles [°]: O1–O2 249.1(1), N1–O1 279.2(1), O1–C17 131.9(2); N1-O1-O2 112.8(1).

This clearly requires more basic and sterically encumbered phosphazenes like **2** for the separation of non-coordinated phenolates (Scheme 2).

The reaction of equimolar quantities of phenol and **2** leads to the precipitation of the expected phenolate **[2H][PhO]** (Figure 3) as colorless crystals in yields up to 95%.[21] The product is highly air sensitive and decomposes above 75 °C. The decomposition of the product in [D_1]chloroform and [D_3]acetonitrile solution was observed by ^{13}C NMR spectroscopy and led to deep blue and strong yellow solutions, respectively, whose color eventually faded.[21]

Salt **[2H][PhO]** is the first example of the non-coordinated phenolate anion. The anion is disordered in a ratio of 94:6.[22] In the major representative the closest C–H···O$^-$ contact of cation and anion (O1B–C31) was determined to 325.9(2) pm, which is in the range of C–H···O$^-$ hydrogen bonds.[18,26] The C–O bond length of the anion in **[2H][PhO]** amounts to 128.7(2) pm and is thus significantly shortened in comparison to the C–O bonds of coordinated anions as present in sodium phenolate (133(1) pm)[27] or in **[1H][PhO(HOPh)]** (131.9(2) pm). This bond shortage points to a significant resonance stabilization of the negative charge, which is also confirmed by a strong upfield shift ($\delta = 5.5$ ppm) of the signal of the *para* positioned proton in the ^{1}H NMR spectrum (Figure 4, top). The C–C distances in free [PhO]$^-$ are slight elongated (138.6(1) pm to 143.6(1) pm) compared to sodium phenolate (138(1) pm to

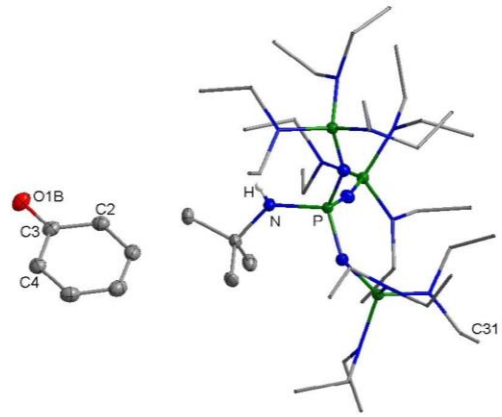

Figure 3. Molecular structure of the salt **[2H][PhO]**.[23] The anion is disordered (94:6). Selected bond lengths [pm]: O1B–C3 128.7(2), C2–C3 143.6(2), C3–C4 142.8(2).

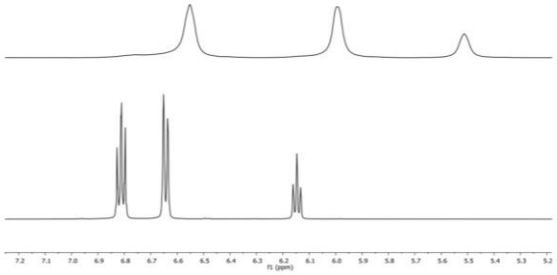

Figure 4. Aromatic region of the ^{1}H NMR spectra of **[2H][PhO]** (top) and **[2H][PhO(HOPh)]** (bottom) in [D_8]THF.

Chemistry–A European Journal | Communication doi.org/10.1002/chem.202003504 | Chemistry Europe European Chemical Societies Publishing

142(1) pm). The corresponding angles within the aromatic system do not differ significantly.

Application of two equivalents of phenol allows the synthesis of the phenol-phenolate compound **[2H][PhO(HOPh)]** (Figure 5) in excellent yields (99%, Scheme 2). The phenol-phenolate salt exhibits a higher thermal stability (m.p. 125 °C) and deteriorates less eagerly in air or in [D_1]chloroform and [D_3]acetonitrile solution than the corresponding non-coordinated phenolate salt **[2H][PhO]**.[21] Hydrogen bonding brings about downfield shifts of the aromatic protons in the ^{1}H NMR spectrum and clean couplings (Figure 4, bottom).

The associated hydrogen bond with an O1–O8 distance of 243.7(2) pm is shortened in comparison to **[1H][PhO(HOPh)]** (249.1(1) pm).[22]

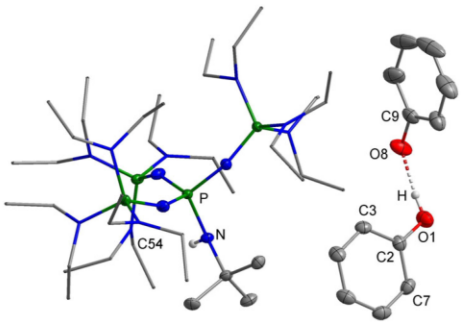

Figure 5. Molecular structure of the salt **[2H][PhO(HOPh)]**.[23] The donor hydrogen atom is disordered at both oxygen atoms with a ratio of 1:1, only one is shown. Selected bond lengths [pm]: O1–O8 243.7(2), O1–C2 131.9(2), O8–C9 132.1(2).

Several papers addressed the redox potentials of various phenols[28] and phenolates[29,30] as determined by (cyclic) voltammetry, preferentially in acetonitrile solution. The anions were preferentially generated in situ via deprotonation with tetraalkylammonium hydroxides. The unsuccessful preparation of the free phenolate anion by deprotonation with ammonium hydroxides[11] and the fast deterioration of non-coordinated phenolates like **[2H][PhO]** in acetonitrile[21] casts doubt on the reported redox potentials.

The now possible selective synthesis of hydrogen bonded phenolate moieties makes the disclosure of the influence of hydrogen bonding on the redox properties of phenolate anions via cyclic voltammetry (CV) conceivable (Figure 6). The rapid reactions of intermediates led to irreversible oxidation processes at low scan rates of 100 mV s^{-1}. Thus, only oxidation potentials (E_{Ox}) can be determined, which are compared with quantum chemical calculations on the BP86/6–311+g(3df,2p) level.[31]

Salt **[2H][PhO]** was oxidized in THF solution at E_{Ox} = −0.12(1) V vs. the Fc/Fc$^+$ couple (black, Figure 6).[21] This value is cathodically shifted in comparison to the estimated value in acetonitrile solution reported in the literature (+0.24 V).[30] Interestingly, the hydrogen bonded phenol-phenolate adduct is oxidized at a more positive potential (E_{Ox} = +0.22(1) V), and resembles the potential reported for the phenolate/phenoxyl

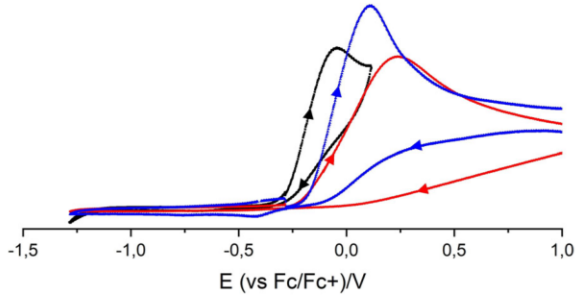

Figure 6. Cyclic voltammograms of **[2H][PhO]** (black), **[2H][PhO(HOPh)]** (red) and **[2H][PhO(HOPh)]** + excess H_2O (concentration of 0.1 M H_2O in the electrolyte solution, blue), recorded in 0.1 M [NBu_4][PF_6]·THF solution at 100 mV s^{-1}.[21] Fc/Fc$^+$ was set at +0.405 V.

couple (+0.24 V).[30] The anodically shifted oxidation potential of [PhO(HOPh)]$^-$ is rationalized by a reduced charge density of the phenolate oxygen in comparison to free [PhO]$^-$. A concentration of 0.1 M H_2O (17 equivalents) was prepared by adding water to the phenol-phenolate electrolyte solution, which leads to a cathodic shift of E_{Ox} (+0.10(1) V, Figure 6). Likewise the addition of water (0.1 M, 0.2 M, 0.7 M) to **[2H][PhO]** results in increasing potentials of E_{Ox} = +0.02(1) V, +0.04(1) V and +0.11(1) V.[21] This clearly underlines that hydrogen bonded adducts of phenolates instead of free phenolates have been oxidized previously.

The presented tendency is confirmed by the calculation of adiabatic ionization potentials (E_i) of phenolates in the gas phase.[31] The influence of hydrogen bonding on the potential of the phenolate anion is more pronounced in the phenol adduct [PhO(HOPh)]$^-$ (E_i = 314.90(1) kJ mol^{-1}) than in the water adduct [PhO(H_2O)]$^-$ (E_i = 267.42(1) kJ mol^{-1}), both significantly differ from the calculated value of the free anion [PhO]$^-$ (E_i = 228.69(1) kJ mol^{-1}).

For the employment of phenolates as strong reducing agents, we selected 2,6-di-*tert*-butyl-4-methoxyphenol (^{MeOtBu2}PhOH) as the substrate of choice (Scheme 3).

Deprotonation of this phenol with **2** clearly furnished the corresponding phenolate salt **[2H][^{MeOtBu2}PhO]** (Figure 7).[21] The salt is significantly more air sensitive than the previously discussed phenolate. Air contact effects a quick color change from yellow to red-brown.

As the closest cation-anion contact in **[2H][^{MeOtBu2}PhO]** a O1–C8 separation of 303.9(1) pm was observed.[22] The O1–C41 bond (129.0(2) pm) is similar to that in the anion of **[2H][PhO]**.

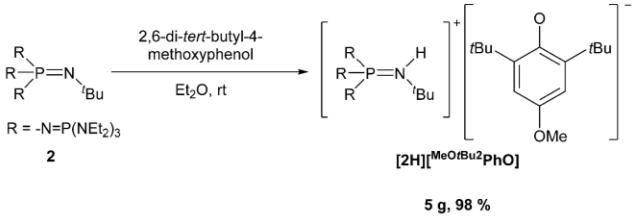

Scheme 3. Synthesis of **[2H][^{MeOtBu2}PhO]**.

Chemistry–A European Journal | Communication doi.org/10.1002/chem.202003504 | Chemist Europe European Chem Societies Publis

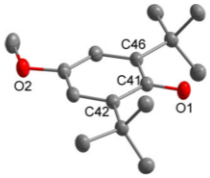

Figure 7. Molecular structure of the anion of **[2H][^{MeOtBu2}PhO]**.[23] Selected bond lengths [pm]: C41–O1 129.0(2), C41–C42 144.8(4), C41–C46 144.9(4).

The anion in **[2H][^{MeOtBu2}PhO]** undergoes a reversible redox reaction at $E^0 = -0.72(1)$ V vs. Fc/Fc^+ (Figure 8), which is significantly lower than the literature data in acetonitrile (−0.45(1) V).[29,30] Thus it has a similar redox potential as zinc and can be classified as an organic zinc reagent.[32]

In order to demonstrate the reducing capability of **[2H][^{MeOtBu2}PhO]**, the reaction with the chemically inert sulfur hexafluoride was investigated (Scheme 4).

SF_6 is the most potent greenhouse gas known to date[33] and has a dramatic impact on the climate due to its high chemical stability.[34] Therefore the chemical degradation of SF_6 has become an important issue of current research.[35,36–38] In ethereal solution the treatment of the phenolate with SF_6 (Scheme 4) was accompanied by a color change from yellow to pink to deep red. The formation of the $[SF_5]^-$ anion was evidenced by ^{19}F NMR spectroscopy featuring a quintet at $\delta =$ 88.7 ppm and a doublet at 59.5 ppm, with a coupling constant of $^2J_{FF} = 45$ Hz (Figure 9).[36,39]

The broad resonance of the fluoride anion in the product was observed in the ^{19}F NMR spectrum at $\delta = -173.0$ ppm.[21] According to the favorable decomposition pathway,[37,38] the

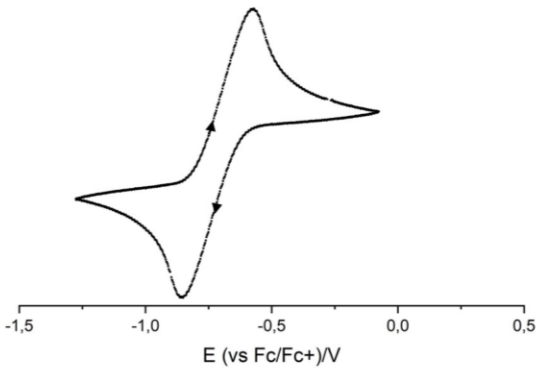

Figure 8. Cyclic voltammogram of **[2H][^{MeOtBu2}PhO]** recorded in 0.1 M $[NBu_4][PF_6]$·THF solution at 100 mV s^{-1}.[21] Fc/Fc^+ was set at +0.405 V.

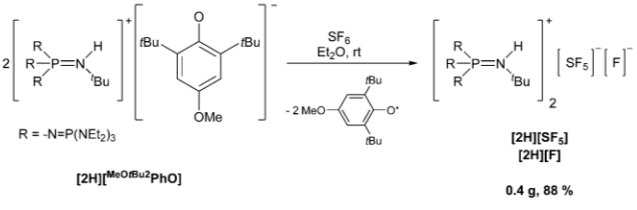

Scheme 4. Activation of SF_6 with phenolate **[2H][^{MeOtBu2}PhO]**.

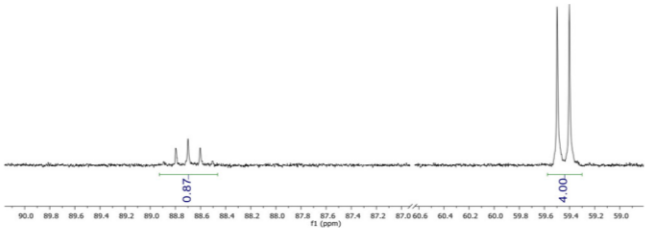

Figure 9. Resonances of the $[SF_5]^-$ anion in the ^{19}F NMR spectrum of the reaction of **[2H][^{MeOtBu2}PhO]** with SF_6.

formed $[SF_6]^{\cdot-}$ radical anion disintegrates into a fluoride anion and an $(SF_5)^{\cdot}$ radical. The latter is further reduced by a second phenolate to obtain the $[SF_5]^-$ anion. The thermally stable salt mixture of **[2H][SF_5]** and **[2H][F]** (dec. > 123 °C) precipitates from the reaction mixture as a colorless solid in high yields (> 88 %).[21] The X-ray structural analysis of a single crystal of **[2H][SF_5]** obtained by slow precipitation from the reaction mixture confirms the presence of the $[SF_5]^-$ anion with its distorted pseudo square-pyramidal geometry.[21,22,36,40]

In conclusion we succeeded in the clean deprotonation of phenol and 2,6-di-*tert*-butyl-4-methoxyphenol by means of the tetraphosphazene base **2**, affording salts of the free phenolate anions in **[2H][PhO]** and in **[2H][^{MeOtBu2}PhO]** in excellent yields (> 95 %). The strength of the base as well as the stoichiometry determines if a phenol-free phenolate salt or a phenol-phenolate adduct is generated. The latter anions were preferentially obtained by deprotonation of phenol with the less basic pyrrolidino monophosphazene **1** or alternatively in the case of **[2H][PhO(HOPh)]** by the employment of two molar equivalents of phenol.

We also disclosed the successful degradation of sulfur hexafluoride (SF_6) in a two-electron reduction process applying **[2H][^{MeOtBu2}PhO]**, leading to the corresponding phosphazenium pentafluorosulfanide and fluoride salts **[2H][SF_5]** and **[2H][F]** in high yields (> 88 %). The use of phosphazenium phenolates for the preparation of highly reactive anions, especially radical anions, is under active study in our laboratory.

Experimental Section

Crystallographic data: Deposition numbers 1973242, 1973243, 1973244, 2002668, and 2002669 contain the supplementary crystallographic data for this paper. These data are provided free of charge by the joint Cambridge Crystallographic Data Centre and Fachinformationszentrum Karlsruhe Access Structures service.

Acknowledgements

We acknowledge the financial support by Merck KGaA and Solvay. We thank Mira Kessler for the calculations of adiabatic ionization potentials and we furthermore thank the Regional Computing Center of the University of Cologne (RRZK) for providing computing time on the DFG-funded High Performance Computing (HPC) system CHEOPS, as well as support. We acknowledge Prof. Dr. Lothar Weber and Dr. Julia Bader for help-

Chemistry–A European Journal | Communication doi.org/10.1002/chem.202003504 | Chemist Europe European Cher Societies Publi

ful discussions. We thank Luisa Koch and Manuel Warkentin for experimental assistance. Open access funding enabled and organized by Projekt DEAL.

Conflict of interest

The authors declare no conflict of interest.

Keywords: hydrogen bond · phenol · phosphazene base · SF_6 activation · weakly coordinating cation

[1] K. C. Gross, P. G. Seybold, *Int. J. Quantum Chem.* **2001**, *85*, 569.

[2] a) Z. Pawlak, J. Magonski, *J. Chem. Soc. Faraday Trans.* **1985**, *81*, 2021; b) R. J. Mayer, M. Breugst, N. Hampel, A. R. Ofial, H. Mayr, *J. Org. Chem.* **2019**, *84*, 8837.

[3] A. M. Buytendyk, J. D. Graham, K. D. Collins, K. H. Bowen, C.-H. Wu, J. I. Wu, *Phys. Chem. Chem. Phys.* **2015**, *17*, 25109.

[4] T. M. Krygowski, H. Szatyłowicz, *J. Phys. Chem. A* **2006**, *110*, 7232.

[5] N. Kornblum, P. J. Berrigan, W. J. Le Noble, *J. Am. Chem. Soc.* **1963**, *85*, 1141.

[6] A. Kütt, V. Movchun, T. Rodima, T. Dansauer, E. B. Rusanov, I. Leito, I. Kaljurand, J. Koppel, V. Pihl, I. Koppel, A. A. Kolomeitsev, *J. Org. Chem.* **2008**, *73*, 2607.

[7] H. Kolbe, *J. Prakt. Chem.* **1874**, *10*, 89.

[8] Z. Marković, S. Marković, N. Manojlović, J. Predojević-Simović, *J. Chem. Inf. Model.* **2007**, *47*, 1520.

[9] a) A. Zouni, H. T. Witt, J. Kern, P. Fromme, N. Krauss, W. Saenger, P. Orth, *Nature* **2001**, *409*, 739; b) Y. Umena, K. Kawakami, J.-R. Shen, N. Kamiya, *Nature* **2011**, *473*, 55; c) J. D. Megiatto Jr., D. D. Méndez-Hernández, M. E. Tejeda-Ferrari, A.-L. Teillout, M. J. Llansola-Portolés, G. Kodis, O. G. Poluektov, T. Rajh, V. Mujica, T. L. Groy, D. Gust, T. A. Moore, A. L. Moore, *Nat. Chem.* **2014**, *6*, 423.

[10] a) T. Steiner, I. Majerz, C. C. Wilson, *Angew. Chem. Int. Ed.* **2001**, *40*, 2651; *Angew. Chem.* **2001**, *113*, 2728; b) A. Chandra, T. Uchimaru, *Int. J. Mol. Sci.* **2002**, *3*, 407; c) A. Sirjoosingh, S. Hammes-Schiffer, *J. Phys. Chem. A* **2011**, *115*, 2367; d) M. Kołaski, A. Kumar, N. J. Singh, K. S. Kim, *Phys. Chem. Chem. Phys.* **2011**, *13*, 991.

[11] R. Goddard, H. M. Herzog, M. T. Reetz, *Tetrahedron* **2002**, *58*, 7847.

[12] A. Albert, E. P. Serjeant, *Ionization Constants of Acids and Bases*, Methuen, London, **1962**.

[13] R. E. Dinnebier, M. Pink, J. Sieler, P. W. Stephens, *Inorg. Chem.* **1997**, *36*, 3398.

[14] J. A. Cowan, J. A. C. Clyburne, M. G. Davidson, R. L. W. Harris, J. A. K. Howard, P. Küpper, M. A. Leech, S. P. Richards, *Angew. Chem. Int. Ed.* **2002**, *41*, 1432 – 1434; *Angew. Chem.* **2002**, *114*, 1490 – 1492.

[15] M. E. Fraser, S. Fortier, A. Rodrigue, J. W. Bovenkamp, *Can. J. Chem.* **1986**, *64*, 816.

[16] M. E. Fraser, S. Fortier, M. K. Markiewicz, A. Rodrigue, J. W. Bovenkamp, *Can. J. Chem.* **1987**, *65*, 2558.

[17] M. G. Davidson, *J. Chem. Soc. Chem. Commun.* **1995**, 919.

[18] M. G. Davidson, A. E. Goeta, J. A. K. Howard, S. Lamb, S. A. Mason, *New J. Chem.* **2000**, *24*, 477.

[19] a) K. C. K. Swamy, C. Sreelatha, R. O. Day, J. Holmes, R. R. Holmes, *Inorg. Chem.* **1991**, *30*, 3126; b) G. Laus, J. Schütz, N. Schuler, V. Kahlenberg, H. Schottenberger, *Z. Kristallogr. New Cryst. Struct.* **2009**, *224*, 117; c) S. E. Bettis, M. W. Mathias, K. L. Martin, *Ga. J. Sci.* **2008**, *66*, 6.

[20] R. F. Weitkamp, B. Neumann, H.-G. Stammler, B. Hoge, *Angew. Chem. Int. Ed.* **2019**, *58*, 14633; *Angew. Chem.* **2019**, *131*, 14775.

[21] Details are given in the supplementary information for this paper.

[22] Details of the X-ray investigation are given in Tables S1–S3 of the Supporting Information for this paper.

[23] Thermal ellipsoids are shown at 50% probability. Hydrogen atoms bonded at carbon atoms and minor occupied disordered atoms are omitted for clarity. Diethylamino groups in $[\mathbf{2H}]^+$ are shown as stick model.

[24] K. Abu-Dari, K. N. Raymond, D. P. Freyberg, *J. Am. Chem. Soc.* **1979**, *101*, 3688.

[25] T. Steiner, *Angew. Chem. Int. Ed.* **2002**, *41*, 48; *Angew. Chem.* **2002**, *114*, 50.

[26] a) R. Taylor, O. Kennard, *J. Am. Chem. Soc.* **1982**, *104*, 5063; b) G. R. Desiraju, *Acc. Chem. Res.* **1991**, *24*, 290; c) T. Steiner, *Cryst. Rev.* **1996**, *6*, 1.

[27] M. Kunert, E. Dinjus, M. Nauck, J. Sieler, *Chem. Ber.* **1997**, *130*, 1461.

[28] a) J. A. Richards, P. E. Whitson, D. H. Evans, *J. Electroanal. Chem. Interfacial Electrochem.* **1975**, *63*, 311; b) L. Kiss, D. Bősz, F. Kovács, H. Li, G. Nagy, S. Kunsági-Máté, *Polym. Bull.* **2019**, *76*, 5849; c) N. L. Zabik, C. N. Virca, T. M. McCormick, S. Martic-Milne, *J. Phys. Chem. B* **2016**, *120*, 8914; d) A. S. Pavitt, E. J. Bylaska, P. G. Tratnyek, *Environ. Sci. Processes Impacts* **2017**, *19*, 339.

[29] L. L. Williams, R. D. Webster, *J. Am. Chem. Soc.* **2004**, *126*, 12441.

[30] P. Hapiot, J. Pinson, N. Yousfi, *New J. Chem.* **1992**, *16*, 877.

[31] Gaussian 09, Revision D.01, M. J. Frisch, G. W. Trucks, H. B. Schlegel, G. E. Scuseria, M. A. Robb, J. R. Cheeseman, G. Scalmani, V. Barone, B. Mennucci, G. A. Petersson, H. Nakatsuji, M. Caricato, X. Li, H. P. Hratchian, A. F. Izmaylov, J. Bloino, G. Zheng, J. L. Sonnenberg, M. Hada, M. Ehara, K. Toyota, R. Fukuda, J. Hasegawa, M. Ishida, T. Nakajima, Y. Honda, O. Kitao, H. Nakai, T. Vreven, J. A. Montgomery, Jr., J. E. Peralta, F. Ogliaro, M. Bearpark, J. J. Heyd, E. Brothers, K. N. Kudin, V. N. Staroverov, R. Kobayashi, J. Normand, K. Raghavachari, A. Rendell, J. C. Burant, S. S. Iyengar, J. Tomasi, M. Cossi, N. Rega, J. M. Millam, M. Klene, J. E. Knox, J. B. Cross, V. Bakken, C. Adamo, J. Jaramillo, R. Gomperts, R. E. Stratmann, O. Yazyev, A. J. Austin, R. Cammi, C. Pomelli, J. W. Ochterski, R. L. Martin, K. Morokuma, V. G. Zakrzewski, G. A. Voth, P. Salvador, J. J. Dannenberg, S. Dapprich, A. D. Daniels, Ö. Farkas, J. B. Foresman, J. V. Ortiz, J. Cioslowski, D. J. Fox, Gaussian, Inc., Wallingford CT, **2013**.

[32] W. M. Haynes, *CRC Handbook of Chemistry and Physics*, CRC Press, London, **2016**.

[33] P. Forster, V. Ramaswamy, P. Artaxo, T. Berntsen, R. Betts, D. W. Fahey, J. Haywood, J. Lean, D. C. Lowe, G. Myhre, *Changes in Atmospheric Constituents and in Radiative Forcing, in: Climate Change 2007: The Physical Science Basis. Contribution of Working Group I to the Fourth Assessment Report of the IPCC*, Cambridge University Press, **2007**.

[34] a) A. F. Holleman, E. Wiberg, N. Wiberg, *Lehrbuch der anorganischen Chemie*, de Gruyter, Berlin [u.a.] **2007**; b) K. Seppelt, *Chem. Rev.* **2015**, *115*, 1296.

[35] a) D. Sevenard, P. Kirsch, A. A. Kolomeitsev, G.-V. Röschenthaler, DE 102 20 901 A1, **2002**; b) R. Basta, B. G. Harvey, A. M. Arif, R. D. Ernst, *J. Am. Chem. Soc.* **2005**, *127*, 11924; c) P. Holze, B. Horn, C. Limberg, C. Matlachowski, S. Mebs, *Angew. Chem. Int. Ed.* **2014**, *53*, 2750; d) L. Zámostná, T. Braun, *Angew. Chem.* **2015**, *127*, 10798; e) T. A. McTeague, T. F. Jamison, *Angew. Chem. Int. Ed.* **2016**, *55*, 15072; *Angew. Chem.* **2016**, *128*, 15296; f) L. Zámostná, T. Braun, *Nachr. Chem.* **2016**, *64*, 829; g) H. Deubner, F. Kraus, *Inorganics* **2017**, *5*, 68; h) D. Rombach, H.-A. Wagenknecht, *Angew. Chem. Int. Ed.* **2020**, *59*, 300; *Angew. Chem.* **2020**, *132*, 306.

[36] F. Buß, C. Mück-Lichtenfeld, P. Mehlmann, F. Dielmann, *Angew. Chem.* **2018**, *130*, 773.

[37] G. Iakobson, M. Pošta, P. Beier, *J. Fluorine Chem.* **2018**, *213*, 51.

[38] M. Rueping, P. Nikolaienko, Y. Lebedev, A. Adams, *Green Chem.* **2017**, *19*, 2571.

[39] W. Heilemann, R. Mews, S. Pohl, W. Saak, *Chem. Ber.* **1989**, *122*, 427.

[40] K. Matsumoto, Y. Haruki, S. Sawada, S. Yamada, T. Konno, R. Hagiwara, *Inorg. Chem.* **2018**, *57*, 14882.

Manuscript received: July 28, 2020
Revised manuscript received: August 4, 2020
Accepted manuscript online: August 10, 2020
Version of record online: ■■ ■■, 0000

Chemistry–A European Journal

Supporting Information

Non-Coordinated Phenolate Anions and Their Application in SF_6 Activation

Robin F. Weitkamp, Beate Neumann, Hans-Georg Stammler, and Berthold Hoge*[a]

1. Experimental Section

1.1 General Part

All chemicals were obtained from commercial sources and used without further purification. Standard high-vacuum techniques were employed throughout all experiments. Non-volatile compounds were handled in a dry N_2 atmosphere using Schlenk techniques.

1.2 Analysis Methods

1.2.1 NMR Spectroscopy

NMR spectra were recorded on a Bruker Avance III 500 spectrometer (^{1}H 500.01 MHz; ^{13}C 125.73 MHz; ^{19}F 470.48 MHz; ^{31}P 202.41 MHz) or on a Bruker Avance III 500 HD spectrometer (^{1}H 500.20 MHz; ^{13}C 125.78 MHz; ^{19}F 470.66 MHz; ^{31}P 202.48 MHz). Positive shifts are downfield from the external standards TMS (^{1}H, ^{13}C), CCl_3F (^{19}F) and H_3PO_4 (^{31}P). The NMR spectra were recorded in the indicated deuterated solvent or in relation to acetone-d_6-filled capillaries.

1.2.2 IR Spectroscopy

IR spectra were recorded on an ALPHA-FT-IR spectrometer (Bruker) using an ATR unit with a diamond crystal for liquids and solids.

1.2.3 Elemental Analyses

Elemental analyses were performed by Mikroanalytisches Laboratorium Kolbe (Oberhausen, Germany). The elemental analysis of **[2H][^{MeO}*t*Bu^{2}PhO]** was performed in the element-analytical laboratory of the Universität Bielefeld using the EURO EA Element Analyzer 2010 (HEKAtech GmbH).

1.2.4 Melting Point

Melting points were measured on a Mettler Toledo Mp70 Melting Point System.

1.2.5 Cyclic Voltammetry

The cyclic voltammetric investigations were performed on a PGSTAT101 potentiostat (Metrohm) using a „three-electrode arrangement“ in a flame-dried 25 mL Schlenk flask under inert atmosphere with a glassy carbon working electrode (2.0(1) mm diameter), a counter electrode (stainless steel 18/8, 2.0(1) mm diameter) and an Ag/AgCl reference electrode in a saturated ethanolic LiCl solution (148 mV vs. SHE). The supporting electrolyte $[NBu_4][PF_6]$ was carefully dried in a high vacuum (10^{-3} mbar). THF was dried over K and freshly distilled prior to use. For every run 0.1 mmol of the substrate and 15 mL of the electrolyte solution were used. The Fc/Fc^+ couple was used as internal standard by adding a small amount (spatula tip) of ferrocene after the measurements. The obtained redox potentials were finally recalculated based on the Fc/Fc^+ couple which was set at +0.405 V vs. SCE.

1.2.6 Mass spectrometry

Nano-ESI mass spectra were recorded using an Esquire 3000 ion trap mass spectrometer (Bruker Daltonik GmbH, Bremen, Germany) equipped with a nano-ESI source. Samples were dissolved in THF and introduced to static nano-ESI using *in-house* pulled glass emitters. Nitrogen served both as nebulizer gas and dry gas. Nitrogen was generated by a Bruker nitrogen generator NGM 11. Helium served as cooling gas for the ion trap and collision gas for mass spectrometry experiments. The mass axis was externally calibrated with ESI-L Tuning Mix (Agilent Technologies, Santa Clara, CA, USA) as calibration standard.

1.3 Syntheses

1.3.1 Synthesis of [1H][PhO(HOPh)]

Phosphazene **1** (524 mg, 1.68 mmol) is dissolved in diethyl ether (10 mL) and phenol (332 mg, 3.528 mmol) is added at ambient temperature. The resulting two-phase system is stirred for 15 minutes and then cooled at -28 °C overnight. The supernatant is removed via a syringe and the product (725 mg, 1.45 mmol, 86 % based on **1**) is isolated as a slight brown crystalline solid after drying in a high vacuum (m.p. > 63 °C).

^{1}H NMR (THF-d_8, rt): δ [ppm] = 1.3 (s, 9 H, $C(CH_3)_3$), 1.8 (m, 12 H, $NCH_2C\mathbf{H}_2$), 3.2 (t, d, $^{3}J_{HH}$ = 7 Hz, $^{3}J_{PH}$ = 4 Hz, 12 H, NCH_2), 6.4 (m, 2 H, *para* H), 6.8 (m, 4 H, *ortho* H), 7.0 (m, 4 H, *meta* H), 11.1 (s, OH).
^{13}C NMR (THF-d_8, rt): δ [ppm] = 26.0 (d, $^{3}J_{PC}$ = 8 Hz, $NCH_2\mathbf{C}H_2$), 31.8 (d, $^{3}J_{PC}$ = 5 Hz, $C(\mathbf{C}H_3)_3$), 47.3 (d, $^{3}J_{PC}$ = 5 Hz, $N\mathbf{C}H_2CH_2$), 52.2 (d, $^{2}J_{PC}$ = 1 Hz, $\mathbf{C}(CH_3)_3$), 114.4 (s, *para* C), 117.0 (s, *ortho* C), 128.3 (s, *meta* C), 163.2 (s, *ipso* C).
^{31}P NMR (THF-d_8, rt): δ [ppm] = 16.3 (s).
IR (ATR): $\tilde{\nu}$ [cm^{-1}] = 3209 (vw, br), 3049 (vw), 2970 (w), 2872 (w), 2691 (w), 2559 (w, br), 1895 (vw), 1807 (vw), 1704 (vw), 1583 (w), 1468 (m), 1412 (w), 1392 (w), 1367 (w), 1347 (w), 1294 (w), 1243 (s), 1226 (s), 1199 (s), 1161 (m), 1128 (m), 1077 (vs), 1017 (vs), 984 (s), 916 (m), 866 (m), 837 (m), 817 (m), 752 (vs), 692 (vs), 617 (m), 582 (m), 567 (m), 547 (m), 514 (s), 493 (s), 453 (m), 435 (m), 403 (m).
elemental analysis of $C_{28}H_{45}N_4O_2P$ (M = 500.7 g/mol): calcd.: C 67.17, H 9.06, N 11.19; found: C 67.07, H 9.14, N 11.13.

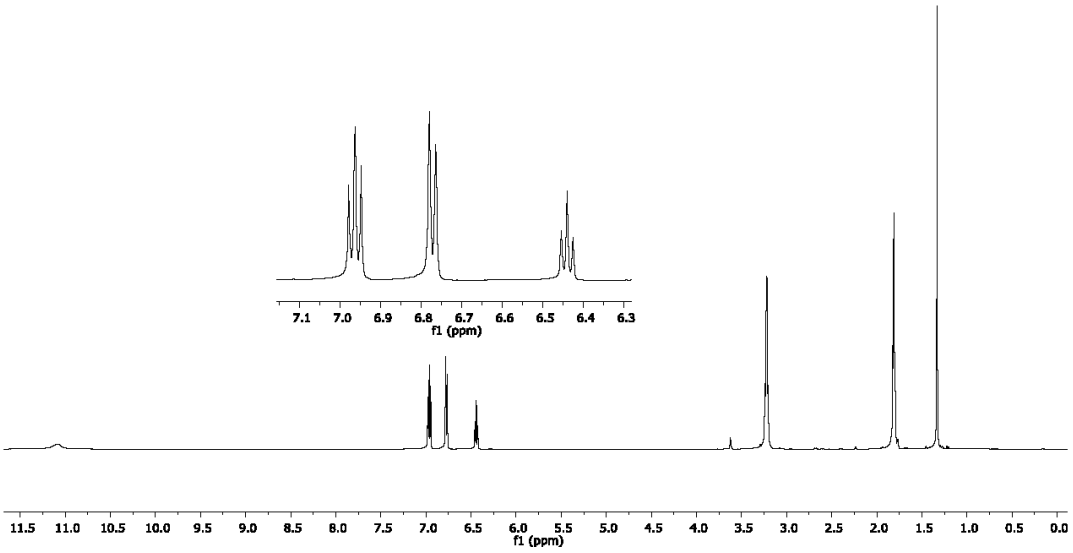

Figure 1. ^{1}H NMR spectrum of **[1H][PhO(HOPh)]** in THF-d_8 (500 MHz).

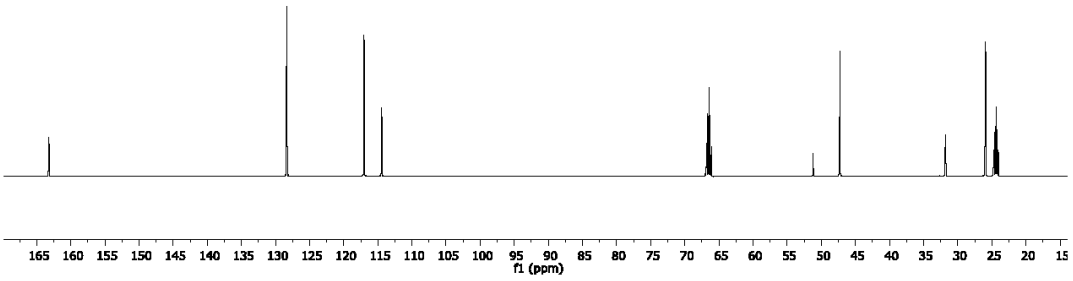

Figure 2. ^{13}C NMR spectrum of **[1H][PhO(HOPh)]** in THF-d_8 (500 MHz).

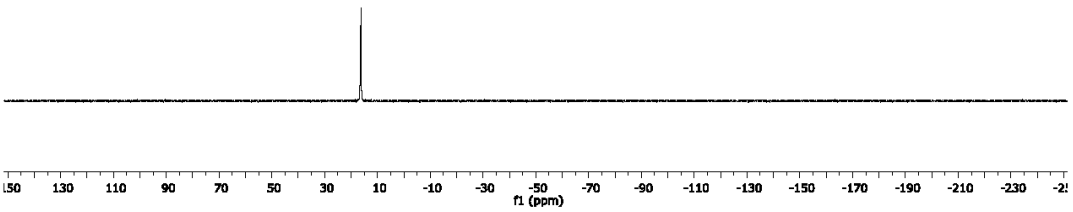

Figure 3. ^{31}P NMR spectrum of **[1H][PhO(HOPh)]** in THF-d_8 (500 MHz).

1.3.2 Synthesis of [2H][PhO]

Phosphazene **2** (1.40 g, 1.57 mmol) is dissolved in diethyl ether (7 mL) and phenol (149 mg, 1.58 mmol) is rapidly added in 3 mL of diethyl ether. The emulsion is stirred for 1.5 hours and cooled to -28 °C overnight, by which a colorless solid precipitates. For the complete precipitation of the product *n*-hexane (4 mL) is added and the supernatant is removed via a syringe. The solid is washed with 4 mL of *n*-hexane and dried in a high vacuum. The product (1.46 g, 1.49 mmol, 95 % based on **2**) is isolated as a colorless solid (dec. > 75 °C).

^{1}H NMR (THF-d_8, rt): δ [ppm] = 1.2 (t, $^{3}J_{HH}$ = 7 Hz, 54 H, CH_3), 1.4 (s, 9 H, $C(CH_3)_3$), 2.3 (d, $^{2}J_{PH}$ = 8 Hz, 1 H, NH), 3.2 (d, q, $^{3}J_{PH}$ = 10 Hz, $^{3}J_{HH}$ = 7 Hz, 36 H, CH_2), 5.5 (s, 1 H, *para* H), 6.0 (m, 2 H, *ortho* H), 6.6 (m, 2 H, *meta* H).
^{13}C NMR (THF-d_8, rt): δ [ppm] = 13.0 (d, $^{3}J_{PC}$ = 4 Hz, CH_3), 31.2 (d, $^{3}J_{PC}$ = 5 Hz, $C(\mathbf{C}H_3)_3$), 39.2 (d, $^{2}J_{PC}$ = 6 Hz, CH_2), 50.5 (d, $^{2}J_{PC}$ = 4 Hz, $\mathbf{C}(CH_3)_3$), 101.8 (s, *para* C), 119.4 (s, *ortho* C), 127.6 (s, *meta* C), 175.0 (s, *ipso* C).
^{31}P NMR (THF-d_8, rt): δ [ppm] = -33.5 (q, d, $^{2}J_{PP}$ = 70 Hz, $^{2}J_{PH}$ = 7 Hz, 1 P, P=NH), 7.8 (d, tridec, $^{2}J_{PP}$ = 70 Hz, $^{3}J_{PH}$ = 10 Hz, 3 P, $(Et_2N)_3P$).
IR (ATR): $\tilde{\nu}$ [cm^{-1}] = 2969 (w), 2930 (w), 2870 (w), 1578 (w), 1538 (vw), 1485 (w), 1462 (w), 1414 (w), 1377 (m), 1350 (w), 1330 (w), 1261 (s), 1227 (m), 1201 (s), 1174 (vs), 1108 (w), 1076 (w), 1054 (w), 1017 (vs), 979 (w), 941 (vs), 848 (m), 795 (s), 740 (m), 699 (s), 691 (s), 614 (m), 590 (w), 509 (vs), 456 (s), 435 (s).
elemental analysis of $C_{46}H_{106}N_{13}OP_4$ (M = 981.3 g/mol): calcd.: C 56.36, H 10.80, N 18.57; found: C 55.66, H 10.69, N 18.31.

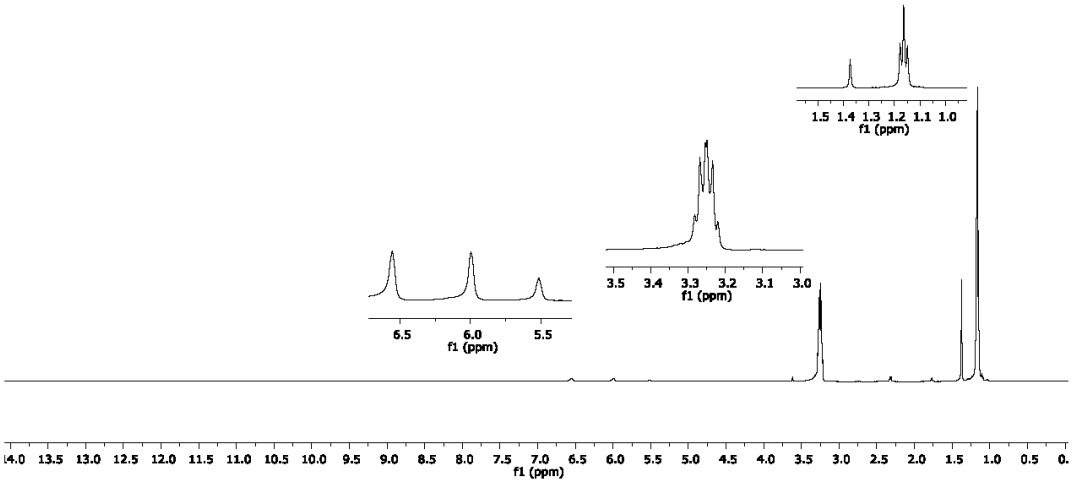

Figure 4. ^{1}H NMR spectrum of **[2H][PhO]** in THF-d_8 (500 MHz).

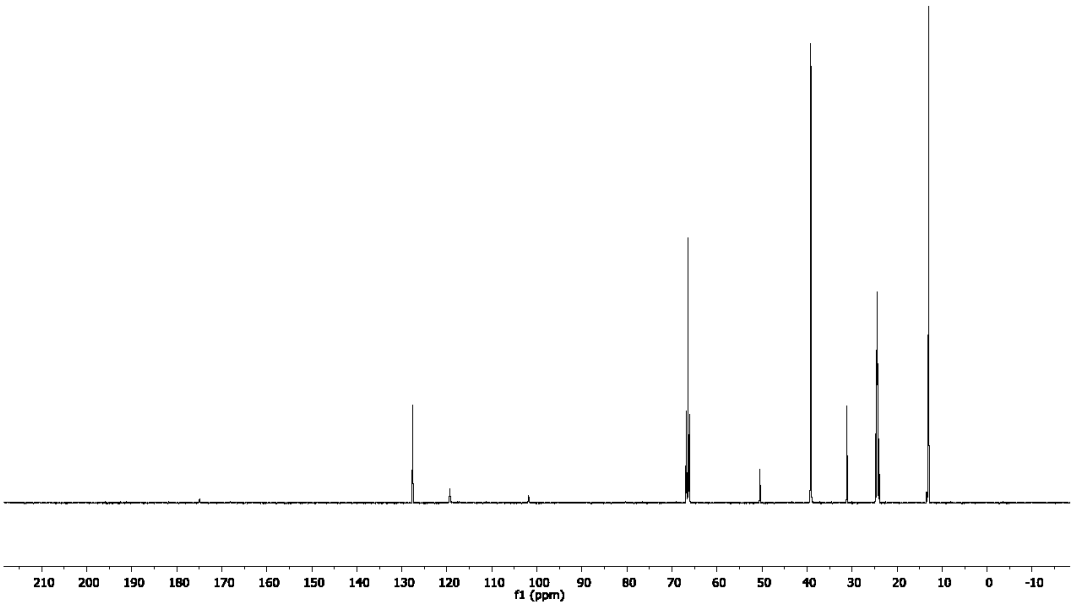

Figure 5. ^{13}C NMR spectrum of **[2H][PhO]** in THF-d_8 (500 MHz).

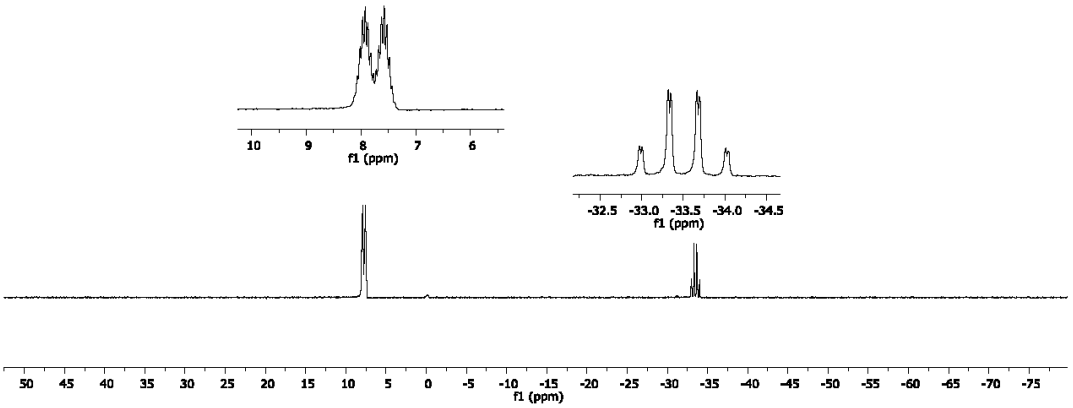

Figure 6. ^{31}P NMR spectrum of **[2H][PhO]** in THF-d_8 (500 MHz).

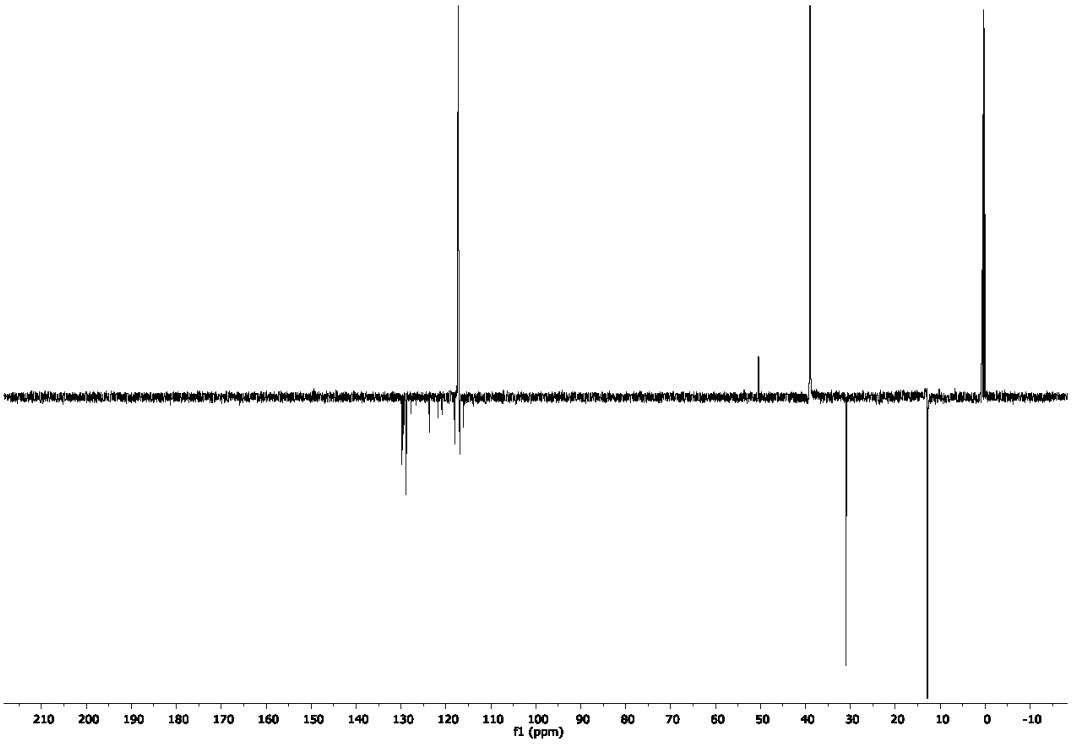

Figure 7. $^{13}C\{^1H\}$ APT NMR spectrum of the resulting decomposition products of **[2H][PhO]** in acetonitrile-d_3 (yellow solution) (500 MHz).

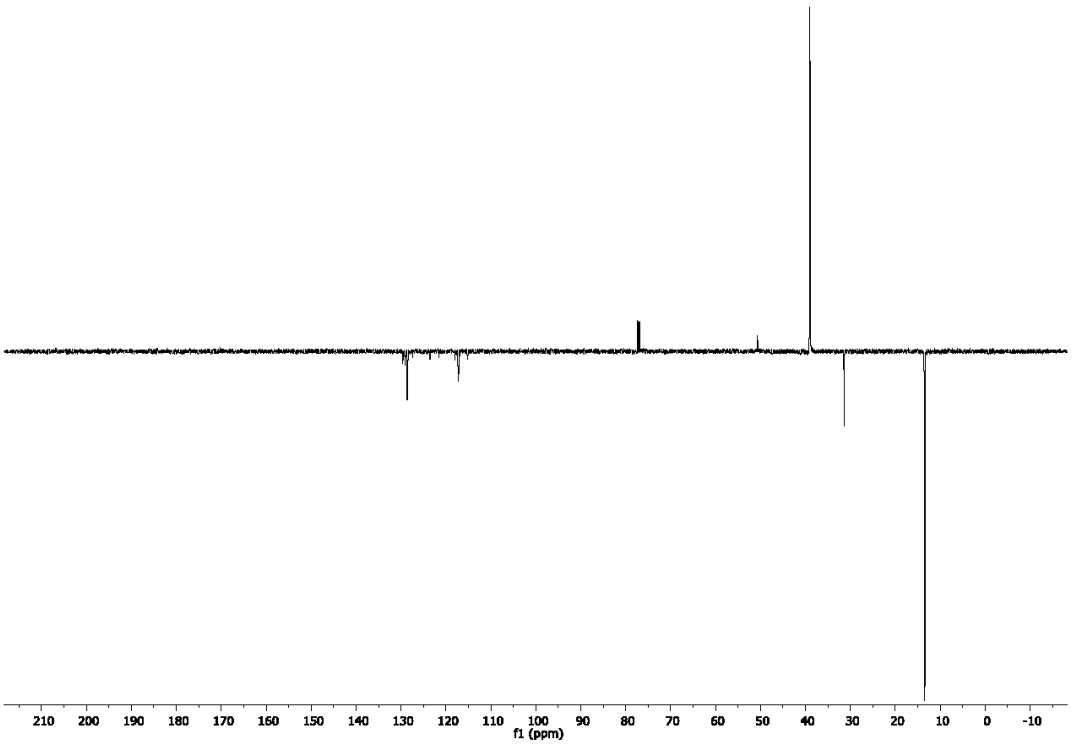

Figure 8. $^{13}C\{^{1}H\}$ APT NMR spectrum of the resulting decomposition products of **[2H][PhO]** in chloroform-d_1 (blue solution) (500 MHz).

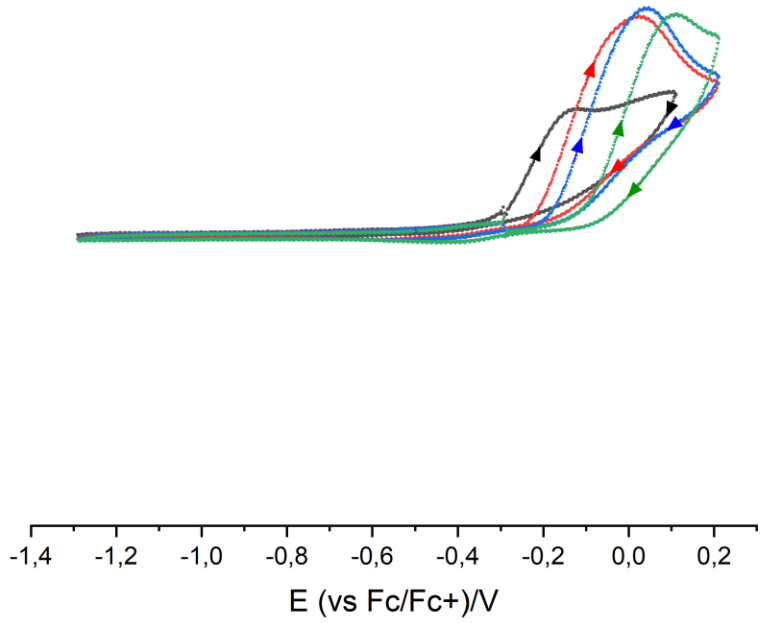

Figure 9. Cyclovoltammograms of **[2H][PhO]** (black) and **[2H][PhO]** with addition of H_2O to obtain concentrations of 0.1 M (28 mg H_2O, red), 0.2 M (59 mg H_2O, blue) and 0.7 M (258 mg H_2O, green) water in the electrolyte solution. Voltammograms recorded in 0.1 M $[NBu_4][PF_6]$ THF solution at 100 mV/s under inert atmosphere with a glassy carbon working electrode (2.0(1) mm), a counter electrode (steel 18/8, 2.0(1) mm) and an Ag/AgCl reference electrode. All potentials were recalculated using the Fc/Fc^+ couple (+0.405 V vs SCE).

1.3.3 Synthesis of [2H][^{MeOtBu2}PhO]

Phosphazene **2** (4.41 g, 4.98 mmol) is dissolved in diethyl ether (15 mL) and 2,6-di-*tert*-butyl-4-methoxyphenol (^{MeOtBu2}PhOH, 1.18 g, 4.99 mmol) in 5 mL diethyl ether is rapidly added to yield an intensely yellow suspension. After stirring for one hour *n*-hexane (10 mL) is added and the supernatant is removed via a syringe. The solid is washed with *n*-hexane (10 mL) and dried in a high vacuum. The product (5.46 g, 4.86 mmol, 98 % based on **2**) is isolated as a highly air sensitive yellow crystalline solid.

The product rapidly decomposes in a melting point capillary upon heating over 40 °C to yield a dark brown solid.

The product dissolves rapidly in acetonitrile and chloroform to yield intensely orange or light pink solutions.

^{1}H NMR (THF-d_8, rt): δ [ppm] = 1.2 (t, $^{3}J_{HH}$ = 7 Hz, 54 H, $NCH_2C\mathbf{H}_3$), 1.4 (s, 9 H, $NC(CH_3)_3$), 1.4 (s, 18 H, $C(CH_3)_3$), 2.2 (d, $^{2}J_{PH}$ = 8 Hz, 1 H, NH), 3.2 (d, q, $^{3}J_{PH}$ = 10 Hz, $^{3}J_{HH}$ = 7 Hz, 36 H, $NC\mathbf{H}_2CH_3$), 3.5 (s, 3 H, OCH_3), 6.4 (s, 2 H, *meta* H).

^{13}C NMR (THF-d_8, rt): δ [ppm] = 13.0 (d, $^{3}J_{PC}$ = 4 Hz, $NCH_2\mathbf{C}H_3$), 29.6 (s, $C(\mathbf{C}H_3)_3$), 31.1 (d, $^{3}J_{PC}$ = 5 Hz, $NC(\mathbf{C}H_3)_3$), 35.0 (s, $\mathbf{C}(CH_3)_3$), 39.1 (d, $^{2}J_{PC}$ = 6 Hz, $N\mathbf{C}H_2CH_3$), 50.5 (d, $^{2}J_{PC}$ = 4 Hz, $N\mathbf{C}(CH_3)_3$), 57.6 (s, OCH_3), 110.8 (s, *meta* C), 133.3 (s, *ortho* C), 140.7 (s, *para* C), 168.0 (s, *ipso* C).

^{31}P NMR (THF-d_8, rt): δ [ppm] = -33.7 (q, d, $^{2}J_{PP}$ = 70 Hz, $^{2}J_{PH}$ = 7 Hz, 1 P, P=NH), 7.7 (d, tridec, $^{2}J_{PP}$ = 70 Hz, $^{3}J_{PH}$ = 10 Hz, 3 P, $(Et_2N)_3P$).

IR (ATR): $\tilde{\nu}$ [cm^{-1}] = 2966 (vw), 2931 (vw), 2870 (w), 1465 (w), 1415 (w), 1377 (w), 1348 (w), 1244 (m), 1201 (s), 1173 (vs), 1102 (w), 1073 (vw), 1053 (w), 1016 (vs), 944 (s), 921 (m), 890 (w), 844 (w), 783 (s), 740 (w), 700 (s), 616 (w), 508 (s), 440 (m).

MS (ESI, pos.) {*m/z* (%) [assignment]}: 887.7 (100) **[2H]$^{+}$**

MS (ESI, neg.) {*m/z* (%) [assignment]}: 235.1 (100) **[^{MeOtBu2}PhO]$^{-}$**

elemental analysis of $C_{55}H_{123}N_{13}O_2P_4$ (M = 1122.6 g/mol): calcd.: C 58.85, H 11.04, N 16.22; found: C 59.24, H 10.74, N 16.12.

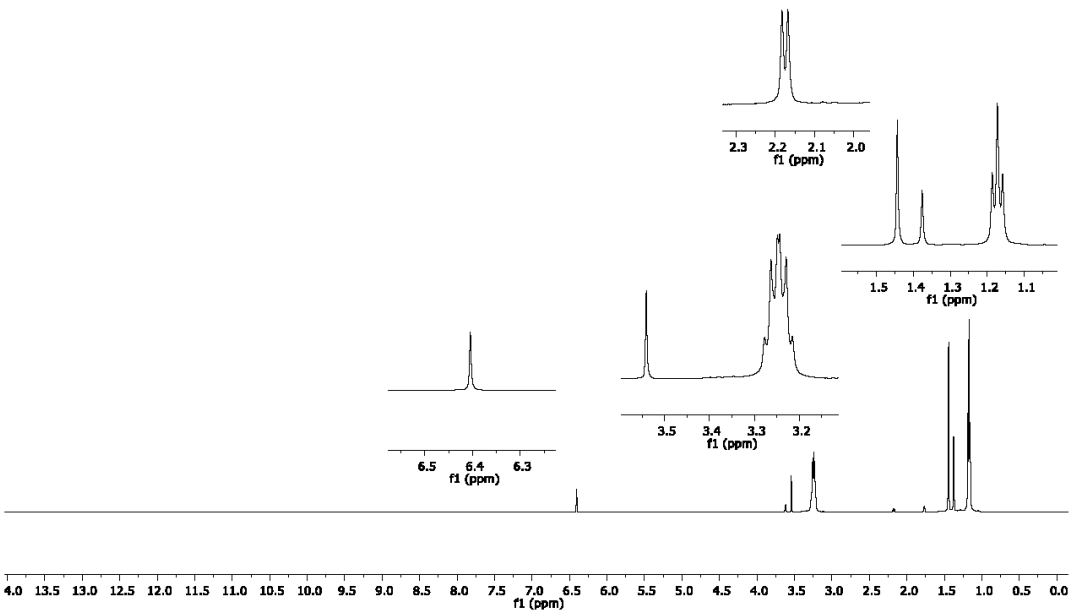

Figure 10. ^{1}H NMR spectrum of **[2H][^{MeOtBu2}PhO]** in THF-d_8 (500 MHz).

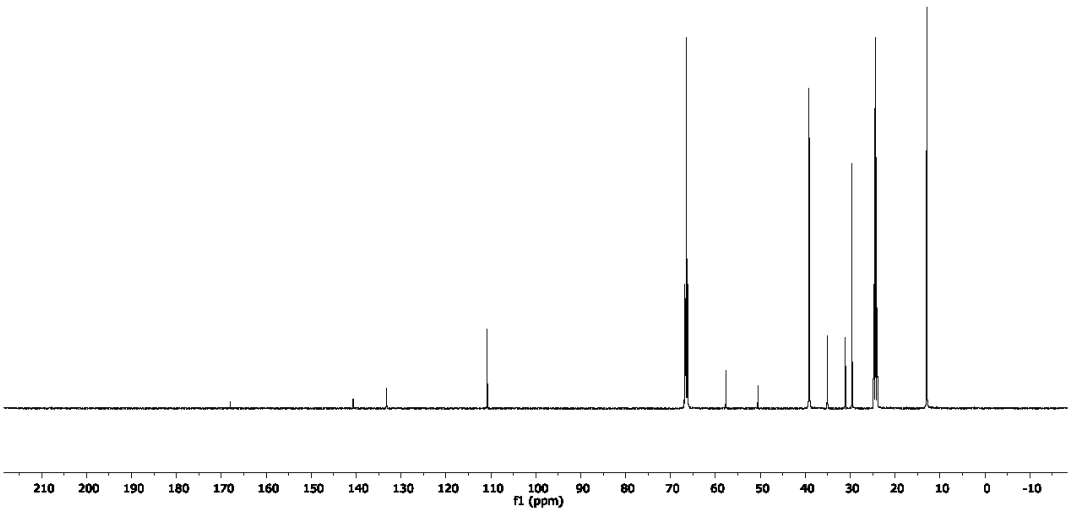

Figure 11. ^{13}C NMR spectrum of **[2H][^{MeOtBu2}PhO]** in THF-d_8 (500 MHz).

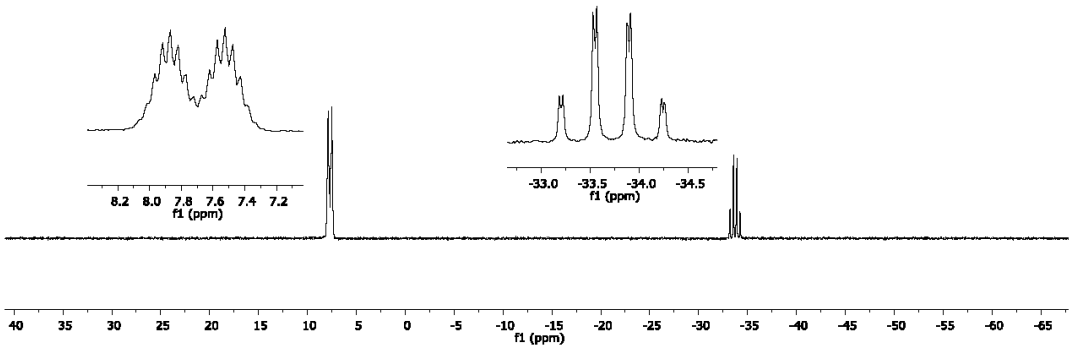

Figure 12. ^{31}P NMR spectrum of **[2H][^{MeOtBu2}PhO]** in THF-d_8 (500 MHz).

1.3.4 Synthesis of [2H][PhO(HOPh)]

Phosphazene **2** (2.25 g, 2.54 mmol) is dissolved in 15 mL of diethyl ether and phenol (0.48 g, 5.09 mmol) in 4 mL of diethyl ether is rapidly added. Immediately a second yellowish phase forms. The emulsion is stirred for an additional hour and then cooled to -28 °C overnight. The supernatant is removed via a syringe and the solid is dried in a high vacuum. The product (2.69 g, 2.50 mmol, 99 %, based on phenol) is isolated as a light-brown crystalline solid (m.p. > 125 °C (dec.)).

^{1}H NMR (THF-d_8, rt): δ [ppm] = 1.1 (t, $^{3}J_{HH}$ = 7 Hz, 54 H, $NCH_2C\mathbf{H}_3$), 1.4 (s, 9 H, $NC(CH_3)_3$), 2.1 (d, $^{2}J_{PH}$ = 8 Hz, 1 H, NH), 3.2 (d, q, $^{3}J_{PH}$ = 10 Hz, $^{3}J_{HH}$ = 7 Hz, 36 H, $NC\mathbf{H}_2CH_3$), 6.1 (m, 2 H, *para* H), 6.6 (m, 4 H, *ortho* H), 6.8 (m, 4 H, *meta* H), 15.1 (s, OH).
^{13}C NMR (THF-d_8, rt): δ [ppm] = 12.9 (d, $^{3}J_{PC}$ = 4 Hz, $NCH_2\mathbf{C}H_3$), 31.1 (d, $^{3}J_{PC}$ = 5 Hz, $NC(\mathbf{C}H_3)_3$), 39.1 (d, $^{2}J_{PC}$ = 6 Hz, $N\mathbf{C}H_2CH_3$), 50.5 (d, $^{2}J_{PC}$ = 4 Hz, $N\mathbf{C}(CH_3)_3$), 110.7 (s, *para* C), 117.4 (s, *ortho* C), 127.7 (s, *meta* C), 167.2 (s, *ipso* C).
^{31}P NMR (THF-d_8, rt): δ [ppm] = -33.7 (q, d, $^{2}J_{PP}$ = 70 Hz, $^{2}J_{PH}$ = 8 Hz, 1 P, P=NH), 7.7 (d, tridec, $^{2}J_{PP}$ = 70 Hz, $^{3}J_{PH}$ = 10 Hz, 3 P, $(Et_2N)_3P$).
IR (ATR): $\tilde{\nu}$ [cm^{-1}] = 2973 (vw), 2965 (w), 2949 (vw), 2934 (vw), 2867 (vw), 1455 (vw), 1376 (w), 1353 (w), 1260 (s), 1222 (w), 1201 (m), 1173 (s), 1157 (s), 1103 (w), 1074 (w), 1056 (w), 1020 (vs), 943 (vs), 867 (w), 845 (w), 822 (m), 782 (s), 750 (s), 695 (vs), 620 (m), 603 (m), 541 (s), 511 (vs), 494 (vs), 482 (m), 445 (s), 408 (vs).
elemental analysis of $C_{52}H_{111}N_{13}O_2P_4$ (M = 1074.4 g/mol): calcd.: C 58.13, H 10.41, N 16.95; found: C 57.89, H 10.22, N 17.03.

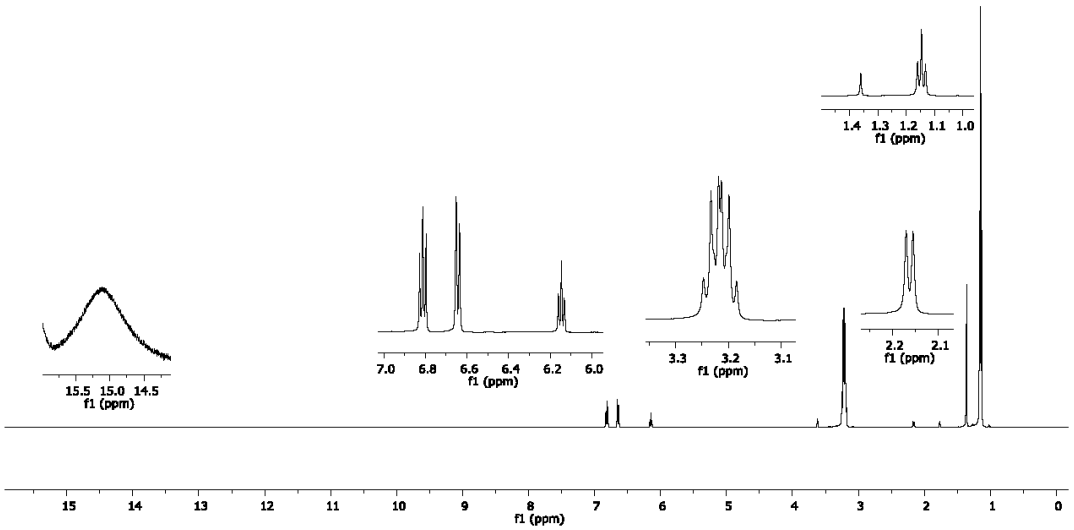

Figure 13. ^{1}H NMR spectrum of **[2H][PhO(HOPh)]** in THF-d_8 (500 MHz).

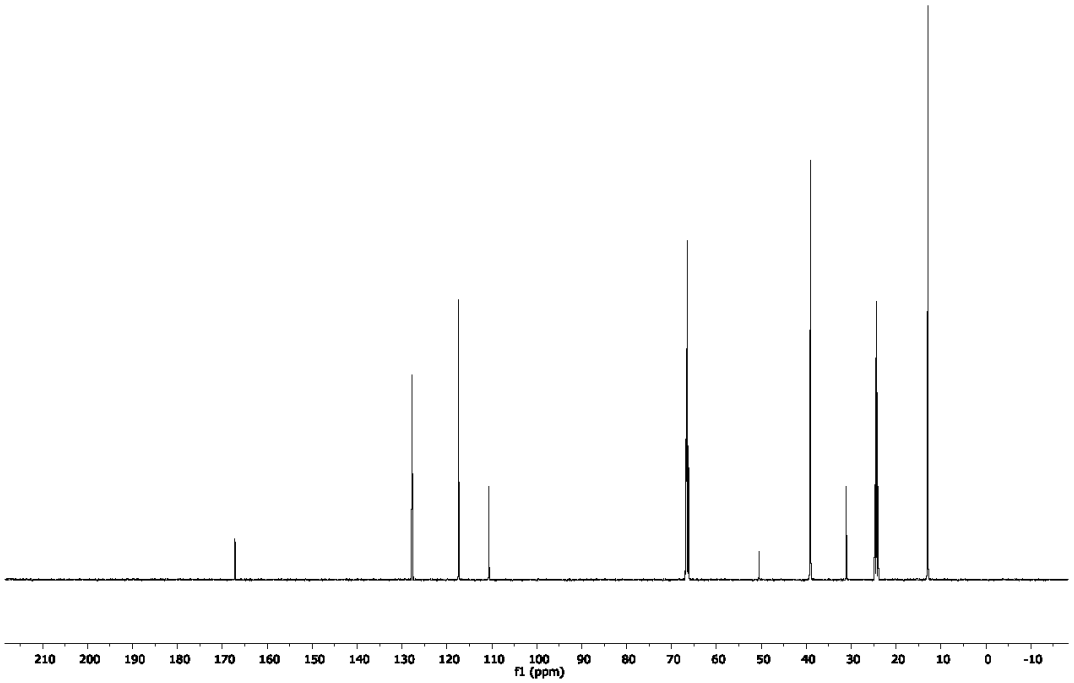

Figure 14. ^{13}C NMR spectrum of **[2H][PhO(HOPh)]** in THF-d_8 (500 MHz).

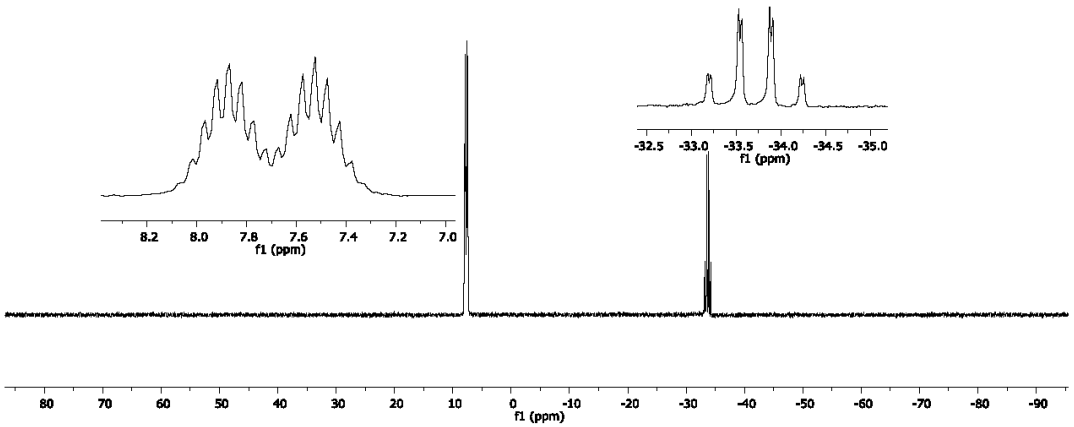

Figure 15. ^{31}P NMR spectrum of **[2H][PhO(HOPh)]** in THF-d_8 (500 MHz).

1.3.5 Activation of SF_6

At -196 °C diethyl ether (15 mL) is condensed onto the salt **[2H][^{MeOtBu2}PhO]** (514 mg, 0.46 mmol), the resulting yellowish emulsion is shortly allowed to warm to room temperature and then sulfur hexafluoride (SF_6) (2.35 mmol) is condensed onto the mixture at -196 °C. The emulsion is again warmed to room temperature and stirred for 4 days. The deep red supernatant of the resulting suspension is removed via a syringe at -40 °C and the solid is washed with cold diethyl ether (3 x 5 mL). A salt mixture of **[2H][SF_5]** and **[2H][F]** (389 mg, 0.38 mmol, 88 %) is isolated as a colorless, highly hygroscopic crystalline solid (dec. > 123 °C).

^{13}C NMR (THF, rt): δ [ppm] = 13.2 (d, $^3J_{PC}$ = 4 Hz, $NCH_2\mathbf{C}H_3$), 31.4 (d, $^3J_{PC}$ = 5 Hz, $NC(\mathbf{C}H_3)_3$), 39.4 (d, $^2J_{PC}$ = 6 Hz, $N\mathbf{C}H_2CH_3$), 50.8 (d, $^2J_{PC}$ = 4 Hz, $N\mathbf{C}(CH_3)_3$).
^{19}F NMR (THF, rt): δ [ppm] = -173.0 (s, br, F^-), 59.4 (s, br, 4 F, $[SF_5]^-$), 88.9 (s, br, 1 F, $[SF_5]^-$).
^{31}P NMR (THF, rt): δ [ppm] = -33.3 (q, d, $^2J_{PP}$ = 70 Hz, $^2J_{PH}$ = 8 Hz, 1 P, P=NH), 8.1 (d, tridec, $^2J_{PP}$ = 70 Hz, $^3J_{PH}$ = 10 Hz, 3 P, $(Et_2N)_3P$).
IR (ATR): $\tilde{\nu}$ [cm^{-1}] = 2966 (vw), 2928 (vw), 2869 (vw), 1774 (br, vw), 1463 (vw), 1414 (vw), 1377 (w), 1349 (w), 1259 (m), 1227 (w), 1202 (m), 1173 (s), 1107 (w), 1054 (w), 1018 (vs), 942 (s), 846 (w), 785 (m), 741 (w), 700 (s), 613 (w), 579 (vs), 511 (vs), 458 (vs), 437 (vs).

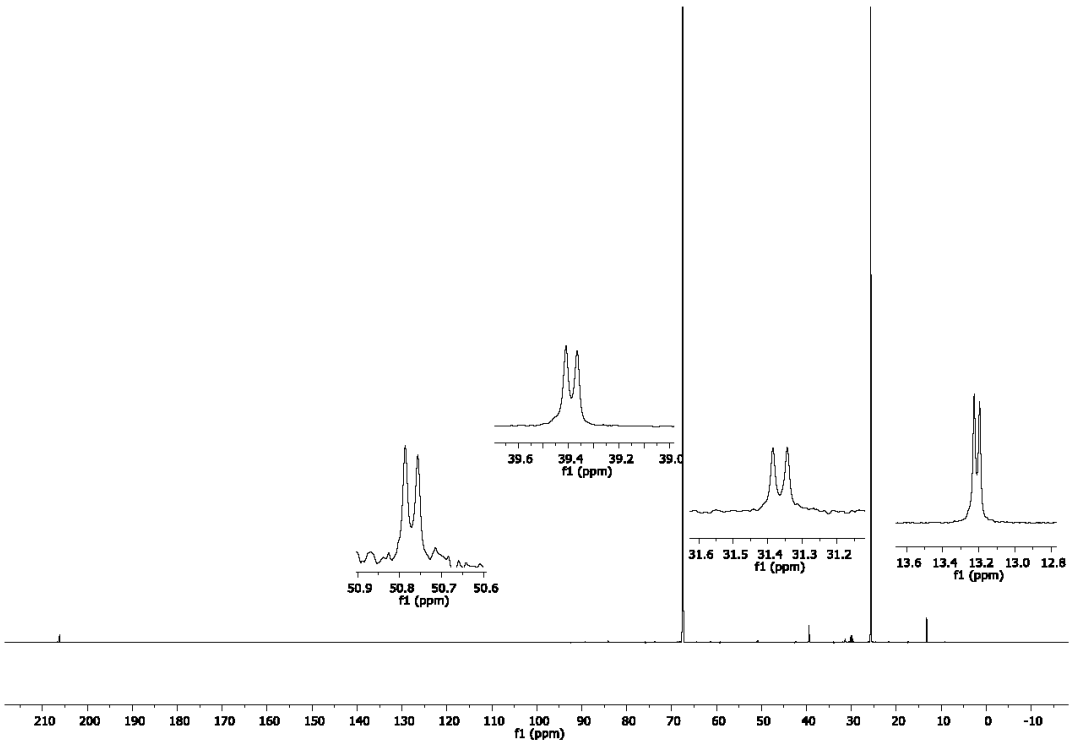

Figure 16. $^{13}C\{^{1}H\}$ NMR spectrum of the salt mixture **[2H][SF_5]** and **[2H][F]** in THF (500 MHz). Lock with acetone-d_6 in a capillary.

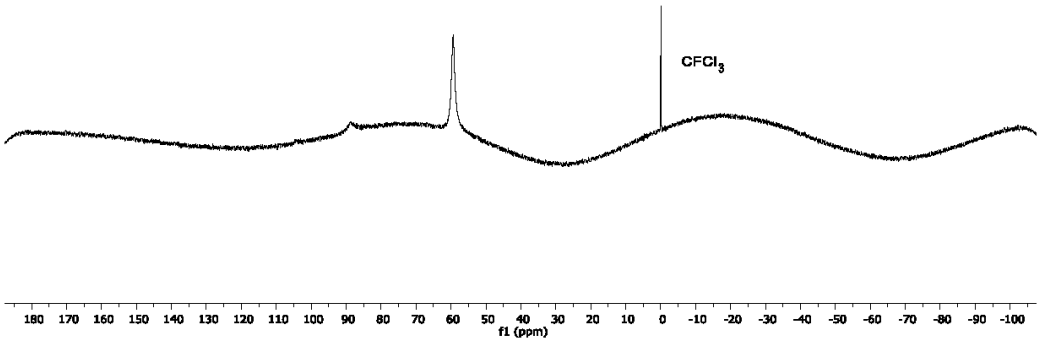

Figure 17. ^{19}F NMR spectrum of the salt mixture **[2H][SF_5]** and **[2H][F]** in THF (500 MHz). Lock with acetone-d_6 in a capillary. $CFCl_3$ as internal standard. SW [ppm] 295.08; O1P [ppm] 40.00.

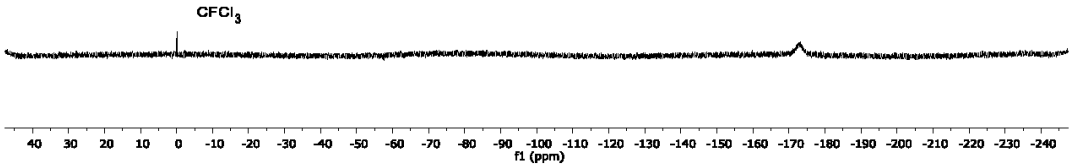

Figure 18. ^{19}F NMR spectrum of the salt mixture **[2H][SF_5]** and **[2H][F]** in THF (500 MHz). Lock with acetone-d_6 in a capillary. $CFCl_3$ as internal standard. SW [ppm] 295.12; O1P [ppm] -100.00.

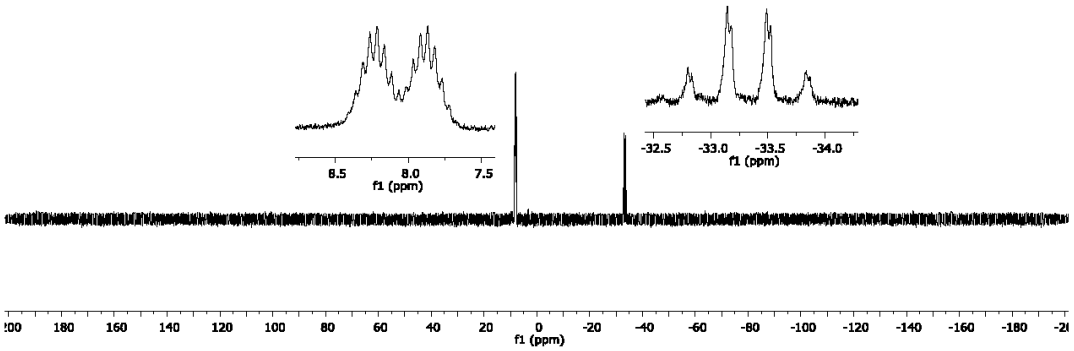

Figure 19. ^{31}P NMR spectrum of the salt mixture **[2H][SF_5]** and **[2H][F]** in THF (500 MHz). Lock with acetone-d_6 in a capillary.

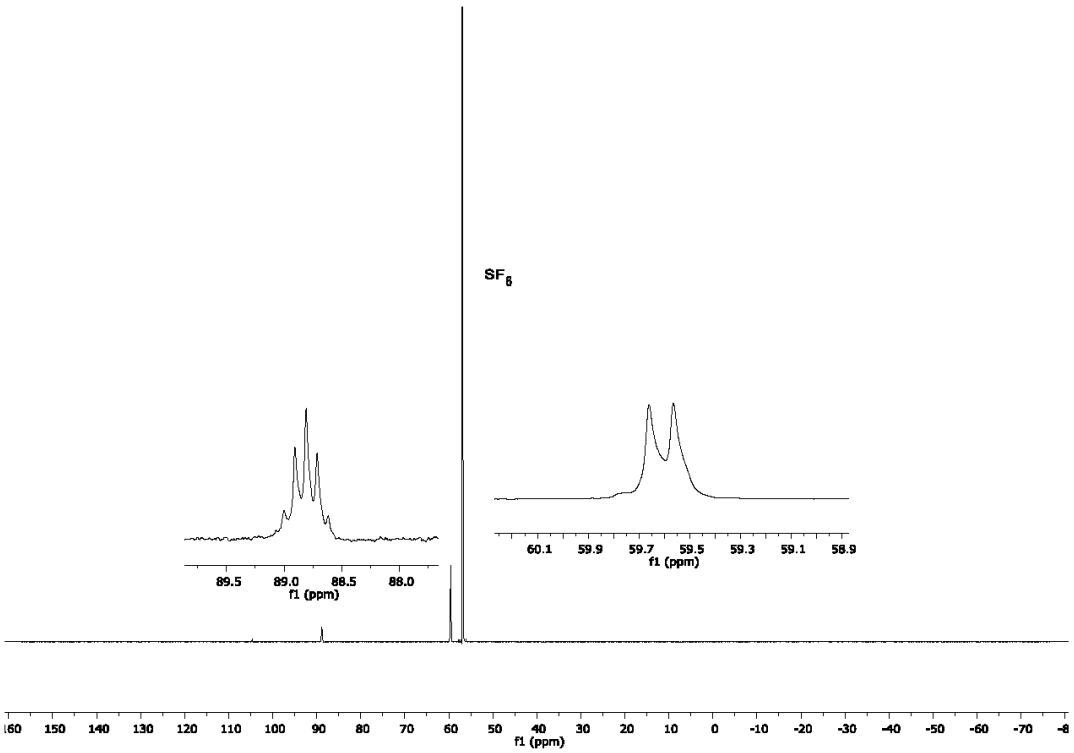

Figure 20. ^{19}F NMR spectrum of the SF_6 activation in Et_2O solution in an FEP tube (500 MHz). Lock with acetone-d_6 in a surrounding NMR tube. SW [ppm] 241.52; O1P [ppm] 40.00.

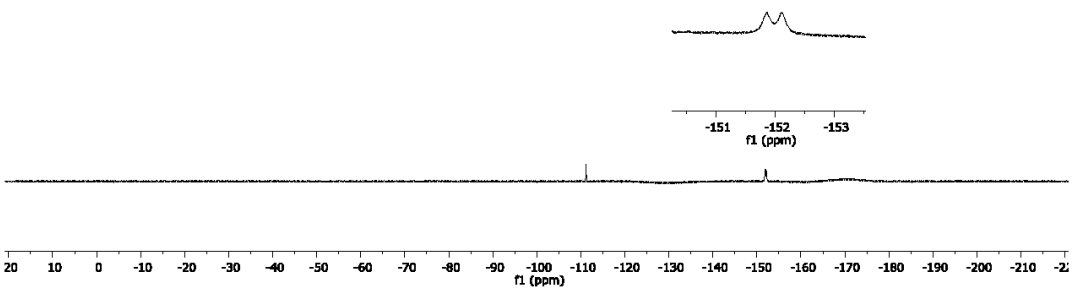

Figure 21. ^{19}F NMR spectrum of the SF_6 activation in Et_2O solution in an FEP tube (500 MHz). Lock with acetone-d_6 in a surrounding NMR tube. The resonance at δ = -152 ppm results from $[HF_2]^-$, which forms over time. SW [ppm] 241.56; O1P [ppm] -100.00.

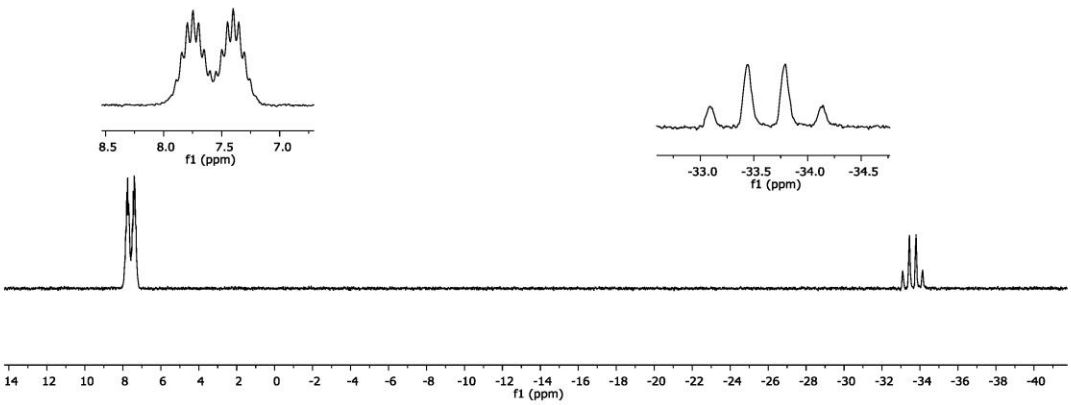

Figure 22. ^{31}P NMR spectrum of the SF_6 activation in Et_2O solution in an FEP tube (500 MHz). Lock with acetone-d_6 in a surrounding NMR tube.

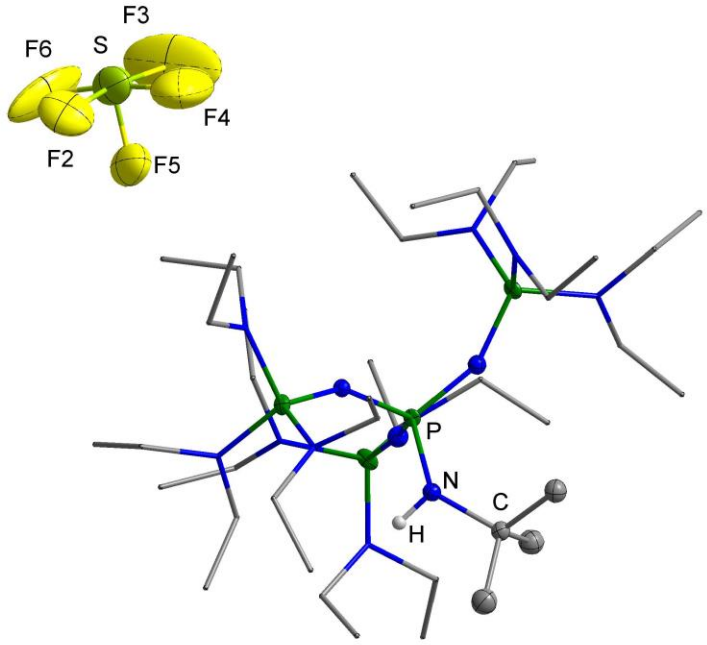

Figure 23. Molecular structure of **[2H][SF_5]** in the solid state. Thermal ellipsoids are shown at 50 % probability. The hydrogen atoms bonded at carbon atoms are omitted for clarity. Diethylamino groups are shown as stick model.

1.4 Details on the X-Ray Diffraction

The crystal data were collected on a Rigaku Supernova diffractometer (Cu-K_α radiation (λ = 154.184 pm) or Mo-K_α radiation (λ = 71.073 pm) at 100.0(2) K.
Using Olex2[1], the structures were solved with the ShelXS[2] structure solution program using direct methods and refined with the ShelXL[3] refinement package using least squares minimization. All hydrogen atoms bonded at nitrogen or oxygen were refined isotropically including the 1:1 disordered ones in **[2H][PhO(HOPh)]**.
Details of the X-ray investigation are given in Tables 1-3. CCDC 1973242-1973244, 2002668 and 2002669 contain the supplementary crystallographic data for this paper. These data can be obtained free of charge via http://www.ccdc.cam.ac.uk/conts/retrieving.html.

Table 1. Structure refinement data of **[1H][PhO(HOPh)]** and **[2H][PhO]**.

compound	**[1H][PhO(HOPh)]**	**[2H][PhO]**
empirical formula	$C_{28}H_{45}N_4O_2P$	$C_{46}H_{105}N_{13}OP_4$
a / pm	1927.213(11)	1293.050(10)
b / pm	1640.156(10)	1952.430(10)
c / pm	8711.71(5)	2285.320(10)
α / °	90	90
β / °	90	102.3290(10)
γ / °	90	90
V / 10^6 pm^3	2753.71(3)	5636.44(6)
Z	4	4
ρ_{calc} / mg·mm^{-3}	1.208	1.155
crystal system	orthorhombic	monoclinic
space group	*Pna*2$_1$	*P*2$_1$/*n*
color shape	yellowish block	colorless irregular
crystal size / mm^{-3}	0.087 × 0.07 × 0.033	0.292 × 0.202 × 0.148
μ / mm^{-1}	1.122	1.581
F(000)	1088.0	2160.0
2θ range for data col. / °	7.078 to 151.786°	6.014 to 152.968°
index ranges	-24 ≤ *h* ≤ 24 -19 ≤ *k* ≤ 20 -10 ≤ *l* ≤ 10	-11 ≤ *h* ≤ 16 -22 ≤ *k* ≤ 24 -28 ≤ *l* ≤ 27
reflections col.	50317	27180
independent refl.	5686	11608
R(int)	0.0343	0.0156
data/restraints/	5686/1/327	11608/0/623

parameter		
goodness-of-fit on F^2	1.046	1.036
R_1 / wR_2 [I>2σ(I)]	0.0249/0.0665	0.0341/0.0883
R_1 / wR_2 (all data)	0.0256/0.0671	0.0357/0.0897
$\Delta\rho_{max/min}$ / e Å^{-3}	0.25/-0.16	0.74/-0.57
CCDC number	1973242	1973243

Table 2. Structure refinement data of **[2H][PhO(HOPh)]** and **[2H][^{MeOtBu2}PhO]**.

compound	**[2H][PhO(HOPh)]**	**[2H][^{MeOtBu2}PhO]**
empirical formula	$C_{52}H_{111}N_{13}O_2P_4$	$C_{55}H_{123}N_{13}O_2P_4$
a / pm	1332.764(8)	1646.26(2)
b / pm	1919.982(10)	1956.90(2)
c / pm	2416.372(14)	2058.51(2)
α / °	90	90
β / °	90.7361(5)	90
γ / °	90	90
V / 10^6 pm^3	6182.70(6)	6631.62(13)
Z	4	4
ρ_{calc} / mg·mm^{-3}	1.154	1.124
crystal system	monoclinic	orthorhombic
space group	$P2_1/c$	$P2_12_12_1$
color shape	colorless block	clear yellow, irregular
crystal size / mm^{-3}	0.244 × 0.144 × 0.135	0.221 × 0.19 × 0.087
μ / mm^{-1}	1.496	1.412
F(000)	2360.0	2480.0
2θ range for data col. / °	5.88 to 153.038°	6.232 to 152.94°

index ranges	$-16 \le h \le 16$ $-24 \le k \le 24$ $-30 \le l \le 30$	$-20 \le h \le 20$ $-24 \le k \le 24$ $-25 \le l \le 16$
reflections col.	126690	59589
independent refl.	12952	13795
R(int)	0.0404	0.0634
data/restraints/ parameter	12952/0/1127	13795/0/699
goodness-of-fit on F^2	1.016	1.030
R_1 / wR_2 [I>2σ(I)]	0.0300/0.0794	0.0413/0.1061
R_1 / wR_2 (all data)	0.0337/0.0823	0.0464/0.1102
$\Delta\rho_{max/min}$ / e Å^{-3}	0.36/-0.35	0.43/-0.36
CCDC number	1973244	2002668

Table 3. Structure refinement data of **[2H][SF_5]**.

compound	**[2H][SF_5]**
empirical formula	$C_{40}H_{100}F_5N_{13}P_4S$
a / pm	1263.54(9)
b / pm	1772.96(9)
c / pm	2459.20(15)
α / °	90
β / °	99.856(6)
γ / °	90
V / 10^6 pm^3	5427.8(6)
Z	4
ρ_{calc} / mg·mm^{-3}	1.241

crystal system	monoclinic
space group	$P2_1/c$
color shape	colorless plate
crystal size / mm^{-3}	0.218 × 0.063 × 0.023
μ / mm^{-1}	2.129
F(000)	2208.0
2θ range for data col. / °	9.978 to 133.182°
index ranges	$-14 \leq h \leq 15$ $-21 \leq k \leq 21$ $-21 \leq l \leq 29$
reflections col.	24230
independent refl.	24230
R(int)	0.1877
data/restraints/ parameter	11517/318/569
goodness-of-fit on F^2	1.656
R_1 / wR_2 [I>2σ(I)]	0.1927/0.4507
R_1 / wR_2 (all data)	0.2679/0.4931
$\Delta\rho_{max/min}$ / e $Å^{-3}$	2.63/-1.70
CCDC number	2002669

References

[1] O. V. Dolomanov, L. J. Bourhis, R. J. Gildea, J. A. K. Howard, H. Puschmann, *J. Appl. Cryst.* **2009**, *42*, 339.

[2] G. M. Sheldrick, *Acta Cryst. A* **2015**, *71*, 3.

[3] G. M. Sheldrick, *Acta Cryst. C* **2015**, *71*, 3.

Anhang 4

The Influence of Weakly Coordinating Cations on the O-H···O$^-$ Hydrogen Bond of Silanol-Silanolate Anions

Robin F. Weitkamp, Beate Neumann, Hans-Georg Stammler and Berthold Hoge

Chem. Eur. J. **2021**, *27*, 915.

Chemistry–A European Journal | Communication
doi.org/10.1002/chem.202004236

Silicon

The Influence of Weakly Coordinating Cations on the O–H···O⁻ Hydrogen Bond of Silanol-Silanolate Anions

Robin F. Weitkamp, Beate Neumann, Hans-Georg Stammler, and Berthold Hoge*[a]

Dedicated to Professor Dr. Herbert W. Roesky on the occasion of his 85th birthday

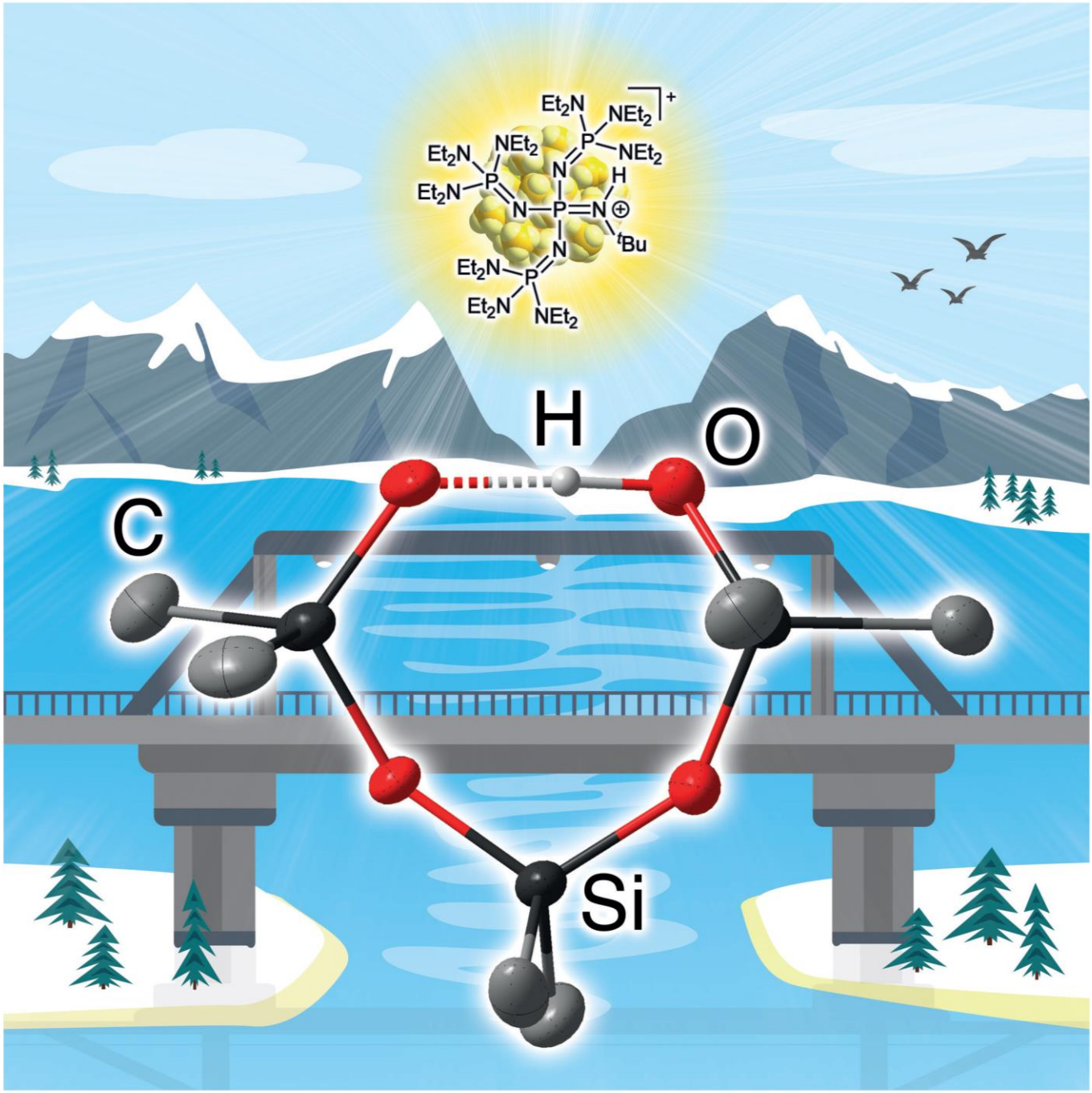

Chemistry–A European Journal | Communication
doi.org/10.1002/chem.202004236
Chemistr Europe
European Chemic Societies Publishi

Abstract: The reaction of a saline phosphazenium hydroxide hydrate with siloxanes led to a novel kind of silanol-silanolate anions. The weakly coordinating behavior of the cation renders the formation of silanol-silanolate hydrogen bonds possible, which otherwise suffer from detrimental silanolate–oxygen cation interactions. We investigated the influence of various weakly coordinating cations on silanol-silanolate motifs, particularly with regard to different cation sizes. While large cations favor the formation of intramolecular hydrogen bonds resulting in cyclic structures, the less bulky tetramethyl ammonium cation encourages the formation of polyanionic silanol-silanolate chains in the solid state.

There is no life without hydrogen bonds.[1–5] The most prominent representative of hydrogen bonding is water. Without hydrogen bonding water would not exist in the well-known form, but would exhibit significant differences in the melting and boiling point, as it is observed for the higher homologue H_2S.[6] Moreover, hydrogen bonding is crucial in supramolecular chemistry, as the helical structure of the DNA, as well as the secondary and tertiary structures of proteins and peptides, are based on those weak interactions.[1–5] Consequently, the understanding of hydrogen bonding is decisive to understand chemistry at all.

Hydrogen bonding is not an exclusive domain in biochemistry. Inorganic compounds besides H_2O show such interactions as well. Silanols[7,8,9] and silanediols[10–13] exhibit distinct tendencies for hydrogen bond formation, which often result in the formation of ring structures. Meanwhile several studies are directed to interactions in silanol-silanol adducts,[8,9,12–14] as well as in silanol-alcohol[15] and in silanol-amine[9,16,17] aggregates. The obtained structures are strongly affected by the presence of solvent molecules capable of hydrogen bonding. Silanols have also found application as catalysts in silanol-hydrogen-bond-assisted coupling reactions[10,11] and CO_2 fixation strategies.[16,18]

Weakly coordinating cations are essential for the investigation of hydrogen bonds in silanol-silanolates, which is clearly clarified by the strong potassium oxygen interaction in the representative potassium silanolate $[K\{O(Ph_2SiO)_2SiPh_2OH\}]_2$ of Sullivan et al.[19] The interaction of the silanolate oxygen with the potassium cation is favored over the formation of a silanol-silanolate hydrogen bond. Thus, ring formation including the potassium ion is observed.

Bulky phosphazenium cations are predestinated for the investigation of non-coordinated anions, such as naked fluoride anions,[20] the hydroxide trihydrate anion[21] or reactive aluminates,[22] and are also capable to stabilize isolated silanol-silanolate anions, as recently reported by us (Figure 1).[23]

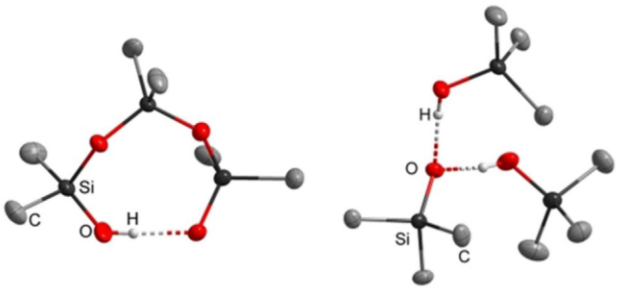

Figure 1. Depiction of selected molecular geometries of silanol-silanolate anions in the solid state featuring the phosphazenium counterion **[1H]**$^+$, reported earlier by us.[23] The cation is not depicted.

The benefits of strong neutral bases like tetraphosphazene **1** ($[(Et_2N)_3P{=}N]_3P{=}N\mathit{t}Bu$) and guanidino monophosphazene **2** ($[(Me_2N)_2C{=}N]_3P{=}N\mathit{t}Bu$) applied in this work (Figure 2) are the high proton affinity paired with the low electrophilicity of the corresponding cations. In the following, we are going to show that in addition to the low coordination ability of these cations, their sizes also play decisive roles in the construction of the observed structural patterns.

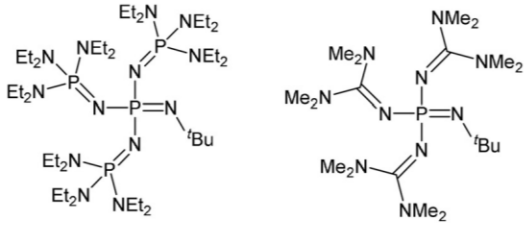

Figure 2. Phosphazene bases applied in this work.

As previously reported by us, silanol-silanolate anions can be synthesized by the reaction of a saline phosphazenium hydroxide hydrate with siloxane species.[23,24] Due to the weak electrophilicity of the cation, anions are formed in which hydrogen bond formation is favored over cation anion interactions. We disclosed that hydrogen bonding is crucial for the existence of highly basic silanolate anions. Similar to the decomposition pathway of the hydroxide trihydrate anion, non-coordinated silanolate anions are not viable in the presence of phosphazenium cation **[1H]**$^+$ due to deprotonation of the cation.[23] The selective syntheses of silanol-silanolate anions without cation anion interactions render a precise investigation of hydrogen

[a] *R. F. Weitkamp, B. Neumann, Dr. H.-G. Stammler, Prof. Dr. B. Hoge*
Centrum für Molekulare Materialien, Fakultät für Chemie
Universität Bielefeld, Universitätsstraße 25, 33615 Bielefeld (Germany)
E-mail: b.hoge@uni-bielefeld.de

Supporting information and the ORCID identification number(s) for the author(s) of this article can be found under:
https://doi.org/10.1002/chem.202004236.

Chemistry–A European Journal | Communication doi.org/10.1002/chem.202004236 | Chemist Europe European Chem Societies Publis

bond formation possible. In the case of dimethyl- (Figure 1, left) or diphenyl-siloxanes[23] the corresponding cyclic $[D_3OH]^-$ anions featuring strong intramolecular hydrogen bonds are particularly stable in the solid state. This is in agreement with the results of Baney and Atkari, who proposed the formation of $[D_3OH]^-$ anions by potentiometric titration experiments of cyclic siloxanes with tetra-*n*-butylammonium hydroxide.[25] In order to examine cation-dependent differences in silanol-silanolate structures, hydroxide salts of the depicted cations in Scheme 1 were applied for the reaction with dimethylsiloxanes.

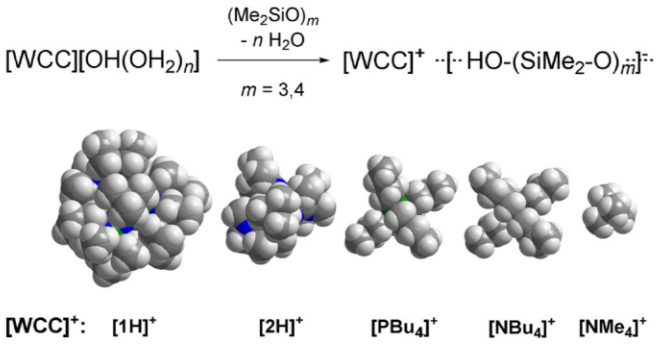

Scheme 1. Reaction of hydroxide hydrate salts of weakly coordinating cations (WCC) with cyclic siloxanes (top) and space filling models of weakly coordinating cations obtained from X-ray investigations (below).

The free tetra- and monophosphazene bases **1**[21] and **2**[24,27] were synthesized according to known literature procedures. The latter was liberated from its hydrochloride salt applying $NaNH_2$ in liquid ammonia as the deprotonation agent.

[1H][OH(OH$_2$)$_n$] was generated by addition of one molar equivalent of water to the free base in *n*-hexane. The subsequent reaction with hexamethylcyclotrisiloxane (D_3) afforded **[1H][D$_3$OH]** in a nearly quantitative yield on a multigram scale. The non-hygroscopic product is well soluble in benzene and chlorobenzene. The ^{29}Si NMR resonance of the silicon atoms adjacent to the intramolecular hydrogen bridge appears as a singlet at $\delta = -23.9$ ppm. The signal of the central silicon atom is slightly highfield shifted to $\delta = -24.1$ ppm. The intramolecular hydrogen bond length (O1–O4 distance) amounts to 242.8(2) pm (Figure 1).[23,26]

Whereas the cation of salt **[1H][OH(OH$_2$)$_n$]** is highly resistant towards hydroxide anions in THF or aqueous solution, phosphazene **2** hydrolyses in H_2O via its hydroxide salt. ^{31}P NMR resonances of unspecified products at $\delta = -5.4$, -0.2 and 1.7 ppm were observed. The resonance at $\delta = 19.7$ ppm is assigned to the phosphorus atom of phosphane oxide $[(Me_2N)_2C{=}N]_3P{=}O$. In the presence of NaOMe in aqueous MeOH, hydrolysis of base **2** leads to the formation of the amide derivative **3**, with a ^{31}P NMR resonance at $\delta = -4.8$ ppm in water. The product was further evidenced by X-ray diffraction (Scheme 2).[26]

The amide **3** is characterized by a cyclic intramolecular hydrogen bridge. The corresponding O1–N1 distance amounts to 278.9(4) pm.

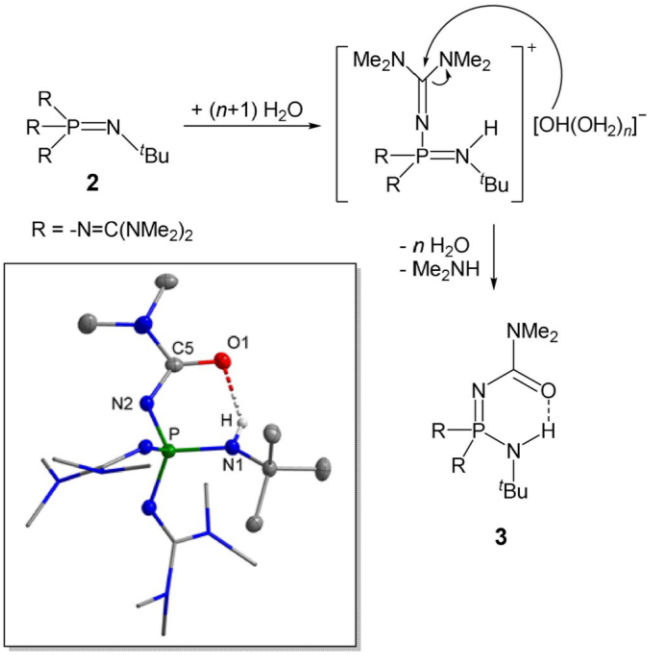

Scheme 2. Hydrolysis of **2** and molecular structure of **3** (box): All hydrogen atoms bonded at carbon atoms are omitted for clarity.[26] Guanidyl groups are shown as stick model. Selected bond lengths [pm]: O1–C5 125.2(5), N2–C5 134.3(5).

Hydrolysis of **[2H]**$^+$ can be efficiently suppressed temporarily if siloxanes like D_3 are present in the mixture prior to the addition of water (Scheme 3).

Thus, the corresponding guanidino phosphazenium salt **[2H][D$_3$OH]** was isolated as pale yellow, highly hygroscopic crystals (98% yield). However, in the presence of $[D_3OH]^-$ cation **[2H]**$^+$ succumbs quite fast to hydrolysis at ambient temperature also resulting in the clean formation of **3**, which hampers a reliable elemental analysis. In the ^{31}P NMR spectrum of **[2H][D$_3$OH]** the resonance of the phosphorus atom in **[2H]**$^+$ is observed as a singlet at $\delta = -10.6$ ppm. In the ^{1}H^{29}Si HMBC NMR spectrum the resonances of the terminal silicon atoms of the anionic ring are slightly downfield shifted ($\delta = -22.8$ ppm) compared to **[1H][D$_3$OH]** ($\delta = -23.7$ ppm).

An X-ray diffraction study of crystals grown from the cooled reaction mixture reveals a cation-anion hydrogen bond interaction with an N1-O4 separation of 285.2(2) pm (Figure 3), which is presumably responsible for the small downfield shift of the terminal ^{29}Si nuclei.[26] The other hydrogen bond within the anion with an O1–O4 distance of 250.8(2) pm is elongated compared to **[1H][D$_3$OH]** (242.8(2) pm).

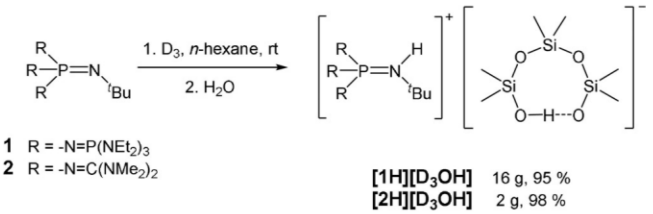

Scheme 3. Syntheses of phosphazenium silanol-silanolates.

Chemistry–A European Journal | Communication doi.org/10.1002/chem.202004236 | Chemist Europe European Cher Societies Publi

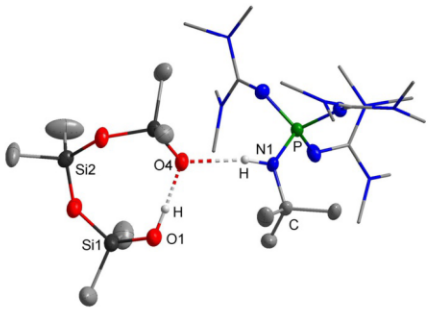

Figure 3. Molecular structure of **[2H][D$_3$OH]** with highlighted cation anion hydrogen bond interaction.[26] Disorder of Si1, C22 and C23 over two sites (76:24). Disordered parts and hydrogen atoms of methyl groups are omitted for clarity. Guanidyl groups are shown as stick model. Selected bond lengths [pm] and angles [°]: N1–P1 162.9(1), N1–O4 285.2(2), O1–O4 250.8(2), O1–Si1 160.7(1), O4–Si3 159.0(1); O1-O4-Si3 116.2(1), O4-O1-Si1 113.9(1), O2-Si2-O3 111.9(3).

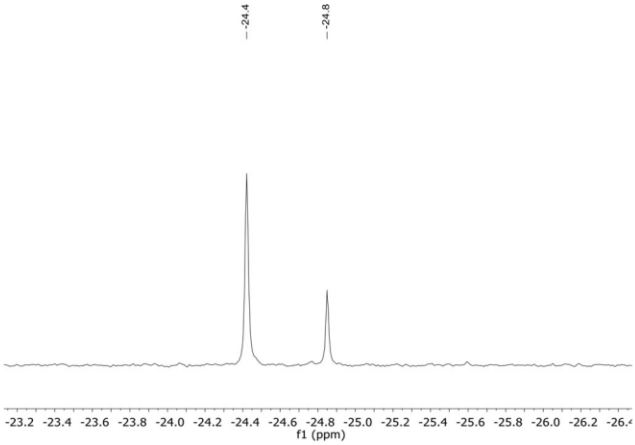

Figure 4. ^{29}Si NMR spectrum of **[NBu$_4$][D$_3$OH]** in Et$_2$O (lock with [D$_6$]acetone in a capillary).

The salt **[2H][D$_3$OH]** decomposes within days at room temperature, and it deteriorates fast above 75 °C with hydrolysis of its cation under formation of **3** (^{31}P shift of the decomposition product at $\delta = 1.0$ ppm in chlorobenzene, lock with [D$_6$]acetone in a capillary) and liberation of cyclic siloxanes, mainly D$_4$.

For the syntheses of phosphonium and ammonium silanolates, the corresponding hydroxides ([NMe$_4$]OH 25 wt. % in MeOH, [NBu$_4$][OH(OH$_2$)$_{30}$], [PBu$_4$]OH 40 wt. % in H$_2$O) were applied. The nature of the employed siloxane source is not decisive, since equilibrium mixtures of linear and cyclic siloxanes are always present in the base assisted reaction and D$_3$ fragments are formed by binding rearrangements. We employed liquid octamethylcyclotetrasiloxane (D$_4$), which additionally acted as the solvent. In the case of [NMe$_4$]OH, the reaction with D$_3$ as siloxane source was performed in ethereal solution.[24] In all cases the excess of siloxane and water can be removed in vacuo after the reaction.[23] The tetra-*n*-butylammonium and tetra-*n*-butylphosphonium silanolates were isolated in yields of 92% and 73% after crystallization from saturated ethereal solutions at −28 °C. The ^{29}Si NMR spectrum of **[NBu$_4$][D$_3$OH]** is depicted in Figure 4. The resonance at $\delta = -24.4$ ppm results from the silicon atoms adjacent to the hydrogen bond.

The X-ray structural investigation reveals the cyclic [D$_3$OH]$^-$ anion in both salts, which is depicted for **[NBu$_4$][D$_3$OH]** as a representative example in Figure 5.[26]

The hydrogen bonds within the obtained [D$_3$OH]$^-$ anions were identified by the O1-O4 distances, which amount to 245.1(1) pm for **[NBu$_4$][D$_3$OH]** and 244.3(1) pm for **[PBu$_4$][D$_3$OH]**. They are well comparable with the value in **[1H][D$_3$OH]**.[23] Both salts are highly hygroscopic and melt within seconds under air. The salt **[NBu$_4$][D$_3$OH]** completely decomposes by a Hofmann-type elimination reaction of the cation above 80 °C in high vacuum. The released products tributylamine and butene were detected via ^{1}H NMR spectroscopy. Cyclic siloxanes are also liberated.[24] While **[NBu$_4$][D$_3$OH]** is stable at room temperature as a crystalline solid under inert atmosphere over months without any traces of decomposition,

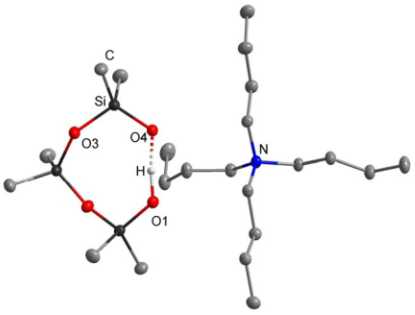

Figure 5. Molecular structure of **[NBu$_4$][D$_3$OH]**.[26] All hydrogen atoms bonded at carbon atoms are omitted for clarity. Thermal ellipsoids are set at 50% probability. Selected bond length [pm]: O1-O4 245.1(1).

the tetra-*n*-butylphosphonium cation in solid **[PBu$_4$][D$_3$OH]** completely hydrolyzes within days under the same conditions. Fast hydrolysis is observed over a few hours in ethereal solution to afford the corresponding tributylphosphane oxide, which is evidenced by ^{31}P NMR spectroscopy at a chemical shift of $\delta = 42.5$ ppm (lit: 42.0 ppm).[28]

From the corresponding reaction of [NMe$_4$]OH with D$_3$ a colorless sticky oil was obtained, which is insoluble in benzene and barely soluble in diethyl ether and chlorobenzene. By layering the oil with diethyl ether and storage at −28 °C, colorless crystals of **[NMe$_4$][D$_3$OH]$_{1/\infty}$** were obtained with a melting point of 75 °C. Its decomposition at ambient temperature, which impedes a reliable elemental analysis, is accompanied by a strong amine odor and a yellow discoloration. The ^{29}Si NMR spectroscopic investigation of a milky chlorobenzene solution of the mixture reveals the presence of six chemically inequivalent silicon atoms. In comparison to previously discussed [WCC][D$_3$OH] salts, the resonances at $\delta = -24.7$ and −24.1 ppm in a ratio of 2:1 are assigned to the silicon atoms of the [D$_3$OH]$^-$ moiety. The X-ray diffraction of a small crystalline fragment reveals a polymeric silanolate anion in **[NMe$_4$][D$_3$OH]$_{1/\infty}$** (Figure 6).[26] In stark contrast to cyclic silanol-silanolate anions of the type [D$_3$OH]$^-$, which were obtained with

Chemistry–A European Journal | Communication
doi.org/10.1002/chem.202004236
Chemist Europe
European Chem Societies Publis

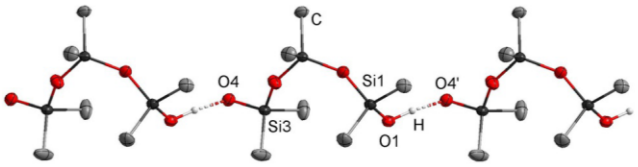

Figure 6. Section of the strand of the $[D_3OH]^-_x$ polyanion along the *x* axis spanned by intermolecular silanol-silanolate hydrogen bonding in **[NMe$_4$][D$_3$OH]**$_{1/\infty}$.[26] All hydrogen atoms bonded at carbon atoms and tetramethylammonium counterions are omitted for clarity. Thermal ellipsoids are set at 50% probability. Selected bond length [pm]: O1—O4′ 247.0(1).

bulky counterions, the small tetramethylammonium cation favors the formation of intermolecular hydrogen bonding in the solid state. Compared to the cyclic anion in **[NBu$_4$][D$_3$OH]**, in which the terminal silanol and silanolate functions exhibit torsion angles of 55.9° (O1-Si1-O2-Si2) and 55.8° (O4-Si3-O3-Si2), the terminal functions in **[NMe$_4$][D$_3$OH]**$_{1/\infty}$ are rotated around the bonds Si1-O2 and Si3-O3 with torsion angles of 123.9° (O1-Si1-O2-Si2) and 132.5° (O4-Si3-O3-Si2). This gives rise to linear polyanionic chains of $[D_3OH]_{1/\infty}^-$ units (Figure 6), which seem to be responsible for the poor solubility of salt **[NMe$_4$][D$_3$OH]**$_{1/\infty}$.

The intermolecular O1–O4′ distance was determined to 247.0(1) pm and is thus slightly elongated in comparison to intramolecular hydrogen bonding in **[1H][D$_3$OH]** (242.8(2) pm) and **[NBu$_4$][D$_3$OH]** (245.1(1) pm). Interestingly, the anionic structural motif of the three $SiMe_2O$ units is maintained.

Accidentally, impurities of potassium hydroxide were present in a flask of $[NMe_4]OH$ and cyclic siloxanes. Gratifyingly, single crystals of salt **[NMe$_4$][K(D$_3$OH)$_2$]** evolved and were analyzed by X-ray crystallography (Figure 7).[26]

The potassium cation is surrounded by two $[D_3OH]^-$ units exhibiting strong potassium silanolate (d(K–O4) = 269.1(2) pm) and silanol-silanolate interactions (d(O4–O8′) = 249.6(2) pm) in a mono-anionic complex. Moreover, this complex is associated to a dimer in the solid state, displaying strong potassium silanolate interactions with a K–O5 separation of 274.4(1) ppm and additional silanol-silanolate hydrogen bonds (d(O1–O5) = 244.5(2) pm). Again, the structural motif of the three $SiMe_2O$ units remains favorable. Similar to the potassium salt presented by Sullivan et al. previously,[19] the potassium ions form strong interactions to silanolate oxygen atoms, which obviously significantly influenced the construction of the formed pattern. This example impressively underlines the need for weakly coordinating cations to observe isolated silanol-silanolate interactions.

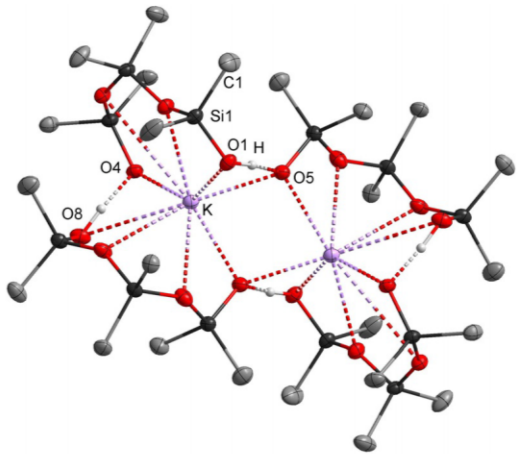

Figure 7. Molecular structure of the dimer of **[NMe$_4$][K(D$_3$OH)$_2$]**.[26] The ammonium cations are not shown. All hydrogen atoms linked to carbon atoms are omitted for clarity. Thermal ellipsoids are set at 50% probability. Selected bond lengths [pm]: K—O4 269.1(2), O1—O5 244.5(2), O4—O8′ 249.6(2).

In conclusion we succeeded in the clean formation of silanol-silanolate salts featuring weakly coordinating cations. In all cases $[D_3OH]^-$ anions containing three siloxane units were delivered, which proves the extraordinary thermal stability of this motif. Phosphazenium silanol-silanolate salts with cyclic anions of the type $[D_3OH]^-$ in **[1H][D$_3$OH]** and **[2H][D$_3$OH]** were obtained in excellent yields (>95%) by the reaction of the free phosphazene bases with water and cyclodimethylsiloxanes. The corresponding tetra-*n*-butylammonium and -phosphonium salts **[NBu$_4$][D$_3$OH]** and **[PBu$_4$][D$_3$OH]** were afforded analogously by use of their hydroxides. All cyclic $[D_3OH]^-$ anions show intramolecular hydrogen bonding, with O–O distances depending on the size and the coordination capability of the applied cation. While an enlargement of non-coordinating cations from $[NBu_4]^+$ to $[\mathbf{1H}]^+$ results in a shortening of the intramolecular hydrogen bond from 245.1(1) pm to 242.8(2) pm, hydrogen bond donating cations like $[\mathbf{2H}]^+$ favor an extension of the formed bond (250.8(2) pm). Downsizing the cation to $[NMe_4]^+$ in **[NMe$_4$][D$_3$OH]**$_{1/\infty}$ benefits the organization of the $[D_3OH]^-$ moieties in a polyanionic strand. In contrast to cyclic $[D_3OH]^-$ anions, an intermolecular hydrogen bond (247.0(1) pm) is predominant in the presence of less bulky counterions.

Acknowledgements

We acknowledge the financial support by Merck KGaA. We thank Prof. Dr. Lothar Weber and Dr. Julia Bader for helpful discussions. Open access funding enabled and organized by Projekt DEAL.

Conflict of interest

The authors declare no conflict of interest.

Keywords: hydrogen bond · phosphazene bases · silanolates · silanol-silanolate · weakly coordinating cations

[1] S. J. Grabowski, *Hydrogen bonding. New insights*, Springer, Dordrecht, **2006**.
[2] G. A. Jeffrey, *An introduction to hydrogen bonding*, Oxford University Press, New York, **1997**.
[3] D. Hadži, Hydrogen Bonding. Papers Presented at the Symposium on Hydrogen Bonding Held at Ljubljana, 29 July-3 August **1957**, Elsevier Science Burlington, **2013**.
[4] T. Steiner, *Angew. Chem. Int. Ed.* **2002**, *41*, 48; *Angew. Chem.* **2002**, *114*, 50.

Chemistry–A European Journal | Communication doi.org/10.1002/chem.202004236 | Chemist Europe European Chem Societies Publis

[5] T. Steiner, *Cryst. Rev.* **1996**, *6*, 1.
[6] J. R. Sabin, *J. Am. Chem. Soc.* **1971**, *93*, 3613.
[7] a) N. Winkhofer, H. W. Roesky, M. Noltemeyer, W. T. Robinson, *Angew. Chem. Int. Ed.* **1992**, *31*, 599; *Angew. Chem.* **1992**, *104*, 670; b) S. Grabowsky, M. F. Hesse, C. Paulmann, P. Luger, J. Beckmann, *Inorg. Chem.* **2009**, *48*, 4384; c) R. West, R. H. Baney, *J. Am. Chem. Soc.* **1959**, *81*, 6145; d) H. Schmidbaur, *Chem. Ber.* **1964**, *97*, 830.
[8] V. Chandrasekhar, R. Boomishankar, S. Nagendran, *Chem. Rev.* **2004**, *104*, 5847.
[9] U. Klingebiel, P. Neugebauer, I. Müller, M. Noltemeyer, I. Usón, *Eur. J. Inorg. Chem.* **2002**, 717.
[10] K. M. Diemoz, J. E. Hein, S. O. Wilson, J. C. Fettinger, A. K. Franz, *J. Org. Chem.* **2017**, *82*, 6738.
[11] A. G. Schafer, J. M. Wieting, A. E. Mattson, *Org. Lett.* **2011**, *13*, 5228.
[12] O. Graalmann, U. Klingebiel, W. Clegg, M. Haase, G. M. Sheldrick, *Chem. Ber.* **1984**, *117*, 2988.
[13] H. Behbehani, B. J. Brisdon, M. F. Mahon, K. C. Molloy, M. Mazhar, *J. Organomet. Chem.* **1993**, *463*, 41.
[14] a) P. Jutzi, U. Schubert, *Silicon chemistry: From the atom to extended systems*, Wiley-VCH, Weinheim, **2003**; b) A. Bleiber, J. Sauer, *Chem. Phys. Lett.* **1995**, *238*, 243; c) C. Reiche, S. Kliem, U. Klingebiel, M. Noltemeyer, C. Voit, R. Herbst-Irmer, S. Schmatz, *J. Organomet. Chem.* **2003**, *667*, 24; d) S. T. Malinovskii, A. Tesuro Vallina, H. Stoeckli-Evans, *J. Struct. Chem.* **2006**, *47*, 1127; e) J. Beckmann, A. Duthie, G. Reeske, M. Schürmann, *Organometallics* **2004**, *23*, 4630.
[15] a) S. A. Bourne, L. R. Nassimbeni, K. Skobridis, E. Weber, *J. Chem. Soc. Chem. Commun.* **1991**, 282; b) E. Weber, W. Seichter, K. Skobridis, D. Alivertis, V. Theodorou, P. Bombicz, I. Csöregh, *J. Inclusion Phenom. Macrocyclic Chem.* **2006**, *55*, 131.
[16] M. d. J. Velásquez-Hernández, A. Torres-Huerta, U. Hernández-Balderas, D. Martínez-Otero, A. Núñez-Pineda, V. Jancik, *Polyhedron* **2017**, *122*, 161.
[17] a) G. Prabusankar, R. Murugavel, R. J. Butcher, *Organometallics* **2004**, *23*, 2305; b) A. E. Goeta, S. E. Lawrence, M. M. Meehan, A. O'Dowd, T. R. Spalding, *Polyhedron* **2002**, *21*, 1689; c) J. O. Bauer, C. Strohmann, *J. Organomet. Chem.* **2015**, *797*, 52; d) D. Marappan, M. Palanisamy, K. Velappan, N. Muthukumaran, P. Ganesan, *Inorg. Chem. Commun.* **2018**, *92*, 101.
[18] J. Pérez-Pérez, U. Hernández-Balderas, D. Martínez-Otero, V. Jancik, *New J. Chem.* **2019**, *43*, 18525.
[19] B. Laermann, M. Lazell, M. Motevalli, A. C. Sullivan, *J. Chem. Soc. Dalton Trans.* **1997**, 1263.
[20] a) R. Schwesinger, R. Link, G. Thiele, H. Rotter, D. Honert, H.-H. Limbach, F. Männle, *Angew. Chem. Int. Ed. Engl.* **1991**, *30*, 1372–1375; *Angew. Chem.* **1991**, *103*, 1376; b) R. Schwesinger, R. Link, P. Wenzl, S. Kossek, *Chem. Eur. J.* **2006**, *12*, 438.
[21] R. F. Weitkamp, B. Neumann, H.-G. Stammler, B. Hoge, *Angew. Chem. Int. Ed.* **2019**, *58*, 14633; *Angew. Chem.* **2019**, *131*, 14775.
[22] N. Tiessen, B. Neumann, H.-G. Stammler, B. Hoge, *Chem. Eur. J.* **2020**, *26*, 13611–13614.
[23] R. F. Weitkamp, B. Neumann, H.-G. Stammler, B. Hoge, *Angew. Chem. Int. Ed.* **2020**, *59*, 5494; *Angew. Chem.* **2020**, *132*, 5536.
[24] Details are given in the Supporting Information for this paper.
[25] R. H. Baney, F. S. Atkari, *J. Organomet. Chem.* **1967**, *9*, 183.
[26] Details of the X-ray investigation are given in Table S1–S3. > Deposition numbers 952716, 2024632, 2024633, 2024634, 2024635, 2024636, and 2024637 contain(s) the supplementary crystallographic data for this paper. These data are provided free of charge by the joint Cambridge Crystallographic Data Centre and Fachinformationszentrum Karlsruhe Access Structures service.
[27] A. A. Kolomeitsev, I. A. Koppel, T. Rodima, J. Barten, E. Lork, G.-V. Röschenthaler, I. Kaljurand, A. Kütt, I. Koppel, V. Mäemets, I. Leito, *J. Am. Chem. Soc.* **2005**, *127*, 17656.
[28] S. Hawkeswood, D. W. Stephan, *Dalton Trans.* **2005**, 2182.

Manuscript received: September 17, 2020
Revised manuscript received: November 6, 2020
Accepted manuscript online: November 12, 2020
Version of record online: December 7, 2020

Chemistry—A European Journal

Supporting Information

The Influence of Weakly Coordinating Cations on the O—H···O$^-$ Hydrogen Bond of Silanol-Silanolate Anions

Robin F. Weitkamp, Beate Neumann, Hans-Georg Stammler, and Berthold Hoge*[a]

1. Experimental Section

1.1 General Part

All chemicals were obtained from commercial sources and used without further purification. Standard high-vacuum techniques were employed throughout all experiments. Non-volatile compounds were handled in a dry N_2 atmosphere using Schlenk techniques.

1.2 Analysis Methods

1.2.1 NMR Spectroscopy

NMR spectra were recorded on a Bruker Model Avance III 300 spectrometer (^{1}H 300.13 MHz; ^{13}C 75.47 MHz; ^{29}Si 59.63 MHz; ^{31}P 121.49 MHz) or on a Bruker Avance III 500 spectrometer (^{1}H 500.01 MHz; ^{13}C 125.73 MHz; ^{29}Si 99.34 MHz; ^{31}P 202.41 MHz) or on a Bruker Avance III 500 HD spectrometer (^{1}H 500.20 MHz; ^{13}C 125.79 MHz; ^{29}Si 99.38 MHz; ^{31}P 202.48 MHz). Positive shifts are downfield from the external standards TMS (^{1}H, ^{13}C, ^{29}Si) and H_3PO_4 (^{31}P). The NMR spectra were recorded in the indicated deuterated solvent or in relation to acetone-d_6 filled capillaries.

1.2.2 IR Spectroscopy

IR spectra were recorded on an ALPHA-FT-IR spectrometer (Bruker) using an ATR unit with a diamond crystal for liquids and solids.

1.2.3 Elemental Analyses

Elemental analyses were performed by Mikroanalytisches Laboratorium Kolbe (Oberhausen, Germany).

1.2.4 Melting Point

Melting points were measured on a Mettler Toledo Mp70 Melting Point System.

1.3 Syntheses

1.3.1 Synthesis of [1H][D$_3$OH]

Phosphazene **1** (13.69 g, 15.5 mmol) is dissolved in 45 mL of *n*-hexane before hexamethylcyclotrisiloxane (3.44 g, 15.5 mmol) is added. After addition of water (0.29 g, 15.5 mmol) two phases separated. After stirring at room temperature overnight, a pale yellow solid precipitates. The supernatant solution is removed via a syringe and the solid is dried in a high vacuum (10^{-3} mbar). The product (16.46 g, 14.6 mmol, 95 % based on **1**) is obtained as a colorless crystalline solid (m.p. 99-101 °C).

^{1}H NMR (C_6D_6, rt): δ [ppm] = 0.6 (s, 6 H, SiO(H_3C)$_2$SiOSi), 0.7 (s, 12 H, (H_3C)$_2$SiOH-OSi(CH_3)$_2$), 1.0 (t, $^{3}J_{HH}$ = 7 Hz, 54 H, CH_3), 1.3 (s, 9 H, C(CH_3)$_3$), 2.1 (d, $^{2}J_{PH}$ = 8 Hz, 1 H, NH), 3.0 (d, q, $^{3}J_{PH}$ = 10 Hz, $^{3}J_{HH}$ = 7 Hz, 36 H, CH_2), 14.0 (s, OH).
^{13}C{^{1}H} NMR (C_6D_6, rt): δ [ppm] = 2.3 (s, SiO(H_3C)$_2$SiOSi), 3.6 (s, (H_3C)$_2$SiOH-OSi(CH_3)$_2$), 13.4 (d, $^{3}J_{PC}$ = 4 Hz, CH_3), 31.3 (d, $^{3}J_{PC}$ = 5 Hz, C(**C**H_3)$_3$), 39.0 (d, $^{2}J_{PC}$ = 6 Hz, CH_2), 50.4 (d, $^{2}J_{PC}$ = 4 Hz, **C**(CH_3)$_3$).
^{29}Si{^{1}H}dept30 NMR (C_6D_6, rt): δ [ppm] = -24.1 (s, SiO(H_3C)$_2$**Si**OSi), -23.9 (s, (H_3C)$_2$**Si**OH-O**Si**(CH_3)$_2$).
^{29}Si{^{1}H}IG NMR (PhCl, rt): δ [ppm] = -24.2 (s, SiO(H_3C)$_2$**Si**OSi), -23.7 (s, (H_3C)$_2$**Si**OH-O**Si**(CH_3)$_2$).
^{31}P NMR (C_6D_6, rt): δ [ppm] = -33.7 (q, d, $^{2}J_{PP}$ = 70 Hz, $^{2}J_{PH}$ = 8 Hz, 1 P, P=NH), 7.6 (d, tridec, $^{2}J_{PP}$ = 70 Hz, $^{3}J_{PH}$ = 10 Hz, 3 P, (Et_2N)$_3$P).
IR (ATR): $\tilde{\nu}$ [cm^{-1}] = 2966 (vw), 2872 (vw), 1627 (vw, vbr), 1464 (vw), 1379 (w), 1351 (w), 1273 (m, br), 1247 (m), 1202 (m), 1175 (s), 1053 (w), 1016 (vs), 940 (vs), 847 (w), 784 (vs), 700 (m), 614 (w), 508 (m), 440 (m).
elemental analysis of $C_{46}H_{119}N_{13}O_4P_4Si_3$ (M = 1126.7 g/mol): calcd.: C 49.04, H 10.65, N 16.16, P 11.00, Si 7.48; found: C 48.61, H 10.64, N 15.89, P 10.98, Si 7.59.

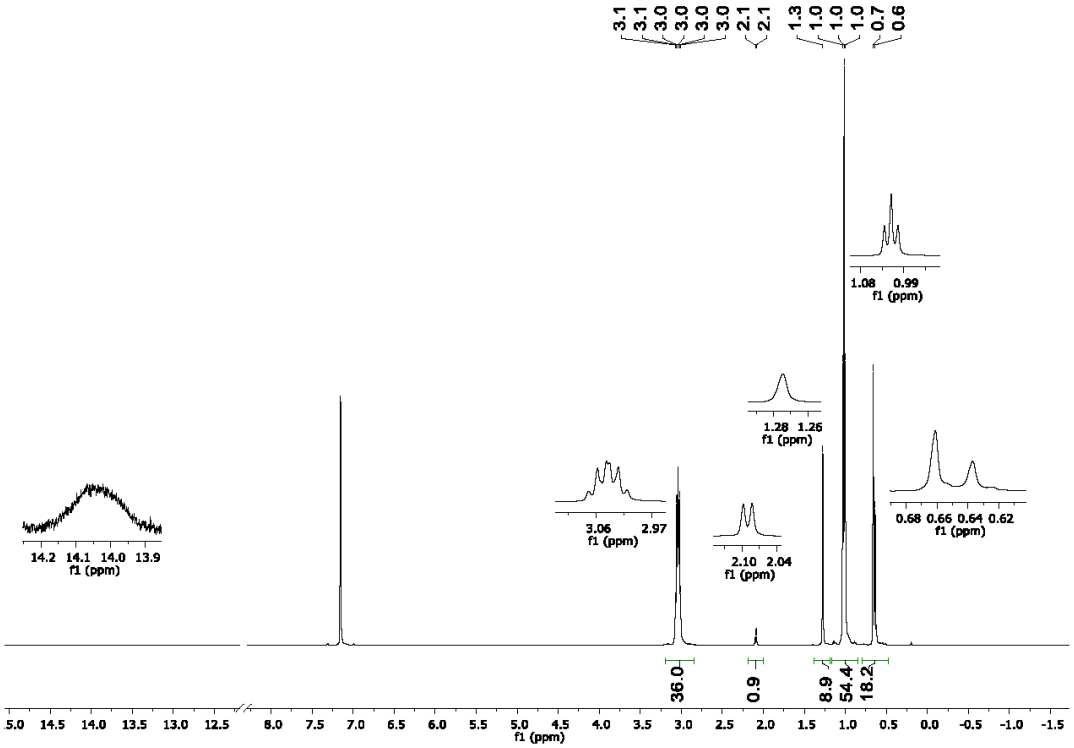

Figure 1. ^{1}H NMR spectrum of **[1H][D$_3$OH]** in benzene-d$_6$ (500 MHz).

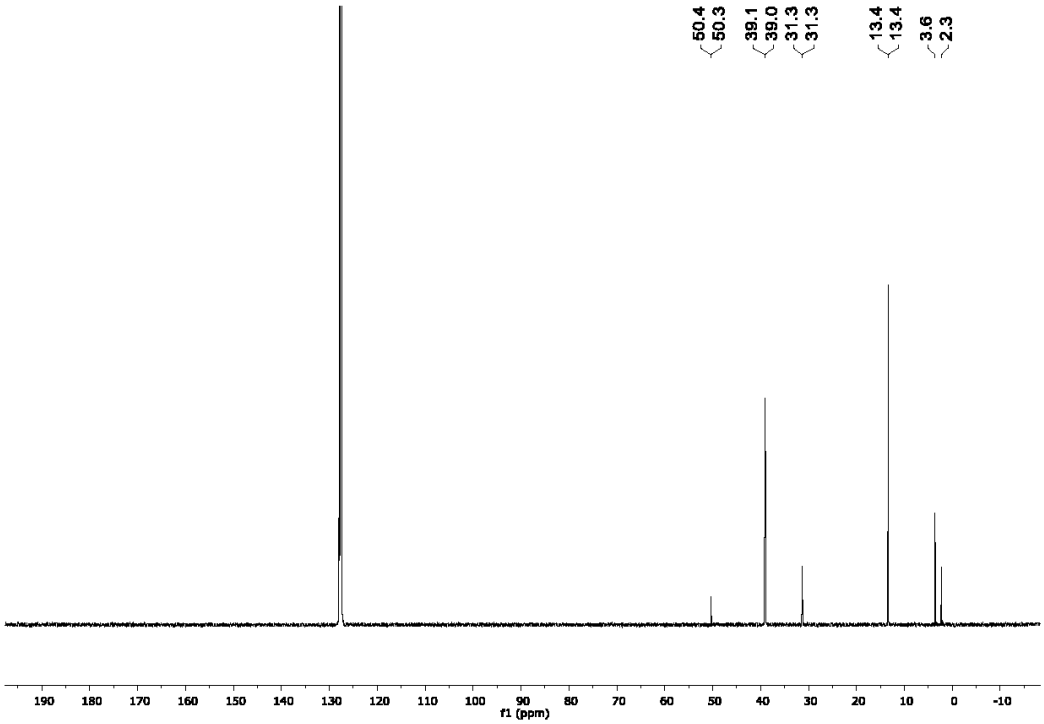

Figure 2. ^{13}C{^{1}H} NMR spectrum of **[1H][D$_3$OH]** in benzene-d$_6$ (500 MHz).

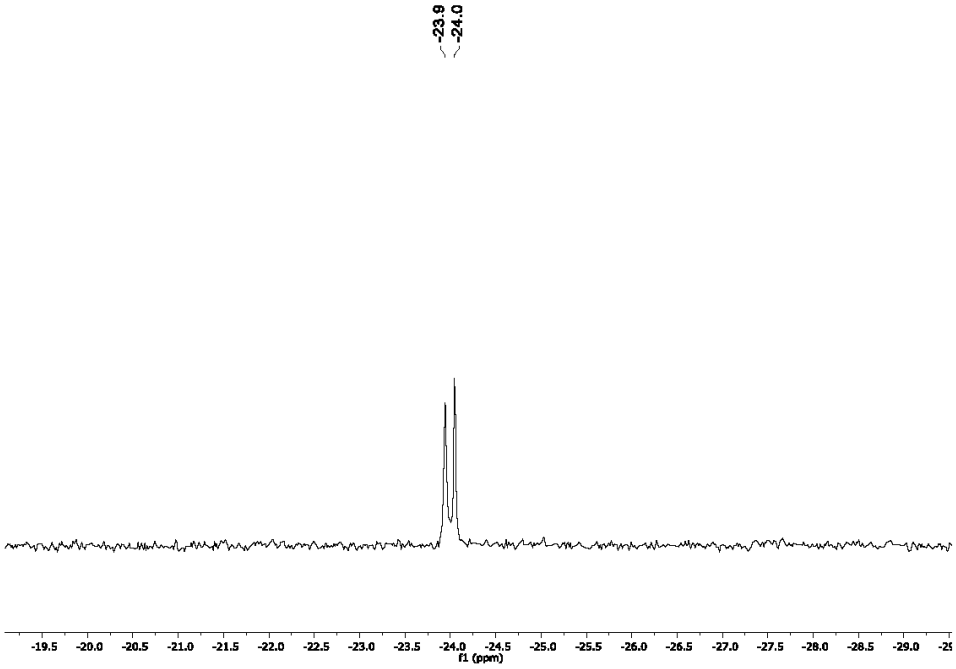

Figure 3. $^{29}Si\{^{1}H\}$dept30 NMR spectrum of **[1H][D$_3$OH]** in benzene-d$_6$ (500 MHz).

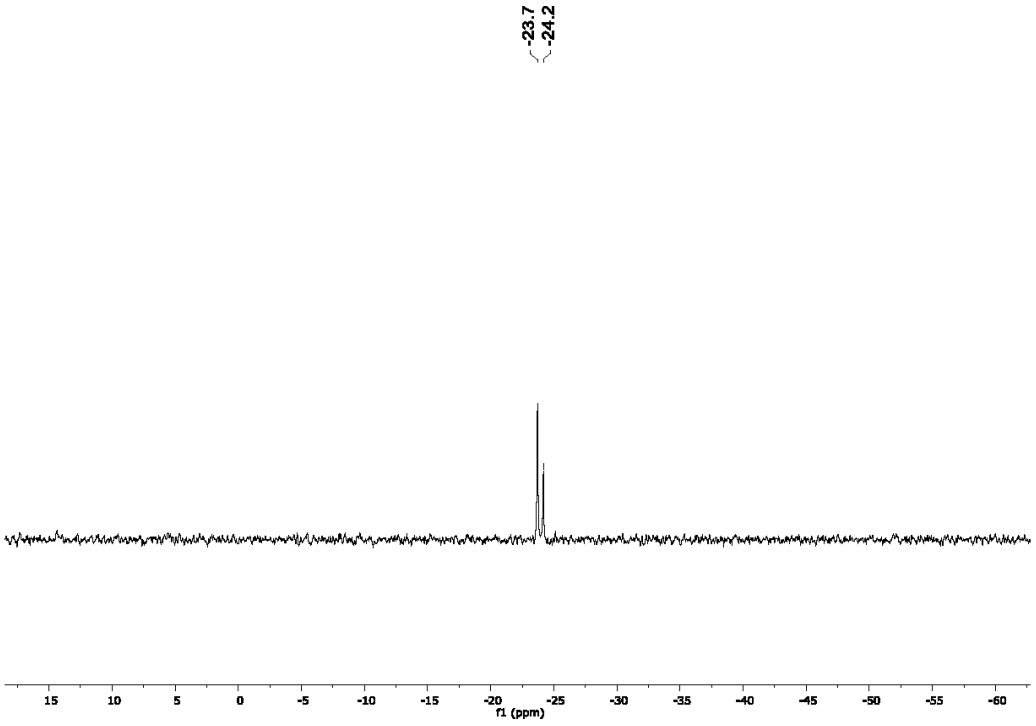

Figure 4. $^{29}Si\{^{1}H\}$IG NMR spectrum of **[1H][D$_3$OH]** in PhCl (300 MHz). Lock with acetone-d$_6$ in a capillary.

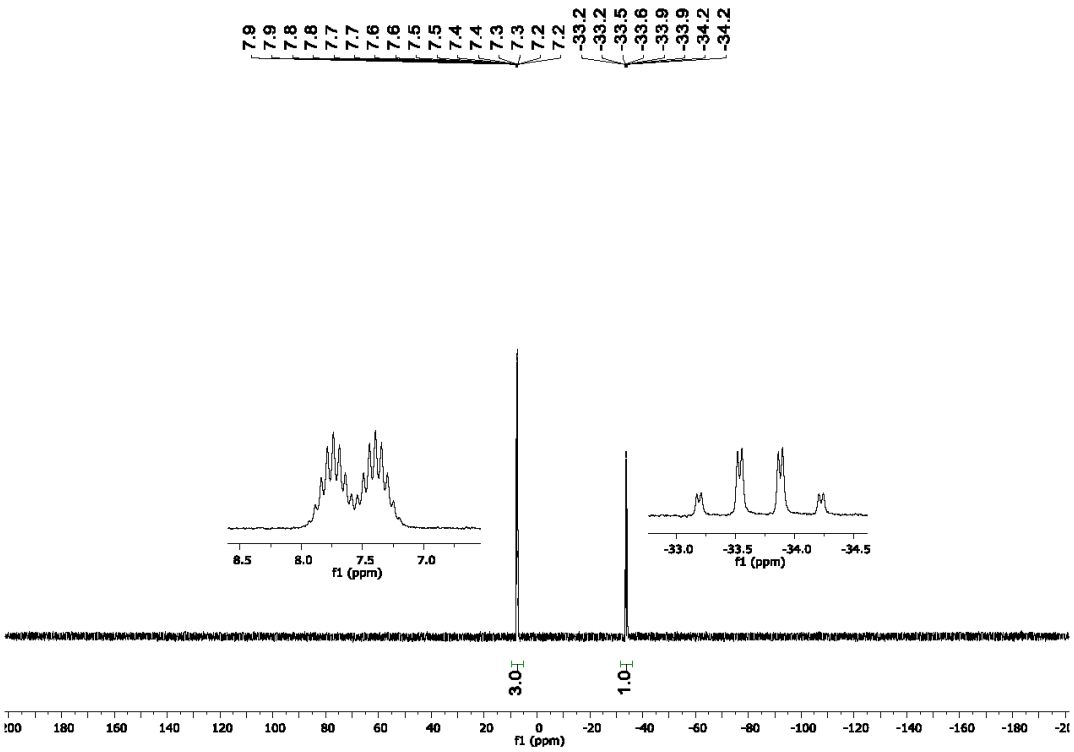

Figure 5. ^{31}P NMR spectrum of **[1H][D$_3$OH]** in benzene-d$_6$ (500 MHz).

1.3.2 Synthesis of [2H][D_3OH]

To a solution of **2** (1.16 g, 2.61 mmol) in 10 mL of *n*-hexane first hexamethylcyclotrisiloxane (593 mg, 2.67 mmol) and then water (57 mg, 3.16 mmol) are added to yield a yellowish second phase. After one hour of stirring, the emulsion was kept at -28 °C overnight, by which a solid precipitated. The supernatant is removed via a syringe and the product (1.75 g, 2.55 mmol, 98 % based on **2**) is isolated as a pale yellow crystalline solid (m.p. 75 °C (dec.)).

The product decomposes at ambient temperature by hydrolysis of **[2H]$^+$**, which is accompanied by a strong amine odor. The ^{31}P NMR resonance of the decomposition product **3** is observed as a singlet at δ = 2.2 ppm in benzene-d_6.

^{1}H NMR (PhCl, rt): δ [ppm] = 0.1 (m, 18 H, $(H_3C)_2SiO$), 1.2 (s, 9 H, $C(CH_3)_3$), 2.5 (s, 36 H, $N(CH_3)_2$), 9.7 (s, br, SiOH).

^{13}C{^{1}H}APT NMR (PhCl, rt): δ [ppm] = 1.9 (s, $SiO(H_3C)_2SiOSi$), 3.1 (s, $(H_3C)_2SiOH$-$OSi(CH_3)_2$), 31.2 (d, $^3J_{PC}$ = 4 Hz, $C(\mathbf{C}H_3)_3$), 39.8 (s, $N(CH_3)_2$), 50.0 (s, $\mathbf{C}(CH_3)_3$), 159.2 (s, C=N).

^{1}H^{29}Si HMBC NMR (PhCl, rt): δ [ppm] = 0.1 / -24.0 ($SiO(\mathbf{H}_3C)_2\mathbf{Si}OSi$), 0.1 / -22.8 (s, $(\mathbf{H}_3C)_2\mathbf{Si}OH$-$O\mathbf{Si}(C\mathbf{H}_3)_2$).

^{29}Si{^{1}H} IG NMR (PhCl, rt): δ [ppm] = -24.2 (s, $SiO(H_3C)_2\mathbf{Si}OSi$), -23.4 (s, $(H_3C)_2\mathbf{Si}OH$-$O\mathbf{Si}(CH_3)_2$).

^{31}P NMR (PhCl, rt): δ [ppm] = -10.6 (s, P=NH).

IR (ATR): $\tilde{\nu}$ [cm^{-1}] = 3008 (vw), 2951 (vw), 2933 (vw), 2896 (vw), 2813 (vw), 1617 (vw), 1543 (vs), 1504 (s), 1472 (m), 1421 (m), 1404 (m), 1375 (s), 1232 (m), 1135 (m), 1044 (s), 1010 (vs), 982 (m), 917 (s), 892 (vs), 787 (vs), 753 (s), 657 (s), 641 (m), 596 (m), 579 (w), 553 (m), 525 (w), 511 (w), 458 (w), 436 (m).

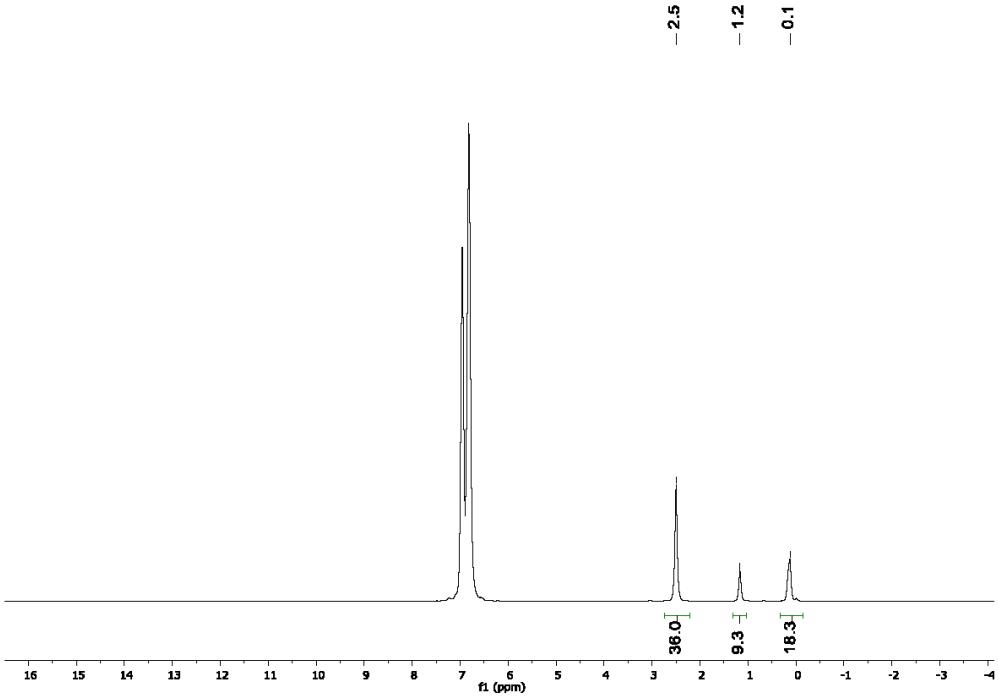

Figure 6. ^{1}H NMR spectrum of **[2H][D$_3$OH]** in PhCl. Lock with acetone-d$_6$ in a capillary (300 MHz).

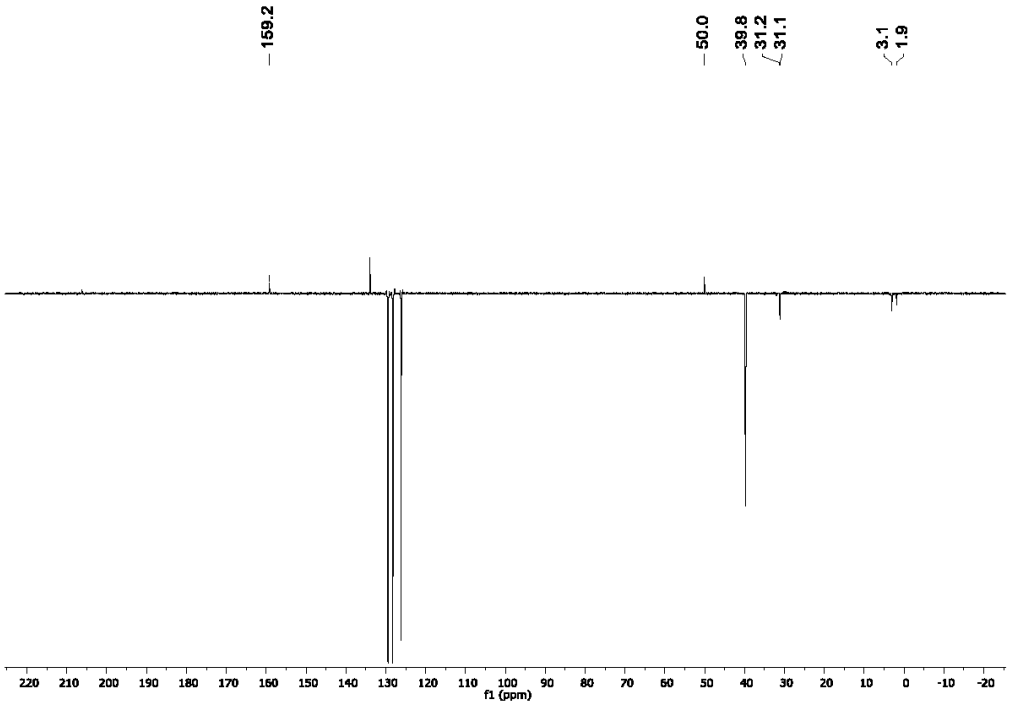

Figure 7. ^{13}C{^{1}H}APT NMR spectrum of **[2H][D$_3$OH]** in PhCl. Lock with acetone-d$_6$ in a capillary (300 MHz).

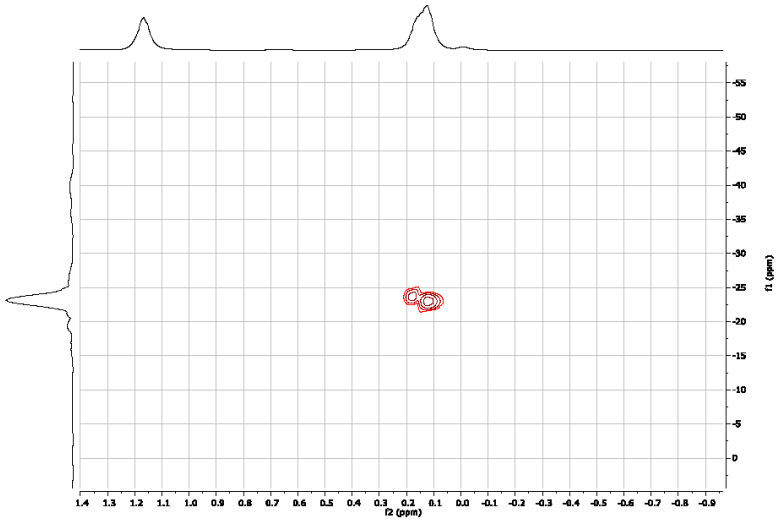

Figure 8. $^{1}H^{29}Si$ HMBC NMR spectrum of **[2H][D$_3$OH]** in PhCl. Lock with acetone-d$_6$ in a capillary (300 MHz).

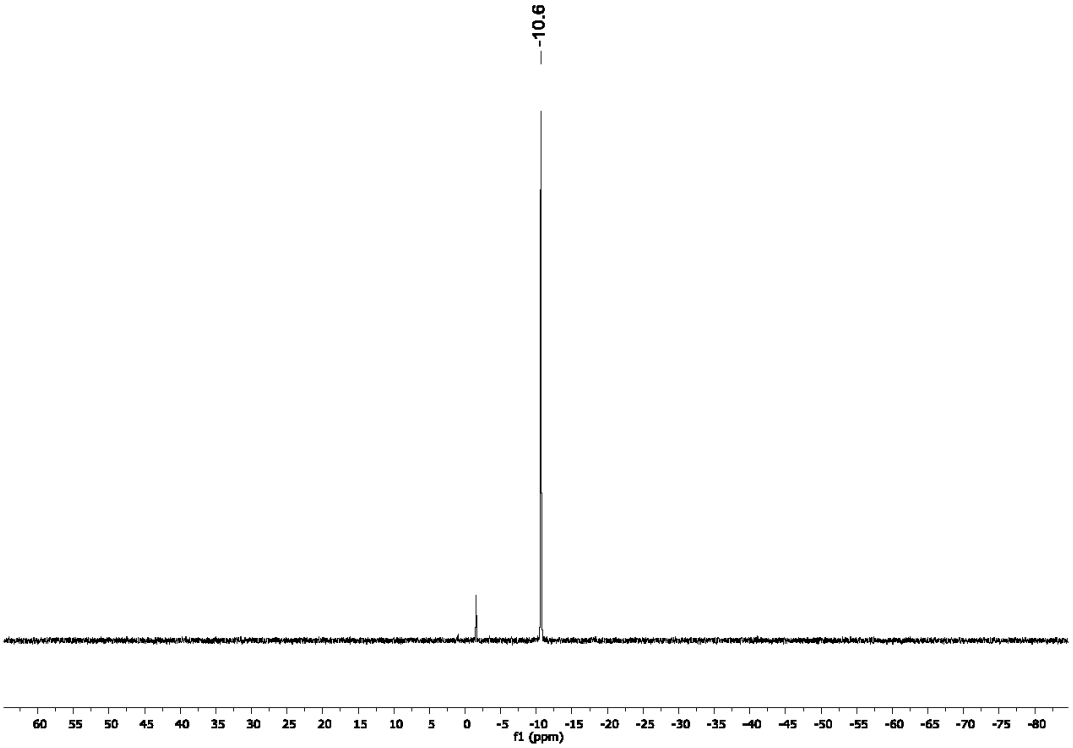

Figure 9. ^{31}P NMR spectrum of **[2H][D$_3$OH]** in PhCl. Lock with acetone-d$_6$ in a capillary (300 MHz).

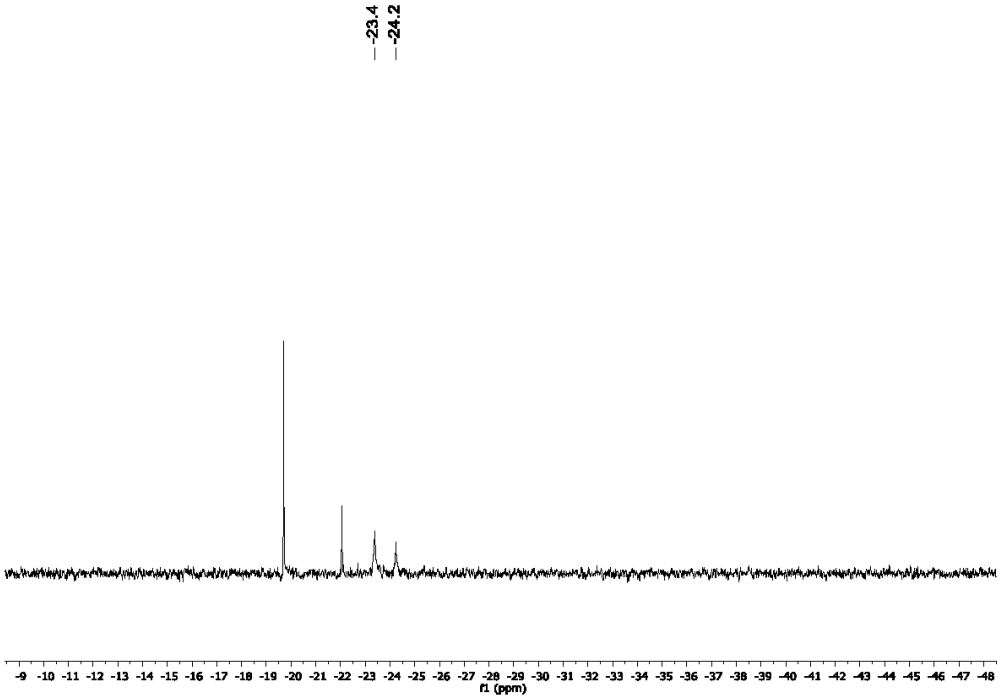

Figure 10. $^{29}Si\{^{1}H\}$ IG NMR spectrum of **[2H][D$_3$OH]** in PhCl after storage at room temperature for several days. Lock with acetone-d_6 in a capillary (500 MHz). A reformation of D_4 and D_5 is observed at δ = -19.7 and -22.1 ppm.

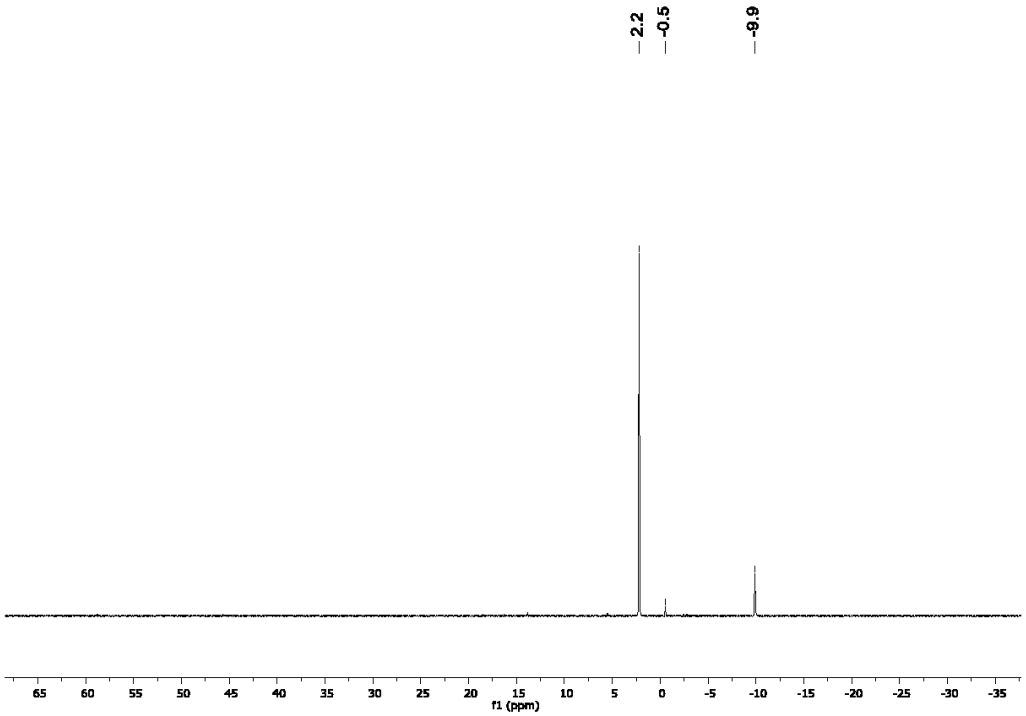

Figure 11. ^{31}P NMR spectrum of **[2H][D$_3$OH]** in benzene-d_6 after storage at room temperature for several days (500 MHz).

1.3.3 Synthesis of [NBu$_4$][D$_3$OH]

Octamethylcyclotetrasiloxane (D_4, 15.0 mL, 50.6 mmol) is added to solid [NBu$_4$][OH(OH$_2$)$_{30}$] (16.86 g, 21.1 mmol) and stirred overnight. All volatile compounds are removed in a high vacuum (10^{-3} mbar) over 24 hours and *n*-pentane (25 mL) is added. The suspension is filtered with a frit (P4) and the solid is washed with *n*-pentane (25 mL). The solid is dissolved in diethylether (135 mL) and recrystallized at -28 °C. The product (9.35 g, 19.4 mmol, 92 % based on [NBu$_4$][OH(OH$_2$)$_{30}$]) is isolated as highly hygroscopic colorless crystals (m.p. 84 °C).
The product decomposes in protic solvents like acetonitrile-d_3 and chloroform-d_1.
Slow thermolysis in vacuo was observed above 80 °C. The volatile products were collected in a cooling trap at -196 °C and analysed via multinuclear NMR spectroscopy. The cation is deprotonated in a Hofmann elimination with liberation of tributylamine, butene and cyclic siloxanes (mainly D_4).

^{1}H NMR (Et$_2$O, rt): δ [ppm] = 0.1 (s, 12 H, (H$_3$C)$_2$SiOH-OSi(CH$_3$)$_2$), 0.2 (s, 6 H, SiO(H$_3$C)$_2$SiOSi), 1.2 (t, $^3J_{HH}$ = 7 Hz, 12 H, NCH$_2$CH$_2$CH$_2$C**H**$_3$), 1.7 (t, q, $^3J_{HH}$ = 7 Hz, $^3J_{HH}$ = 7 Hz, 8 H, NCH$_2$CH$_2$C**H**$_2$CH$_3$), 2.0 (m, 8 H, NCH$_2$C**H**$_2$CH$_2$CH$_3$), 3.8 (m, 8 H, NC**H**$_2$CH$_2$CH$_2$CH$_3$), 14.6 (s, br, SiOH).
^{13}C{^{1}H} NMR (Et$_2$O, rt): δ [ppm] = 0.9 (s, SiO(H$_3$C)$_2$SiOSi), 2.3 (s, (H$_3$C)$_2$SiOH-OSi(CH$_3$)$_2$), 13.3 (s, NCH$_2$CH$_2$CH$_2$**C**H$_3$), 19.9 (s, NCH$_2$CH$_2$**C**H$_2$CH$_3$), 25.0 (s, NCH$_2$**C**H$_2$CH$_2$CH$_3$), 59.0 (s, N**C**H$_2$CH$_2$CH$_2$CH$_3$).
^{29}Si{^{1}H} IG NMR (Et$_2$O, rt): δ [ppm] = -24.9 (s, SiO(H$_3$C)$_2$**Si**OSi), -24.4 (s, (H$_3$C)$_2$**Si**OH-O**Si**(CH$_3$)$_2$).
IR (ATR): $\tilde{\nu}$ [cm^{-1}] = 2959 (w), 2939 (vw), 2915 (vw), 2872 (vw), 1497 (vw), 1470 (vw), 1379 (vw), 1255 (w), 1244 (m), 1108 (w), 1046 (s), 1020 (s), 873 (w), 853 (w), 793 (vs), 762 (m), 694 (w), 659 (m), 644 (w), 557 (w), 512 (w), 450 (w).
elemental analysis of $C_{22}H_{55}NO_4Si_3$ (M = 481.9 g/mol): calcd.: C 54.83, H 11.50, N 2.91, Si 17.48; found: C 54.52, H 11.49, N 2.88, Si 17.16.

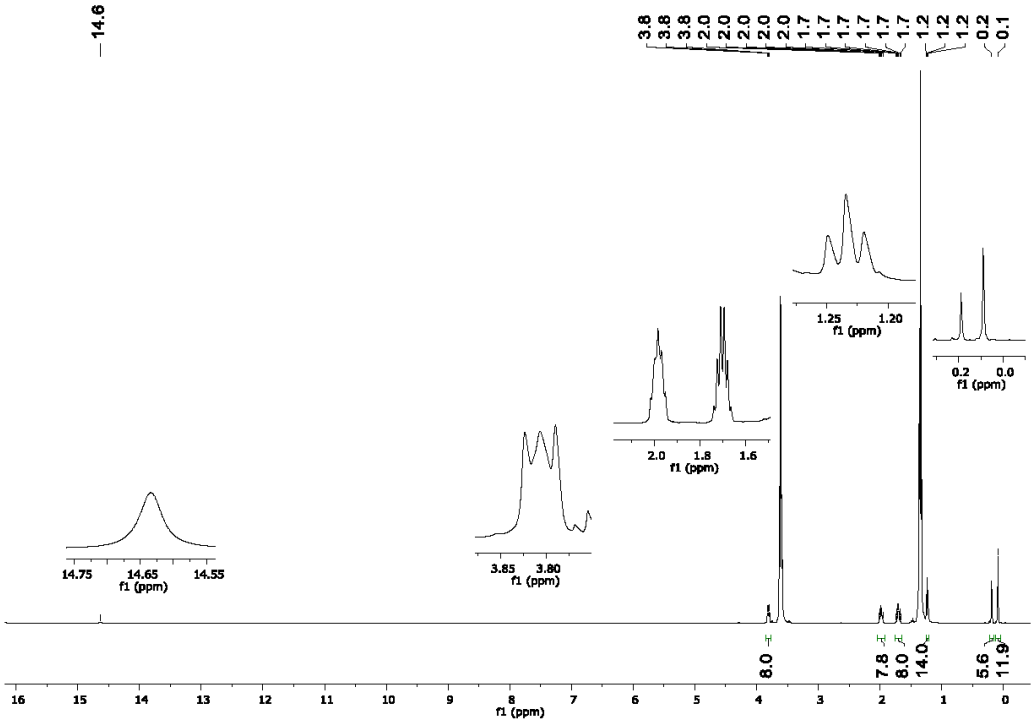

Figure 12. ^{1}H NMR spectrum of **[NBu$_4$][D$_3$OH]** in Et_2O. Lock with acetone-d_6 in a capillary (500 MHz).

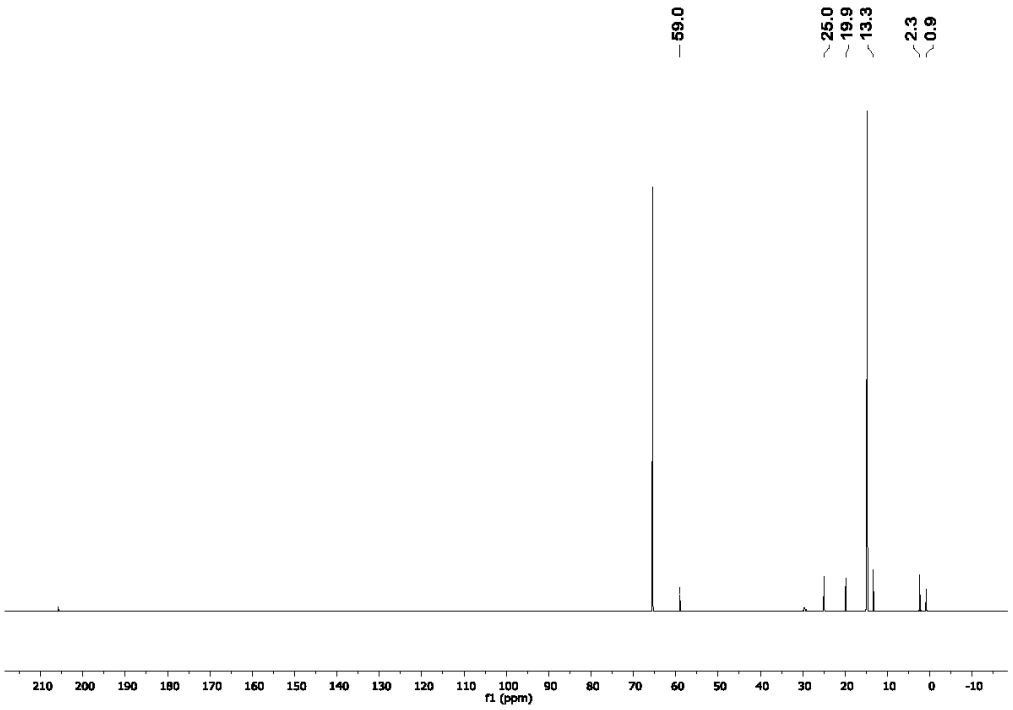

Figure 13. $^{13}C\{^{1}H\}$ NMR spectrum of **[NBu$_4$][D$_3$OH]** in Et_2O. Lock with acetone-d_6 in a capillary (500 MHz).

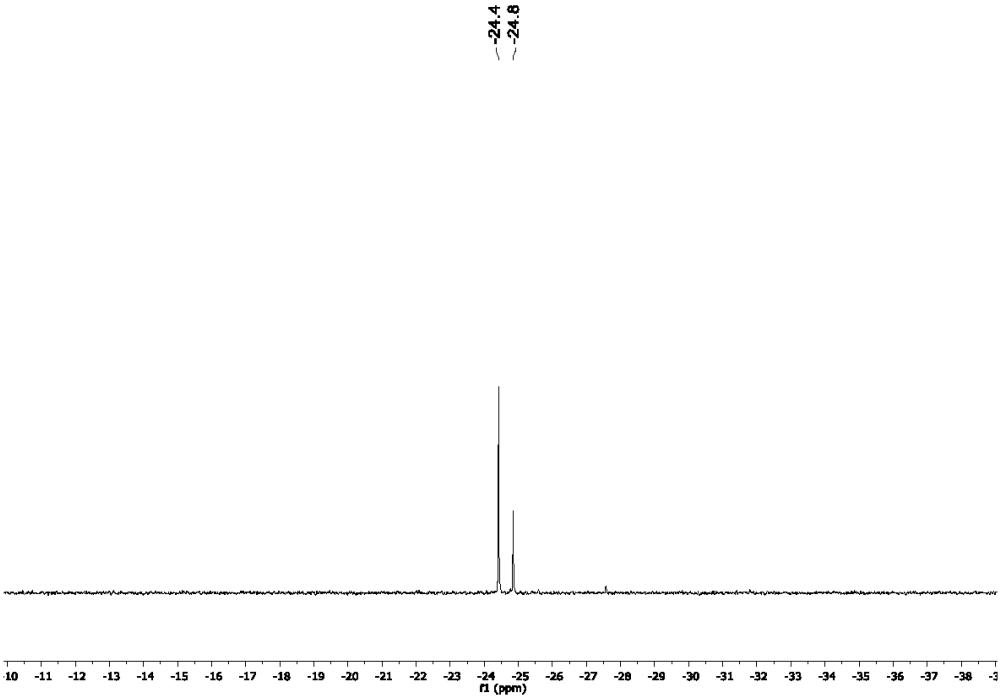

Figure 14. $^{29}Si\{^{1}H\}$ IG NMR spectrum of **[NBu$_4$][D$_3$OH]** in Et_2O. Lock with acetone-d_6 in a capillary (500 MHz).

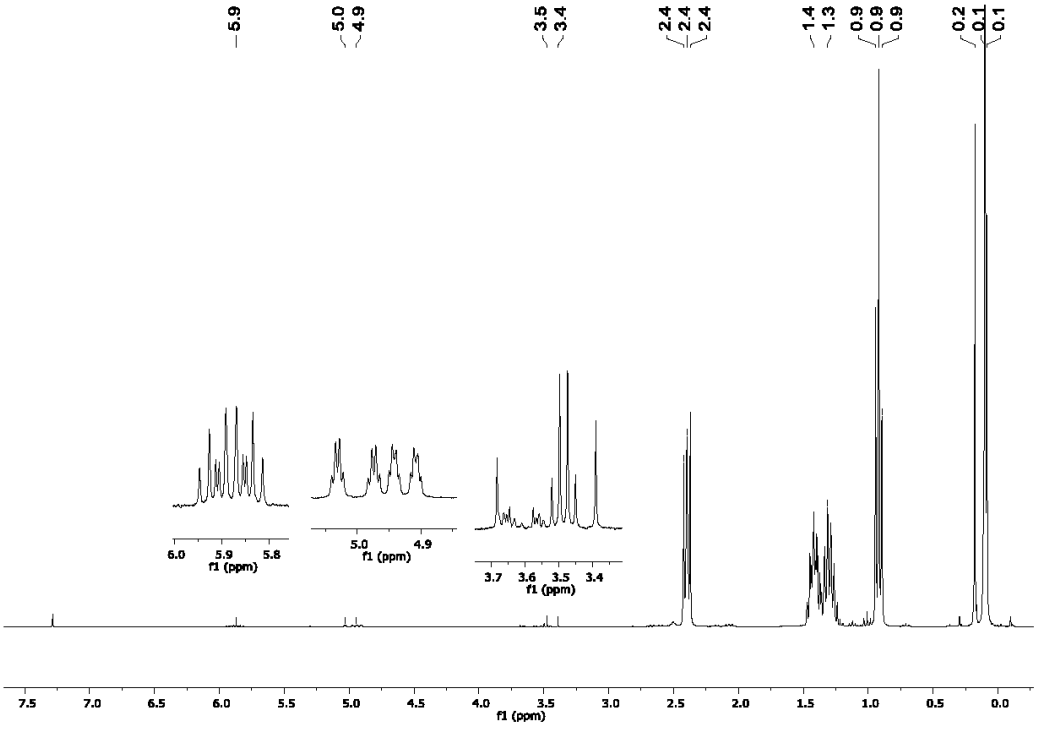

Figure 15. ^{1}H NMR spectrum of the collected gaseous decomposition products of the vacuum thermolysis of **[NBu$_4$][D$_3$OH]** in $CDCl_3$ (300 MHz).

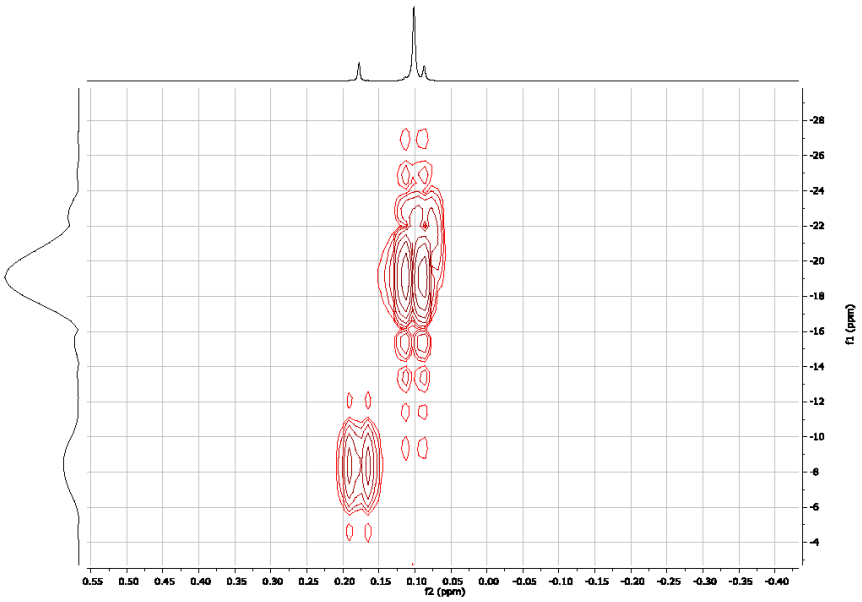

Figure 16. $^{1}H^{29}Si$ HMBC NMR spectrum of the collected gaseous decomposition products of the vacuum thermolysis of **[NBu$_4$][D$_3$OH]** in $CDCl_3$ (300 MHz).

1.3.4 Synthesis of [PBu$_4$][D$_3$OH]

Octamethylcyclotetrasiloxane (D$_4$, 3.60 g, 12.14 mmol) is added to [PBu$_4$]OH (40 wt.% in H$_2$O, 5.93 g, 8.58 mmol) and stirred for 45 minutes. All volatile compounds are removed in a high vacuum (10^{-3} mbar) over 2 days and the product is recrystallized from Et$_2$O (20 mL) at -28 °C afterwards. The product (3.13 g, 6.27 mmol, 73 % based on [PBu$_4$]OH) is isolated as highly hygroscopic colorless crystals (m.p. 71 °C).

The product rapidly decomposes by hydrolysis of the tetra-*n*-butylphosphonium cation in ethereal solution and in the solid state.

^{1}H NMR (Et$_2$O, rt): δ [ppm] = 0.6 (m, 12 H, (H$_3$C)$_2$SiOH-OSi(CH$_3$)$_2$), 0.7 (s, 6 H, SiO(H$_3$C)$_2$SiOSi), 1.7 (m, 12 H, PCH$_2$CH$_2$CH$_2$C**H**$_3$), 2.3 (m, 16 H, PCH$_2$C**H**$_2$C**H**$_2$CH$_3$), 3.4 (m, 8 H, PC**H**$_2$CH$_2$CH$_2$CH$_3$), 15.7 (s, br, SiOH).

^{13}C{^{1}H} NMR (Et$_2$O, rt): δ [ppm] = -1.3 (m, SiO(H$_3$C)$_2$SiOSi), 0.0 (m, (H$_3$C)$_2$SiOH-OSi(CH$_3$)$_2$), 11.0 (s, PCH$_2$CH$_2$CH$_2$**C**H$_3$), 16.4 (d, $^1J_{PC}$ = 47 Hz, P**C**H$_2$CH$_2$CH$_2$CH$_3$), 22.0 (d, $^2J_{PC}$ = 15 Hz, PCH$_2$**C**H$_2$CH$_2$CH$_3$), 22.2 (d, $^3J_{PC}$ = 5 Hz, PCH$_2$CH$_2$**C**H$_2$CH$_3$).

^{29}Si{^{1}H} IG NMR (Et$_2$O, rt): δ [ppm] = -26.4 (s, SiO(H$_3$C)$_2$**Si**OSi), -25.5 (s, (H$_3$C)$_2$**Si**OH-O**Si**(CH$_3$)$_2$).

^{31}P NMR (Et$_2$O, rt): δ [ppm] = 33.7 (s).

IR (ATR): $\tilde{\nu}$ [cm^{-1}] = 2956 (w), 2901 (vw), 2873 (vw), 1465 (vw), 1423 (vw), 1380 (vw), 1310 (vw), 1247 (m), 1153 (w), 1097 (w), 1045 (s), 1024 (s), 908 (w), 850 (w), 788 (vs), 765 (m), 694 (w), 656 (w), 643 (w), 563 (w), 514 (w), 447 (w).

elemental analysis of C$_{22}$H$_{55}$O$_4$PSi$_3$ (M = 498.9 g/mol): calcd.: C 52.93, H 11.11, P 6.21, Si 16.89; found: C 53.00, H 11.09, P 6.23, Si 16.88.

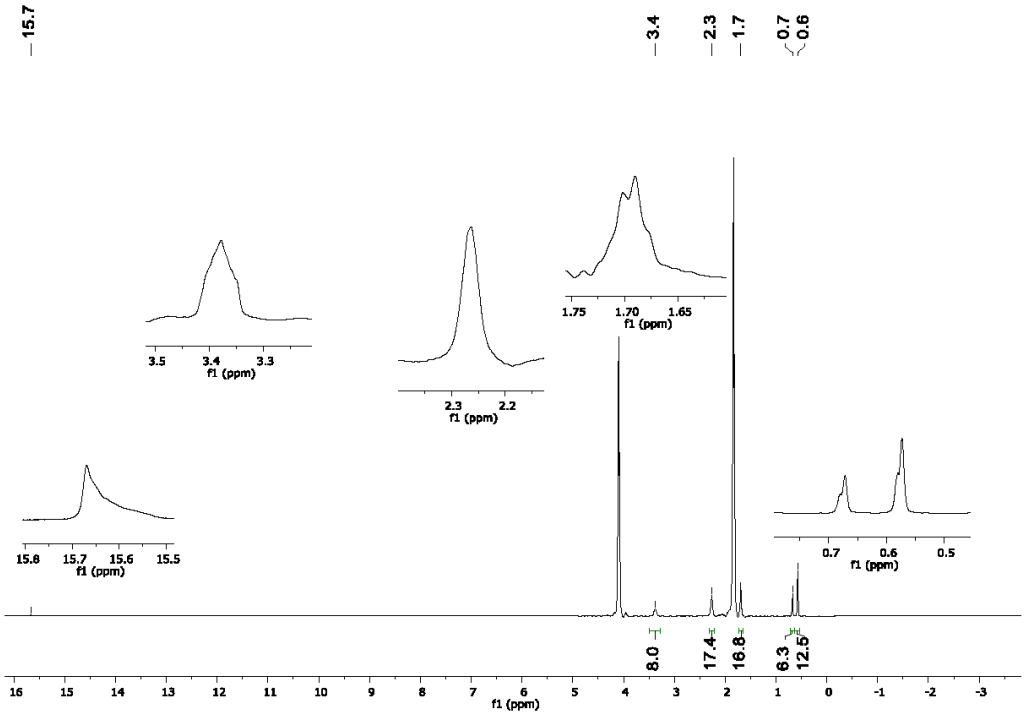

Figure 17. ^{1}H NMR spectrum of **[PBu$_4$][D$_3$OH]** in Et$_2$O. Lock with acetone-d$_6$ in a capillary (500 MHz).

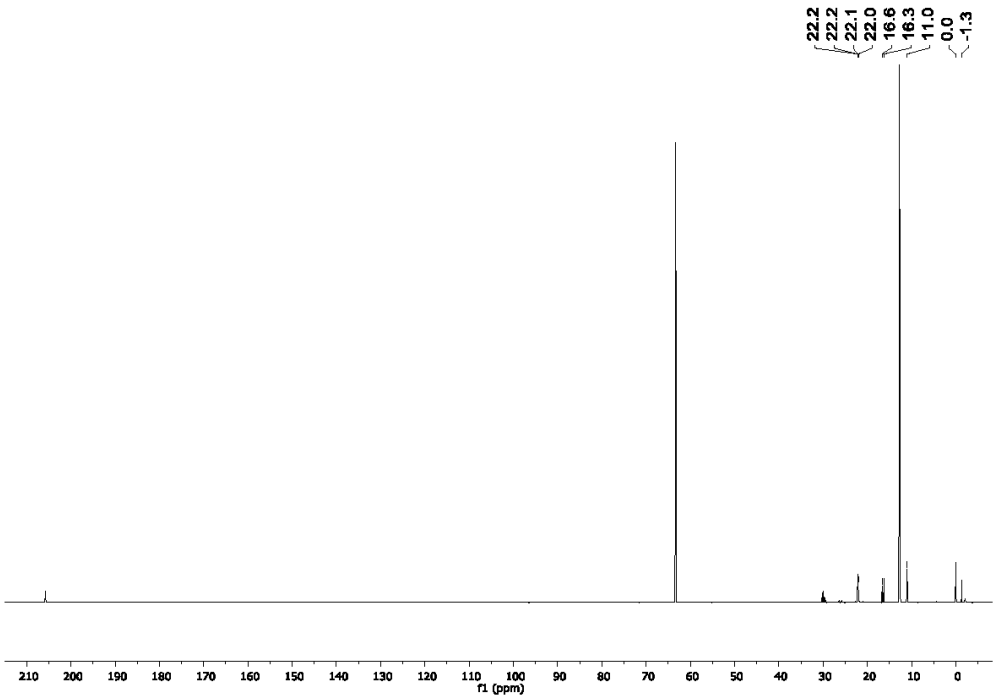

Figure 18. ^{13}C{^{1}H} NMR spectrum of **[PBu$_4$][D$_3$OH]** in Et$_2$O. Lock with acetone-d$_6$ in a capillary (500 MHz).

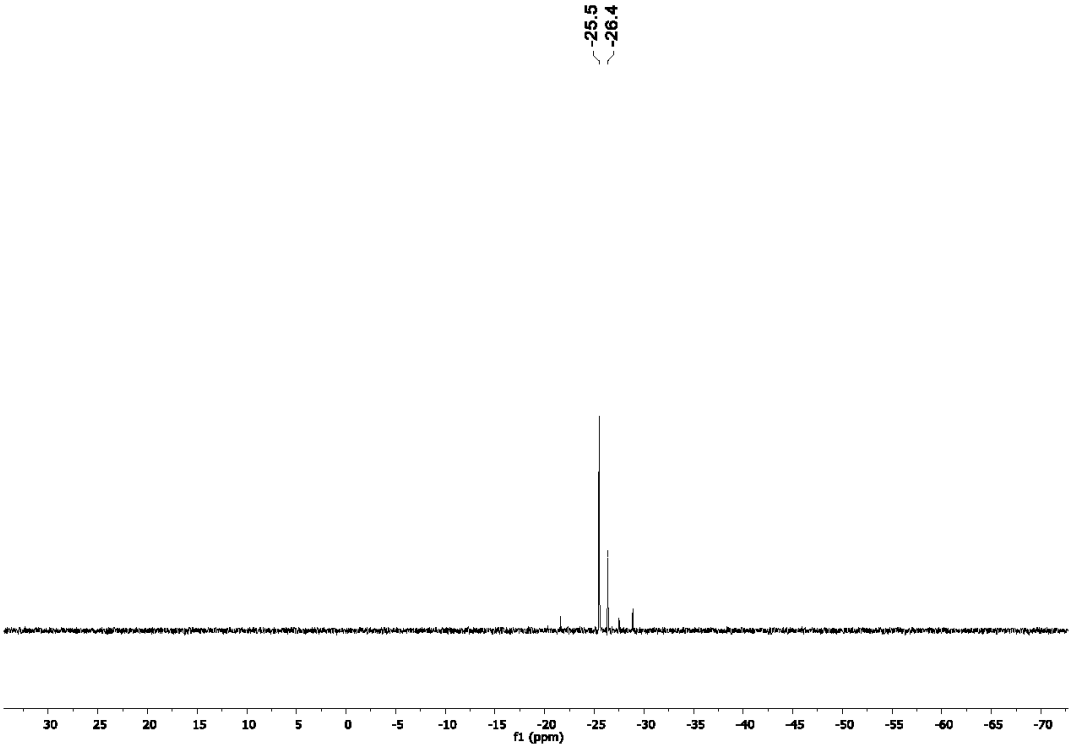

Figure 19. $^{29}Si\{^{1}H\}$ IG NMR spectrum of **[PBu$_4$][D$_3$OH]** in Et_2O. Lock with acetone-d_6 in a capillary (500 MHz).

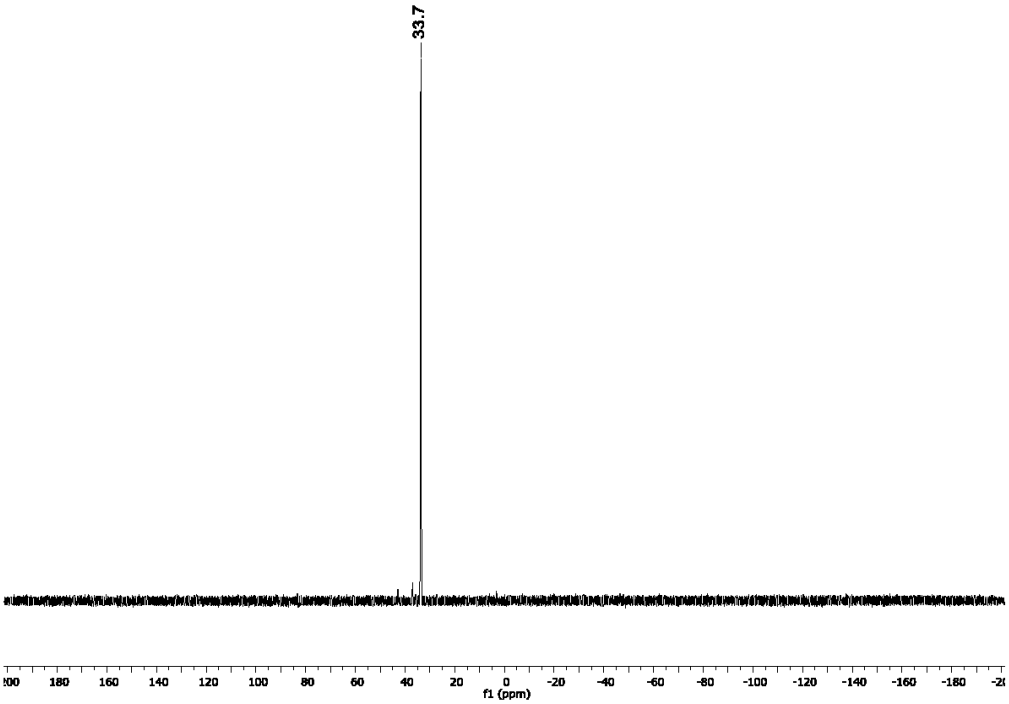

Figure 20. ^{31}P NMR spectrum of **[PBu$_4$][D$_3$OH]** in Et_2O. Lock with acetone-d_6 in a capillary (500 MHz).

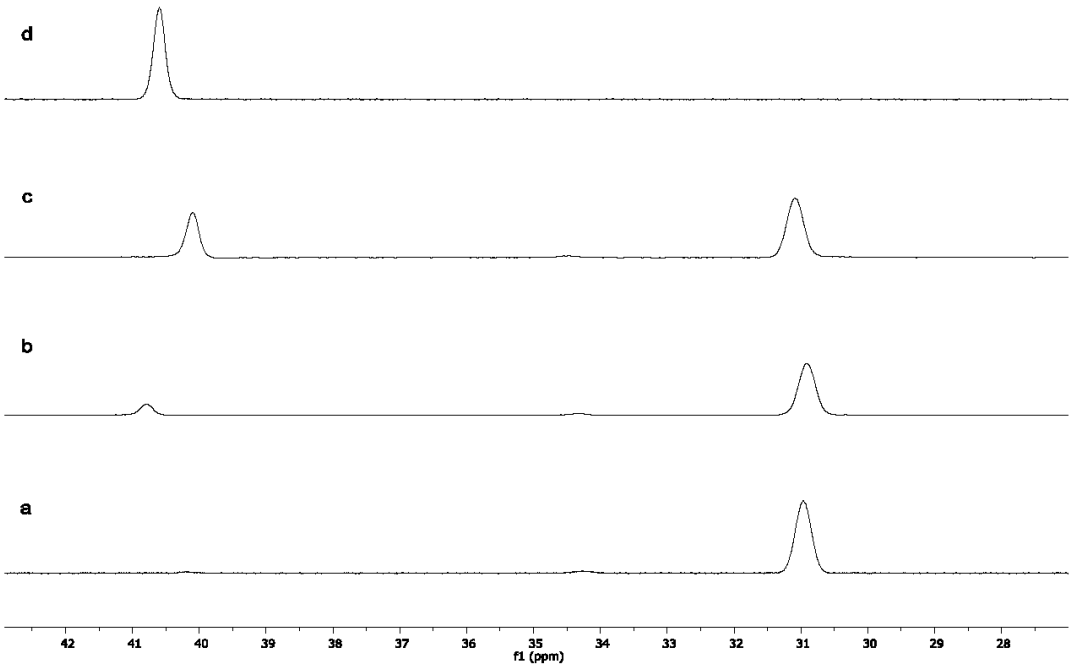

Figure 21. ^{31}P NMR spectra of the time dependent hydrolysis of **[PBu$_4$][D$_3$OH]** in Et_2O. Lock with acetone-d_6 in a capillary (500 MHz). ^{31}P NMR spectra measured: a) immediately; b) after a few hours; c) over night; d) after several days at ambient temperature.

1.3.5 Synthesis of $[NMe_4][D_3OH]_{1/\infty}$

Hexamethylcyclotrisiloxane (D_3, 1.38 g, 6.21 mmol) is dissolved in Et_2O (7 mL) and $[NMe_4]OH$ (25 wt.% in MeOH, 2.27 g, 6.23 mmol) is added. The obtained suspension becomes clear while stirring overnight. All volatile compounds are removed in a high vacuum (10^{-3} mbar). The product (1.86 g, 5.93 mmol, 95 % based on $[NMe_4]OH$) is obtained as a colorless, highly hygroscopic sticky oil. Crystallization from ethereal solution at -28 °C affords a highly hygroscopic microcrystalline solid (m.p. 75 °C).
The product rapidly decomposes at ambient temperature under hydrolysis of the tetramethylammonium cation, which is accompanied by a color change to yellow and a strong amine odor.

^{1}H NMR (PhCl, rt): δ [ppm] = -0.4 to -0.3 (m, 18 H, $(H_3C)_2SiO$), 2.7 (s, 12 H, $N(CH_3)_4$), 13.7 (s, br, SiOH).
$^{13}C\{^{1}H\}$ NMR (PhCl, rt): δ [ppm] = 1.2 (s, $SiO(H_3C)_2SiOSi$), 2.5 (s, $(H_3C)_2SiOH$-$OSi(CH_3)_2$), 54.3 (s, $N(CH_3)_4$).
$^{29}Si\{^{1}H\}$ IG NMR (PhCl, rt): δ [ppm] = -28.3 (s), -27.8 (s), -26.2 (s), -26.0 (s), -24.7 (s, $SiO(H_3C)_2$**Si**OSi), -24.1 (s, $(H_3C)_2$**Si**OH-O**Si**$(CH_3)_2$).
IR (ATR): $\tilde{\nu}$ [cm^{-1}] = 3021 (vw), 2953 (vw), 2897 (vw), 2819 (vw), 1493 (w), 1409 (vw), 1248 (m), 1014 (s), 948 (m), 920 (m), 901 (m), 845 (m), 766 (vs), 661 (m), 552 (w), 457 (w).

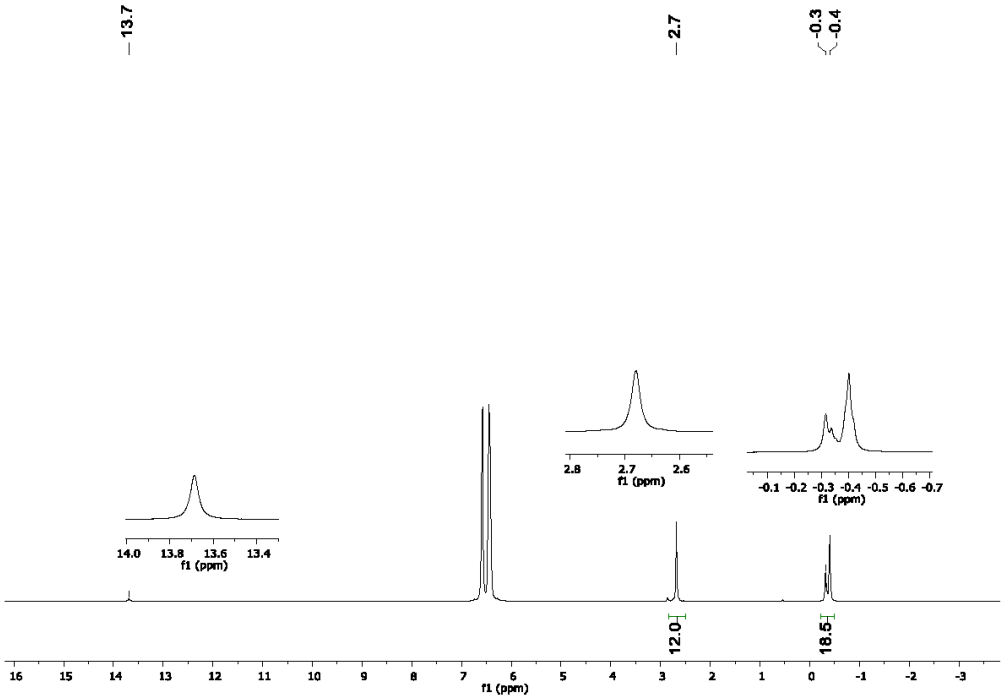

Figure 22. ^{1}H NMR spectrum of **[NMe$_4$][D$_3$OH]**$_{1/\infty}$ in PhCl. Lock with acetone-d$_6$ in a capillary (500 MHz).

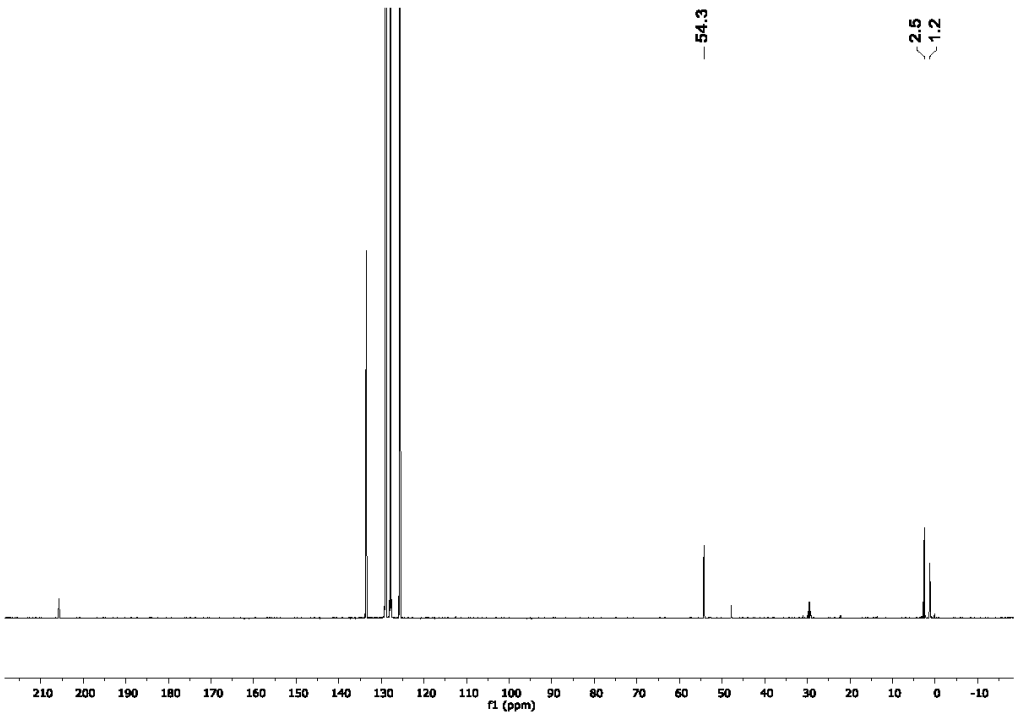

Figure 23. ^{13}C{^{1}H} NMR spectrum of **[NMe$_4$][D$_3$OH]**$_{1/\infty}$ in PhCl. Lock with acetone-d$_6$ in a capillary (500 MHz).

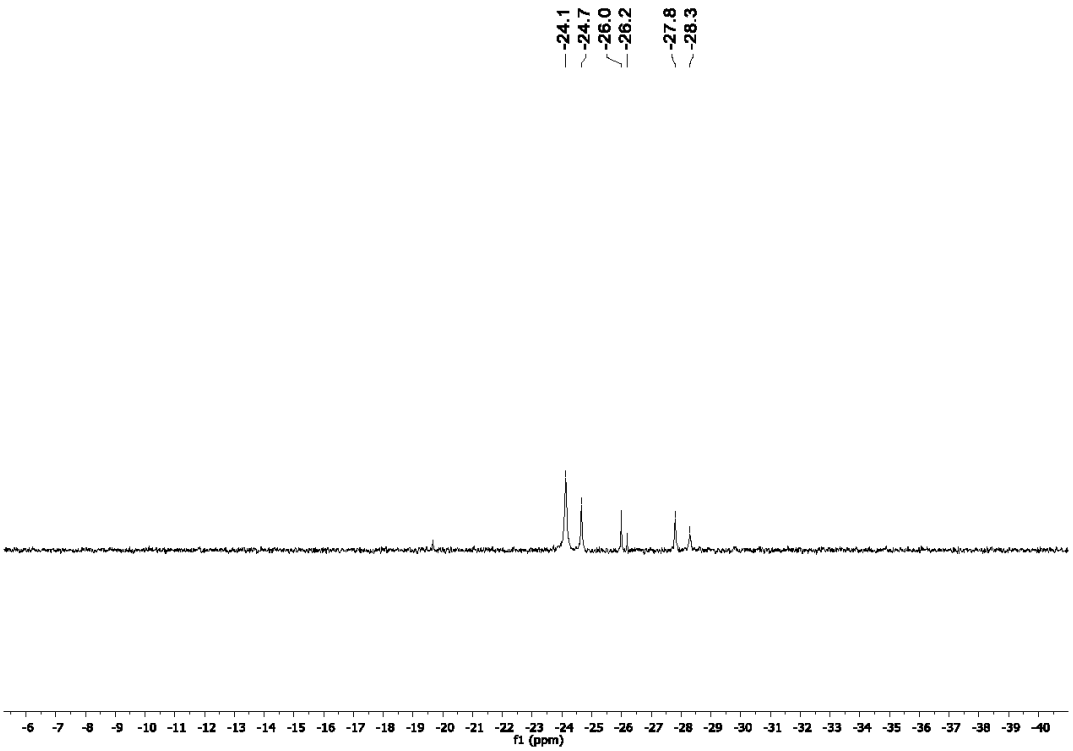

Figure 24. $^{29}Si\{^{1}H\}$ IG NMR spectrum of **[NMe$_4$][D$_3$OH]**$_{1/\infty}$ in PhCl. Lock with acetone-d$_6$ in a capillary (500 MHz).

1.4 Details on the X-Ray Diffraction

The crystal data were collected on a Rigaku Supernova diffractometer (Cu-K_α radiation (λ = 154.184 pm) at 100.0(2) K).

Using Olex2[1], the structures were solved with the ShelXT[2] structure solution program using direct methods and refined with the ShelXL[3] refinement package using least squares minimization. The donor hydrogen atoms were refined isotropically in all these structures.

In **[1H][D_3OH]**, N13, C35-C38 are disordered in a ratio of 94:6, the minor occupied atoms were restrained using ISOR. The P4-N13 and P4-N13B distances were restrained to be same as well as the distances O1-HA and O4-HB. The ratio of HA:HB was refined to 506(6):494(6). Using a model without this disorder, the U_{eq} value of this hydrogen atom becomes unreasonably large and the R-values increase slightly.

Details of the X-ray investigation are given in Tables 1-3. CCDC 1952716 and 2024632-2024637 contain the supplementary crystallographic data for this paper. These data can be obtained free of charge via http://www.ccdc.cam.ac.uk/conts/retrieving.html.

Table 1. Structure refinement data of **[1H][D_3OH]**, **[2H][D_3OH]** and **[NBu_4][D_3OH]**.

compound	**[1H][D_3OH]**	**[2H][D_3OH]**	**[NBu_4][D_3OH]**
empirical formula	$C_{46}H_{119}N_{13}O_4P_4Si_3$	$C_{25}H_{65}N_{10}O_4PSi_3$	$C_{22}H_{55}NO_4Si_3$
a / pm	1101.915(13)	1127.02(2)	1063.768(8)
b / pm	2358.13(3)	1885.81(3)	1805.527(12)
c / pm	2495.13(3)	1975.27(3)	1546.990(10)
α / °	90	90	90
β / °	93.5860(11)	105.7492(18)	98.0714(7)
γ / °	90	90	90
V / 10^6 pm^3	6470.81(13)	4040.51(12)	2941.81(4)
Z	4	4	4
ρ_{calc} / $mg \cdot mm^{-3}$	1.157	1.126	1.088
crystal system	monoclinic	monoclinic	monoclinic
space group	$P2_1/c$	$P2_1/c$	$P2_1/n$
color shape	colorless needles	colorless fragment	colorless irregular
crystal size / mm^{-3}	0.29 × 0.09 × 0.05	0.08 × 0.06 × 0.01	0.24 × 0.15 × 0.12
μ / mm^{-1}	1.985	1.785	1.674
F(000)	2480.0	1496.0	1072.0
2θ range for data col. / °	5.2 to 144.3	6.6 to 153.0	7.6 to 152.9
index ranges	$-13 \le h \le 13$ $-28 \le k \le 28$ $-30 \le l \le 30$	$-14 \le h \le 14$ $-21 \le k \le 23$ $-24 \le l \le 20$	$-13 \le h \le 12$ $-22 \le k \le 22$ $-19 \le l \le 19$
reflections col.	74329	31666	55188
independent refl.	12607	8342	6140
R(int)	0.0321	0.0375	0.0303
data/restraints/	12607/122/719	8342/725/463	6140/0/491

parameter			
goodness-of-fit on F^2	1.025	1.044	1.037
R_1 / wR_2 [I>2σ(I)]	0.0339/0.0834	0.0385/0.1028	0.0267/0.0714
R_1 / wR_2 (all data)	0.0429/0.0884	0.0437/0.1072	0.0282/0.0726
$\Delta\rho_{max/min}$ / e Å^{-3}	0.34/-0.37	0.31/-0.47	0.30/-0.24
CCDC number	1952716	2024632	2024633

Table 2. Structure refinement data of **[PBu$_4$][D$_3$OH]**, **[NMe$_4$][D$_3$OH]$_{1/\infty}$** and **3**.

compound	**[PBu$_4$][D$_3$OH]**	**[NMe$_4$][D$_3$OH]$_{1/\infty}$**	**3**
empirical formula	$C_{22}H_{55}O_4PSi_3$, $[C_4H_{10}O]_{squeezed}$	$C_{10}H_{31}NO_4Si_3$	$C_{17}H_{40}N_9OP$
a / pm	1159.33(4)	818.959(10)	1185.894(12)
b / pm	1288.56(5)	866.405(12)	1519.387(14)
c / pm	1293.82(3)	2586.53(3)	2610.80(3)
α / °	94.440(3)	90	90
β / °	100.378(3)	90	98.7960(10)
γ / °	109.237(3)	90	90
V / 10^6 pm^3	1775.45(11)	1835.27(4)	4648.89(8)
Z	2	4	8
ρ_{calc} / mg·mm^{-3}	1.072	1.135	1.193
crystal system	triclinic	orthorhombic	monoclinic
space group	*P*-1	$P2_12_12_1$	*Pc*
color shape	colorless irregular	colorless plate	colorless needle
crystal size / mm^{-3}	0.35 × 0.26 × 0.24	0.29 × 0.16 × 0.04	0.36 × 0.04 × 0.02
μ / mm^{-1}	1.880	2.445	1.255
F(000)	636.0	688.0	1824.0

2θ range for data col. / °	7.0 to 154.2	6.8 to 1532.0	5.8 to 153.1
index ranges	$-14 \le h \le 14$ $-16 \le k \le 16$ $-16 \le l \le 14$	$-10 \le h \le 10$ $-10 \le k \le 10$ $-32 \le l \le 32$	$-14 \le h \le 14$ $-19 \le k \le 18$ $-32 \le l \le 32$
reflections col.	32048	48329	108757
independent refl.	7373	3822	19206
R(int)	0.0452	0.0603	0.0611
data/restraints/ parameter	7373/72/285	3822/0/287	19206/2/1079
goodness-of-fit on F^2	1.094	1.044	1.036
R_1 / wR_2 [I>2σ(I)]	0.0536/0.1513	0.0238/0.0607	0.0387/0.0945
R_1 / wR_2 (all data)	0.0588/0.1573	0.0254/0.0620	0.0473/0.0995
$\Delta\rho_{max/min}$ / e Å^{-3}	1.08/-0.56	0.27/-0.18	0.40/-0.27
Flack parameter	-	-0.011(10)	0.10(2)
CCDC number	2024634	2024635	2024636

Table 3. Structure refinement data of **$[NMe_4][K(D_3OH)_2]$**.

compound	**$[NMe_4][K(D_3OH)_2]$**
empirical formula	$C_{32}H_{100}K_2N_2O_{16}Si_{12}$
a / pm	1178.68(5)
b / pm	1216.96(6)
c / pm	1216.96(6)
α / °	100.829(4)
β / °	93.251(3)
γ / °	118.521(5)

V / 10^6 pm^3	1649.99(14)
Z	1
ρ_{calc} / mg·mm^{-3}	1.192
crystal system	triclinic
space group	*P*-1
color shape	colorless irregular
crystal size / mm^{-3}	0.21 x 0.11 x 0.08
μ / mm^{-1}	3.793
F(000)	640
2θ range for data col. / °	6.75 to 153.40
index ranges	$-14 \leq h \leq 14$ $-15 \leq k \leq 15$ $-17 \leq l \leq 17$
reflections col.	25456
independent refl.	6794
R(int)	0.0759
data/restraints/ parameter	6794/0/489
goodness-of-fit on F^2	1.022
R_1 / wR_2 [I>2σ(I)]	0.0409/0.0869
R_1 / wR_2 (all data)	0.0644/0.0974
$\Delta\rho_{max/min}$ / e Å^{-3}	0.54/-0.07
Flack parameter	-
CCDC number	2024637

References

[1] O. V. Dolomanov, L. J. Bourhis, R. J. Gildea, J. A. K. Howard, H. Puschmann, *J. Appl. Cryst.* **2009**, *42*, 339.

[2] G. M. Sheldrick, *Acta Cryst. A* **2015**, *71*, 3.

[3] G. M. Sheldrick, *Acta Cryst. C* **2015**, *71*, 3.

Anhang 5

Non-Coordinated and Hydrogen Bonded Phenolate Anions as One-Electron Reducing Agents

Robin F. Weitkamp, Beate Neumann, Hans-Georg Stammler and Berthold Hoge

Chem. Eur. J. **2021**, *[accepted]*.
DOI: 10.1002/chem.202005123.

Anhang

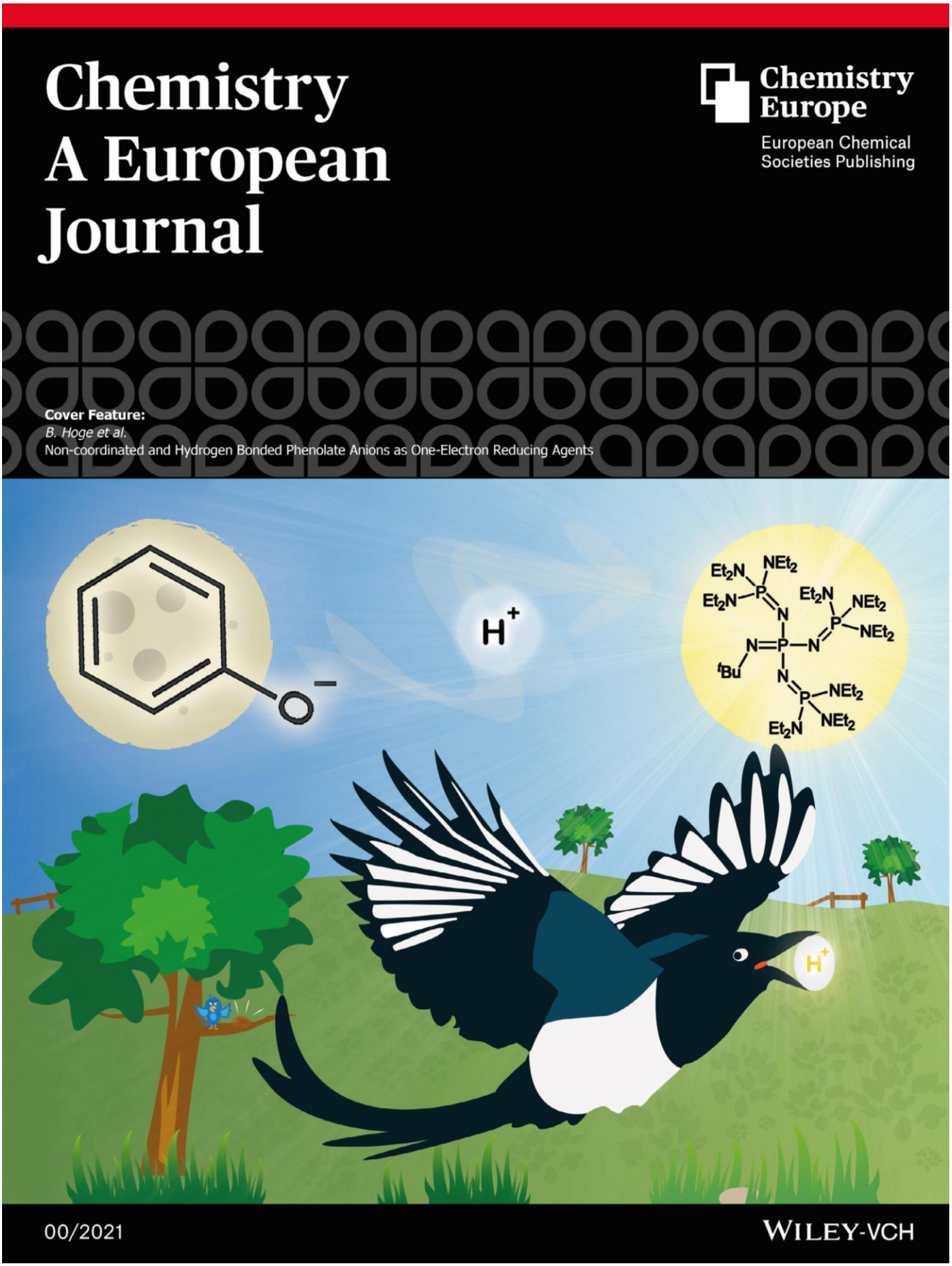
Chemistry
A European
Journal
Chemistry
Europe
European Chemical
Societies Publishing
Cover Feature:
B. Hoge et al.
Non-coordinated and Hydrogen Bonded Phenolate Anions as One-Electron Reducing Agents
H+
00/2021
WILEY-VCH

Anhang

Non-coordinated and hydrogen bonded phenolate anions as one-electron reducing agents

Robin F. Weitkamp, Beate Neumann, Hans-Georg Stammler and Berthold Hoge*[a]

Dedication ((optional))

[a] M. Sc. R. F. Weitkamp, B. Neumann, Dr. H.-G. Stammler, Prof. Dr. B. Hoge
Centrum für Molekulare Materialien
Fakultät für Chemie, Universität Bielefeld,
Universitätsstraße 25, 33615 Bielefeld (Germany)
E-mail: b.hoge@uni-bielefeld.de

Abstract: Here we present the syntheses of non-coordinated electron-rich phenolate anions via deprotonation of the corresponding alcohols with an extremely powerful perethyl tetraphosphazene base (Schwesinger base). The application of uncharged phosphazenes renders the selective preparation of anionic phenol-phenolate and phenolate hydrates possible, which allows the investigation of hydrogen bonding in these species. Hydrogen bonding brings about decreased redox potentials relative to the corresponding non-coordinated phenolate anions. The latter show redox potentials of up to -0.72(1) V vs. SCE, which is comparable to that of zinc metal, thus qualifying their application as organic zinc mimics. We utilized phenolates as reducing agents for the generation of radical anions in addition to the corresponding phenoxyl radicals. A tetracyanoethylene radical anion salt was synthesized and fully characterized as a representative example. We also present the activation of sulfur hexafluoride (SF_6) with phenolates in an SET reaction. Thereby the nature of the respective phenolate determines whether simple fluorides or pentafluorosulfanide ($[SF_5]^-$) salts are formed.

Introduction

Phenol and phenolates are key compounds in applied chemistry, as documented by the industrial Kolbe-Schmitt process.[1] Moreover, a variety of fundamental reactions within the biosphere, such as the photosynthesis, are strongly related to phenolic functionalities.[2,3]

Phenol represents the simplest aromatic alcohol with a pronounced tendency for hydrogen bond formation, which strongly governs the acidity of the present OH functions.[4] Phenol derivatives with a higher acidity than phenol are deprotonated by tetraalkylammonium hydroxides, yielding the corresponding ammonium phenolates.[5] Interestingly, as reported by Reetz *et al.*, all attempts to isolate the non-coordinated phenolate $[H_5C_6\text{-}O]^-$ ($[PhO]^-$) anion by deprotonation with tetra-*n*-butylammonium hydroxide invariantly led to a phenol-phenolate adduct featuring a moderately strong hydrogen bond (O-O distance of 247.1(5) pm).[6] Pronounced hydrogen bonding is also present in imidazolium phenolates, which feature strong C-H···O$^-$ cation-anion interactions.[7,8]

The investigation of hydrogen bonding in proton-coupled electron transfer processes is of growing interest, particularly because of its relevance towards the photosystem.[3,9] The high basicity of the tetraphosphazene base $[(Et_2N)_3P{=}N]_3P{=}N\textit{t}Bu$ (**1**) is sufficient for the deprotonation of phenol, as discussed previously.[chem.202003504] The proton of the corresponding phosphazenium cation $\mathbf{[1H]^+}$ is well shielded towards nucleophilic attack, which allows the isolation of salts with non-coordinated phenolate anions. Thus, in the absence of cation-anion interactions, the effect of hydrogen bonding on the redox properties of phenolate anions can be investigated in detail. The presence of water also effects the oxidation potential of phenol,[chem.202003504] which casts doubt on the reported phenolate redox data from the literature, which were obtained from phenolates generated by deprotonation with tetraalkylammonium hydroxide hydrates in acetonitrile solution.[10,11] The elucidation of the influence of hydrogen bonding requires uncharged phosphazene bases for the deprotonation of phenols to create a definite design of hydrogen bonded phenol-phenolate adducts or phenolate hydrates. Here, in contrast to the application of alkylammonium hydroxide hydrates, the degree of hydration can be controlled exactly by the added amount of water to the reaction. Furthermore, hydrogen bonding also strongly influences light absorption and emission of fluorophores.[12] This phenomenon is also observed for 2-naphtholate anions,[13] and the fluorescence of 2-naphtholate was investigated in more detail in the presence of imidazolium-based ionic liquids, which are able to form C-H···O$^-$ hydrogen bonds.[8,14] Therefore it is obvious to investigate light absorption and emission of the non-coordinated 2-naphtholate anion in comparison to its free 2-naphthole and its adduct with the anion.

Phenolate anions possess a pronounced tendency for single-electron transfer (SET) reactions, as the resulting phenoxyl radicals are well stabilized by electron delocalization. Obviously, we are interested in testing phosphazenium phenolates as electron donors in SET processes. As depicted in Scheme 1, neutral electrophiles are reduced under liberation of stable phenoxyl radicals, which are reluctant to further reactions, and by the generation of the corresponding phosphazenium salts of reactive radical anions $[E]^{\bullet-}$.

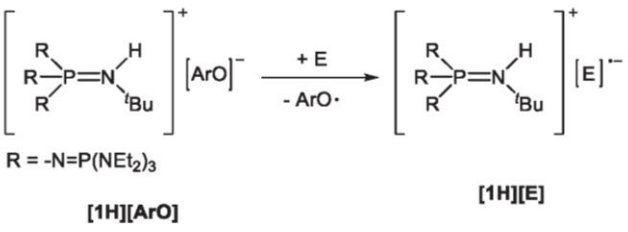

Scheme 1. Application of phosphazenium phenolates as reducing agent.

The applied phenolate should fulfil several prerequisites as a high electron density leading to a sufficiently negative redox potential. Bulky substituents in 2, 4 and 6 position are necessary for the stabilization of phenoxyl radicals by mitigating its nucleophilicity and by obstracting their dimerization.[11] Consistantly, we selected 2,6-di-*tert*-butyl substituted phenolates as the substrates of choice.

Results and Discussion

Syntheses of non-coordinated phenolate anions

The perethyl tetraphosphazene base **1** was synthesized on a multigram scale according to the procedure described previously.[15,16] The reaction of **1** with phenols in ethereal solution affords the corresponding salts as microcrystalline solids in excellent yields (> 95 %, Scheme 2). Importantly, the products are devoid of significant cation-anion contacts.

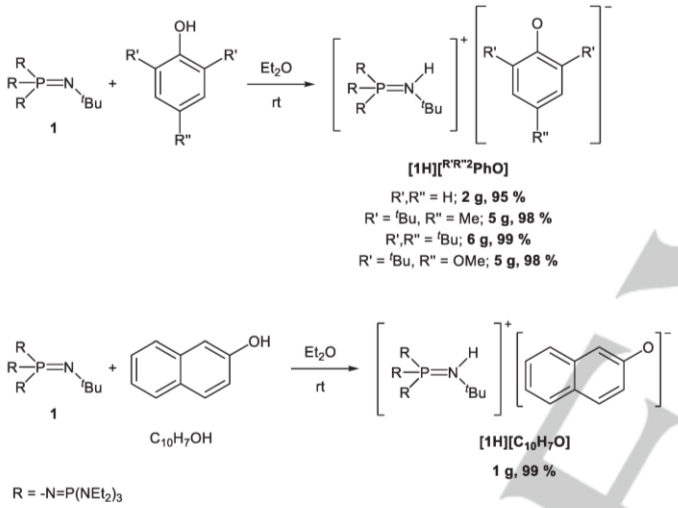

Scheme 2. Synthesis of non-coordinated phenolate salts using **1**.

Whereas salts **[1H][PhO]**, **[1H][^{MetBu2}PhO]** and **[1H][^{tBu3}PhO]** are colorless, salt **[1H][^{MeOtBu2}PhO]** shows a deep yellow color. The deprotonation of 2-naphthol ($C_{10}H_7OH$, Scheme 2) afforded the saline naphtholate **[1H][$C_{10}H_7O$]** with the non-coordinated anions in nearly quantitative yield as fluorescent green crystals. All compounds are air sensitive and by oxidation change their color to yellow, purple, brown or rust-red, while the color of **[1H][$C_{10}H_7O$]** quickly fades. The salts deteriorate in Brønsted acids and solvents like chloroform, dichloromethane and acetonitrile. Thus, handling these phenolates in THF or ethereal solution is indispensable. The novel phenolates were fully characterized and molecular structures were elucidated by single crystal X-ray diffraction (Figure 1) using crystals collected from the cooled ethereal reaction mixtures.

As discussed previously,[chem.202003504] salt **[1H][PhO]** exhibits the first non-coordinated phenolate $[H_5C_6\text{-}O]^-$ anion as building block. The ^{13}C NMR resonance of the C-O$^-$ carbon atom in $[PhO]^-$ (δ = 175.0 ppm) is significantly deshielded in comparison to the anions $[C_{10}H_7O]^-$ (δ = 173.7 ppm), $[^{MetBu2}PhO]^-$ (δ = 170.2 ppm), $[^{tBu3}PhO]^-$ (δ = 170.3 ppm) and $[^{MeOtBu2}PhO]^-$ [chem.202003504] (δ = 168.0 ppm). The corresponding C-O$^-$ distances of these substituted phenolates do not differ significantly from that of $[PhO]^-$ (128.7(2) pm, Table 1), but are shortened compared to coordinated anions as in NaOPh (133(1) pm).[17]

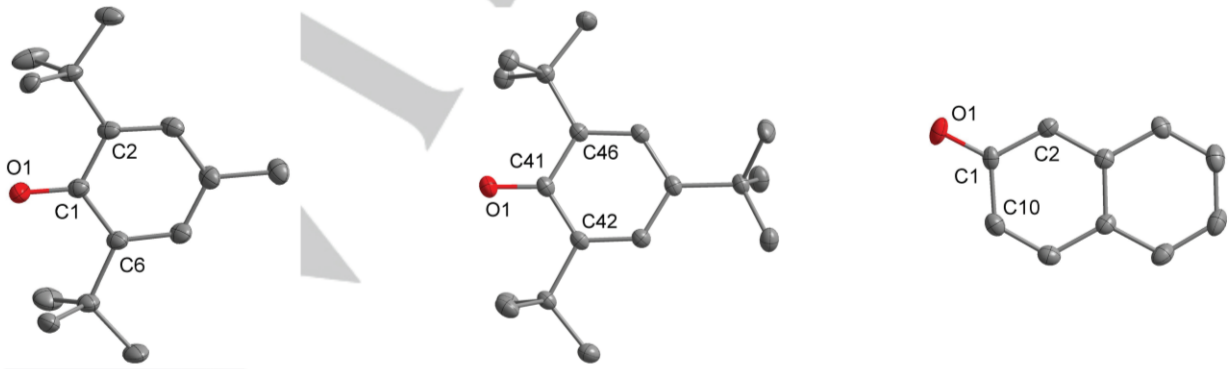

Figure 1. Molecular structures of non-coordinated phenolate anions in **[1H][^{MetBu2}PhO]** (left), **[1H][^{tBu3}PhO]** (middle) and **[1H][$C_{10}H_7O$]** (right). Thermal ellipsoids are shown at 50 % probability. The hydrogen atoms bonded at carbon atoms are omitted for clarity. Selected bond lengths [pm]: left: C1-O1 128.5(2), C1-C2 144.9(2), C1-C6 144.8(2); middle: C41-O1 129.8(2), C41-C42 144.3(2), C41-C46 144.8(2); right: C1-O1 128.4(2), C1-C2 142.1(2), C1-C10 145.8(2).

Table 1. Selected bond lengths, angles and redox potentials (E^0) of non-coordinated and hydrogen bonded phenolate anions with **[1H]⁺** as the counterion. For disordered molecules the values of the major representatives are depicted.

anion	bond	distance / pm	angle / °[a]	E^0 / V[b]
$[PhO]^-$	C-O⁻	128.7(2)	115.0(1)	-0.12(1)[c]
$[^{MefBu2}PhO]^-$	C-O⁻	128.5(2)	116.5(2)	-0.62(1)
$[^{fBu3}PhO]^-$	C-O⁻	129.8(2)	116.4(1)	-0.52(1)
$[^{MeOfBu2}PhO]^-$	C-O⁻	129.0(2)	116.8(3)	-0.72(1)
$[C_{10}H_7O]^-$	C-O⁻	128.4(2)	114.3(1)	-0.15(1)[c]
$[PhO(H_2O)]^-$	C-O⁻	129.8(1)	115.4(8)	-0.04(1)[c]
	O(H)-O⁻	260.8(7)		
		265.2(7)		
$[(PhO)_2H]^-$	C-O⁻	131.9(2)	117.2(1)	+0.22(1)[c]
		132.1(2)	118.0(1)	
	O(H)-O⁻	243.7(2)		
$[(^{MeOfBu2}PhO)_2H]^-$	C-O⁻	131.3(1)	118.0(1)	-0.70(1)
		136.0(1)	120.5(1)	
	O(H)-O⁻	247.0(1)		
$[(C_{10}H_7O)_2H]^-$	C-O⁻	132.1(2)	118.1(1)	+0.08(1)[c]
		133.0(6)	115.8(3)	
	O(H)-O⁻	238.5(4)		

[a] The ortho-ipso-ortho carbon atom angle relative to the C-O⁻ function is depicted. [b] Voltammograms recorded in 0.1 M $[NBu_4][PF_6]$ THF solution at 100 mV/s under inert atmosphere with a glassy carbon working electrode (2.0(1) mm), a counter electrode (steel 18/8, 2.0(1) mm) and an Ag/AgCl reference electrode. All potentials were calibrated to the Fc/Fc^+ couple (+0.405 V vs. SCE). [c] Due to irreversible redox reaction, only the oxidation potential (E_{Ox}) is displayed.

For the sake of a complete picture, we additionally tested the deprotonation of ^{MeOfBu2}PhOH with tetra-*n*-butylammonium hydroxide (triacontahydrate) in a mixture of diethyl ether and THF with a subsequent work-up. Since the in situ deprotonation leads to the formation of the hydrate **$[NBu_4][^{MeOfBu2}PhO(H_2O)_n]$**, we focused on the investigation of a possible liberation of the free anion $[^{MeOfBu2}PhO]^-$ by drying the hydrate in a high vacuum. The powderous pale yellow solid, which was obtained after removal of all volatiles, shows a signal of the C-O⁻ carbon atom at δ = 164.1 ppm in the ^{13}C NMR spectrum, which is upfield shifted by about 4 ppm compared to **$[1H][^{MeOfBu2}PhO]$** (δ = 168.0 ppm). In the IR spectrum no OH stretching vibration is observed, which points to the absence of OH groups evoked by phenol or water. Recrystallization of the salt from a diethyl ether / THF solution at -28 °C afforded single crystals suitable for X-ray analysis. The investigation shows the free anion in **$[NBu_4][^{MeOfBu2}PhO]$**, which is not hydrated and does not show any significant contacts to the cation with the shortest C-H···O⁻ contact of O1-C47* with 340.6(2) ppm (symmetry code C47* (-1/2 + X, 3/2 - Y, 1 - Z). The C1-O1 distance of 129.3(2) ppm is not different from that in the phosphazenium salt. However, air sensitivity evidenced by a color change from yellow to green is attenuated relative to that of the phosphazenium analogue.

Syntheses of hydrogen bonded phenolates

A selective preparation of phenol-phenolate anions is effected by the deprotonation of phenol by half a molar equivalent of phosphazene **1**, or in case of **$[1H][PhO(H_2O)]$** by deprotonation of phenol prior to the addition of one molar equivalent of water (Scheme 3).

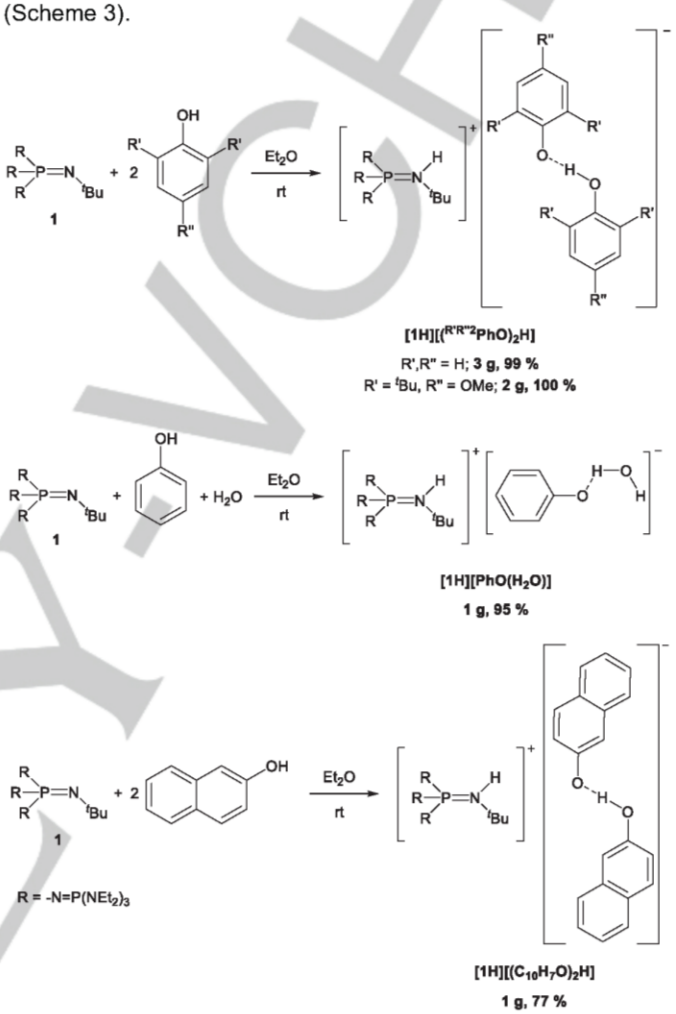

Scheme 3. Syntheses of salts featuring anionic hydrogen bonded phenolate adducts by application of phosphazene **1**.

Salt **$[1H][(PhO)_2H]$** incorporates the anion with an asymmetric, moderately strong hydrogen bond[18] with d(O1-O8) = 243.7(2) pm and therefore the ^{13}C NMR resonance of the C-O⁻ carbon atoms of δ = 167.2 ppm is upfield shifted in comparison to free $[PhO]^-$ (δ = 175.0 ppm).[chem.202003504]

The monohydrate **$[1H][PhO(H_2O)]$** is accessible in excellent yields (95 %). Figure 2 displays the aromatic regions of the ^{1}H NMR spectra of $[PhO]^-$ and its adducts. Hydrogen bonding of $[PhO]^-$ with water and phenol brings about significant lowfield shifts of the signals and an improved resolution of couplings. The latter may be rationalized by a reduced delocalization of the negative charge over the aromatic system, evoked by charge withdrawing hydrogen bonding.

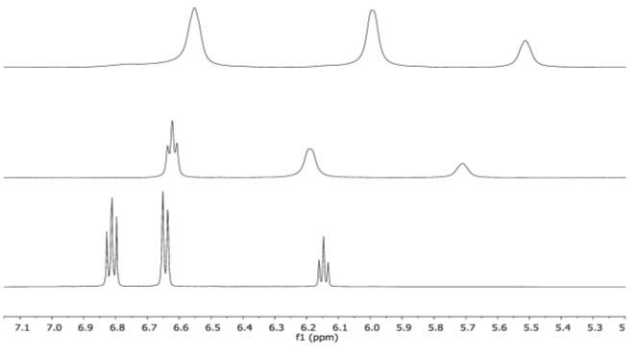

Figure 2. Aromatic region of the ^{1}H NMR spectra of **[1H][PhO]** (top), **[1H][PhO(H$_2$O)]** (middle) and **[1H][(PhO)$_2$H)]** (bottom) in THF-d$_8$.

In accordance, the ^{13}C NMR resonance of the C-O$^-$ carbon atom in [PhO(H$_2$O)]$^-$ (173.6 ppm) is slightly upfield shifted relative to [PhO]$^-$ (175.0 ppm) and shielded relative to [(PhO)$_2$H]$^-$ (167.2 ppm).

Colorless **[1H][PhO(H$_2$O)]** deteriorates above 92 °C and thus, is more temperature sensitive than **[1H][PhO]** (dec. > 115 °C) with a non-coordinated [PhO]$^-$ anion. The OH vibration modes are detected as a single sharp resonance at 3350 cm^{-1}. Single crystals for X-ray crystallography were grown from the ethereal reaction mixture at -28 °C. In the solid state the phenolate monohydrate anion forms a dimer, in which two phenolate hydrates are associated via hydrogen bonding (Figure 3). Interestingly, the water molecules do not show μ_2 bridging between two phenolate anions, but are arranged linearly in a zigzag array. The water molecules are disordered in a 1:1 ratio due to symmetry. The hydrogen bonds with O1-O2 and O1*-O2B distances of 260.8(7) pm and 265.2(7) pm, respectively, are significantly elongated compared to phenol-phenolate hydrogen bonding in **[1H][(PhO)$_2$H]** (243.7(2) pm). The O2-O2B distance of 293.1(5) pm is remarkably long.

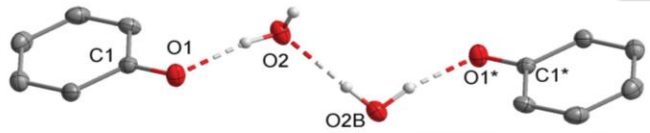

Figure 3. Molecular structure of the formed dianion of salt **[1H][PhO(H$_2$O)]**. Thermal ellipsoids are shown at 50 % probability. Hydrogen atoms bonded at carbon atoms and disordered atoms are omitted for clarity. The cation is not shown. The hydrate water molecules are disordered (1:1). Symmetry code of O1* and C1*: (1-X, 1-Y, -Z). Selected bond lengths [pm] and angles [°]: O1-C1 129.8(1), O1-O2 260.8(7), O2-O2B 293.1(5), O1*-O2B 265.2(7); O1-O2-O2B 117.0(1), O1*-O2B-O2 109.7(2).

All attempts to crystallize hemi-, di- or trihydrates of [PhO]$^-$ suitable for X-ray analysis by adding the respective amounts of water to **[1H][PhO]** resulted in the formation of amorphous solids. The investigation of diffracting crystals solely shows the presence of **[1H][PhO(H$_2$O)]**.

The naphthol-naphtholate salt **[1H][(C$_{10}$H$_7$O)$_2$H]** is accessible in a 77 % yield (Scheme 3) as a colorless solid with a melting point of 76 °C. Regarding the major representative of salt **[1H][(C$_{10}$H$_7$O)$_2$H]** (Figure 4), the anion contains the strongest observed hydrogen bond within all phenolate adducts herein with an O-O separation of 238.5(4) pm. The respective OH vibration mode is detected at 3379 cm^{-1}, and thus is slightly shifted to higher wavenumbers in comparison to [PhO(H$_2$O)]$^-$. Interestingly, in the IR spectra of all other hydrogen bonded phenolates this mode is not observed.

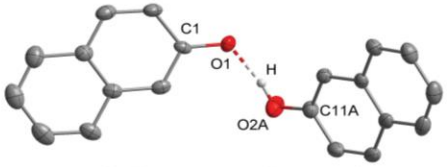

Figure 4. Molecular structure of salt **[1H][(C$_{10}$H$_7$O)$_2$H]**. Thermal ellipsoids are shown at 50 % probability. Hydrogen atoms bonded at carbon atoms and disordered atoms are omitted for clarity. The cation is not shown. The 2-naphthol molecule is disordered (70:30). Selected bond lengths [pm]: O1-C1 132.1(2), O2A-C11A 133.0(6), O1-O2A 238.5(4).

Interestingly, **[1H][(C$_{10}$H$_7$O)$_2$H]** containing the hydrogen bonded anion appears colorless, which is in stark contrast to green **[1H][C$_{10}$H$_7$O]** featuring the non-coordinated anion. UV/Vis spectra in dry THF solution clearly reveal the bathochromic absorbance shift of [C$_{10}$H$_7$O]$^-$ into the visible range with two local maxima at about λ = 412 nm and 439 nm, while the absorbance of [(C$_{10}$H$_7$O)$_2$H]$^-$ is hypsochromically shifted and observed below 400 nm (Figure 6, left), which agrees with the lack of color. The influence of hydrogen bonding is also visible in fluorescence spectra (Figure 6, right). Fluorescence emission spectra were recorded in dry THF with an excitation wavelength of λ_{ex} = 320 nm. The fluorescence of the non-coordinated 2-naphtholate anion in **[1H][C$_{10}$H$_7$O]** is of high intensity and displays one strong fluorescence maximum at λ_{em} = 462 nm with a Stokes shift of 9605 cm^{-1}. The adduct in [(C$_{10}$H$_7$O)$_2$H]$^-$ displays comparatively low intense fluorescence and exhibits four fluorescence maxima at λ_{em} = 344 nm, 360 nm, 427 nm and 458 nm (Stokes shifts of 2181, 3472, 7831 and 9416 cm^{-1}). It is remarkable, that the bands of [C$_{10}$H$_7$O]$^-$ at λ_{em} = 462 nm and of [(C$_{10}$H$_7$O)$_2$H]$^-$ at λ_{em} = 458 nm are close together, which may suggest a dissociation of the hydrogen bonded adduct in the excited state prior to emission. However, mechanistic insights will be discussed elsewhere.

Bulky *tert*-butyl substituents in 2 and 6 positions of phenol do not prevent the formation of hydrogen bonded adducts, as shown for the phenol-phenolate anion in **[1H][(**^{MeO}^{t}^{Bu2}**PhO)$_2$H]**, which can be easily obtained in a quantitative yield as a green solid (Scheme 3). However, the hydrogen bond with an O1-O3 distance of 247.0(1) pm is slightly elongated compared to **[1H][(PhO)$_2$H]** (243.7(2) pm), which may result from steric repulsion (Figure 5).

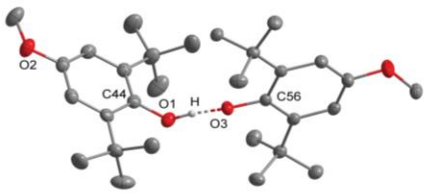

Figure 5. Molecular structure of the anion of salt **[1H][(**^{MeO}^{t}^{Bu2}**PhO)$_2$H]**. Thermal ellipsoids are shown at 50 % probability. The hydrogen atoms bonded at carbon atoms are omitted for clarity. The cation is not shown. Selected bond lengths [pm]: O1-O3 247.0(1), O1-C44 136.0(1), O3-C56 131.3(2).

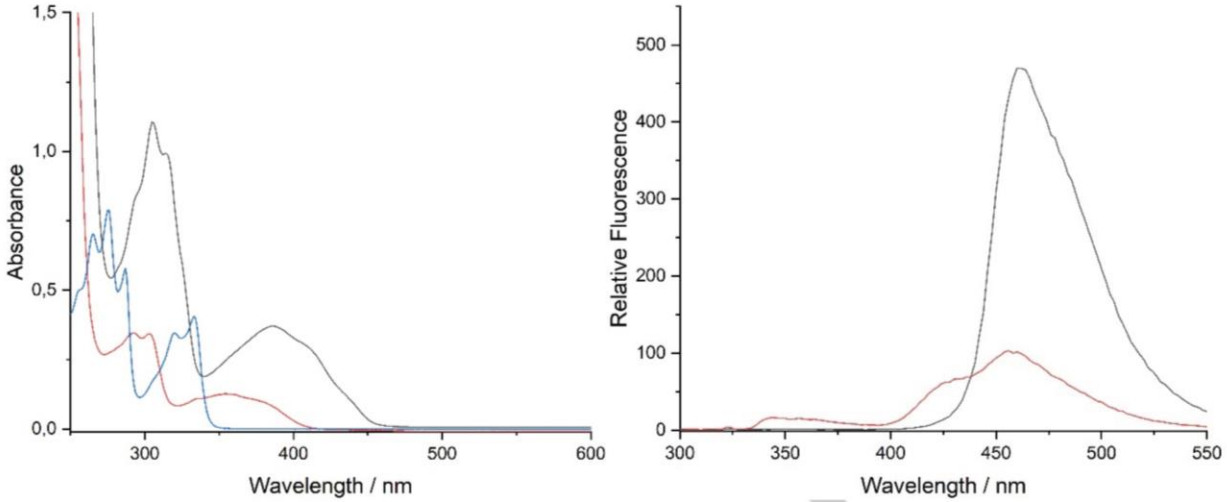

Figure 6. UV/Vis absorption spectrum (left, 32 µM) of 2-naphthole ($C_{10}H_7OH$, blue), **[1H][$C_{10}H_7O$]** (black) and **[1H][$(C_{10}H_7O)_2H$]** (red) and fluorescence emission spectra (right, 200 µM, λ_{ex} = 320 nm) of **[1H][$C_{10}H_7O$]** (black) and **[1H][$(C_{10}H_7O)_2H$]** (red).

The ^{13}C NMR resonance of the C-O^- carbon atoms adjacent to the hydrogen bond are upfield shifted (δ = 158.5 ppm) compared to free [^{MeOtBu2}PhO]$^-$ (δ = 168.0 ppm). Clearly, hydrogen bonding seems responsible for a reduced air-sensitivity, but increased thermal sensitivity (dec. > 74 °C, **[1H][^{MeOtBu2}PhO]** dec. > 118 °C).

Cyclovoltammetry of phenolates

The non-coordinated and hydrogen bonded phenolates were analysed by cyclic voltammetric (CV) measurements under inert conditions (Table 1, Figure 7). THF as the solvent and [NBu_4][PF_6] as the electrolyte were carefully dried prior to use. The substituted non-coordinated phenolate anions show the familiar trend of redox values, known from the literature.[11]

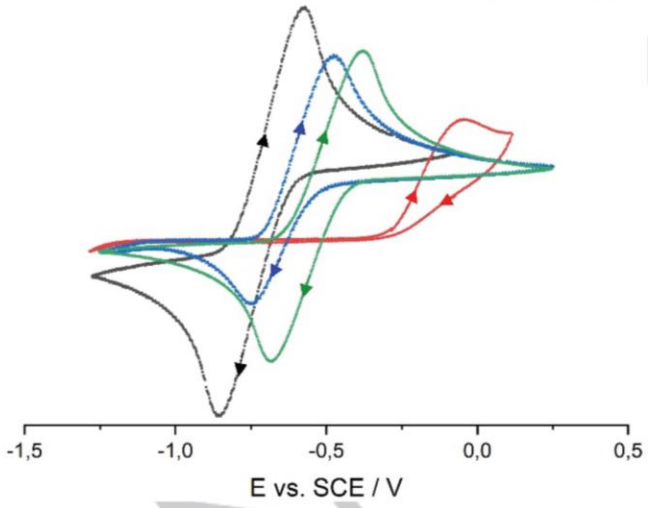

Figure 7. Cyclovoltammograms of non-coordinated phenolates: **[1H][PhO]** (red), **[1H][^{tBu3}PhO]** (green), **[1H][^{MetBu2}PhO]** (blue) and **[1H][^{MeOtBu2}PhO]** (black). Voltammograms recorded in 0.1 M [NBu_4][PF_6] THF solution at 100 mV/s under inert atmosphere with a glassy carbon working electrode (2.0(1) mm), a counter electrode (steel 18/8, 2.0(1) mm) and an Ag/AgCl reference electrode. All potentials were calibrated to the Fc/Fc^+ couple (+0.405 V vs. SCE).

The determined redox potentials of substituted phenolates vary from E^0 = -0.72(1) V vs. SCE for [^{MeOtBu2}PhO]$^-$ to -0.52(1) V vs. SCE for [^{tBu3}PhO]$^-$. These values exceed the reported literature data[11] in acetonitrile solution by about 0.3 V. The anion [^{MeOtBu2}PhO]$^-$ has the most negative redox potential of the here prepared phenolates and reaches that of zinc, which qualifies the anion as an organic zinc mimic.[19] In contrast to the reversible redox reaction of the sterically encumbered phenolates [^{MeOtBu2}PhO]$^-$ and [^{tBu3}PhO]$^-$, the [PhO]$^-$ anion shows an irreversible oxidation at E_{Ox} = -0.12(1) V vs. SCE due to a facile recombination of the formed radicals.[20] The anions [$C_{10}H_7O$]$^-$ and [^{MetBu2}PhO]$^-$ are irreversibly oxidized as well.

According to CV measurements, the anion of the salt **[NBu_4][^{MeOtBu2}PhO]** exhibits the same redox potential of E^0 = -0.72(1) V vs. SCE as **[1H][^{MeOtBu2}PhO]**. However, the air sensitivity is reduced and the ease of color change upon air contact from yellow to green significantly decreases.

Since the reported potentials of phenolate salts in the literature were preferentially determined in aqueous acetonitrile solution with alkylammonium hydroxide hydrates as the deprotonation agent, the influence of conceivable hydrogen bonding on the obtained potentials is neglected.[10,11] The application of **1** enables the investigation with regard to the influence of hydrogen bonding on the oxidation potentials of phenolates.

In keeping with this, we now focused on cyclic voltammetric investigation of the non-coordinated phenolate anion [PhO]$^-$, as well as of the adducts [PhO(H_2O)]$^-$ and [$(PhO)_2H$]$^-$. We further looked at the influence of bulky substituents in 2 and 6 positions on the adduct formation and the resulting redox properties.

As described before, the oxidation potential of salt **[1H][PhO]** was determined to E_{Ox} = -0.12(1) V vs. SCE.[chem.202003504] This value is significantly cathodically

shifted compared to the reported literature data in acetonitrile solution (+0.24 V vs. SCE).[11]

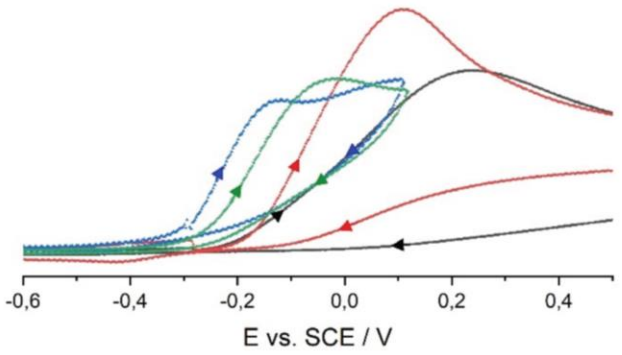

Figure 8. Cyclovoltammograms of **[1H][PhO]** (blue), **[1H][PhO(H$_2$O)]** (green), **[1H][(PhO)$_2$H]** (black) and **[1H][(PhO)$_2$H]** + excess H_2O (concentration of 0.1 M H_2O in the electrolyte solution, red). Voltammograms recorded in 0.1 M $[NBu_4][PF_6]$ THF solution at 100 mV/s under inert atmosphere with a glassy carbon working electrode (2.0(1) mm), a counter electrode (steel 18/8, 2.0(1) mm) and an Ag/AgCl reference electrode. All potentials were calibrated to the Fc/Fc^+ couple (+0.405 V vs. SCE).

Hydrogen bonding to water in the phenolate monohydrate salt **[1H][PhO(H$_2$O)]** brings about an anodic shift of E_{Ox} to -0.04(1) V vs. SCE (Figure 8). The potential of the anion in **[1H][(PhO)$_2$H]** with a value of E_{Ox} = +0.22(1) V vs. SCE experienced an even stronger anodic shift. This trend is confirmed by calculated ionization potentials at the BP86/6-311+g(3df,2p) level of theory,[21] according to which the non-coordinated anion $[PhO]^-$ (E_i = 228.69(1) kJ/mol) is significantly influenced by hydrogen bonding to a water molecule in $[PhO(H_2O)]^-$ (E_i = 267.42(1) kJ/mol).[chem.202003504] The hydrogen bond donation capability in $[(PhO)_2H]^-$ is characterized by a further increase of E_i to 314.90(1) kJ/mol.

The observations may be rationalized by a reduced charge density on the phenolate oxygen atom, which is affected by the strength of the formed hydrogen bond interaction. Moreover, the strength of the hydrogen bond influences the dissociation of the adduct in solution. Thus, assuming that excessive amounts of water displace phenol in **[1H][(PhO)$_2$H]** in the equilibrium reaction, the increased oxidation potential points to the formation of phenolate-water aggregates (Figure 8).[chem.202003504]

The investigation of analogous 2-naphtholate anions deliver similar trends of the observed oxidation potentials as for $[PhO]^-$ anions. The determined value of **[1H][C$_{10}$H$_7$O]** with E_{Ox} = -0.15(1) V vs. SCE shifts significantly with formation of the hydrogen bond in **[1H][(C$_{10}$H$_7$O)$_2$H]** (E_{Ox} = +0.08(1) V vs. SCE, Figure 9). Also in this case, E_{Ox} of the non-coordinated anion in $[C_{10}H_7O]^-$ is clearly shifted compared to the literature data (+0.10 V vs. SCE).[11] As expected, the subsequent addition of water to the **[1H][C$_{10}$H$_7$O]** electrolyte solution (0.1 M, 0.2 M, and 0.6 M H_2O) leads to gradually shifts of E_{Ox} (+0.00(1) V, +0.01(1) V, +0.03(1) V vs. SCE, Figure 9). The picture gets completed by treatment of **[1H][(C$_{10}$H$_7$O)$_2$H]** with an excess of H_2O, which shifts the oxidation potential cathodically (E_{Ox} = +0.06(1) V vs. SCE).

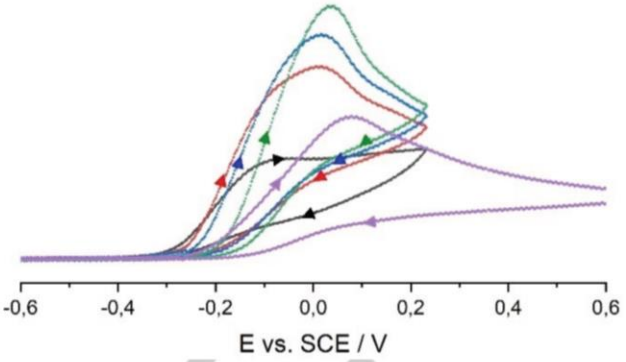

Figure 9. Cyclovoltammograms of **[1H][C$_{10}$H$_7$O]** (black), **[1H][(C$_{10}$H$_7$O)$_2$H]** (purple) and **[1H][C$_{10}$H$_7$O]** with concentrations of 0.1 M (red), 0.2 M (blue) and 0.6 M H_2O (green) in the electrolyte solution. Voltammograms recorded in 0.1 M $[NBu_4][PF_6]$ THF solution at 100 mV/s under inert atmosphere with a glassy carbon working electrode (2.0(1) mm), a counter electrode (steel 18/8, 2.0(1) mm) and an Ag/AgCl reference electrode. All potentials were calibrated to the Fc/Fc^+ couple (+0.405 V vs. SCE).

Interestingly, CV measurements of the hydrogen bonded adduct in **[1H][(^{MeOtBu2}PhO)$_2$H]** reveal a similar redox potential (-0.70(1) V vs. SCE, Figure 10) as for the non-coordinated phenolate $[^{MeOtBu2}PhO]^-$ (-0.72(1) V vs. SCE).

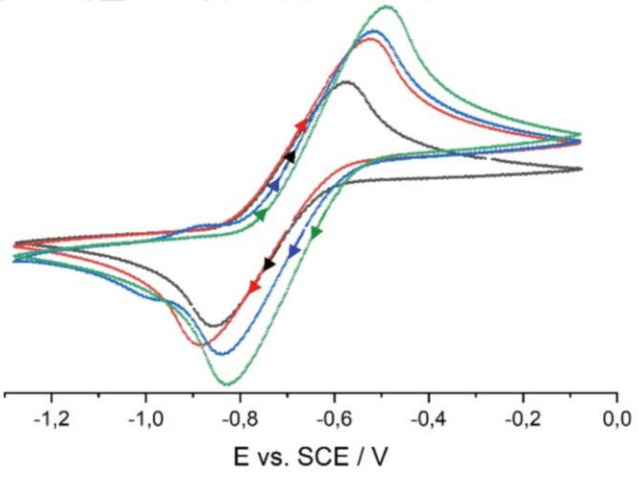

Figure 10. Cyclovoltammograms of **[1H][^{MeOtBu2}PhO]** (black), **[1H][(^{MeOtBu2}PhO)$_2$H]** (red) and **[1H][(^{MeOtBu2}PhO)$_2$H]** with concentrations of 0.1 M (blue) and 0.2 M H_2O (green) in the electrolyte solution. Voltammograms recorded in 0.1 M $[NBu_4][PF_6]$ THF solution at 100 mV/s under inert atmosphere with a glassy carbon working electrode (2.0(1) mm), a counter electrode (steel 18/8, 2.0(1) mm) and an Ag/AgCl reference electrode. All potentials were calibrated to the Fc/Fc^+ couple (+0.405 V vs. SCE).

In comparison to phenolate $[PhO]^-$ and $[(PhO)_2H]^-$, the small redox shift between $[^{MeOtBu2}PhO]^-$ and $[(^{MeOtBu2}PhO)_2H]^-$ may be rationalized by weaker hydrogen bonding in $[(^{MeOtBu2}PhO)_2H]^-$ relative to $[(PhO)_2H]^-$. This fact could possibly lead to a more pronounced dissociation of $[(^{MeOtBu2}PhO)_2H]^-$ in solution and could be responsible for the small redox shift between the coordinated and non-coordinated anion. Subsequent addition of water to the **[1H][(^{MeOtBu2}PhO)$_2$H]**-electrolyte solution leads to further anodically shifted potentials of E^0 = -0.68(1) V and -0.66(1) V vs. SCE (0.1 M and 0.2 M H_2O). Likewise, the addition of water (0.05 M, 0.1 M, 0.4 M and 1.9 M) to **[1H][^{MeOtBu2}PhO]** in the electrolyte solution lowers the observed redox potentials (E^0 = -0.71(1) V, -0.70(1) V, -0.66(1) V and -0.58(1) V vs. SCE).

Phenolates for one-electron reductions

Having non-coordinated phenolate anions and their hydrogen bonded adducts in hand, the second part of this paper is focused on their reducing properties in SET reactions.

In general, radical anions are accessible by electrochemical reduction processes or by single-electron transfer reactions. Especially organic representatives featuring conjugated π-systems exhibit low lying π*-orbitals and enable the formation of stable radical anions. The "*E. coli* "[22,23] of electron transfer reagents is the well known electron-acceptor tetracyanoethylene (TCNE),[24] which is attracting considerable interest for applications in organic semiconductor materials[25] or organic magnets.[26]

The reduction of tetracyanoethylene to its radical anion $[TCNE]^{\cdot-}$ is usually instrumented by the reaction with alkali or transition metals, like elemental potassium or copper, but can also be effected by potassium iodide.[27] The incorporated metal cations may be replaced by other cations via salt metathesis reactions.[28]

As discussed before, non-coordinated phenolate anions as one electron transfer reagents should be of low nucleophilicity and the formed phenoxyl radicals should not undergo any further reactions. For this purpose, salt **[1H][^{MefBu2}PhO]** is reacted with TCNE in ethereal solution (Scheme 4).

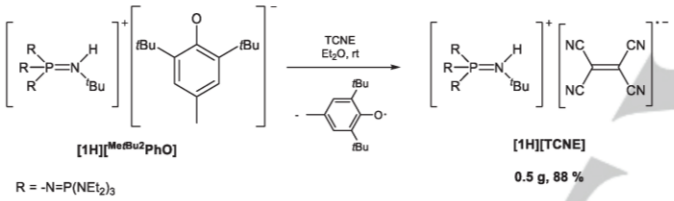

Scheme 4. Synthesis of **[1H][TCNE]** by one electron reduction of TCNE applying phenolate salt **[1H][^{MefBu2}PhO]**.

A rapid electron transfer is observed, which is accompanied by an immediate color change from colorless to green-yellow. Advantageously, the formed radical anion salt **[1H][TCNE]** precipitates from the reaction mixture as a deep-orange solid in an 88 % yield. The phenoxyl radicals can be completely removed by extraction with diethyl ether. The formation of **[1H][TCNE]** is ascertained by elemental analysis and X-ray investigation (Figure 11).

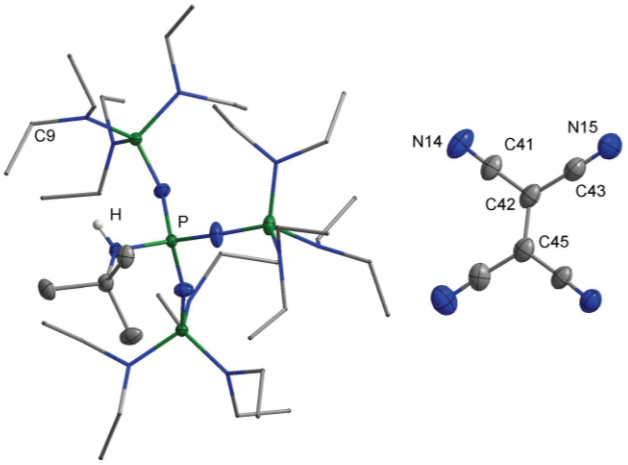

Figure 11. Molecular structure of the radical anion salt **[1H][TCNE]**. Thermal ellipsoids are shown at 50 % probability. The hydrogen atoms bonded at carbon and the minor occupied disordered $N(C_2H_5)_2$ group are omitted for clarity. Diethylamino groups are shown as stick model. Selected bond lengths [pm] and angles [°]: C41-C42 141.5(1), C42-C43 142.8(1), C42-C45 141.7(1), N14-C41 114.4(1), N15-C43 114.6(1); C41-C42-C43 118.9(2), C41-C42-C45 120.7(2), C43-C42-C45 120.3(2).

Although the formation of the dimeric $[TCNE]_2^{2-}$ dianion is known,[29] the $[TCNE]^{\cdot-}$ radical anion in **[1H][TCNE]** is strictly monomeric. This anion is well separated from the counterion with the closest contact of N15-C9 with 326.6(1) pm. The C42-C45 bond in **[1H][TCNE]** of 141.7(1) pm well compares with that of calculated and isolated $[TCNE]^{\cdot-}$ radical anions.[23,28,30]

With the application of the "*E. coli* "[22,23] of electron transfer reagents we confirmed the proof of concept for the preparation of radical anion salts with a weakly coordinating phosphazenium cation, which originates from phosphazenium phenolates.

In view of the severe environmental pollution caused by our economy, which is evident in the climate change on our planet, we tried to find further practical applications for the newly synthesized phosphazenium phenolates.

Sulfur hexafluoride is the strongest greenhouse gas presently known. Its extreme chemical inertness has a dramatic impact on our climate.[31] Clearly, methods for the successful degradation of sulfur hexafluoride are urgently required. Numerous papers are addressing SF_6 activation with transition metal complexes of titanium,[32] rhodium,[33] platinum,[34] chromium and vanadium,[35] as well as of nickel.[36] In all cases the principal reactions lead to corresponding sulfido and fluoride metal complexes. The activation of SF_6 can also be performed electrochemically[37] or by single-electron transfer reactions, as demonstrated by the reaction of SF_6 with alkali metals in liquid ammonia.[38] SET reactions of SF_6 with organic electron donors,[39,40] TEMPOLi[41] and also photo-activated systems[42] have been described. The mechanism for the SF_6 degradation is not completely understood. While some papers claim that the activation proceeds via an SET prior to the disintegration of the corresponding $[SF_6]^{\cdot-}$ radical anion,[39,41,43] Dielmann *et al.* postulate a nucleophilic activation with the use of highly electron rich phosphanes.[44]

In this context, the reducing properties of all synthesized non-coordinated phenolate anions were tested for the activation of SF_6 (Scheme 5).

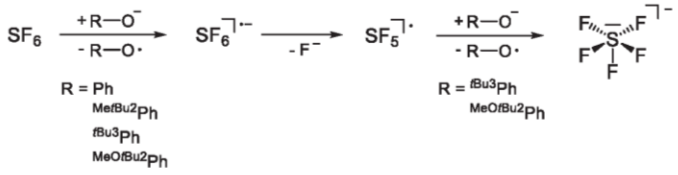

Scheme 5. Activation of SF_6 with phosphazenium phenolate salts.

As previously reported,[chem.202003504] treatment of the strongest reducing reagent **[1H][^{MeOfBu2}PhO]** with SF_6 in ethereal solution leads to the spontaneous formation of the pentafluorosulfanide anion ($[SF_5]^-$) and a color change from yellow to deep red, for which the corresponding liberated phenoxyl radicals seem responsible.

The formation of the pentafluorosulfanide anion from SF_6 is reported to proceed via two single-electron transfer steps (Scheme 5).[39,41] The intermediately formed radical anion $[SF_6]^{\cdot-}$ of the first reduction step disintegrates into F^- and an $(SF_5)^{\cdot}$ radical, and the latter is reduced by a second phenolate to obtain the $[SF_5]^-$ anion.

The reaction of F^- with the borosilicate glass surface leads to the formation of several fluorides, mainly $[HF_2]^-$, as evidenced by ^{19}F NMR spectroscopy. Storage of the collected red ethereal ^{MeOfBu2}PhO· phenoxyl radical solution at -28 °C and most likely diffusion of water and oxygen into the solution afforded green crystals of the corresponding decomposition product 2,6-di-*tert*-butylbenzoquinone, which was authenticated by single crystal X-ray diffraction. The reaction of the ammonium salt **[NBu$_4$][^{MeOfBu2}PhO]** with sulfur hexafluoride also leads to the formation of $[SF_5]^-$. However, the rate of the reaction seems significantly decreased compared to its phosphazenium analogue, and the anion $[SF_5]^-$ was detected not before three days of reaction time.

The treatment of SF_6 with tri-*tert*-butyl phenolate **[1H][^{fBu3}PhO]** in THF as well enables the formation of the $[SF_5]^-$ anion and fluorides (mainly $[HF_2]^-$), as evidenced by ^{19}F NMR spectroscopy. The characteristic resonances of the pseudo square-pyramidal $[SF_5]^-$ anion[44,45][chem.202003504] are observed in the ^{19}F NMR spectrum as a quintet at δ = 88.9 ppm and a doublet at 59.5 ppm, both showing the characteristic $^2J_{FF}$ coupling of 45 Hz.[44] The colorless reaction solution turns deep blue over time, which well agrees with the color of the free phenoxyl radical.[46] ^{19}F NMR spectroscopic investigations manifest the stability of the $[SF_5]^-$ anion in solution in the presence of phenoxyl radicals over weeks of storage at ambient temperature.

The phenolates **[1H][^{MefBu2}PhO]** and **[1H][PhO]** are also utilized for SF_6 activation. However, in sharp contrast to the sterically encumbered 2,4,6-tri-*tert*-butyl- and 2,6-di-*tert*-butyl-4-methoxy- substituted phenolates, the reactions of **[1H][^{MefBu2}PhO]** and **[1H][PhO]** with SF_6 did not lead to the formation of the pentafluorosulfanide anion, but only afforded fluorides. Since $[^{MefBu2}PhO]^-$ and $[PhO]^-$ show a chemical irreversibility in CV experiments, this observation may be rationalized by the reaction of phenoxyl radicals with intermediates prior to the generation of the $[SF_5]^-$ anion. The hydrogen bonded anionic adduct in **[1H][(^{MeOfBu2}PhO)$_2$H]** was also reacted with SF_6. After stirring of the reaction mixture over three days, the solution turned red and the formation of $[SF_5]^-$ was monitored by ^{19}F NMR spectroscopy. In contrast to the reaction with the non-coordinated anion $[^{MeOfBu2}PhO]^-$, the rate of the formation of $[SF_5]^-$ by $[(^{MeOfBu2}PhO)_2H]^-$ was also significantly decreased. Presumably by the presence of phenolic OH functions, several unspecified fluorine containing products were further formed and detected by ^{19}F NMR spectroscopy.

Interestingly, the reducing agent tetrakis(dimethylamino)ethylene (TDAE) is reported to be not capable for the SF_6 activation,[39] although TDAE is an even stronger reducing agent (E^0 = -0.78 V vs. SCE) than all presented phenolate anions herein. This suggests the conclusion that the redox strength itself is not the only factor for a successful reduction of sulfur hexafluoride. In accordance to Dielmann *et al.*[44] one possible explanation for the success of the SF_6 activation with phenolates invokes a nucleophilic interaction of a phenolate anion with a fluorine atom of SF_6, which may support the subsequent activation by single-electron transfer.

Conclusion

We succeeded in high-yield syntheses of a series of non-coordinated phenolate anions by deprotonation of the corresponding alcohols with the tetraphosphazene base **1**. The phenolate anions show significantly shortened C-O$^-$ bonds (128.4(2) pm to 129.8(2) pm) compared to coordinated phenolate anions like in NaOPh (133(1) pm). With phosphazene **1** hydrogen bonded phenol-phenolate and phenolate hydrates are accessible by the deprotonation of phenol in the presence of one equivalent of phenol or water, respectively. This renders the investigation of the influence of hydrogen bonding on the redox potentials of phenolate anions possible. The latter were studied by cyclic voltammetric measurements and reveal significant shifts of the oxidation potentials of $[PhO]^-$ (-0.12(1) V vs. SCE) by contact to a water molecule (-0.04(1) V vs. SCE) or to a phenol molecule (+0.22(1) V vs. SCE). The same trend was observed by comparison of the non-coordinated 2-naphtholate salt **[1H][C$_{10}$H$_7$O]** (-0.15(1) V) with the 2-naphthol adduct in **[1H][(C$_{10}$H$_7$O)$_2$H]** (+0.08(1) V). The latter anion displays the strongest observed hydrogen bond within all presented phenol-phenolates with an O-O separation of 238.5(4) pm, which results in a hypsochromic shift of the absorption into the UV light relative to $[C_{10}H_7O]^-$, which displays two absorption bands in the visible light (412 and 439 nm). The strong hydrogen bond is also perceptible in fluorescence emission spectra. The non-coordinated anion displays a single fluorescence maximum at λ_{em} = 462 nm (λ_{ex} = 320 nm, Stokes-shift 9605 cm^{-1}). In contrast, the fluorescence of the adduct is of less intensity and exhibits several maxima at λ_{em} = 344, 360, 427 and 458 nm, respectively. The hydrogen bond in the phenol-phenolate adduct **[1H][(^{MeOfBu2}PhO)$_2$H]** featuring bulky *tert*-butyl substituents in 2 and 6 position is slightly elongated (O-O distance 247.0(1) pm) compared to the non-substituted analogue $[(PhO)_2H]^-$ (243.7(2) pm). Consequently, the redox potential of the free phenolate $[^{MeOfBu2}PhO]^-$ (-0.72(1) V vs. SCE) is only minor influenced by hydrogen bonding to the phenol with a difference of 20 mV.

We also disclosed the potential of non-coordinated phenolates as one-electron reducing agents. By application of tetracyanoethylene as the "*E. coli* "[22,23] of electron transfer reagents, we presented the possibility for the preparation of radical anion salts from phosphazenium phenolates and isolated

the corresponding salt **[1H][TCNE]** in high yield (88 %). We further described the reduction of the chemically inert sulfur hexafluoride with phosphazenium phenolates, which in case of the sterically encumbered phenolates [^{MeOtBu2}PhO]$^-$ and [^{tBu3}PhO]$^-$ resulted in the formation of pentafluorosulfanide anions. The reduction with other phenolates merely gave fluorides.

Experimental Section

Materials, Instrumentation, Methods

All chemicals were obtained from commercial sources and used without further purification. All solvents were carefully dried and freshly distilled prior to use. Standard high-vacuum techniques were employed throughout all experiments. Non-volatile compounds were handled in a dry N_2 atmosphere using Schlenk techniques. Syntheses of phosphazene **1**,[15,16] phenolates **[1H][PhO]**, **[1H][^{MeOtBu2}PhO]** and **[1H][(PhO)$_2$H]** and the reaction of **[1H][^{MeOtBu2}PhO]** with SF_6 were performed according to literature procedures.[chem.202003504]

NMR spectra were recorded on a Bruker Avance III 500 spectrometer (^{1}H 500.01 MHz; ^{13}C 125.73 MHz; ^{19}F 470.48 MHz; ^{31}P 202.41 MHz) or on a Bruker Avance III 500 HD spectrometer (^{1}H 500.20 MHz; ^{13}C 125.78 MHz; ^{19}F 470.66 MHz; ^{31}P 202.48 MHz). Positive shifts are downfield from the external standards TMS (^{1}H, ^{13}C), CCl_3F (^{19}F) and H_3PO_4 (^{31}P). The NMR spectra were recorded in the indicated deuterated solvent or in relation to acetone-d_6-filled capillaries.

IR spectra were recorded on an ALPHA-FT-IR spectrometer (Bruker) using an ATR unit with a diamond crystal for liquids and solids.

Elemental analyses were performed by Mikroanalytisches Laboratorium Kolbe (Oberhausen, Germany). The elemental analyses of **[1H][(^{MeOtBu2}PhO)$_2$H]**, **[1H][PhO(H$_2$O)]** were performed in the element-analytical laboratory of the Universität Bielefeld using the EURO EA Element Analyzer 2010 (HEKAtech GmbH).

Melting points were measured on a Mettler Toledo Mp70 Melting Point System.

The UV/Vis spectroscopic investigations were performed using the UV/Vis-spectroscopy-system 8453 (Agilent) with a closable cuvette (d = 1 cm) containing a stirring bar (8 mm) under inert atmosphere at 20 °C. The cuvette was heated to 100 °C for 30 minutes prior to each measurement. All samples were prepared in flame-dried Schlenk flasks with concentrations of about 32 µM in THF, which was carefully dried over K and freshly distilled prior to use.

The fluorescence emission spectra were recorded on a RF-5301PC (Shimadzu) in a quartz glass cuvette (d = 1 cm) applying substance concentrations of 200 µM in THF. All samples were prepared in flame-dried Schlenk flasks using THF, which was carefully dried over K and freshly distilled prior to use. The samples were excited with a Xenon lamp at λ_{ex} = 320 nm.

The cyclic voltammetric investigations were performed on a PGSTAT101 potentiostat (Metrohm) using a „three-electrode arrangement“ in a flame-dried 25 mL Schlenk flask under inert atmosphere with a glassy carbon working electrode (2.0(1) mm diameter), a counter electrode (stainless steel 18/8, 2.0(1) mm diameter) and an Ag/AgCl reference electrode in a saturated ethanolic LiCl solution (148 mV vs. SHE). The supporting electrolyte [NBu_4][PF_6] was carefully dried in a high vacuum (10^{-3} mbar). THF was dried over K and freshly distilled prior to use. For every run 0.1 mmol of the substrate and 15 mL of the electrolyte solution were used. The Fc/Fc$^+$ couple was used as internal standard by adding a small amount (spatula tip) of ferrocene after the measurements. The obtained redox potentials were finally recalculated based on the Fc/Fc$^+$ couple which was set at E^0(Fc/Fc$^+$) = +0.405 V vs. SCE. In case of **[1H][PhO]** and **[1H][C$_{10}$H$_7$O]** the addition of ferrocene leads to changes in the observed oxidation potentials, and therefore E^0(Fc/Fc$^+$) = +0.673 V vs Ag/AgCl was used as the external reference for the recalculation vs. SCE.

Nano-ESI mass spectra were recorded using an Esquire 3000 ion trap mass spectrometer (Bruker Daltonik GmbH, Bremen, Germany) equipped with a nano-ESI source. Samples were dissolved in THF and introduced to static nano-ESI using *in-house* pulled glass emitters. Nitrogen served both as nebulizer gas and dry gas. Nitrogen was generated by a Bruker nitrogen generator NGM 11. Helium served as cooling gas for the ion trap and collision gas for mass spectrometry experiments. The mass axis was externally calibrated with ESI-L Tuning Mix (Agilent Technologies, Santa Clara, CA, USA) as calibration standard.

The crystal data were collected on a Rigaku Supernova diffractometer (Cu-K_α radiation (λ = 154.184 pm) or Mo-K_α radiation (λ = 71.073 pm) at 100.0(2) K. Using Olex2,[47] the structures were solved with the ShelXT[48] structure solution program using direct methods and refined with the ShelXL[49] refinement package using least squares minimization. All hydrogen atoms bonded at nitrogen or oxygen were refined isotropically including the 1:1 disordered ones in **[1H][(PhO)$_2$H]**. Details of the X-ray investigation are given in Tables 2-3. CCDC 2035834-2035838, 2045902-2045903 contain the supplementary crystallographic data for this paper. These data can be obtained free of charge via http://www.ccdc.cam.ac.uk/conts/retrieving.html.

Synthesis of [1H][^{MetBu2}PhO]

Phosphazene **1** (4.17 g, 4.70 mmol) is dissolved in 20 mL of diethyl ether and the solution of 2,6-di-*tert*-butyl-4-methylphenol (^{MetBu2}PhOH, 1.04 g, 4.71 mmol) in 6 mL of diethyl ether is rapidly added. After 15 minutes a colorless solid separates. The suspension is stirred for additional 3 days (30 minutes are sufficient) and *n*-hexane (10 mL) is added. The slight purple supernatant is removed via a syringe and the colorless solid is washed with additional 10 mL of *n*-hexane. After drying in a high vacuum the product (5.11 g, 4.62 mmol, 98 %, based on 2,6-di-*tert*-butyl-4-methylphenol) is isolated as a colorless solid (dec. > 111 °C). Suitable crystals for XRD were grown from the ethereal reaction mixture at -28 °C. ^{1}H NMR (500 MHz, [D$_8$]THF, rt): δ=1.2 (t, $^3J_{H,H}$ = 7 Hz, 54 H, NCH$_2$C**H**$_3$), 1.4 (s, 9 H, NC(CH$_3$)$_3$), 1.4 (s, 18 H, C(CH$_3$)$_3$), 2.1 (s, 3 H, CH$_3$), 2.2 (d, $^2J_{P,H}$ = 8 Hz, 1 H, NH), 3.2 (d, q, $^3J_{P,H}$ = 10 Hz, $^3J_{H,H}$ = 7 Hz, 36 H, NC**H**$_2$CH$_3$), 6.4 ppm (s, 2 H, meta H); ^{13}C NMR (500 MHz, [D$_8$]THF, rt): δ=12.9 (d, $^3J_{P,C}$ = 4 Hz, NCH$_2$**C**H$_3$), 21.6 (s, CH$_3$), 29.8 (s, C(**C**H$_3$)$_3$), 31.1 (d, $^3J_{P,C}$ = 5 Hz, NC(**C**H$_3$)$_3$), 34.8 (s, **C**(CH$_3$)$_3$), 39.1 (d, $^2J_{P,C}$ = 6 Hz, N**C**H$_2$CH$_3$), 50.5 (d, $^2J_{P,C}$ = 4 Hz, N**C**(CH$_3$)$_3$), 105.7 (s, para C), 122.9 (s, ortho C), 134.0 (s, meta C), 170.2 ppm (s, ipso C); ^{31}P NMR (500 MHz, [D$_8$]THF, rt): δ=-33.7 (q, d, $^2J_{P,P}$ = 70 Hz, $^2J_{P,H}$ = 8 Hz, 1 P, P=NH), 7.7 ppm (d, tridec, $^2J_{P,P}$ = 70 Hz, $^3J_{P,H}$ = 10 Hz, 3 P, (Et$_2$N)$_3$P); IR (ATR): $\tilde{\nu}$=2964 (w), 2932 (w), 2870 (w), 2160 (vw), 1973 (vw), 1595 (vw), 1465 (w), 1420 (w), 1377 (m), 1350 (w), 1276 (s), 1226 (w), 1201 (s), 1173 (vs), 1107 (w), 1074 (w), 1054 (w), 1017 (vs), 942 (s), 887 (w), 848 (w), 793 (s), 741 (w), 700 (s), 612 (m), 508 (vs), 448 (s), 437 (s), 399 (m), 379 (m) cm^{-1}; MS (ESI, pos.) {*m/z* (%) [assignment]}: 886.7 (100) **[1H]$^+$**; MS (ESI, neg.) {*m/z* (%) [assignment]}: 219.1 (100) **[^{MetBu2}PhO]$^-$**; elemental analysis calcd (%) for $C_{55}H_{123}N_{13}OP_4$: C 59.70, H 11.20, N 16.46; found: C 59.74, H 11.13, N 16.34.

Synthesis of [1H][^{tBu3}PhO]

Phosphazene **1** (4.86 g, 5.49 mmol) is dissolved in 20 mL of diethyl ether and the solution of 2,4,6-tri-*tert*-butylphenol (^{tBu3}PhOH, 1.44 g, 5.50 mmol) in 5 mL of diethyl ether is rapidly added. Immediately a colorless solid precipitates from the slightly yellow mixture. The suspension is stirred for additional 3 days (30 minutes are sufficient) and *n*-hexane (10 mL) is added. The slightly yellow supernatant is removed via a syringe and the solid is washed with additional 10 mL of *n*-hexane. After drying in a high vacuum the product (6.24 g, 5.43 mmol, 99 %, based on ^{tBu3}PhOH) is

isolated as a colorless solid (dec. > 196 °C). Suitable crystals for XRD were grown from the ethereal reaction mixture at -28 °C. ^{1}H NMR (500 MHz, [D$_8$]THF, rt): δ=1.2 (t, $^{3}J_{H,H}$ = 7 Hz, 54 H, NCH$_2$C**H**$_3$), 1.2 (s, 9 H, para C(CH$_3$)$_3$), 1.4 (s, 9 H, NC(CH$_3$)$_3$), 1.5 (s, 18 H, ortho C(CH$_3$)$_3$), 2.2 (d, $^{2}J_{P,H}$ = 8 Hz, 1 H, NH), 3.3 (d, q, $^{3}J_{P,H}$ = 10 Hz, $^{3}J_{H,H}$ = 7 Hz, 36 H, NC**H**$_2$CH$_3$), 6.7 ppm (s, 2 H, meta H); ^{13}C NMR (500 MHz, [D$_8$]THF, rt): δ=13.0 (d, $^{3}J_{P,C}$ = 4 Hz, NCH$_2$**C**H$_3$), 29.9 (s, ortho C(**C**H$_3$)$_3$), 31.1 (d, $^{3}J_{P,C}$ = 5 Hz, NC(**C**H$_3$)$_3$), 32.4 (s, para C(**C**H$_3$)$_3$), 33.5 (s, para **C**(CH$_3$)$_3$), 35.3 (s, ortho **C**(CH$_3$)$_3$), 39.1 (d, $^{2}J_{P,C}$ = 6 Hz, N**C**H$_2$CH$_3$), 50.1 (d, $^{2}J_{P,C}$ = 4 Hz, N**C**(CH$_3$)$_3$), 118.4 (s, ortho C), 119.5 (s, para C), 133.1 (s, meta C), 170.3 ppm (s, ipso C); ^{31}P NMR (500 MHz, [D$_8$]THF, rt): δ=-33.7 (q, d, $^{2}J_{P,P}$ = 70 Hz, $^{2}J_{P,H}$ = 8 Hz, 1 P, P=NH), 7.7 ppm (d, tridec, $^{2}J_{P,P}$ = 70 Hz, $^{3}J_{P,H}$ = 10 Hz, 3 P, (Et$_2$N)$_3$P); IR (ATR): $\tilde{\nu}$=2965 (vw), 2934 (w), 2870 (w), 1466 (w), 1425 (w), 1375 (m), 1352 (w), 1307 (s), 1290 (vs), 1239 (w), 1223 (w), 1203 (s), 1176 (vs), 1105 (w), 1073 (vw), 1055 (w), 1019 (vs), 1001 (m), 943 (s), 920 (m), 887 (w), 869 (w), 845 (w), 828 (vw), 793 (s), 779 (m), 737 (w), 702 (s), 609 (m), 510 (vs), 484 (s), 433 (s), 401 (w) cm^{-1}; MS (ESI, pos.) {*m/z* (%) [assignment]}: 886.5 (100) **[1H]$^+$**; MS (ESI, neg.) {*m/z* (%) [assignment]}: 261.1 (100) **[^{tBu3}PhO]$^-$**; elemental analysis calcd (%) for C$_{58}$H$_{129}$N$_{13}$OP$_4$: C 60.65, H 11.32, N 15.85; found: C 60.76, H 11.46, N 15.73.

Synthesis of [NBu$_4$][^{MeOtBu2}PhO]

Tetra-*n*-butylammonium hydroxide triacontahydrate (641 mg, 0.80 mmol) is suspended in diethyl ether (10 mL) and THF (2 mL) and the solution of 2,6-di-*tert*-butyl-4-methoxyphenol (^{MeOtBu2}PhOH, 189 mg, 0.80 mmol) in 5 mL of diethyl ether is rapidly added to yield a yellow suspension. After stirring for two hours the solvent is removed under reduced pressure and the product is dried in a high vacuum overnight. The product (338 mg, 0.72 mmol, 90 % based on ^{MeOtBu2}PhOH) is isolated as a pale yellow crystalline solid (dec. > 77 °C). The product slowly decomposes upon air contact, which results in a color change to green. Suitable crystals for XRD were grown from a saturated THF/Et$_2$O solution at -28 °C. ^{1}H NMR (500 MHz, [D$_8$]THF, rt): δ=1.0 (t, $^{3}J_{H,H}$ = 7 Hz, 12 H, NCH$_2$CH$_2$CH$_2$C**H**$_3$), 1.4 (m, 8 H, NCH$_2$CH$_2$C**H**$_2$CH$_3$), 1.5 (s, 18 H, C(CH$_3$)$_3$), 1.8 (m, 8 H, NCH$_2$C**H**$_2$CH$_2$CH$_3$), 3.5 (m, 8 H, NC**H**$_2$CH$_2$CH$_2$CH$_3$), 3.6 (s, 3 H, OCH$_3$), 6.5 ppm (s, 2 H, meta H); ^{13}C NMR (500 MHz, [D$_8$]THF, rt): δ=13.2 (s, NCH$_2$CH$_2$CH$_2$**C**H$_3$), 19.7 (s, NCH$_2$CH$_2$**C**H$_2$CH$_3$), 24.1 (s, NCH$_2$**C**H$_2$CH$_2$CH$_3$), 29.7 (s, C(**C**H$_3$)$_3$), 35.0 (s, **C**(CH$_3$)$_3$), 57.0 (s, OCH$_3$), 58.7 (s, N**C**H$_2$CH$_2$CH$_2$CH$_3$), 111.0 (s, meta C), 135.0 (s, ortho C), 143.3 (s, para C), 164.0 ppm (s, ipso C); IR (ATR): $\tilde{\nu}$=2941 (w), 2895 (w), 2873 (w), 2821 (vw), 1488 (w), 1461 (m), 1410 (vs), 1376 (w), 1366 (m), 1349 (w), 1312 (w), 1282 (w), 1248 (w), 1210 (m), 1196 (w), 1161 (w), 1150 (vw), 1103 (vw), 1066 (vs), 1029 (vw), 924 (w), 890 (w), 853 (w), 811 (vw), 788 (w), 779 (s), 750 (w), 739 (w), 685 (vw), 650 (vw), 603 (vw), 572 (vw), 562 (vw), 538 (vw), 521 (vw), 496 (vw), 470 (vw), 461 (vw), 438 (w), 406 (vw), 383 (w) cm^{-1}; MS (ESI, pos.) {*m/z* (%) [assignment]}: 242.2 (100) **[NBu$_4$]$^+$**; MS (ESI, neg.) {*m/z* (%) [assignment]}: 235.1 (48) **[^{MeOtBu2}PhO]$^-$**.

Synthesis of [1H][C$_{10}$H$_7$O]

Phosphazene **1** (774 mg, 0.87 mmol) is dissolved in diethyl ether (15 mL) and the solution of 2-naphthol (C$_{10}$H$_7$OH, 126 mg, 0.87 mmol) in 5 mL of diethyl ether is rapidly added to yield a green-yellow fluorescent solution from which a solid precipitates. The suspension is stirred for 5 minutes and then cooled to -28 °C overnight. The supernatant solution is removed via a syringe and the product (887 mg, 0.86 mmol, 99 % based on **1**) is isolated after drying in a high vacuum as a fine fluorescent green crystalline solid (dec. > 107 °C). Exposure to air results in a fast discoloration. Suitable crystals for XRD were grown from the ethereal reaction mixture at -28 °C. ^{1}H NMR (500 MHz, [D$_8$]THF, rt): δ=1.2 (t, $^{3}J_{H,H}$ = 7 Hz, 54 H, NCH$_2$C**H**$_3$), 1.4 (s, 9 H, NC(CH$_3$)$_3$), 2.3 (d, $^{2}J_{P,H}$ = 8 Hz, 1 H, NH), 3.2 (d, q, $^{3}J_{P,H}$ = 10 Hz, $^{3}J_{H,H}$ = 7 Hz, 36 H, NC**H**$_2$CH$_3$), 6.1 (s, 1 H, aryl H), 6.3 (m, 1 H, aryl H), 6.5 (m, 1 H, aryl H), 6.7 (m, 1 H, aryl H), 7.0 (m, 1 H, aryl H), 7.1 (m, 1 H, aryl H), 7.1 ppm (m, 1 H, aryl H); ^{13}C NMR (500 MHz, [D$_8$]THF, rt): δ=13.0 (d, $^{3}J_{P,C}$ = 4 Hz, NCH$_2$**C**H$_3$), 31.1 (d, $^{3}J_{P,C}$ = 5 Hz, NC(**C**H$_3$)$_3$), 39.1 (d, $^{2}J_{P,C}$ = 6 Hz, N**C**H$_2$CH$_3$), 50.5 (d, $^{2}J_{P,C}$ = 4 Hz, N**C**(CH$_3$)$_3$), 107.5 (aryl C), 111.7 (aryl C), 122.0 (aryl C), 122.3 (aryl C), 126.3 (aryl C), 126.6 (aryl C), 129.0 (aryl C), 139.3 (aryl C), 173.7 ppm (C-O$^-$); ^{31}P NMR (500 MHz, [D$_8$]THF, rt): δ=-33.7 (q, d, $^{2}J_{P,P}$ = 70 Hz, $^{2}J_{P,H}$ = 7 Hz, 1 P, P=NH), 7.7 ppm (d, tridec, $^{2}J_{P,P}$ = 70 Hz, $^{3}J_{P,H}$ = 10 Hz, 3 P, (Et$_2$N)$_3$P); IR (ATR): $\tilde{\nu}$=2967 (vw), 2931 (vw), 2868 (vw), 1602 (vw), 1585 (vw), 1543 (vw), 1490 (vw), 1462 (w), 1433 (w), 1375 (w), 1353 (w), 1278 (s), 1254 (s), 1227 (m), 1202 (s), 1172 (vs), 1104 (m), 1054 (w), 1019 (vs), 941 (vs), 844 (w), 832 (m), 789 (m), 756 (w), 734 (m), 721 (w), 705 (s), 693 (s), 625 (w), 614 (m), 593 (w), 524 (s), 508 (vs), 467 (vs), 455 (s), 431 (s), 418 (s), 496 (m), 386 (m) cm^{-1}; MS (ESI, pos.) {*m/z* (%) [assignment]}: 886.8 (100) **[1H]$^+$**; MS (ESI, neg.) {*m/z* (%) [assignment]}: 143.0 (100) **[C$_{10}$H$_7$O]$^-$**, 287.1 (5) **[(C$_{10}$H$_7$O)$_2$H]$^-$**; elemental analysis calcd for C$_{50}$H$_{107}$N$_{13}$OP$_4$: C 58.28, H 10.47, N 17.67; found: C 58.32, H 10.76, N 17.03.

Synthesis of [1H][(C$_{10}$H$_7$O)$_2$H]

Phosphazene **1** (714 mg, 0.81 mmol) is dissolved in diethyl ether (10 mL) and the solution of 2-naphthol (C$_{10}$H$_7$OH, 232 mg, 1.61 mmol) in 5 mL of diethyl ether is rapidly added to yield a strong green-blue fluorescent solution. The fluorescence disappears after the complete addition of 2-naphthol and a second light green phase forms. The emulsion is stirred for 5 minutes and is then cooled to -28 °C overnight. Since no precipitation of the desired product occurs, the upper phase is removed via a syringe and the lower phase is evaporated to dryness. After drying in a high vacuum the product (733 mg, 0.62 mmol, 77 % based on **1**) is isolated as a colorless crystalline solid (m.p. 76 °C). Suitable crystals for XRD were grown from a concentrated ethereal solution at -28 °C. ^{1}H NMR (500 MHz, [D$_8$]THF, rt): δ=1.1 (t, $^{3}J_{H,H}$ = 7 Hz, 54 H, NCH$_2$C**H**$_3$), 1.3 (s, 9 H, NC(CH$_3$)$_3$), 2.1 (d, $^{2}J_{P,H}$ = 8 Hz, 1 H, NH), 3.2 (d, q, $^{3}J_{P,H}$ = 10 Hz, $^{3}J_{H,H}$ = 7 Hz, 36 H, NC**H**$_2$CH$_3$), 6.8 (m, 2 H, aryl H), 7.0 (m, 2 H, aryl H), 7.0 (m, 2 H, aryl H), 7.2 (m, 2 H, aryl H), 7.4 (m, 4 H, aryl H), 7.5 ppm (m, 2 H, aryl H); ^{13}C NMR (500 MHz, [D$_8$]THF, rt): δ=12.9 (d, $^{3}J_{P,C}$ = 4 Hz, NCH$_2$**C**H$_3$), 31.0 (d, $^{3}J_{P,C}$ = 5 Hz, NC(**C**H$_3$)$_3$), 39.0 (d, $^{2}J_{P,C}$ = 6 Hz, N**C**H$_2$CH$_3$), 50.4 (d, $^{2}J_{P,C}$ = 4 Hz, N**C**(CH$_3$)$_3$), 108.6 (aryl C), 117.7 (aryl C), 123.5 (aryl C), 124.7 (aryl C), 125.6 (aryl C), 126.9 (aryl C), 127.1 (aryl C), 137.0 (aryl C), 165.1 ppm (C-O); ^{31}P NMR (500 MHz, [D$_8$]THF, rt): δ=-33.7 (q, d, $^{2}J_{P,P}$ = 70 Hz, $^{2}J_{P,H}$ = 7 Hz, 1 P, P=NH), 7.7 ppm (d, tridec, $^{2}J_{P,P}$ = 70 Hz, $^{3}J_{P,H}$ = 10 Hz, 3 P, (Et$_2$N)$_3$P); IR (ATR): $\tilde{\nu}$=3379 (vw), 3044 (vw), 2970 (w), 2929 (vw), 2870 (vw), 1621 (vw), 1597 (vw), 1561 (vw), 1499 (vw), 1465 (vw), 1453 (w), 1417 (w), 1378 (m), 1349 (w), 1312 (m), 1295 (m), 1249 (s), 1226 (m), 1202 (s), 1171 (vs), 1112 (w), 1074 (w), 1055 (w), 1017 (vs), 941 (s), 865 (w), 842 (s), 789 (s), 742 (vs), 699 (vs), 610 (s), 536 (s), 515 (vs), 471 (s), 453 (s), 427 (s) cm^{-1}; MS (ESI, pos.) {*m/z* (%) [assignment]}: 886.9 (100) **[1H]$^+$**; MS (ESI, neg.) {*m/z* (%) [assignment]}: 143.1 (100) **[C$_{10}$H$_7$O]$^-$**, 287.1 (7) **[(C$_{10}$H$_7$O)$_2$H]$^-$**; elemental analysis calcd for C$_{60}$H$_{115}$N$_{13}$O$_2$P$_4$: C 61.36, H 9.87, N 15.50; found: C 61.32, H 9.78, N 15.05.

Synthesis of [1H][(^{MeOtBu2}PhO)$_2$H]

Phosphazene **1** (1.31 g, 1.47 mmol) is dissolved in diethyl ether (10 mL) and the solution of 2,6-di-*tert*-butyl-4-methoxyphenol (^{MeOtBu2}PhOH, 699 mg, 2.96 mmol) in 5 mL of diethyl ether is rapidly added to yield a deep green-yellow solution. The solution is stirred for 5 minutes and then cooled to -28 °C overnight by which green crystals precipitate. The supernatant solution is removed via a syringe and the product (2.00 g, 1.47 mmol, 100 % based on **1**) is isolated after drying in a high vacuum as a fine green crystalline powder (m.p. (dec.) > 74 °C). Exposure to air results in a slow decomposition accompanied by a color change from green to brown-green. Suitable crystals for XRD were grown from the ethereal reaction mixture at -28 °C. ^{1}H NMR (500 MHz, [D$_8$]THF, rt): δ=1.2 (t, $^{3}J_{H,H}$ = 7 Hz, 54 H, NCH$_2$C**H**$_3$), 1.4 (s, 9 H, NC(CH$_3$)$_3$), 1.4 (s, 36 H, C(CH$_3$)$_3$), 2.2 (d, $^{2}J_{P,H}$ = 8 Hz, 1 H, NH), 3.2 (d, q, $^{3}J_{P,H}$ = 10 Hz, $^{3}J_{H,H}$ = 7 Hz, 36 H, NC**H**$_2$CH$_3$), 3.6 (s, 6 H, OCH$_3$), 6.5 (s, 4 H, meta H), 10.5 ppm (s, br, OH); ^{13}C NMR (500 MHz, [D$_8$]THF, rt): δ=12.9 (d, $^{3}J_{P,C}$ = 4 Hz, NCH$_2$**C**H$_3$), 30.3 (s, C(**C**H$_3$)$_3$), 31.1 (d, $^{3}J_{P,C}$ = 5 Hz, NC(**C**H$_3$)$_3$), 35.0 (s, **C**(CH$_3$)$_3$), 39.1 (d, $^{2}J_{P,C}$ = 6 Hz, N**C**H$_2$CH$_3$), 50.5 (d, $^{2}J_{P,C}$ = 4 Hz, N**C**(CH$_3$)$_3$), 55.5 (s, OCH$_3$), 109.8 (s, meta C), 138.5 (s, ortho C), 147.6 (s, para C), 158.5 ppm (s, ipso C); ^{31}P NMR (500 MHz, [D$_8$]THF, rt): δ=-33.7 (q, d, $^{2}J_{P,P}$ = 70 Hz, $^{2}J_{P,H}$ = 7 Hz, 1 P, P=NH), 7.7 ppm (d, tridec, $^{2}J_{P,P}$ = 70 Hz, $^{3}J_{P,H}$ = 10 Hz, 3 P,

$(Et_2N)_3P$); IR (ATR): $\tilde{\nu}$=2961 (w), 2934 (w), 2869 (w), 1461 (w), 1441 (vw), 1411 (w), 1376 (m), 1352 (m), 1279 (s), 1223 (w), 1203 (s), 1176 (vs), 1108 (w), 1056 (m), 1019 (vs), 942 (vs), 891 (w), 848 (m), 817 (w), 791 (s), 779 (vs), 740 (m), 703 (vs), 682 (m), 643 (m), 608 (s), 587 (m), 537 (vs), 525 (s), 509 (vs), 479 (s), 463 (vs), 453 (vs), 438 (vs), 405 (s), 390 (s) cm^{-1}; MS (ESI, pos.) {*m/z* (%) [assignment]}: 886.9 (100) **[1H]$^+$**; MS (ESI, neg.) {*m/z* (%) [assignment]}: 235.1 (85) **[^{MeOtBu2}PhO]$^-$**; elemental analysis calcd for $C_{70}H_{147}N_{13}O_4P_4$: C 61.87, H 10.90, N 13.40; found: C 61.69, H 11.67, N 12.83.

Synthesis of [1H][PhO(H$_2$O)]

Phosphazene **1** (579 mg, 0.65 mmol) is dissolved in 7 mL of diethyl ether and the solution of phenol (61 mg, 0.65 mmol) in 2 mL of diethyl ether is rapidly added. Immediately a second pale yellow phase forms. Subsequently water (15 mg, 0.83 mmol) is added and the emulsion is stirred for an additional hour prior to cooling to -28 °C. The supernatant is removed from the colorless crystalline solid via a syringe and the solid is dried in a low vacuum (down to 10 mbar). The product (618 mg, 0.62 mmol, 95 %, based on phenol) is isolated as a colorless, slight hygroscopic, sticky crystalline solid (dec. > 92 °C). Suitable crystals for XRD were grown from the ethereal reaction mixture at -28 °C. ^{1}H NMR (500 MHz, [D$_8$]THF, rt): δ=1.2 (t, $^3J_{H,H}$ = 7 Hz, 54 H, $NCH_2C\mathbf{H}_3$), 1.4 (s, 9 H, $NC(CH_3)_3$), 2.2 (d, $^2J_{P,H}$ = 8 Hz, 1 H, NH), 3.2 (d, q, $^3J_{P,H}$ = 10 Hz, $^3J_{H,H}$ = 7 Hz, 36 H, $NC\mathbf{H}_2CH_3$), 4.3 (s, br, 2 H, H_2O), 5.7 (s, 1 H, para H), 6.2 (s, 2 H, ortho H), 6.6 ppm (m, 2 H, meta H); ^{13}C NMR (500 MHz, [D$_8$]THF, rt): δ=13.0 (d, $^3J_{P,C}$ = 4 Hz, $NCH_2\mathbf{C}H_3$), 31.1 (d, $^3J_{P,C}$ = 5 Hz, $NC(\mathbf{C}H_3)_3$), 39.1 (d, $^2J_{P,C}$ = 6 Hz, $N\mathbf{C}H_2CH_3$), 50.5 (d, $^2J_{P,C}$ = 4 Hz, $N\mathbf{C}(CH_3)_3$), 104.5 (s, para C), 119.0 (s, ortho C), 127.6 (s, meta C), 173.6 ppm (s, ipso C); ^{31}P NMR (500 MHz, [D$_8$]THF, rt): δ=-33.7 (q, d, $^2J_{P,P}$ = 70 Hz, $^2J_{P,H}$ = 8 Hz, 1 P, P=NH), 7.7 ppm (d, tridec, $^2J_{P\,P}$ = 70 Hz, $^3J_{P\,H}$ = 10 Hz, 3 P, $(Et_2N)_3P$); IR (ATR): $\tilde{\nu}$=3350 (vw), 3047 (vw), 2967 (w), 2930 (vw), 2867 (w), 1577 (w), 1538 (vw), 1484 (w), 1460 (w), 1415 (vw), 1377 (w), 1350 (w), 1326 (w), 1259 (s), 1227 (w), 1201 (s), 1175 (vs), 1108 (w), 1054 (w), 1018 (vs), 979 (m), 942 (vs), 848 (m), 821 (w), 795 (m), 740 (m), 699 (s), 691 (s), 614 (w), 590 (w), 513 (vs), 486 (s), 457 (s), 435 (s) cm^{-1}; MS (ESI, pos.) {*m/z* (%) [assignment]}: 886.9 (100) **[1H]$^+$**; MS (ESI, neg.) {*m/z* (%) [assignment]}: 92.9 (100) **[PhO]$^-$**; elemental analysis calcd for $C_{46}H_{107}N_{13}O_2P_4$: C 55.34, H 10.80, N 18.24; found: C 54.88, H 10.77, N 17.28.

Synthesis of [1H][TCNE]

The salt **[1H][^{MetBu2}PhO]** (522 mg, 0.47 mmol) is suspended in 12 mL of diethyl ether and a solution of tetracyanoethylene (64 mg, 0.50 mmol) in 10 mL of diethyl ether is rapidly added. Immediately a deep green-yellow suspension forms. The suspension is stirred for 5 minutes and then cooled to -28 °C overnight. The supernatant is removed via a syringe, the solid is washed with diethyl ether (2 x 10 mL) and dried in a high vacuum. The product (422 mg, 0.42 mmol, 88 %, based on **[1H][^{MetBu2}PhO]**) is isolated as an orange solid (dec. > 86 °C). Suitable crystals for XRD were grown from the ethereal reaction mixture at -28 °C. IR (ATR): $\tilde{\nu}$= 2968 (vw), 2932 (vw), 2869 (vw), 2182 (vw), 2143 (w), 2123 (vw), 1465 (vw), 1414 (vw), 1378 (w), 1350 (w), 1267 (m, br), 1225 (w), 1202 (s), 1175 (vs), 1108 (w), 1054 (w), 1018 (vs), 942 (vs), 920 (m), 845 (w), 794 (s), 738 (w), 699 (s), 612 (m), 510 (vs), 442 (s), 408 (m) cm^{-1}; MS (ESI, pos.) {*m/z* (%) [assignment]}: 886.6 (100) **[1H]$^+$**; MS (ESI, neg.) {*m/z* (%) [assignment]}: 127.8 (37) $[TCNE]^{\cdot-}$; HRMS (ESI, pos.) m/z calcd for $C_{40}H_{100}N_{13}P_4$: 886.71696; found: 886.7177; HRMS (ESI, neg.) m/z calcd for C_6N_4: calcd.: 128.01284; found: 128.0128; elemental analysis calcd for $C_{46}H_{100}N_{17}P_4$: C 54.42, H 9.93, N 23.45; found: C 55.57, H 10.11, N 22.65.

Activation of SF$_6$

General procedure: The phosphazenium phenolate salt (60 mg) is filled into a Young NMR tube containing an acetone-d_6 filled capillary. First THF or Et_2O (0.4 mL) as the solvent is condensed onto the salt at -196 °C prior to the condensation of an excess of SF_6 (3 mbar, 0.075 mmol) onto the mixture. The reaction is allowed to warm to ambient temperature and the course of the reaction is monitored by ^{19}F NMR spectroscopy.

Table 2. Structure refinement data of **[1H][PhO(H$_2$O)]**, **[1H][^{tBu3}PhO]**, **[NBu$_4$][^{MeOtBu2}PhO]** and **[1H][(^{MeOtBu2}PhO)$_2$H]**.

Compound	**[1H][PhO(H$_2$O)]**	**[1H][^{tBu3}PhO]**	**[NBu$_4$][^{MeOtBu2}PhO]**	**[1H][(^{MeOtBu2}PhO)$_2$H]**
empirical formula	$C_{46}H_{107}N_{13}O_2P_4$	$C_{58}H_{129}N_{13}OP_4$	$C_{31}H_{59}NO_2$	$C_{82}H_{177}N_{13}O_7P_4$
a / pm	1270.911(14)	1570.493(16)	919.264(10)	4964.04(4)
b / pm	1334.105(14)	1952.776(17)	1726.121(16)	4964.04(4)
c / pm	1727.395(19)	2297.32(2)	3817.73(3)	2016.72(2)
α / °	81.8859(9)	90	90	90
β / °	85.2605(9)	103.5089(11)	90	90
γ / °	79.5752(9)	90	90	120
V / 10^6 pm^3	2846.76(5)	6850.55(12)	6057.82(10)	43037.5(8)
Z	2	4	8	18
ρ_{calc} / mg·mm^{-3}	1.165	1.114	1.048	1.098
crystal system	triclinic	monoclinic	orthorhombic	trigonal
space group	*P*-1	$P2_1/c$	$P2_12_12_1$	*R*-3
crystal size / mm^{-3}	0.332 x 0.258 x 0.096	0.301 x 0.093 x 0.067	0.339 x 0.142 x 0.12	0.424 x 0.381 x 0.247
μ / mm^{-1}	0.180	1.365	0.476	1.145
F(000)	1100.0	2544.0	2144.0	15768.0
2θ range for data col. / °	5.36 to 72.636	5.788 to 153.198	4.63 to 153.718	6.986 to 154.76
index ranges	$-21 \le h \le 21$ $-22 \le k \le 22$ $-28 \le l \le 28$	$-19 \le h \le 19$ $-24 \le k \le 21$ $-28 \le l \le 28$	$-11 \le h \le 11$ $-21 \le k \le 21$ $-48 \le l \le 47$	$-50 \le h \le 61$ $-59 \le k \le 65$ $-24 \le l \le 25$
reflections col.	275615	60331	123549	149772
independent refl.	27575	14264	12696	19943
R(int)	0.0610	0.0418	0.0605	0.0490
data/restraints/ parameter	27575/0/1027	14264/0/719	12696/0/1087	19943/0/1263
goodness-of-fit on F^2	1.041	1.017	1.037	1.044
R_1 / wR_2 [I>2σ(I)]	0.0377/0.0915	0.0369/0.0931	0.0311/0.0768	0.0382/0.0990
R_1 / wR_2 (all data)	0.0559/0.1005	0.0426/0.0969	0.0336/0.0786	0.0401/0.1006
$\Delta\rho_{max/min}$ / e Å^{-3}	0.59/-0.43	0.54/-0.42	0.21/-0.16	0.91/-0.42
remarks	The water molecule is disordered with a ratio of 1:1		Inversion twin with a ratio of 1:1	A solvent mask was calculated, 2154 electrons were found, this is consistent with the presence of three molecules of diethylether per formula unit, which count 2268 electrons.
CCDC number	2035834	2035835	2035836	2035837

Table 3. Structure refinement data of **[1H][$C_{10}H_7O$]**, **[1H][$(C_{10}H_7O)_2H$]** and **[1H][TCNE]**.

Compound	**[1H][$C_{10}H_7O$]**	**[1H][$(C_{10}H_7O)_2H$]**	**[1H][TCNE]**
empirical formula	$C_{50}H_{107}N_{13}OP_4$	$C_{60}H_{115}N_{13}O_2P_4$	$C_{46}H_{100}N_{17}P_4$
a / pm	1321.29(3)	1625.06(3)	1111.084(6)
b / pm	1413.71(3)	1804.57(3)	2734.353(13)
c / pm	1630.93(3)	2300.42(4)	1927.356(13)
α / °	94.8840(18)	90	90
β / °	95.9651(17)	97.1688(15)	97.9077(6)
γ / °	105.357(2)	90	90
V / 10^6 pm^3	2901.55(12)	6693.34(19)	5799.81(6)
Z	2	4	4
ρ_{calc} / mg·mm^{-3}	1.179	1.166	1.163
crystal system	triclinic	monoclinic	monoclinic
space group	*P*-1	$P2_1/n$	$P2_1/n$
color shape			
crystal size / mm^{-3}	0.241 x 0.146 x 0.05	0.353 x 0.269 x 0.112	0.427 x 0.237 x 0.23
μ / mm^{-1}	0.177	0.163	1.563
F(000)	1132.0	2568.0	2220.0
2θ range for data col. / °	5.222 to 72.964	5.174 to 72.638	5.646 to 153.29
index ranges	-21 ≤ *h* ≤ 22 -22 ≤ *k* ≤ 23 -27 ≤ *l* ≤ 26	-27 ≤ *h* ≤ 27 -30 ≤ *k* ≤ 30 -38 ≤ *l* ≤ 38	-13 ≤ *h* ≤ 13 -34 ≤ *k* ≤ 34 -23 ≤ *l* ≤ 23
reflections col.	91248	355625	104415
independent refl.	26937	32422	12103
R(int)	0.0347	0.0783	0.0650
data/restraints/ parameter	26937/0/1123	32422/0/1236	12103/7/655
goodness-of-fit on F^2	1.048	1.031	1.047
R_1 / wR_2 [I>2σ(I)]	0.0417/0.0951	0.0438/0.1030	0.0380/0.0993
R_1 / wR_2 (all data)	0.0629/0.1040	0.0695/0.1151	0.0420/0.1027
$\Delta\rho_{max/min}$ / e Å^{-3}	0.89/-0.63	0.54/-0.38	0.53/-0.46
remarks	The anion and some ethyl groups are disordered with a ratio of 90:10, one ethyl group is disordered in a ratio of 59:41. Disordered atoms close together were constrained to have equivalent thermal parameters.	One Naphtol molecule is disordered with a ratio of 70:30. The hydrogen atom is disordered between the two oxygen atoms with a ratio of 1:1. Disordered atoms close together were constrained to have equivalent thermal parameters	Disorder of one -$N(Me)_2$ group over two sites (57:43). Bond lengths within this disorder were restraint to be equal.
CCDC number	2045902	2045903	2035838

Acknowledgements

We acknowledge the financial support by Merck KGaA and Solvay. We thank Mira Kessler for the calculations of adiabatic ionization potentials and we furthermore thank the Regional Computing Center of the University of Cologne (RRZK) for providing computing time on the DFG-funded High Performance Computing (HPC) system CHEOPS, as well as support. We thank Fridolin Röhs for UV/Vis absorption measurements and the Group of Prof. Dr. Volker Wendisch for providing time on the spectrofluorophotometer. We thank Prof. Dr. Lothar Weber and Dr. Julia Bader for helpful discussions. We thank Manuel Warkentin for experimental assistance.

Keywords: hydrogen bond • phenol • phenolate • radical anion • SF_6 activation

[1] a) H. Kolbe, *J. Prakt. Chem.* **1874**, *10*, 89; b) Z. Marković, S. Marković, N. Manojlović, J. Predojević-Simović, *J. Chem. Inf. Model* **2007**, *47*, 1520.

[2] a) A. Zouni, H. T. Witt, J. Kern, P. Fromme, N. Krauss, W. Saenger, P. Orth, *Nature* **2001**, *409*, 739; b) Y. Umena, K. Kawakami, J.-R. Shen, N. Kamiya, *Nature* **2011**, *473*, 55.

[3] J. D. Megiatto, D. D. Méndez-Hernández, M. E. Tejeda-Ferrari, A.-L. Teillout, M. J. Llansola-Portolés, G. Kodis, O. G. Poluektov, T. Rajh, V. Mujica, T. L. Groy et al., *Nat. Chem.* **2014**, *6*, 423.

[4] a) A. Chandra, T. Uchimaru, *Int. J. Mol. Sci.* **2002**, *3*, 407; b) N. Hayashi, K. Sato, Y. Sato, M. Iwagami, N. Nishimura, J. Yoshino, H. Higuchi, T. Sato, *J. Org. Chem.* **2011**, *76*, 5747; c) M. Kołaski, A. Kumar, N. J. Singh, K. S. Kim, *Phys. Chem. Chem. Phys.* **2011**, *13*, 991.

[5] A. Kütt, V. Movchun, T. Rodima, T. Dansauer, E. B. Rusanov, I. Leito, I. Kaljurand, J. Koppel, V. Pihl, I. Koppel et al., *J. Org. Chem.* **2008**, *73*, 2607.

[6] R. Goddard, H. M. Herzog, M. T. Reetz, *Tetrahedron* **2002**, *58*, 7847.

[7] a) J. A. Cowan, J. A. C. Clyburne, M. G. Davidson, R. L. W. Harris, J. A. K. Howard, P. Küpper, M. A. Leech, S. P. Richards, *Angew. Chem. Int. Ed.* **2002**, *41*, 1432-1434; b) J. A. Cowan, J. A. C. Clyburne, M. G. Davidson, R. L. W. Harris, J. A. K. Howard, P. Küpper, M. A. Leech, S. P. Richards, *Angew. Chem.* **2002**, *114*, 1490; c) J. P. Canal, T. Ramnial, D. A. Dickie, J. A. C. Clyburne, *Chem. Commun.* **2006**, 1809; d) J. K. W. Chui, T. Ramnial, J. A. C. Clyburne, *Comments Inorg. Chem.* **2003**, *24*, 165.

[8] N. Kuhn, C. Maichle-Mößmer, M. Steimann, *Z. Naturforsch., B: Chem. Sci.* **2009**, *64*, 835.

[9] a) A. Sirjoosingh, S. Hammes-Schiffer, *J. Phys. Chem. A* **2011**, *115*, 2367; b) C. Costentin, M. Robert, J.-M. Savéant, *Phys. Chem. Chem. Phys.* **2010**, *12*, 11179; c) L. Benisvy, R. Bittl, E. Bothe, C. D. Garner, J. McMaster, S. Ross, C. Teutloff, F. Neese, *Angew. Chem. Int. Ed.* **2005**, *44*, 5314; d) Y. Fang, L. Liu, Y. Feng, X.-S. Li, Q.-X. Guo, *J. Phys. Chem. A* **2002**, *106*, 4669; e) D. L. Jenson, B. A. Barry, *J. Am. Chem. Soc.* **2009**, *131*, 10567; f) I. J. Rhile, T. F. Markle, H. Nagao, A. G. DiPasquale, O. P. Lam, M. A. Lockwood, K. Rotter, J. M. Mayer, *J. Am. Chem. Soc.* **2006**, *128*, 6075; g) I. J. Rhile, J. M. Mayer, *J. Am. Chem. Soc.* **2004**, *126*, 12718; h) M. Sjödin, T. Irebo, J. E. Utas, J. Lind, G. Merényi, B. Akermark, L. Hammarström, *J. Am. Chem. Soc.* **2006**, *128*, 13076.

[10] L. L. Williams, R. D. Webster, *J. Am. Chem. Soc.* **2004**, *126*, 12441.

[11] P. Hapiot, J. Pinson, N. Yousfi, *New J. Chem.* **1992**, *16*, 877.

[12] a) S. Xie, S. Manuguri, O. Ramström, M. Yan, *Chem. - Asian Journal* **2019**, *14*, 910; b) L. Yang, S. Nian, G. Zhang, E. Sharman, H. Miao, X. Zhang, X. Chen, Y. Luo, J. Jiang, *Sci. Rep.* **2019**, *9*, 11640; c) I. G. Alty, D. W. Cheek, T. Chen, D. B. Smith, E. Q. Walhout, C. J. Abelt, *J. Phys. Chem. A* **2016**, *120*, 3518.

[13] L. M. Tolbert, S. M. Nesselroth, *J. Phys. Chem.* **1991**, *95*, 10331.

[14] a) V. Kumar, S. Pandey, *ChemPhysChem* **2013**, *14*, 491; b) V. Kumar, S. Pandey, *J. Phys. Chem. B* **2012**, *116*, 12030.

[15] R. F. Weitkamp, B. Neumann, H.-G. Stammler, B. Hoge, *Angew. Chem. Int. Ed. Engl.* **2019**, *58*, 14633.

[16] R. F. Weitkamp, B. Neumann, H. ‐ G. Stammler, B. Hoge, *Angew. Chem.* **2019**, *131*, 14775.

[17] M. Kunert, E. Dinjus, M. Nauck, J. Sieler, *Chem. Ber.* **1997**, *130*, 1461.

[18] T. Steiner, *Angew. Chem. Int. Ed.* **2002**, *41*, 48.

[19] W. M. Haynes, *CRC Handbook of Chemistry and Physics*, CRC Press, London, **2016**.

[20] N. L. Zabik, C. N. Virca, T. M. McCormick, S. Martic-Milne, *J. Phys. Chem. B* **2016**, *120*, 8914.

[21] M. J. Frisch, G. W. Trucks, H. B. Schlegel, G. E. Scuseria, M. A. Robb, J. R. Cheeseman, G. Scalmani, V. Barone, B. Mennucci, G. A. Petersson et al., *Gaussian 09, Revision D.01*, Gaussian, Inc., Wallingford CT, **2013**.

[22] B. Olbrich-Deussner, W. Kaim, R. Gross-Lannert, *Inorg. Chem.* **1989**, *28*, 3113.

[23] J. S. Miller, *Angew. Chem. Int. Ed.* **2006**, *45*, 2508.

[24] D. N. Dhar, *Chem. Rev.* **1967**, *67*, 611.

[25] Z.-I. Yoshida, T. Sugimoto, *Angew. Chem.* **1988**, *100*, 1633.

[26] a) J. S. Miller, J. C. Calabrese, A. J. Epstein, R. W. Bigelow, J. H. Zhang, W. M. Reiff, *J. Chem. Soc., Chem. Commun.* **1986**, 1026; b) J. S. Miller, *Inorg. Chem.* **2000**, *39*, 4392; c) J. S. Miller, A. J. Epstein, *Chem. Commun.* **1998**, 1319.

[27] O. Webster, W. Mahler, R. Benson, *J. Org. Chem.* **1960**, *25*, 1470.

[28] J.-M. Lü, S. V. Rosokha, J. K. Kochi, *J. Am. Chem. Soc.* **2003**, *125*, 12161.

[29] a) J. J. Novoa, P. Lafuente, R. E. Del Sesto, J. S. Miller, *Angew. Chem. Int. Ed.* **2001**, *40*, 2540; b) J. J. Novoa, P. Lafuente, R. E. Del Sesto, J. S. Miller, *Angew. Chem.* **2001**, *113*, 2608; c) R. E. Del Sesto, J. S. Miller, P. Lafuente, J. J. Novoa, *Chem. Eur. J.* **2002**, *8*, 4894; d) J. S. Miller, J. J. Novoa, *Acc. Chem. Res.* **2007**, *40*, 189; e) J. Casado, P. M. Burrezo, F. J. Ramírez, J. T. L. Navarrete, S. H. Lapidus, P. W. Stephens, H.-L. Vo, J. S. Miller, F. Mota, J. J. Novoa, *Angew. Chem.* **2013**, *125*, 6549; f) J. Casado, P. Mayorga Burrezo, F. J. Ramírez, J. T. López Navarrete, S. H. Lapidus, P. W. Stephens, H.-L. Vo, J. S. Miller, F. Mota, J. J. Novoa, *Angew. Chem. Int. Ed. Engl.* **2013**, *52*, 6421; g) A. G. Graham, F. Mota, E. Shurdha, A. L. Rheingold, J. J. Novoa, J. S. Miller, *Chem. Eur. J.* **2015**, *21*, 13240; h) A. G. Graham, M. V. Fedin, J. S. Miller, *Chem. Eur. J.* **2017**, *23*, 12620; i) M. Capdevila-Cortada, J. Ribas-Arino, A. Chaumont, G. Wipff, J. J. Novoa, *Chem. Eur. J.* **2016**, *22*, 17037.

[30] a) J. S. Miller, J. C. Calabrese, H. Rommelmann, S. R. Chittipeddi, J. H. Zhang, W. M. Reiff, A. J. Epstein, *J. Am. Chem. Soc.* **1987**, *109*, 769; b) B. Milián, R. Pou-Amérigo, M. Merchán, E. Ortí, *ChemPhysChem* **2005**, *6*, 503; c) S. Flandrois, K. Ludolf, H. J. Keller, D. Nöthe, S. R. Bondeson, Z. G. Soos, D. Wehe, *Mol. Cryst. Liq. Cryst.* **2011**, *95*, 149; d) Z.-h. Cui, H. Lischka, T. Mueller, F. Plasser, M. Kertesz, *ChemPhysChem* **2014**, *15*, 165.

[31] a) P. Forster, V. Ramaswamy, P. Artaxo, T. Berntsen, R. Betts, D. W. Fahey, J. Haywood, J. Lean, D. C. Lowe, G. Myhre et al., *Changes in Atmospheric Constituents and in Radiative Forcing, in: Climate Change 2007: The Physical Science Basis. Contribution of Working Group I to the Fourth Assessment Report of the IPCC, Cambridge University Press, 2007.*; b) K. Seppelt, *Chem. Rev.* **2015**, *115*, 1296; c) L. Zámostná, T. Braun, *Nachr. Chem.* **2016**, *64*, 829.

[32] R. Basta, B. G. Harvey, A. M. Arif, R. D. Ernst, *J. Am. Chem. Soc.* **2005**, *127*, 11924.

[33] a) M. Wozniak, T. Braun, M. Ahrens, B. Braun-Cula, P. Wittwer, R. Herrmann, R. Laubenstein, *Organometallics* **2017**, *37*, 821; b) L. Zámostná, T. Braun, *Angew. Chem.* **2015**, *127*, 10798; c) L. Zámostná, T. Braun, B. Braun, *Angew. Chem. Int. Ed. Engl.* **2014**, *53*, 2745.

[34] C. Berg, T. Braun, M. Ahrens, P. Wittwer, R. Herrmann, *Angew. Chem.* **2017**, *129*, 4364.

[35] B. G. Harvey, A. M. Arif, A. Glöckner, R. D. Ernst, *Organometallics* **2007**, *26*, 2872.

[36] a) P. Holze, B. Horn, C. Limberg, C. Matlachowski, S. Mebs, *Angew. Chem. Int. Ed. Engl.* **2014**, *53*, 2750; b) P. Holze, B. Horn, C. Limberg, C. Matlachowski, S. Mebs, *Angew. Chem.* **2014**, *126*, 2788.

[37] M. Govindan, R. Adam Gopal, I. S. Moon, *Chem. Eng. J.* **2020**, *382*, 122881.

[38] H. Deubner, F. Kraus, *Inorganics* **2017**, *5*, 68.

[39] M. Rueping, P. Nikolaienko, Y. Lebedev, A. Adams, *Green Chem.* **2017**, *19*, 2571.

[40] D. Sevenard, P. Kirsch, A. A. Kolomeitsev, G.-V. Röschenthaler, DE 102 20 901 A1, **2002**.

[41] G. Iakobson, M. Pošta, P. Beier, *J. Fluorine Chem.* **2018**, *213*, 51.

[42] a) T. A. McTeague, T. F. Jamison, *Angew. Chem. Int. Ed. Engl.* **2016**, *55*, 15072; b) D. Rombach, H.-A. Wagenknecht, *Angew. Chem. Int. Ed. Engl.* **2020**, *59*, 300; c) P. Tomar, T. Braun, E. Kemnitz, *Chem. Commun.* **2018**, *54*, 9753.

[43] a) L. Zhong, S. Ji, F. Wang, Q. Sun, S. Chen, J. Liu, B. Hai, L. Tang, *J. Fluorine Chem.* **2019**, *220*, 61; b) A. Akhgarnusch, R. F. Höckendorf, M. K. Beyer, *J. Phys. Chem. A* **2015**, *119*, 9978; c) A. Rosa, F. Brüning, S.V.K. Kumar, E. Illenberger, *Chem. Phys. Lett.* **2004**, *391*, 361; d) R. E. Weston, *J. Phys. Chem.* **1995**, *99*, 13150; e) E. C. M. Chen, L. ‐ R. Shuie, E. Desai D' sa, C. F. Batten, W. E. Wentworth, *J. Chem. Phys.* **1988**, *88*, 4711; f) G. E. Streit, *J. Chem. Phys.* **1982**, *77*, 826.

[44] F. Buß, C. Mück-Lichtenfeld, P. Mehlmann, F. Dielmann, *Angew. Chem.* **2018**, *130*, 5045.

[45] K. Matsumoto, Y. Haruki, S. Sawada, S. Yamada, T. Konno, R. Hagiwara, *Inorg. Chem.* **2018**, *57*, 14882.

[46] a) E. R. Altwicker, *Chem. Rev.* **1967**, *67*, 475; b) E. Müller, K. Ley, W. Kiedaisch, *Chem. Ber.* **1954**, *87*, 1605; c) V. W. Manner, T. F. Markle, J. H. Freudenthal, J. P. Roth, J. M. Mayer, *Chem. Commun.* **2008**, 256.

[47] O. V. Dolomanov, L. J. Bourhis, R. J. Gildea, J. A. K. Howard, H. Puschmann, *J. Appl. Cryst.* **2009**, *42*, 339.

[48] O. Graalmann, U. Klingebiel, W. Clegg, M. Haase, G. M. Sheldrick, *Chem. Ber.* **1984**, *117*, 2988.

[49] G. M. Sheldrick, *Acta Cryst. C* **2015**, *71*, 3.

Anhang 6

Phosphorus Containing Superbases: Recent Progress in the Chemistry of Electron Abundant Phosphines and Phosphazenes

Robin F. Weitkamp, Beate Neumann, Hans-Georg Stammler and Berthold Hoge

Chem. Eur. J. **2021**, *[prepared manuscript]*.

MINIREVIEW

Phosphorus Containing Superbases: Recent Progress in the Chemistry of Electron Abundant Phosphines and Phosphazenes

Robin F. Weitkamp,* Beate Neumann, Hans-Georg Stammler and Berthold Hoge*[a]

Dedication ((optional))

((Insert Picture for Frontispiece here [18.0×18.0 cm]))

[a] M. Sc. R. F. Weitkamp, B. Neumann, Dr. H.-G. Stammler, Prof. Dr. B. Hoge
Centrum für Molekulare Materialien
Fakultät für Chemie, Universität Bielefeld,
Universitätsstraße 25, 33615 Bielefeld (Germany)
E-mail: b.hoge@uni-bielefeld.de

Abstract: The renaissance of superbases is primarily based on their pronounced capability for a large variety of chemical transformations under mild reaction conditions. Four major set screws are available for the selective tuning of the basicity: the nature of the basic center (N, P, …), the degree of electron donation by substituents to the central atom, the possibility for charge delocalization and the energy gain by hydrogen bonding. Within the past decades, a plethora of neutral electron rich phosphine and phosphazene bases appeared in the literature. Their outstanding properties and advantages over inorganic or charged bases have made them now indispensable as auxiliary bases in deprotonation processes. Also, their utilization in catalysis or as ligands in coordination chemistry is highlighted due to broad-spread interest. Here we give an update of the chemistry of basic phosphines and phosphazenes.

1. Introduction

This mini review discusses the recent progress of the chemistry of selected non-charged electron abundant phosphines and phosphazenes within the past five years. Their broad applicability as superbases or as ligands made them flourish to highly important tools in organic and inorganic chemistry and indispensable in catalytic chemistry.[1]

The lone pair of electrons at the P-atom in phosphines PR_3 marked them out as Lewis bases. Substituents R on phosphorus are strongly governing its donor capability as obvious by the comparison of calculated ionization potentials IP_v and electron affinities EA_v of tris(trifluoromethyl)phosphine and trimethylphosphine (Figure 1). While electron donating groups evoke energetically increased HOMO-LUMO levels accompanied by an increased donor strength and basicity, electron withdrawing groups stabilize the HOMO and LUMO significantly and thus decreas the donation ability and basicity of those species.[2]

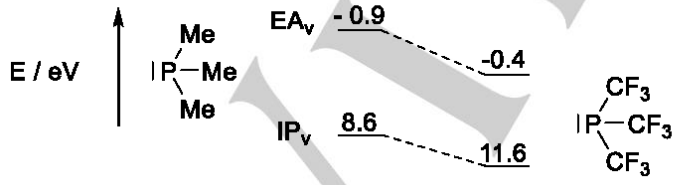

Figure 1. Ionization potential (IP_v) and electron affinity (EA_v) of trimethylphosphine and tris(trifluoromethyl)phosphine (B3LYP/6-311+G(d,p)).[2,3]

It is well known that electron poor phosphines as weakly basic ligands result in electron deficient transition metal complexes.[4,5,6,7,8] The devise of phosphines with stronger σ-donating properties is of growing interest, since N-heterocyclic carbenes (NHC) as strong σ-donor ligands have already surpassed the donor capability of simple alkylphosphines.[5,8,9]

Tris(pyrrolidinyl)phosphine exhibits similar ligating properties as tri(*n*-butyl)phosphine, which can be explained by π-donation of free lone pairs of the N-atoms.[10] Counterintuitively, the exchange of one π-donating but σ-electron-withdrawing amino substituent by one alkyl group affords the corresponding more basic bis(pyrrolidinyl)alkylphosphines, featuring similar donor properties as tri(*tert*)butylphosphine.[11] Thus it is obvious, that increasing the basicity and the overall donor strength is achieved by the implementation of strongly π-donating N-based functionalities, which are able to compensate the electron withdrawing effect of the contact nitrogen atoms.

This concept may also be applied for the design of phosphazenes (phosphanimines) of the type $R_3P{=}NR'$. In this case protonation and metal-coordination is affected by the nitrogen atom of the imino group, which represents the Lewis basicity center. The overall donor capacity of the nitrogen lone pair is improved by π-donating amino substituents on phosphorus which also mitigate the positive charges at the P-centers by π-back donation.[12–15]

The proton affinity as well as the gas-phase basicity of phosphazenes and phosphines have been chosen as a qualitative measure for their basicity and overall electron donation ability, respectively.[14,16,17,18]

In the following we will highlight modern superbase design and will also discuss important applications. First of all, we briefly mention historical milestones in the development of phosphazene and phosphine compounds with strong donor substituents.

Robin Weitkamp received his M.Sc. degree from Bielefeld University, Germany, in 2018 under the supervision of B. Hoge. Currently, he performs his Ph.D. thesis in the group of B. Hoge. His academic research is focused on the chemistry of phosphazene bases and the generation of non-coordinated anions.

Berthold Hoge received his Ph.D. in inorganic chemistry at Wuppertal University in Germany with R. Eujen in 1997. After his postdoc with K. O. Christe at the University of Southern California in the United States (1998), he started his habilitation mentored by D. Naumann at the University of Cologne, Germany, which he has accomplished in 2004. He was promoted to professor in inorganic chemistry in 2009 at

Bielefeld University in Germany, with the focus on molecular chemistry containing fluorine, phosphorus and silicon.

The roots of phosphazene chemistry date back to the year 1919, when Staudinger presented the first iminophosphoranes **1**, which were obtained by reaction of triorganophosphines with organic azides (Scheme 1).[19] Most commonly, the transiently formed phosphazides evade isolation and suffer from liberation of N_2.

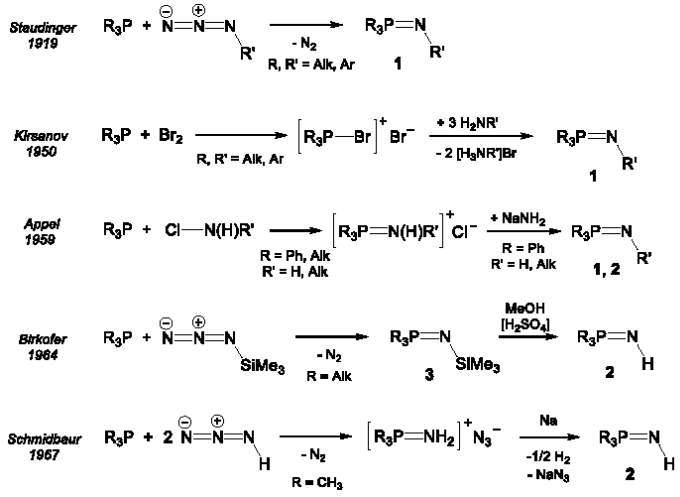

Scheme 1. Preparation of iminophosphoranes.

The protocol of Staudinger represents the most efficient and nowadays, preferably used pathway to a variety of iminophosphoranes.[20,21,22,23] However, it should be kept in mind that the use of sensitive azides is always hazardous due to violent decompositions,[24] which is particularly true for hydrazoic acid (HN_3).

The strategy presented by Kirsanov in 1950 utilizes a halogeno triorganophosphonium halide, which is converted to the corresponding iminophosphoranes **1** by primary amines (Scheme 1).[25] This method circumvents the need of dangerous and possibly non-existent azides, delivering products in high yields.

A few years later in 1959, Appel *et al.* succeeded in the isolation of the first iminophosphorane Ph_3P=NH (**2a**) by the deprotonation of the corresponding iminium halide with sodium amide in liquid ammonia.[26,27] Iminophosphoranes **2** of the general formula R_3P=NH are accessible by the reaction of phosphines with chloramines.[27,28] Another convenient method for the synthesis of **2** was developed by Birkofer in 1964 via Staudinger reactions of phosphines with trimethylsilylazide and the subsequent acid catalyzed hydrolysis of initially obtained trimethylsilyl iminophosphoranes **3** in methanol (Scheme 1).[22,29] The reaction of phosphines with hydrazoic acid and the subsequent reaction with sodium in liquid ammonia is also described.[30,31]

The availability of iminophosphoranes **2** has opened the door to a rich chemistry, e. g. the formation of metalorganic iminophosphoranes **4** and **6** resulting from deprotonation of **2** with organolithium bases[30–33] (Scheme 2) or from adducts **5** with organometallic compounds among others ($AlMe_3$, $GaMe_3$, $ZnMe_2$, …).[30,31,33,34] In order to study electron abundant iminophosphoranes, Issleib *et al.* decided to incorporate electron donating dimethylamino groups at the imino phosphorus atom in **2**.[35] The syntheses of the mono- to tris(dimethylamino) derivatives were performed according to the procedure by Appel *et al.* (Scheme 1 and 2) via the reaction of phosphines with chloramines and the subsequent deprotonation.[26–28] This series was completed by Goubeau *et al.* in 1974 with the tetrakis(dimethylamino)phosphonium ion.[20] Two years later in 1976, Schmutzler *et al.* further explored properties of (dimethylamino)iminophosphoranes **3** and reported on the first entirely dialkylamino substituted diphosphazene $(Me_2N)_3P$=N-$P(NMe_2)_2$=N-$SiMe_3$ (**7**, Scheme 2).[23]

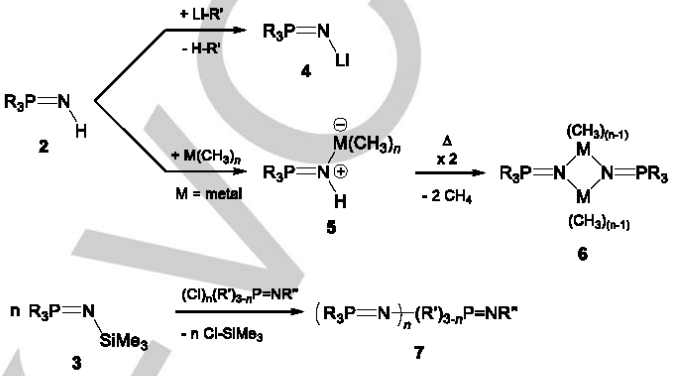

Scheme 2. Selected reactions of iminophosphoranes and functionalization possibilities.

Phosphazenylphosphines **8** as early examples of electron rich phosphines were first described by Schmidbaur in 1968.[33] Their syntheses are based upon the reaction of lithium imino(trialkyl)phosphoranes **4** with chloro(dialkyl)phosphines (Scheme 3)[33] but also proceeds via transmetalation of **3** with chlorophosphines.[36] Due to the high electron density at the tricoordinate phosphorus atom in **8**, facile alkylation of phosphazenylphosphines with alkylhalides affords bis(trialkylphosphine)iminium salts (**9**, Scheme 3).[36] These cations show a high thermal stability and moreover are resistant towards acids and bases.[37] Consistently, representatives like bis(triphenylphosphine)iminium (PNP^+) salts, first prepared by Appel *et al.*[37] in 1961, finds frequent application as appropriate cation sources in the stabilization and crystallization of salts featuring reactive anions.[38]

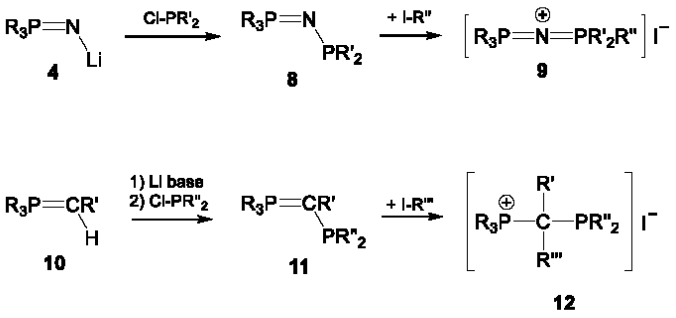

Scheme 3. Comparison of phosphazenylphosphines and phosphinealkylenephosphines.

More than three decades after Staudinger's seminal synthesis of the isoelectronic phosphonium methanides or

methylene phosphoranes **10** in 1919,[39] Wittig discovered their utility as reactants in a carbonyl-olefination process when brought in contact with aldehydes and ketones.[40] The so-called Wittig reaction remains to be one of the most important methods in olefin syntheses.[41] Through deprotonation and conversion with chlorophosphines, Issleib and co-workers succeeded in the functionalization of **10** and reported on first examples of C-phosphino methylene phosphoranes or ylidylphosphines **11** (YPhos, $Ph_3P=C(R)\text{-}PR'_2$, Scheme 3),[42] of which numerous representatives are known by today.[43] In stark contrast to the reactivity of **8** towards alkylhalides, alkylation of ylidylphosphines **11** occurs at the central carbon atom, resulting in salt-like phosphinomethyl phosphonium halides **12** (Scheme 3). This behavior is rationalized by the high negative charge density at carbon expressed by a zwitterionic resonance structure.[44–47] Investigations on diphosphinomethane[48] and diphosphinomethanides[49] are also relevant in this context.

Carbodiphosphoranes of the general formula $R_3P=C=PR_3$ (**13**) are isoelectronic to iminiumdiphosphorane cations **9** (Scheme 4).

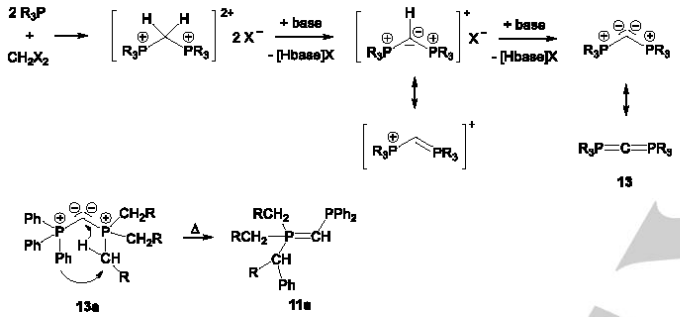

Scheme 4. Carbodiphosphorane preparation and comparison with iminiumdiphosphorane.

The first symmetric perphenylated carbodiphosphorane $Ph_3P=C=PPh_3$ was synthesized by Ramirez *et al.* in 1961,[50] and was followed by non-symmetric examples by Appel in 1978.[51] Due to ylid-ylene resonance structures, carbodiphosphoranes **13** can formally be regarded as bisylides with a twofold negative charge at the central carbon atom (Scheme 4). Consequently they act as strong carbon bases in a twofold protonation process towards Brønsted acids.[50,51] The negative charge at the carbon atom of **13** was demonstrated by their capability to function as bridging four-electron ligands in coordination chemistry.[52,53] At higher temperatures carbodiphosphoranes as **13a** with α-CH units may rearrange under formation of ylidylphosphines **11a** (Scheme 4).[51]

Verkade and co-workers have discovered another important group of superbasic electron rich phosphines, denoted "Verkade bases" (**14**). During their investigation of pentacoordinated phosphatranes of the general formula $[HP(XCH_2CH_2)_3N]^+$ (X = O, NMe) with tricyclic aminetriol[54,55] and triaminoamine[56,57] substituents (Scheme 5), they revealed unusually robust P-H bonds. The remarkably high proton affinity of **14** is caused by a stabilizing electron pair donation of the central nitrogen atom to the cationic center within the tricyclic substituent (Scheme 5), which was also subject of theoretical calculations.[58]

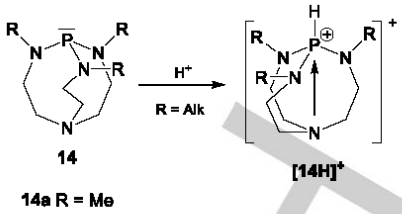

Scheme 5. "Verkade bases" **14**.

Oxaphosphatranes resists clean deprotonation due to the large tendency of the anticipated free base towards polymerization.[59] The corresponding highly stable pro-azaphosphatranes **14** ("Verkade bases") are smoothly liberated with KO*t*Bu.[57,59,60,61] With a $^{MeCN}pK_{BH^+}$ value of 32.9 for the methyl derivative **14a**, pro-azaphosphatranes are of similar basicity as diphosphazenes $(R_2N)_3P=N\text{-}(R_2N)_2P=N\textit{t}Bu$ (**16**, Scheme 6),[61–63] which were published a few years later by Schwesinger. The superbasic phosphines of Verkade type are useful reagents in organic syntheses[64] and enable a large bandwidth of reactions under mild reaction conditions, like the trimerization of isocyanates to isocyanurates,[65,66] as well as syntheses of important oxazoles and pyrroles,[67] or monoalkylations[68] and dehydrohalogenation reactions.[69,70] Pro-azaphosphatranes have also found application as auxiliary bases in Michael addition[71] or 1,2-addition reactions.[72]

Later, when Schwesinger's activities were focused on the preparation and investigation of superbasic proton sponges as auxiliary bases in dehydrohalogenation reactions,[73–77] he observed the outstanding proton-accepting properties of amino-substituted phosphanimines and laid the foundation stone of the wide field of the so called "Schwesinger bases".[12,13,15,63,78,79,80] High thermal stability, reluctance towards oxygen and base hydrolysis,[80,81,82] as well as their easy accessibility on large scales were crucial for their great success in synthetic chemistry.

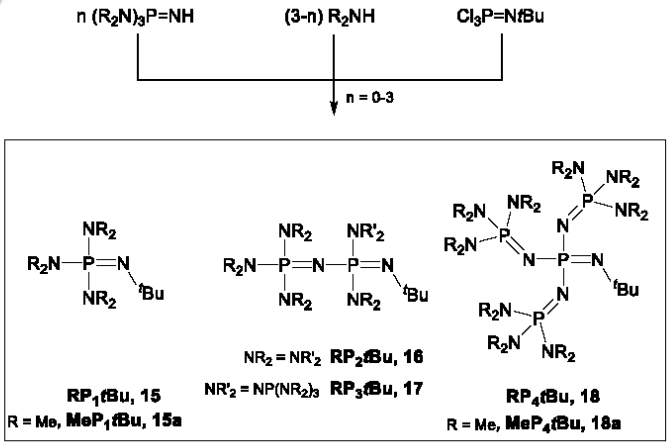

Scheme 6. Preparation of Schwesinger bases.

Phosphazene bases exhibit extremely high $^{MeCN}pK_{BH^+}$ values, which range from 26.9[12,15,79] for monophosphazene $(Me_2N)_3P=N\textit{t}Bu$ (**MeP$_1$*t*Bu**, **15a**) up to 42.7[63] for tetraphosphazene $[(Me_2N)_3P=N]_3P=N\textit{t}Bu$ (**MeP$_4$*t*Bu**, **18a**) (Scheme 6). As previously described, the superbasicity of

phosphazenes is due to π-donating phosphazenyl- or dialkylamino substituents bonded at phosphorus, which further allows an excellent delocalization of the engendered positive charge of the cations.[12,15] This is illustrated by the resonance structures of the protonated permethyl monophosphazene base **[MeP$_1$*t*BuH]$^+$** (**[15aH]$^+$**) in Scheme 7.

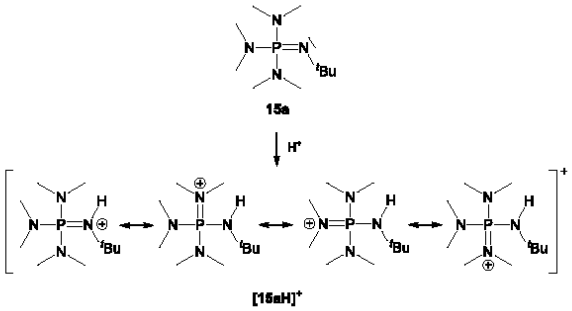

Scheme 7. Resonance structures of **[MeP$_1$*t*BuH]$^+$** (**[15aH]$^+$**).

The further "homologization" to penta- and heptaphosphazenes results in an only marginal increase in basicity and for the latter in a drastically sensitivity towards acids and air.[63]

The bulky phosphazene homologues **18** combine high basicity with low nucleophilicity,[12,13,15,63,73–77] which recommends their versatile employment in dehydrohalogenation reactions,[12,15,63] biarylether couplings[83] and alkylation reactions[1] among others.[57,84]

The direct basicity comparison of Verkade's phosphine $N(CH_2CH_2NMe)_3P$ **14a** with the analogous tricyclic Verkade's iminophosphorane $N(CH_2CH_2NMe)_3P{=}NR$ and the acyclic iminophosphorane $(Me_2N)_3P{=}NR$ **15** revealed the highest basicity for the phosphine within the row: $N(CH_2CH_2NMe)_3P$ > $N(CH_2CH_2NMe)_3P{=}NR$ > $(Me_2N)_3P{=}NR$.[85] Moreover, the cyclic imine derivative is more basic than the acyclic compound. Although Verkade's bases **14** are capable in dehydrohalogenation reactions of secondary and tertiary alkyl halides,[69,70] a pronounced nucleophilicity of this base leads to alkylation with primary alkyl halides as well as an eager formation of coordination adducts with Lewis acids.[55,59,65,66,86] The well accessibility of the P-atoms of the free bases also applies to the PH-functions of the respective protonated forms, and thus suggest that Verkade's bases **14** can not be employed for the realization of non-coordinated or "naked" anions. Alkylamino saturated phosphazenium ions offer themselves for the investigation of naked anions, like the naked fluoride anion.[82,87] However, salt metathesis reactions are required, which are often accompanied by poor solubilities or solvent removal issues. Encumbered phosphazene bases like **18** (Scheme 6) can take remedial action. Since neutral phosphazenes can be handled in common non-acidic and non-polar solvents, deprotonation of even weak acids affords the corresponding highly reactive non-coordinated anions.[88] Due to the central location of the accepted proton in a steric shielded molecule pocket, coordination and a dynamic proton exchange are hampered.

2. Recent results and discussions

2.1. Electron rich phosphines

Electron rich phosphines are available with a variety of different substituents.[4] They play a paramount role as ligands in transition metal catalysis[11,89] and their syntheses are increasingly supported by computational predictions.[90] Their development in recent decades has been accompanied by an impressive variety of commercially available phosphines for nearly every desired demand. Profound discussion, however, would go beyond the scope of this mini review. Thus, in the following chapters we will focus on recent achievements to phosphines of Dielmann, Sundermeyer and Gessner carrying strongly electron donating imidazoline-2-ylidenamino, pyridinylidenamino, phosphazenyl and ylidyl groups.

2.1.1 Mono and bidentate Imidazolin-2-ylidenamino phosphines (IAPs)

Dielmann and co-workers obtain electron rich phosphines by employment of strongly π-donating imidazolidine-2-ylidenamino or imidazoline-2-ylidenamino substituents (Scheme 8).[5,8,91]

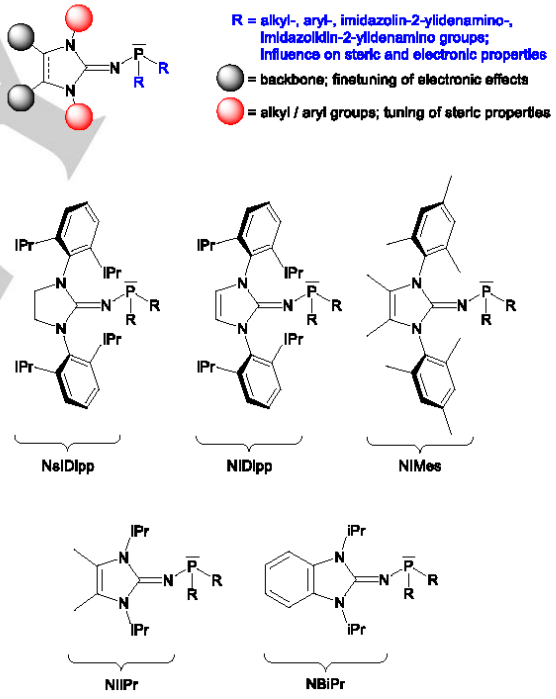

Scheme 8. IAPs of Dielmann *et al.*[5,8,91–93]

Imidazolidine-2-ylidenamino groups already excelled in syntheses of exotic donor free phosphinonitrene[94] and iminophosphonium cations[95] via lowering the electrophilicity at phosphorus. Advantageously, the incorporated NHC backbones have been broadly investigated, and thus enable efficient and easy tuning of steric and electronic properties (Scheme 8). The established syntheses of IAPs are depicted in Scheme 9. The NHC backbones are builded up by starting from imidazolium and imidazolidinium salts followed by the subsequent deprotonation with KO*t*Bu prior to the conversion via a Staudinger reaction with

trimethylsilylazide.[5,8,91–93,96] Established high yield syntheses (iPr > 99 %, *t*Bu 56 %) of dialkyl-IAPs **19a-c**, **20** and **21a-b** proceed via transmetalation of TMS-imidazolin-2-ylidenamines with R_2PCl or in case of $P(NIMes)_2(iPr)$ (**19c**) with PCl_3 and subsequent alkylation with iPrMgCl (Scheme 9).[5,8]

The NIiPr-groups are INTRODUCED via the free imine as building block, which can be furnished by hydrolysis of the corresponding TMS-compound in methanol.[97] Deprotonation of H-NIiPr with *n*-BuLi and conversion with $(iPr)_2PCl$ and $iPrPCl_2$ affords mono- and bis-substituted IAPs **22a** and **22b**, respectively, in high yields of over 87 %. However, the tris-compound of **22c** is isolated as the stable adduct $P(NIiPr)_3 \cdot LiCl$ due to the presence of intermediary formed LiCl from the reaction with PCl_3. LiCl may be separated by heating to 130 °C in *n*-hexane, which affords free $P(NIiPr)_3$ (**22c**) in a 34 % yield. In a more convenient route the respective imine itself is employed as the base and used in a quantitative manner (Scheme 9).[91,98] However, while $(NIiPr)(iPr)_2P$ (**22a**) is easily liberated, H-NIiPr is not sufficient for the deprotonation of $[H\text{-}P(NIiPr)_2(iPr)]Cl$ (**[22bH]Cl**) and $[H\text{-}P(NIiPr)_3]Cl$ (**[22cH]Cl**), thus deprotonation of these compounds is accomplished with KO*t*Bu and delivers the desired phosphines in high yields (> 89 %).[91]

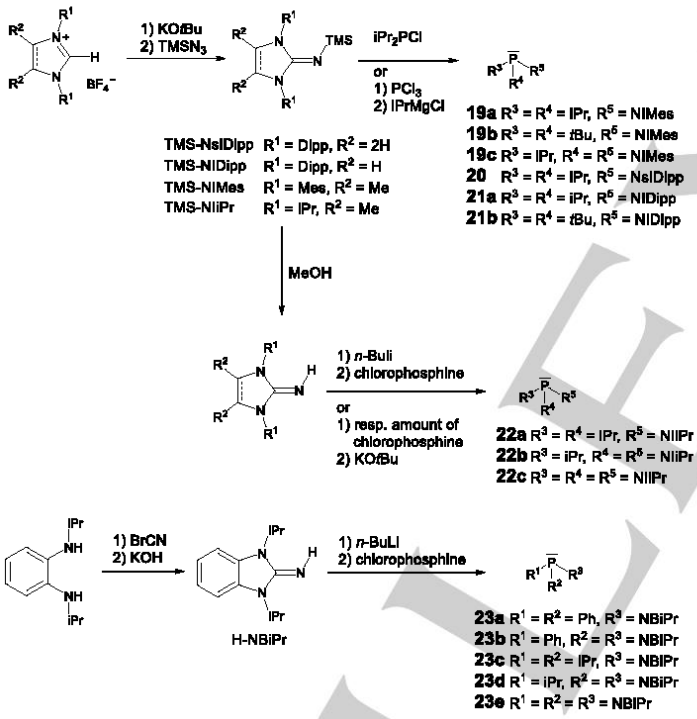

Scheme 9. IAPs of Dielmann *et al.*[5,8,91–93,99]

Compound $P(NIiPr)_3$ (**22c**) represents the strongest base within investigated IAPs with an experimental $^{THF}pK_{BH+}$ value of 31.0 ($^{MeCN}pK_{BH+}$ = 38.8).[91]

Benzimidazoline-IAPs **23a-e** are viable in yields of over 84 % via lithiation of H-NBiPr and subsequent reaction with the respective chlorophosphines.[5,8,92] Interestingly, employing this strategie $P(NBiPr)_3$ (**23e**) is accessible without incorporation of LiCl, for which the stronger electron releasing character of NIiPr-groups relative to NBiPr may be responsible.

Electron rich and strongly Lewis basic IAPs have found application in the activation of small molecules as SF_6,[100,101] CO_2[91,92] and SO_2,[102] and they readily form complexes with transition metals,[5,8,91–93,98] which excel outstanding catalytic activities in Suzuki-Miyaura cross-couplings and hydroamination reactions. Moreover, they were employed in FLP systems for the polymerization of methyl methacrylate.[103]

The π-donating power of NIiPr-groups does not only remarkably increase the Lewis and Brønsted basicity at phosphorus, but also evoke an increased hydridic character of the PH-unit in $[H\text{-}P(NIiPr)_3]^+$ (**[22cH]$^+$**). A salt exchange reaction with NaX (X = $B(C_6F_5)_4^-$ or $BAr^F{}_4^-$) and the subsequent hydrid abstraction affords the first phosphorus dication $[P(NIiPr)_3][X]_2$.[104]

Chelating IAPs **24-26** were also synthesized by the Dielmann group, whereas the phosphine moieties were either connected via a ferrocene,[5,8] a 1,3-bis(imidazolin-2-ylidenamino)propylene or a phenylene backbone (Scheme 10).[99] The 1,3-bis(imidazolin-2-ylidenamino)propylene group is built up from the respective dicarbene followed by the reaction with N_2O and hydrochloric acid. The desired product was isolated in a 93 % yield after deprotonation and the subsequent addition of $PCl(iPr)_2$.[99]

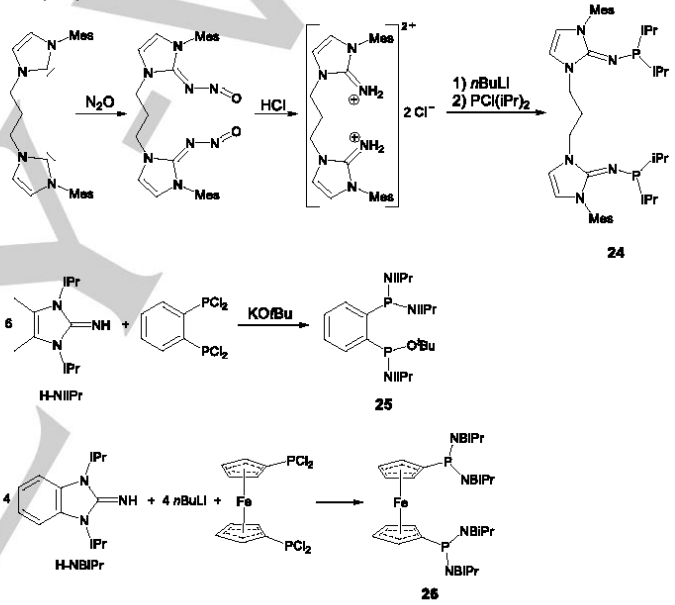

Scheme 10. Bidentate IAPs of Dielmann *et al.*[99]

The ferrocene backbone is easily incorporated by the reaction of H-NBiPr with a lithium base and the subsequent addition of bis(dichlorophosphino)ferrocene by which diphosphine **26** is isolated in a 81 % yield.[5,8] In contrast to that, and most likely due to steric repulsion, the analogous reaction of bis(dichlorophosphino)benzene with H-NIiPr as the base and nucleophile solely afforded the chloro-tris(NIiPr) intermediate. All attempts to substitute the chlorine atom by an additional NIiPr group remained challenging and thus substitution by a *tert*-butoxide moiety was performed instead to obtain the diphosphine **25**.

All bidentate phosphine ligands were successfully employed for the generation of electron rich gold(I), palladium(II) and nickel(0) chelate complexes.[99]

2.1.2 Pyridinylidenamino phosphines (PyAPs)

Taking the results of Nifantyev *et al.* in consideration,[105] Dielmann and co-workers realized PyAPs (pyridinylidenaminophosphines) **27-29** via incorporation of readily available and strongly π-donating pyridinylidenamino substituents in order to manifest cheap and easy to prepare electron rich phosphines for broad range applications as ligands or their employment in stoichiometric quantities (Scheme 11).[100,101,106] A comparison of the calculated gas-phase basicities of IAPs and PyAPs based on the representative examples $P(NIiPr)_3$ (**22c**, 288.0 kcal/mol) and PyAP $P(\text{-}N{=}C_5H_4N\text{-}n\text{Bu})_3$ (**27e**, 284.3 kcal/mol) reveal similar proton affinities.[100,101]

Aminopyridines represent cheap and commercially available starting materials and promise short straight forward PyAP syntheses. Analogous to imidazoline-2-ylidenamino substituents, the electronic and steric finetuning of aminopyridines is easily viable via incorporated substituents (Scheme 11).

Starting from 2- or 4-aminopyridinium salts the deprotonation with KHMDS and subsequent reaction with R_2PCl delivers the respective mono-PyAPs **27a-d** and **28a-d** in excellent yields (> 84 %).[106]

As previously reported by Dielmann and co-workers tris-PyAP $P(\text{-}N{=}C_5H_4N\text{-}n\text{Bu})_3$ (**27e**, Scheme 11) may be generated in THF solution by treatment of PCl_3 with five equivalents of imine $HN{=}C_5H_4N\text{-}n\text{Bu}$ and the subsequent deprotonation with KHMDS. However, the clean isolation of **27e** is hampered by incorporation of KCl in the stable coordination adduct **27e**·KCl. Due to increased steric hindrance at the imine nitrogen atom, the respective 2-pyridinylidenamino groups have been proven beneficial for the liberation of the corresponding free tris-2-pyridinylidenamino phosphines **29a** and **29b** from their HBF_4 salts in yields over 81 %.

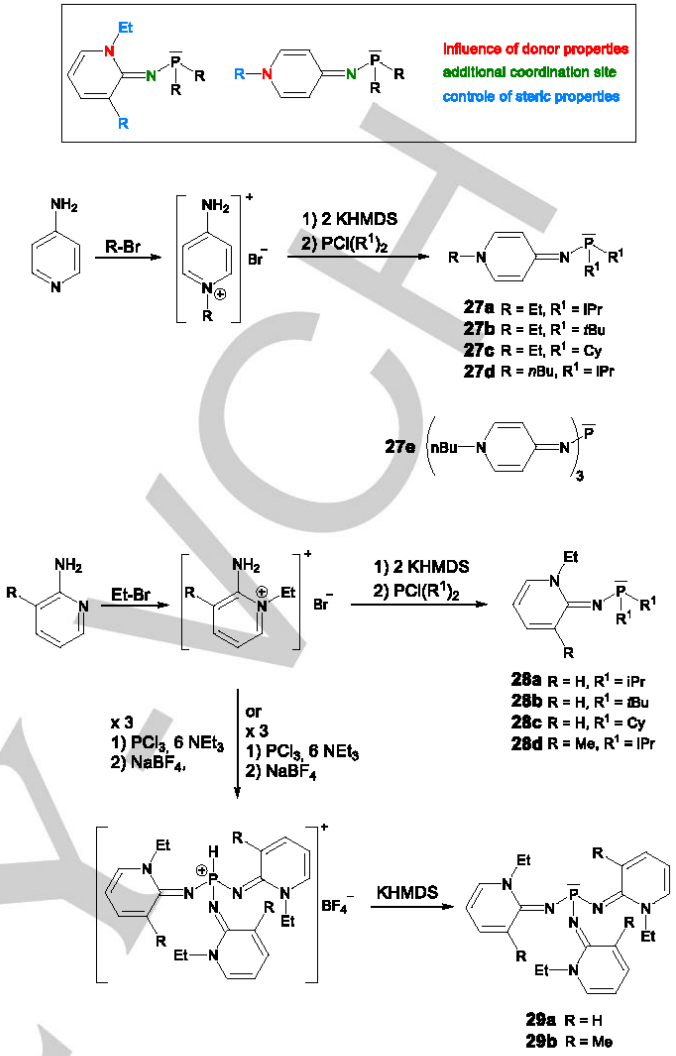

Scheme 11. PyAPs of Dielmann *et al.* and structure of **27e**.[100,101,106]

The pronounced Lewis basicity of PyAPs **27-29** is documented by ready formation of complexes with Cu(I), Au(I) and Pd(II) compounds and moreover excel in the activation of small molecules as SO_2 and CO_2 via incorporation as stable Lewis base adducts.[106] The in situ generation of PyAP **27e** and the subsequent disintegration of SF_6 is also reported.[100,101]

2.1.3 Phosphazenyl phosphines (PAPs)

Like all electron rich phosphines, phosphazenylphosphines (PAPs) represent strong Lewis and Brønsted bases, which is perceptible in their coordination properties.[7,107]

Sundermeyer *et al.* developed the strongest phosphine bases known so far via attachment of Schwesinger's phosphazenyl groups at the tricoordinate P-atom.[108–110]

The monophosphazenylphosphines **30a-d** are produced by treatment of PCl_3 with the respective phosphanimine $(R_2N)_3P{=}NSiMe_3$ followed by aminolyses. The applied phosphanimine derivatives are synthesized via Staudinger reaction with trimethylsilyl azide.[36,110]

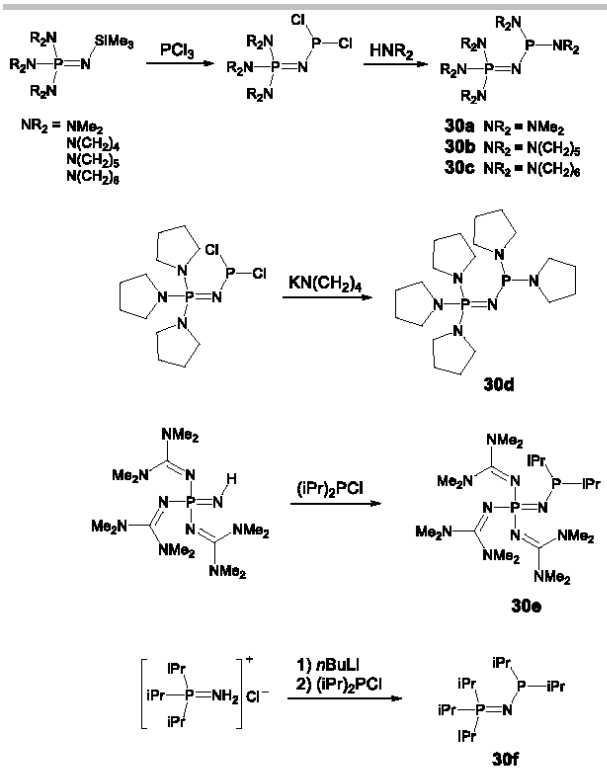

Scheme 12. Syntheses of mono PAPs.[108–111]

Phosphazenylphosphines **31a** and **31b** as well as the biphosphazenyl derivative (dma)P_6P (**32**) are only accessible in their protonated form by starting from $(Me_2N)_2PCl$ or $(Et_2N)_2PCl$, respectively, and reaction with mono- or diphosphazenes in THF solution (Scheme 13).[108–110] Advantageously, the employed dialkylaminochlorophosphines contain the build-in auxiliary base, which avoids the formation of inseparable mixtures of phosphonium and ammonium salts as the products. The subsequent anion exchange reaction with $NaBF_4$ delivers the desired tetrafluoroborate salts in excellent yields (> 83 %, Scheme 13).

The unsymmetrical substituted (dma)P_4P (**33**) is also obtained as the HBF_4 salt by reaction of PAP **30a** with either $[(Me_2N)_3P{=}NH_2][BF_4]$ and $(Me_2N)_3P{=}N{-}P(NMe_2)_2{=}NH$ or $[(Me_2N)_3P{=}N{-}P(NMe_2)_2{=}NH_2]Br$ and $(Me_2N)_3P{=}NH$, respectively, with subsequent salt exchange (Scheme 13).

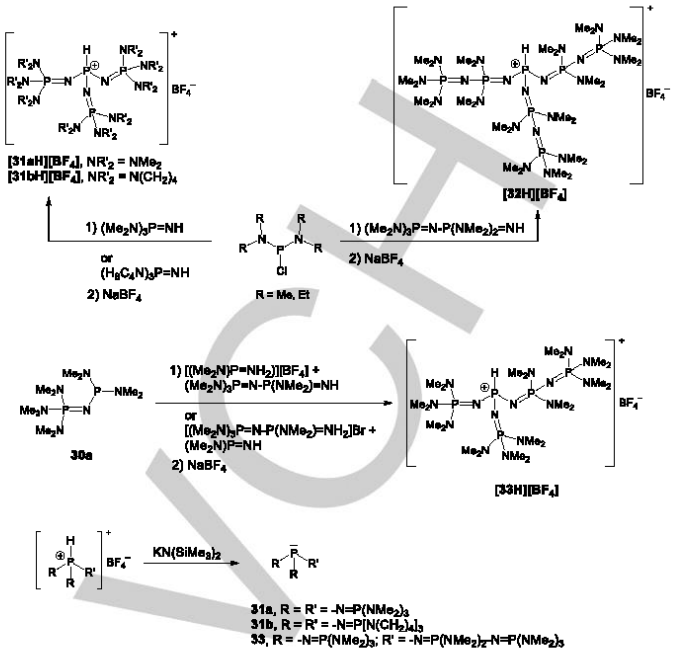

Scheme 13. Syntheses of tris PAPs.[108–110]

The free P_3P and P_4P bases **31a-b** and **33** can be liberated from their corresponding phosphonium tetrafluoroborates with potassium hexamethyldisilazide (KHMDS) in toluene solution, yielding the desired products as colorless solids in high yields (> 79 %, Scheme 13). Unfortunately, the deprotonation of the higher homologue [(dma)P_6PH][BF_4] (**[32H][BF_4]**) remains a challenge.[108,109] It could neither be realized with potassium in liquid ammonia or ethylenediamine, nor with several lithium bases (*n*- and *t*-BuLi, lithium di-*iso*-propylamide), among others.[108,109] Solely in the presence of an excessive amount of $NaNH_2$ or potassium pyrrolidide in THF solution, the free base **32** could be generated and characterized by NMR spectroscopy.

The obtained PAPs exhibit experimental $^{THF}pK_{BH+}$ values of 34.9 for (dma)P_3P (**31a**) and 36.7 for (pyrr)P_3P (**31b**), respectively, and up to 37.2 for (dma)P_4P (**33**).[108,109] The $^{THF}pK_{BH+}$ values of PAPs largely exceed that of the methyl Verkade superbase **14a** ($^{THF}pK_{BH+}$ = 24.1) and Dielmanns IAP P(NIiPr)$_3$ (**22c**, $^{THF}pK_{BH+}$ = 31.0), and may further surpass Schwesinger's methyl tetraphosphazene superbase **MeP$_4$*t*Bu** (**18a**, $^{THF}pK_{BH+}$ = 33.9) and **pyrrP$_4$*t*Bu** (**18b**, $^{THF}pK_{BH+}$ = 35.3).[17,18] The respective mono-PAPs **30a-d** are significantly less basic with calculated $^{MeCN}pK_{BH+}$ values of 26.4 for methyl derivative **30a** up to 31.5 for pyrrolidyl derivative **30d**.[110] The corresponding piperidyl- and azepanyl derivatives **30b** and **30c** show similar $^{MeCN}pK_{BH+}$ values.

In addition to the remarkable high observed proton affinities of PAPs, they surpass the Lewis basicity of IAPs, PyAPs and YPhos ligands, which is also mirrored in their coordination chemistry.[108,109]

Complementing the row of dialkyl PAPs, Dielmann established the syntheses of phosphazenylphosphines **30e** and **30f**, and gold(I) complexes thereof.[111]

2.1.4 Ylidylphosphines

Phosphonium ylides, bisylides and yldiides are 1,2-dipolar compounds with a high electron density at the central carbon atom.[44–47,112] Thus, they act as strong carbon bases and show a significant tendency for the addition of electrophiles.[18,42] During research on ylide and yldiide compounds as ligands in transition metal complexes and the stabilization of reactive low-valent main group elements, Gessner and coworkers connected the strongly π-donating ylidyl groups as substituents to phosphorus and obtained electron abundant ylidylphosphines (YPhos).[113,114,115]

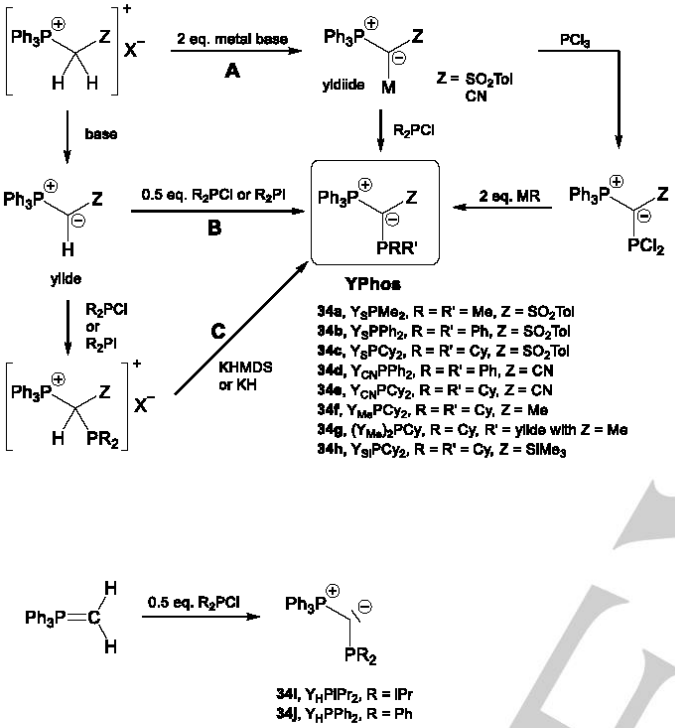

Scheme 14. Syntheses of YPhos ligands.

Three simple reaction paths **A**-**C** in Scheme 14 were presented to synthesize ylidylphosphines starting from alkylphosphonium salts, which can be easily prepared via reaction of the respective phosphine with alkylhalides (Scheme 14).[116–120] Depending on the nature of Z, double deprotonation with metal bases and subsequent nucleophilic substitution at halophosphines deliver the desired YPhos ligands **34a-e** in moderate to high yields of 69-92 % (route **A**).[116,119] As demonstrated for **34a**, the detour via reaction of yldiides with PCl_3 (70 %) and alkylation with organolithium or Grignard reagents is also feasible, but requires the isolation of sensitive intermediates.[116,119] In case of cheap starting materials, the way **B** is recommendable. Reaction of ylides with halophosphines and deprotonation by a second equivalent of ylide as the auxiliary base afforded the target molecules.[116,118–120] The route **C** is accomplished via reaction of ylides with halophosphines, but requires an additional equivalent of base as KH or KHMDS. Routes **B** and **C** are reported to proceed in a one pot synthesis and are therefore the preferable preparation methods.

The corresponding ylidylphosphines Y_HPiPr_2 (**34i**) and Y_HPPh_2 (**34j**) were synthesized by Dielmann and co-workers in high yields (> 85 %) in analogy to the preparation method of Issleib and Lindner[42] via the reaction of ylide H_2CPPh_3 with the respective chlorophosphine (Scheme 14).[111]

YPhos ligands represent valuable electron rich phosphines, which was demonstrated by their readily formation of transition metal complexes, such as gold(I)[111,114,116,119] or palladium[115,117,118,120] complexes, which have been successfully employed as catalysts in amination and hydroamination reactions, as well as alpha arylation with arylchlorides among others.[121]

2.2 Phosphazenes

While highly electron-rich phosphines generally find application in transition metal catalyses, low nucleophilic phosphazene superbases have been preferably established in deprotonation reactions, which is particularly obvious with regard to the huge variety of commercially available tailor-made phosphazenes as auxiliary bases for nearly every purpose.

2.2.1 Basicity enhancement by hydrogen bonding

While several useful methods are known to increase the basicity of phosphazene bases, the group of Sundermeyer studied the stabilizing effect of hydrogen bonding in detail and thereby designed the first phosphazene superbase **TDMPP** (**35**) with an increased basicity due to multiple intramolecular hydrogen bonding (Scheme 15).[122]

Phosphazene **35** is obtained as its corresponding phosphazenium tetrafluoroborate by the reaction of 3-dimethylamino-1-propylamine with PCl_5 and subsequent salt metathesis reaction in 68 % yield. The following deprotonation with KO*t*Bu proceeds nearly quantitatively (98 %).

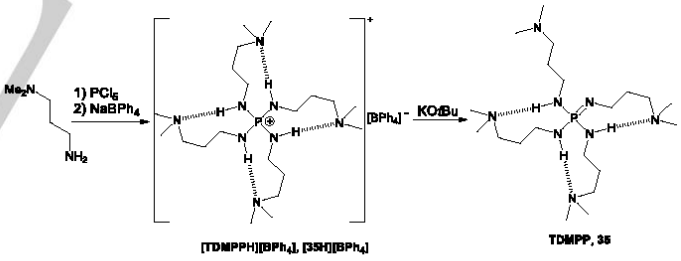

Scheme 15. Synthesis of **TDMPP** (**35**).

X-ray crystallographic analyses revealed shorter and thus stronger hydrogen bonds within the protonated base **[35H]$^+$** with N-(H)···N distances of 296 pm, compared to free **35** with distances of 300 to 305 pm.[122]

Due to multiple intramolecular hydrogen bonding, **35** exhibits a basicity of $^{MeCN}pK_{BH+}$ = 30.4, which is enhanced by up to 2.9 and 1.5 orders of magnitude relative to the presently known monophosphazenes $(Me_2N)_3P{=}NMe$ and $[(H_2C)_4N]_3P{=}NEt$.[17,122]

2.2.2 Proton sponges derived from phosphazenes

The combination of Alders proton sponge 1,8-bis(dimethylamino)naphthalene (**DMAN**)[75,123] with superbasic

phosphazenyl fragments constitute the class of phosphazene proton sponges (Scheme 16).[124–128]

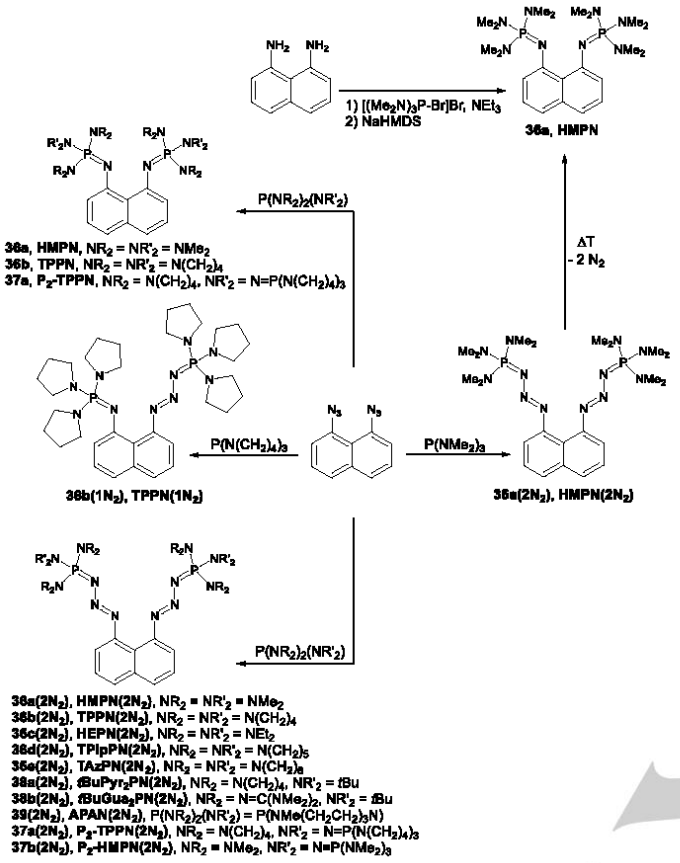

Scheme 16. Phosphazenyl and phosphazide proton sponges.

Sundermeyer's prototypical **HMPN** (1,8-bis(hexamethyltriaminophosphazenyl)naphthalene, **36a**) published in 2005 is accessible via Kirsanov reaction with subsequent deprotonation (43 %, Scheme 16).[124–126,128] **HMPN** (**36a**) has a proton affinity of PA = 274 kcal/mol and a $^{MeCN}pK_{BH+}$ value of 29.9, and is thus 12 orders of magnitude more basic than **DMAN** and 4 orders more basic than **TMGN** (1,8-bis(tetramethylguanidyl)naphthalene).[124,129] Since the success of Kirsanov type reactions is limited for sterically demanding groups, the pyrrolidine-derivative **TPPN** (**36b**) and its higher homologue **P$_2$-TPPN** (**37a**) are only viable via Staudinger reactions starting from 1,8-bis(diazido)naphthalene. The proton pincer ligands **36b** and **37a** reach extremely high $^{MeCN}pK_{BH+}$ values of 32.3 and 42.1, respectively,[125,126] whereas a significant nucleophilicity of phosphazenyl proton sponges was observed in the reaction with ethyl iodide. While in case of **37a** complete protonation in a dehydrohalogenation reaction is observed, for the less bulky proton sponges **36a** and **36b** alkylation is favored over elimination reactions. This is also the case for alkyl substituted biphosphazenyl proton sponges.[128] The corresponding mono substituted naphthalene derivatives were shown to be significantly less basic, which is due to the loss of stabilizing intramolecular hydrogen bonding in the protonated form.[124,125]

Interestingly, Sundermeyer *et al.* observed a significant stability of biphosphazides as intermediates in the Staudinger reactions and obtained the respective compounds in moderate to high yields (Scheme 16).[110,126] By definite reaction conditions also monophosphazide **36b(1N$_2$)** could be prepared (Scheme 16).

Except compounds **36a(2N$_2$)**, **36b(2N$_2$)** and **37a(2N$_2$)**, which feature relatively small NR_2-groups and thus are prone to thermally induced nitrogen extrusion to yield the phosphazenes **36a-b** and **37a**, all other biphosphazides are highly stable even at elevated temperatures, for which the bulky substituents were made responsible.[126]

Due to their high nucleophilicity, the proton sponges do not only act as proton acceptors, but also readily form pincer complexes with Lewis acids, such as $AlMe_3$ and $GaMe_3$.[128]

2.2.3 Chiral phosphazenes

The employment of chiral organocatalysts bearing strongly basic phosphazene moieties for the activation of only weakly acidic pronucleophiles has been introduced for the first time in the asymmetric Henry reaction by Ooi *et al.* in 2007.[130–132]

The ready availability of chiral phosphazenes[133] and their outstanding catalytic activity in enantioselective sulfa-Michael addition reactions,[134] Mannich-type reactions,[135] cycloaddition reactions,[136,137] hydrophosphinylations[138,139] as well as 1,2- and 1-4-addition reactions[140] among others has moved them into the focus of current interest. Rigid chiral iminophosphoranes are excellent reagents for challenging enantioselective reactions, as well.[141] As an illustration the chiral iminophosphoranes **40** of Dixon,[134,140,142,143] spiro-phosphazenes **41** of Ooi[130,144] and chiral guanidinophosphazenes **44** and **45** of Terada[135–139,145,146,147,148] are depicted in Scheme 17, but will not be discussed in more detail, since latest advances and achievements has been reviewed recently.[131,132,149] The chiral phosphazenes **43** and **42** of Suna[150] and Anders[151] are also included (Scheme 17).

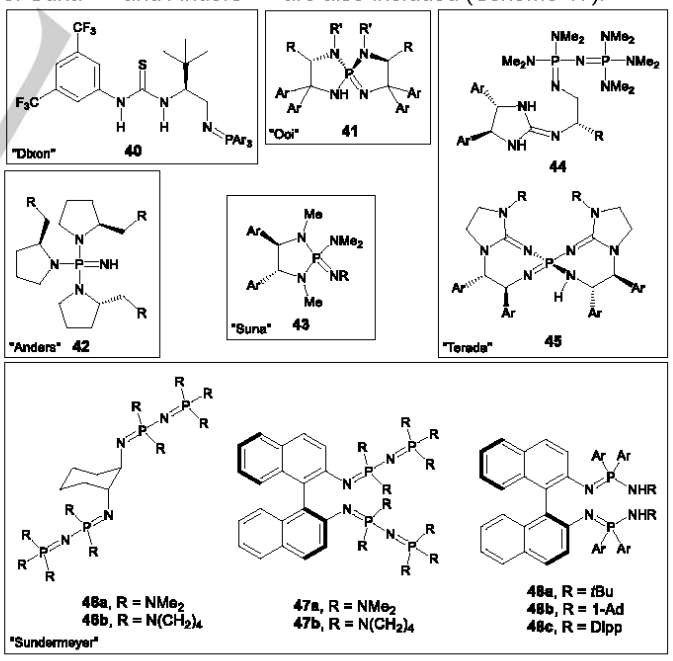

Scheme 17. Chiral phosphazene bases.

The basicity of chiral phosphazenes can be increased by the homologization strategy of Schwesinger,[12,15] which was realized by Terada with the cooperative binary base catalyst **44**

consisting of a biphosphazenyl unit bound to a guanidyl substituent (Scheme 17), and which has proven beneficial for enantioselective direct Mannich-type reactions.[146,148]

Sundermeyer *et al.* focused on two biphosphazene units connected via binaphthyl[127] or cyclohexyl[152] backbones in **47a-b** and **46a-b**. Whereas biphosphazenes **47a-b** can be regarded as proton sponge derivatives, the cyclohexyl derivatives **46a-b** cannot be considered as such due to the lack of N-electron pair repulsion.[152]

Chiral phosphazene bases are accessible via prominent methods as Staudinger reactions of phosphines with chiral azide compounds,[142] via Kirsanov type reactions,[127,152] via condensation of chiral amines,[151] diamines[130] or guanidines[145] with PCl_5, and combinations thereof.[150]

2.2.4 Carbon superbases containing phosphazenyl groups

As already mentioned, phosphorus ylides behave like phosphonium-substituted carbanions,[44–47] and are thus significantly more basic than their corresponding phosphanimine analogues.[18,42] Recent achievements in carbodiphosphorane chemistry have been summarized by Alcarazo[53] and will not be discussed in more detail here. However, it should be briefly noted, that Gessner *et al.* recently explored a Lewis basic diamino-substituted carbodiphosphorane, with strong C-donor properties, and preferentially binds to neutral metals and main group elements via the carbon center instead of the amino groups.[153]

In order to design a Brønsted carbon superbase that overcomes the basicity of Schwesinger's commercially available tetraphosphazenes **18** and additionally features a significantly decreased molecular weight, Sundermeyer and co-workers focused on the classical proton sponge concept and brought the basicity centers of phosphonium ylides in spatial proximity.[154,155]

The nucleophilic substitution of 1,8-bis(bromomethyl)naphthalene with $P(NMe_2)_3$ and the subsequent deprotonation with benzyl potassium afforded the desired carbon-based proton sponge **MHPN** (**49**) in a 84 % yield (Scheme 18). NMR spectroscopic titration experiments reavealed a significantly enhanced basicity of **49** ($^{MeCN}pK_{BH+}$ = 33.3) relative to the biphosphazenyl proton sponge **HMPN** (**36a**, $^{MeCN}pK_{BH+}$ = 29.9),[154,155] although no rigid hydrogen bond interaction is found in **[49H]$^+$**. The "acidic" proton bound at carbon undergoes a rather rapid exchange or "proton hopping" between both basicity centers, which is accompanied by an increased kinetic barrier relative to classical proton sponges. Thus, definite CH and CH_2 resonances can be observed by ^{1}H NMR spectroscopy and X-ray diffraction confirms predicted different structures of $CP(NMe_2)_3$ groups in **[49H]$^+$**.

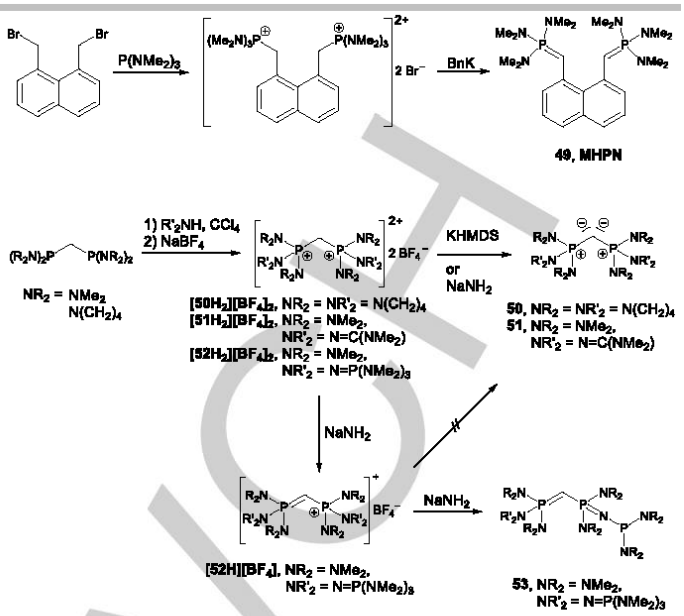

Scheme 18. Syntheses of carbodiphosphoranes.

Since no beneficial basicity increase by interaction of two carbon basicity centers in spatial proximity was proven, the direct comparison of ylide **49** with ylide $Me_2C{=}P(NMe_2)_3$ ($^{MeCN}pK_{BH+}$ = 37.7)[18] suggests a possibly larger increase by implementation of strongly electron donating substituents at the carbon basicity center. For this purpose, Sundermeyer *et al.* developed a series of carbodiphosphorane derivatives **50**-**52** containing $-P(NR_2)_2(NR'_2)$ groups at carbon, whereas NR'_2 represents already awarded phosphazenyl , tetramethylguanidyl (TMG) or simple amino groups.[156] Starting from readily available bis(dimethylaminophosphino)methane or the respective pyrrolidyl derivative, oxidative amination with CCl_4 afforded the desired dicationic species in all cases (Scheme 18), which were transferred into their air and water stable HBF_4 salts according to described literature procedures. The neutral carbodiphosphoranes **50** ($^{THF}pK_{BH+}$ = 30.1 - 32.9) and **51** ($^{THF}pK_{BH+}$ = 35.8) were liberated via twofold deprotonation with KHMDS or $NaNH_2$ in yields of 60 % and 70 %, respectively.[156] Guanidyl derivative **51** is the strongest carbon base presently known and surpasses ylide $H_2C{=}P(2,4,6\text{-}(MeO)_3\text{-}C_6H_2)_2Ph$ with a $^{THF}pK_{BH+}$ value of 33.5.[18]

The higher dicationic phosphazenyl homologue **[52H$_2$]$^{2+}$** can be efficiently transferred into the mono cation **[52H]$^+$** by treatment with $NaNH_2$ (69 %, Scheme 18). A second deprotonation step at the carbon atom, however, does not occur. In contrast to the desired carbodiphosphorane **52** (calculated $^{THF}pK_{BH+}$ = 39.1), Sundermeyer obtained the phosphazenylphosphine **53** as the selective product via elimination of a peripheric dimethylamino group, by which he clearly demonstrated a potential basicity limit for dimethylaminophosphazene-incorporated superbases.[156]

2.2.5 Non-coordinated anions with phosphazene bases

Most commonly, phosphazene bases are required for the deprotonation of only weakly acidic pronucleophiles, as the trifluoromethane building block in nucleophilic

trifluoromethylations.[157,158,159] Moreover, the low Lewis-acidity of the corresponding phosphazenium cation renders the formation of non-coordinated "naked" anions possible, which feature a drastically increased reactivity. Combinations of phosphazene bases with protic reactants are thus frequently used as metal-free promotors in anionic polymerizations,[160] as of γ-butyrolactone,[161] methyl methacrylate,[162] cyclosiloxanes[163,164] or in copolymerizations of epoxides.[165]

Clearly, the nature of the respective non-coordinated anionic species is of broad interest for the elucidation of structural features and the stability of intermediates, as well as an insight in conceivable reaction pathways, as prerequisites for an improved fabrication of products and reliable quantum chemical predictions.

Recently, the first hydroxide trihydrate devoid of significant cation-anion interactions was obtained and structurally elucidated by deprotonation of four equivalents of water with the perethyl tetraphosphazene base **18c** (Scheme 19).[157,159]

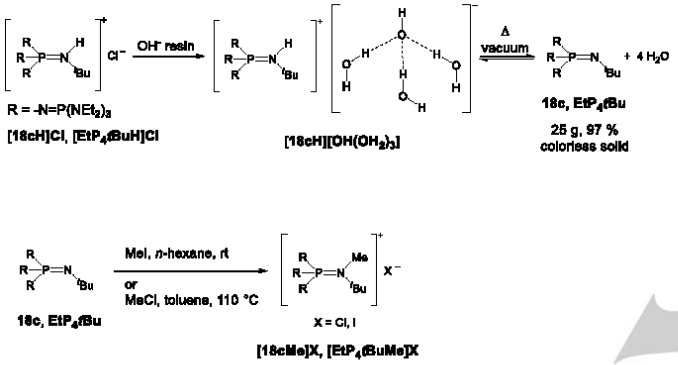

Scheme 19. Liberation of tetraphosphazene **18c** via its hydroxide hydrate salt and ensured methylation.[157,159]

Normally, in mixtures consisting of free and protonated phosphazene base **18c** a high kinetic proton exchange barrier is evidenced at ambient temperature by the presence of two separated signal sets with characteristic $^2J_{PP}$ couplings of 29 Hz and 70 Hz as observable in Figure 3. In keeping with this, the ^{31}P NMR spectroscopic titration of the free base **18c** with water in chlorobenzene displays a single signal set with a continuous increasing $^2J_{PP}$ coupling from 29 to 70 Hz with increasing amounts of water (Figure 2).[157,159] Addition of four equivalents of water afforded the hydroxide trihydrate anion as a saline phosphazenium salt, showing the characteristic $^2J_{PP}$ coupling of 70 Hz, whereas the $^2J_{PH}$ coupling constant of 8 Hz is only resolved in the presence of an excess of water.

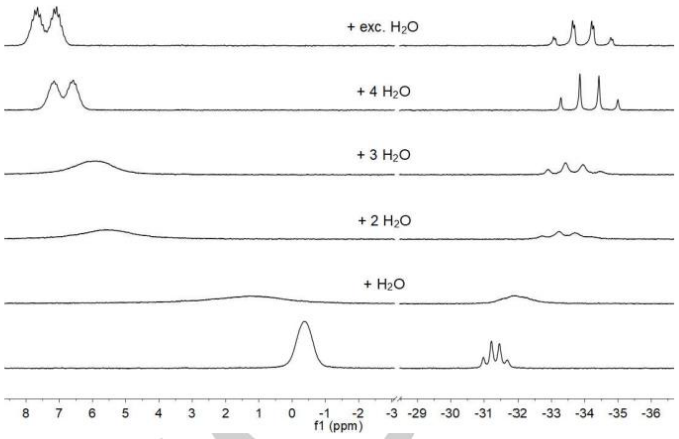

Figure 2. ^{31}P NMR spectroscopic titration of **EtP$_4$** with different amounts of water in chlorobenzene. Lock with acetone-d_6 in a capillary. Bottom: free base; top: with an excess of water.[157,159]

The ^{31}P NMR titration of the free tetraphosphazene **18c** with *tert*-butanol surprisingly delivers the two familiar signal sets for the free and the protonated base (Figure 3), which reflects a significantly impeded proton exchange in comparison to the hydroxide salt.

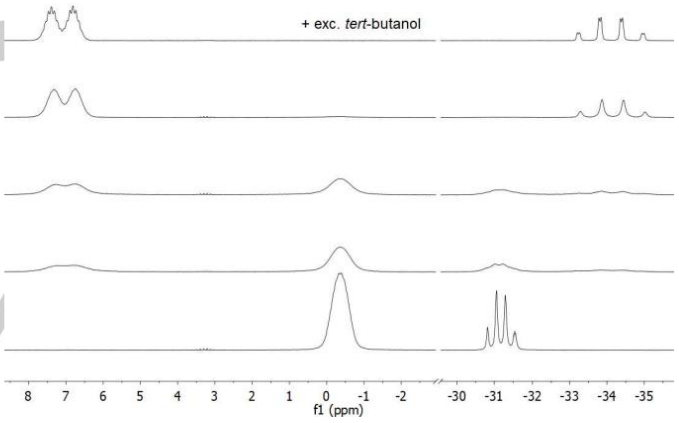

Figure 3. ^{31}P NMR spectroscopic titration of **EtP$_4$** with *tert*-butanol in chlorobenzene. Lock with acetone-d_6 in a capillary. Bottom: free base; top: with an excess of *tert*-butanol.

Employment of three equivalents of the alcohol leads to complete protonation of **18c** and suggests the formation of a *tert*-butanolate anion with two *tert*-butanol solvate molecules. This prediction is confirmed by X-ray analysis of single crystals of **[18cH][*t*BuO(HO*t*Bu)$_2$]**[166] obtained from a cooled *n*-hexane reaction mixture (Figure 4).

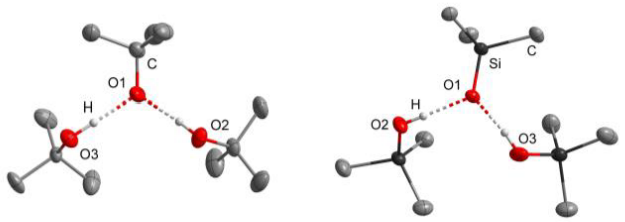

Figure 4. Anions of the phosphazenium salts **[18cH][Me$_3$SiO(HOSiMe$_3$)$_2$]** and **[18cH][*t*BuO(HO*t*Bu)$_2$]**.[167,168] The cation **[18cH]$^+$** is not depicted.

The O1-O2 and O1-O3 distances in the anion amount to 258.2(2) and 253.0(2) pm, respectively, and are similar to those observed in the trimethylsilanolate anion [Me$_3$SiO(HOSiMe$_3$)$_2$]$^-$ previously reported by us (Figure 4).[167,168] Solid **[18cH][*t*BuO(HO*t*Bu)$_2$]** decomposes rapidly upon warming to room temperature and reformation of the free base **18c** is evident by ^{31}P NMR spectroscopy.

Generally solvated anions [OH(OH$_2$)$_3$]$^-$, [*t*BuO(HO*t*Bu)$_2$]$^-$ and [Me$_3$SiO(HOSiMe$_3$)$_2$]$^-$ are prone to loss of the solvate shell, with concomitant deprotonation of their phosphazenium cations **[18cH]$^+$**.[157,159,167,168]

As the most common way for the deprotonation of phosphazenium salts involves hazardous and self-igniting amides in liquid ammonia,[12,15,63,157,159,167,168] which also causes serious waste disposal problems, alternative strategies for the liberation of **18c** and other tetraphosphazenes **18** from their hydrochlorides are urgently required.

For this purpose the salt metathesis reaction of **[18cH]Cl** with a strongly basic OH$^-$ anion exchange resin and the subsequent thermolysis of the obtained phosphazenium hydroxide hydrate have been proven beneficial and affords the free base in high quantity and yield (97 %, Scheme 19).[157,159]

In order to trap a naked hydroxide anion, the "acidic" iminium functionality of **[18cH]$^+$** needs protection. The substitution of the proton by a methyl group in **[18cMe]$^+$** seems promising and can be incorporated by alkylation of base **18c** with methyl halides (Scheme 19).[63] While methylation of **18c** is performed quantitatively with MeI in *n*-hexane at ambient temperature, the analogous reaction with MeCl solely afforded the protonated base under the same conditions, however, methylation is favored over protonation in toluene at elevated temperatures.

The methylated base **[18cMe]$^+$** features a characteristic quartet of quartet splitting with $^2J_{PP}$ and $^3J_{PH}$ couplings of 77 and 14 Hz. The described procedure for the generation a phosphazenium hydroxide salt by means of a basic anion exchange resin was applied. The subsequent drying in a high vacuum at ambient temperature resulted in the deterioration of the phosphazenium cation **[18cMe]$^+$** and delivered a mixture of products. Multinuclear NMR spectroscopy suggests the decomposition of the *tert*-butyl group of the iminium functionality as the main decomposition pathway. Thus, the generation of a naked hydroxide anion in the presence of peralkylated phosphazenium cation **[18cMe]$^+$** seems to exceed the limits of the respective protocol.

Phosphazenium hydroxides, which can be employed as polymerization initiator for cyclosiloxanes,[160,164] react readily with siloxane species in a stoichiometric manner. We recently showed, that in the presence of weakly coordinating phosphazenium ion **[18cH]$^+$** an insertion of the OH$^-$ anion into a silicon-oxygen bond furnished silanol-silanolate anions as products, that are devoid of significant cation-anion interactions.[167–169] Whereas the reaction with hexamethyldisiloxane delivers the [Me$_3$SiO(HOSiMe$_3$)$_2$]$^-$ anion, the analogous reaction with hexamethyl or hexaphenyl cyclotrisiloxanes leads to cyclic [(R'$_2$SiO)$_3$OH]$^-$ ([D$_3$OH]$^-$) silanol-silanolates featuring strong intramolecular hydrogen bonds (O-O separation in the range of 242.8(2) to 242.9(2) pm).[167,168]

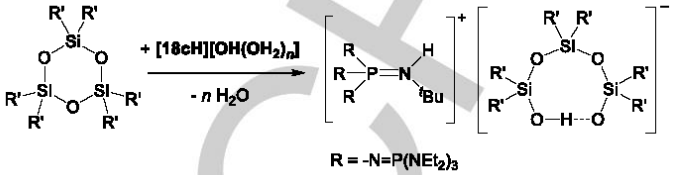

Scheme 20. Syntheses of [D$_3$OH]$^-$ anions.[167,168]

Furthermore we showed, that hydrogen bonding patterns in silanolate anions strongly depend on the employed counterions, as cyclic moieties are favored in the presence of bulky cations, whereas in the presence of small tetramethylammonium cations intermolecular hydrogen bonds are predestinated, leading to indefinite strands of [D$_3$OH]$^-$ anions.[169] [10.1002/chem.202004236]

Besides the discovery of isolated silanol-silanolate hydrogen bridges devoid of cation-anion interactions,[167,168] [10.1002/chem.202004236] the nature and characteristics of non-coordinated phenolate anions and their hydrogen bonded adducts were elucidated with the aid of pyrrolidine monophosphazene **pyrrP$_1$*t*Bu** (**15b**) and tetraphosphazene **18c**.[170] Interestingly, the deprotonation of the acidic phenol H$_5$C$_6$-OH molecule (pK_{BH+} = 9.98)[171] with **15b** solely afforded the hydrogen bonded anionic phenol-phenolate moiety with an additional cation-anion interaction.

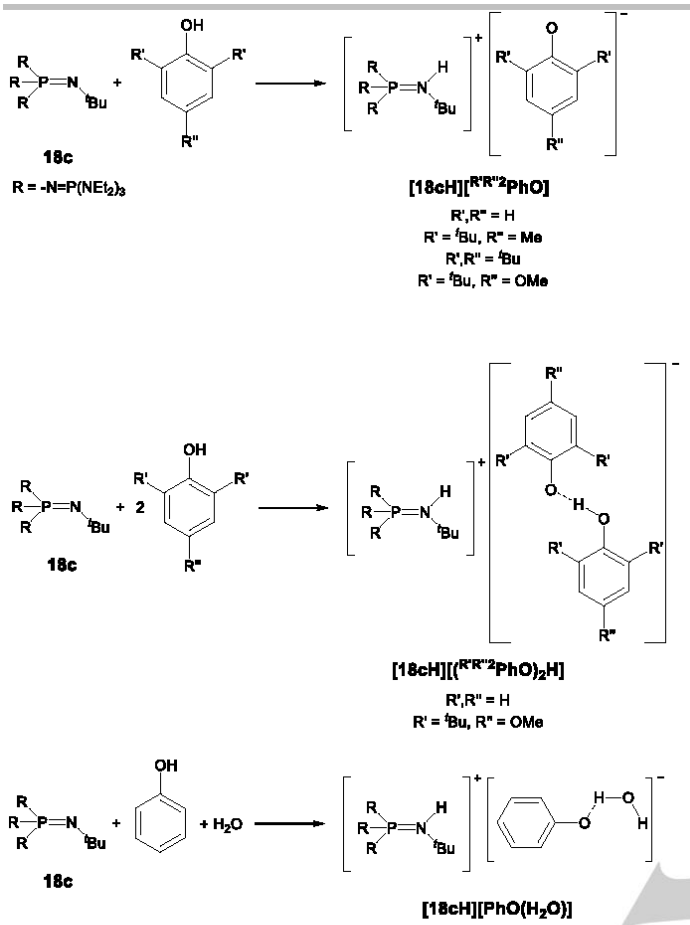

Scheme 21. Syntheses of non-coordinated phenolate anions and their adducts employing **18c**.[170]

In contrast to that, the more powerful tetraphosphazene **18c** allows the complete deprotonation and the realization of the first non-coordinated phenolate $[H_5C_6\text{-}O]^-$ anion (Scheme 21).[170] Moreover, several electron rich phenolates were quantitatively synthesized and show comparable reducing properties as zinc with redox potentials of up to -0.72 V vs. SCE. Those phosphazenium phenolates found application in activating the inert and most effective greenhouse gas SF_6 to produce pentafluorosulfanide $[SF_5]^-$ and fluoride salts.[170] Moreover, sterically encumbered phenolates are excellent reducing agents for the syntheses of radical anion salts featuring weakly coordinating phosphazenium cation **[18cH]$^+$**, which represents a main subject of our current interest.

Beyond that, neutral phosphazene **18c** render the selective design of hydrogen bonded phenol-phenolates or phenolate hydrates possible (Scheme 21), by which we were able to show the tremendous impact of hydrogen bonding on the redox properties of phenolate anions, which is especially important for mechanistic insights of the photosystem II.[170] Since reported redox potentials of phenolates were commonly obtained by deprotonation with alkylammonium hydroxides,[172] the effect of hydrogen bonded water molecules was neglected. We clearly demonstrated the hydrogen bond induced oxidation potential shifts of non-coordinated phenolate $[PhO]^-$ (E_{Ox} = -0.12(1) V vs SCE) relative to its adducts $[PhO(H_2O)]^-$ (E_{Ox} = -0.04(1) V vs SCE) and $[PhO(HOPh)]^-$ (E_{Ox} = +0.22(1) V vs. SCE) and verified the results with quantum chemical calculations at the BP86/6-311+g(3df,2p) level of theory.[170]

3. Conclusions and outlook

In this mini review, we have given an account on the most recent developments of the chemistry of electron-rich phosphines and phosphazenes. Strategies to increase the Lewis and Brønsted basicity of electron-rich phosphines are based upon the introduction of strongly π-donating substituents. The phosphazenyl groups introduced by Schwesinger are particularly suitable for this purpose, as they exert a considerable influence on the electronic structure of the central atom via the homologization strategy. The corresponding phosphazenyl phosphines (PAPs) can even surpass the basicity of Schwesinger's commercially available tetraphosphazene bases. Furthermore, incorporation of NHC-based imidazolin-2-ylideneamino groups have also proven beneficial. The known NHC backbones allow efficient fine-tuning of the electronic and steric properties of the corresponding imidazolin-2-ylideneaminophosphines (IAPs). Similar donating abilities have also been demonstrated for pyridinyliden-2-amino groups in pyridinyliden-2-amino phosphines (PyAPs), which are extremely cheap alternatives to IAPs. Ylidyl groups in ylidylphosphines (YPhos) are also suitable for enhancing the Lewis basicity and to generate efficient transition metal catalysts.

Since Schwesinger's homologization concept for increasing the basicity of phosphazenes has already reached its limits, there are versatile approaches to increase the basicity by steric effects. For example, it has been shown that the basicity of phosphazenes is significantly increased by the formation of intramolecular hydrogen bonds in its protonated form. It is also possible to combine the structure of proton sponges with electron-donating phosphazenyl groups, thus exceeding the basicity of the conventional proton sponge 1,8-bis(dimethylamino)naphthalene by several orders of magnitude. The inclusion of chiral substituents at phosphorus or the attachment of phosphazene units to chiral backbones have enabled the preparation of a variety of chiral phosphazenes, allowing the catalytic and stereoselective conversion of weakly acidic pronucleophiles.

In contrast to superbasic phosphines, which tend to add electrophiles and are therefore used for transition metal-catalyzed coupling reactions, sterically encumbered tetraphosphazene bases offer the possibility to deprotonate weakly acidic compounds and, due to their low tendency for coordination, allow the study of the corresponding non-coordinated anions.

Acknowledgements

We thank Prof. Dr. Lothar Weber and Dr. Julia Bader for helpful discussions.

Keywords: Phosphine • Phosphazene • superbase • electron-rich • naked anion

[1] T. Ishikawa, *Superbases for Organic Synthesis. Guanidines, amidines and phosphazenes and related organocatalysts*, John Wiley & Sons, Ltd, Chichester, UK, **2009**.

[2] M. Wiesemann, B. Hoge, *Chem. Eur. J.* **2018**, *24*, 16457.

[3] M. J. Frisch, G. W. Trucks, H. B. Schlegel, G. E. Scuseria, M. A. Robb, J. R. Cheeseman, G. Scalmani, V. Barone, B. Mennucci, G. A. Petersson et al., *Gaussian 09*, *Revision D.01*, Gaussian, Inc., Wallingford CT, **2013**.

[4] C. A. Tolman, *Chem. Rev.* **1977**, *77*, 313.

[5] M. A. Wünsche, P. Mehlmann, T. Witteler, F. Buß, P. Rathmann, F. Dielmann, *Angew. Chem. Int. Ed. Engl.* **2015**, *54*, 11857.

[6] a) N. Allefeld, B. Neumann, H.-G. Stammler, N. Ignat'ev, B. Hoge, *Chem. Eur. J.* **2015**, *21*, 12326; b) M. F. Ernst, D. M. Roddick, *Inorg. Chem.* **1989**, *28*, 1624; c) M. M. Rahman, H. Y. Liu, K. Eriks, A. Prock, W. P. Giering, *Organometallics* **1989**, *8*, 1; d) S. A. Hayes, R. J. F. Berger, B. Neumann, N. W. Mitzel, J. Bader, B. Hoge, *Dalton Trans.* **2010**, *39*, 5630.

[7] H. G. Ang, Y. M. Cai, L. L. Koh, W. L. Kwik, *J. Chem. Soc., Chem. Commun.* **1991**, *3*, 850.

[8] M. A. Wünsche, P. Mehlmann, T. Witteler, F. Buß, P. Rathmann, F. Dielmann, *Angew. Chem.* **2015**, *127*, 12024.

[9] a) J. A. Mata, F. E. Hahn, E. Peris, *Chem. Sci.* **2014**, *5*, 1723; b) E. Peris, *Chem. Rev.* **2018**, *118*, 9988.

[10] K. G. Moloy, J. L. Petersen, *J. Am. Chem. Soc.* **1995**, *117*, 7696.

[11] M. L. Clarke, D. J. Cole-Hamilton, A. M. Z. Slawin, J. D. Woollins, *Chem. Commun.* **2000**, 2065.

[12] R. Schwesinger, H. Schlemper, *Angew. Chem.* **1987**, *99*, 1212.

[13] R. Schwesinger, *Chimia* **1985**, *39*, 269.

[14] E. D. Raczyńska, J.-F. Gal, P.-C. Maria, *Chem. Rev.* **2016**, *116*, 13454.

[15] R. Schwesinger, H. Schlemper, *Angew. Chem. Int. Ed. Engl.* **1987**, *26*, 1167-1169.

[16] a) B. Kovacević, Z. B. Maksić, *Chem. Commun.* **2006**, 1524; b) I. Leito, I. A. Koppel, I. Koppel, K. Kaupmees, S. Tshepelevitsh, J. Saame, *Angew. Chem. Int. Ed. Engl.* **2015**, *54*, 9262; c) Z. B. Maksić, B. Kovačević, R. Vianello, *Chem. Rev.* **2012**, *112*, 5240; d) T. Allman, R. G. Goel, *Can. J. Chem.* **1982**, *60*, 716; e) I. Kaljurand, I. A. Koppel, A. Kütt, E.-I. Rõõm, T. Rodima, I. Koppel, M. Mishima, I. Leito, *J. Phys. Chem. A* **2007**, *111*, 1245; f) I. Leito, I. A. Koppel, I. Koppel, K. Kaupmees, S. Tshepelevitsh, J. Saame, *Angew. Chem.* **2015**, *127*, 9394.

[17] I. Kaljurand, J. Saame, T. Rodima, I. Koppel, I. A. Koppel, J. F. Kögel, J. Sundermeyer, U. Köhn, M. P. Coles, I. Leito, *J. Phys. Chem. A* **2016**, *120*, 2591.

[18] J. Saame, T. Rodima, S. Tshepelevitsh, A. Kutt, I. Kaljurand, T. Haljasorg, I. A. Koppel, I. Leito, *J. Org. Chem.* **2016**, *81*, 7349.

[19] a) H. Staudinger, E. Hauser, *HCA* **1921**, *4*, 861; b) H. Staudinger, J. Meyer, *HCA* **1919**, *2*, 635.

[20] P. Haasemann, J. Goubeau, *Z. Anorg. Allg. Chem.* **1974**, *408*, 293.

[21] a) Y.G. Gololobov, I. N. Zhmurova, L. F. Kasukhin, *Tetrahedron* **1981**, *37*, 437; b) Y. G. Gololobov, L. F. Kasukhin, *Tetrahedron* **1992**, *48*, 1353.

[22] L. Birkofer, S. M. Kim, *Chem. Ber.* **1964**, *97*, 2100.

[23] O. Schlak, W. Stadelmann, O. Stelzer, R. Schmutzler, *Z. Anorg. Allg. Chem.* **1976**, *419*, 275.

[24] a) S. Bräse, C. Gil, K. Knepper, V. Zimmermann, *Angew. Chem.* **2005**, *117*, 5320; b) S. Bräse, C. Gil, K. Knepper, V. Zimmermann, *Angew. Chem. Int. Ed.* **2005**, *44*, 5188.

[25] a) A. V. Kirsanov, *Izv. Akad. Nauk SSSR, Ser. Khim.* **1950**, 426; b) A. V. Kirsanov, *Zh. Obshch. Khim.* **1952**, *88*.

[26] R. Appel, A. Hauss, *Angew. Chem.* **1959**, *71*, 626.

[27] R. Appel, A. Hauss, *Chem. Ber.* **1960**, *93*, 405.

[28] H. H. Sisler, A. Sarkis, H. S. Ahuja, R. J. Drago, N. L. Smith, *J. Am. Chem. Soc.* **1959**, *81*, 2982.

[29] W. Wolfsberger, *Z. Naturforsch., B: Chem. Sci.* **1978**, *33*, 1452.

[30] H. Schmidbaur, G. Jonas, *Angew. Chem. Int. Ed. Engl.* **1967**, *6*, 449.

[31] H. Schmidbaur, G. Jonas, *Angew. Chem.* **1967**, *79*, 413.

[32] H. Schmidbaur, G. Jonas, *Chem. Ber.* **1967**, *100*, 1120.

[33] H. Schmidbaur, G. Jonas, *Chem. Ber.* **1968**, *101*, 1271.

[34] a) H. Schmidbaur, G. Kuhr, U. Krüger, *Angew. Chem.* **1965**, *77*, 866; b) H. Schmidbaur, G. Kuhr, U. Krüger, *Angew. Chem. Int. Ed. Engl.* **1965**, *4*, 877; c) H. Schmidbaur, W. Wolfsberger, *Chem. Ber.* **1967**, *100*, 1000; d) H. Schmidbaur, W. Wolfsberger, H. Kröner, *Chem. Ber.* **1967**, *100*, 1023.

[35] K. Issleib, M. Lischewski, *Synth. React. Inorg. Met.-Org. Chem.* **1973**, *3*, 255.

[36] W. Wolfsberger, H. H. Pickel, H. Schmidbaur, *Z. Naturforsch., B: Chem. Sci.* **1971**, *26*, 979.

[37] R. Appel, A. Hauss, *Z. Anorg. Allg. Chem.* **1961**, *311*, 290.

[38] a) J. K. Ruff, W. J. Schlientz, R. E. Dessy, J. M. Malm, G. R. Dobson, M. N. Memering in *Inorganic Syntheses*, John Wiley & Sons, Ltd, **2007**, pp. 84–90; b) C. Bolli, J. Gellhaar, C. Jenne, M. Keßler, H. Scherer, H. Seeger, R. Uzun, *Dalton Trans.* **2014**, *43*, 4326; c) R. Eujen, B. Hoge, D. J. Brauer, *Inorg. Chem.* **1997**, *36*, 3160; d) L. Mann, E. Hornberger, S. Steinhauer, S. Riedel, *Chem. Eur. J.* **2018**, *24*, 3902.

[39] H. Staudinger, J. Meyer, *Helv. Chim. Acta* **1919**, *2*, 619.

[40] a) G. Wittig, G. Geissler, *Justus Liebigs Ann. Chem.* **1953**, *580*, 44; b) B. E. Maryanoff, A. B. Reitz, *Chem. Rev.* **1989**, *89*, 863.

[41] a) A. Maercker, *The Wittig Reaction. Organic Reactions*, Wiley, New York, **1965**; b) P. A. Byrne, D. G. Gilheany, *Chem. Soc. Rev.* **2013**, *42*, 6670.

[42] K. Issleib, R. Lindner, *Justus Liebigs Ann. Chem.* **1966**, *699*, 40.

[43] a) H. Schmidbaur, A. Schier, S. Lauteschlaeger, J. Riede, G. Mueller, *Organometallics* **1984**, *3*, 1906; b) H. Schmidbaur, C. Paschalidis, G. Reber, G. Müller, *Chem. Ber.* **1988**, *121*, 1241.

[44] H. Lischka, *J. Am. Chem. Soc.* **1977**, *99*, 353.

[45] H. Schmidbaur, *Angew. Chem. Int. Ed. Engl.* **1983**, *22*, 907.

[46] L. T. Scharf, D. M. Andrada, G. Frenking, V. H. Gessner, *Chem. Eur. J.* **2017**, *23*, 4422.

[47] H. Schmidbaur, *Angew. Chem.* **1983**, *95*, 980.

[48] a) H. Schmidbaur, U. Deschler, B. Milewski-Mahrla, *Chem. Ber.* **1983**, *116*, 1393; b) R. Appel, K. Geisler, H.-F. Schöler, *Chem. Ber.* **1979**, *112*, 648.

[49] K. Issleib, H. P. Abicht, *J. Prakt. Chem.* **1970**, *312*, 456.

[50] F. Ramirez, N. B. Desai, B. Hansen, N. McKelvie, *J. Am. Chem. Soc.* **1961**, *83*, 3539.

[51] R. Appel, G. Erbelding, *Tetrahedron Lett.* **1978**, *19*, 2689.

[52] a) H. Schmidbaur, O. Gasser, *Angew. Chem. Int. Ed. Engl.* **1976**, *15*, 502; b) H. Schmidbaur, O. Gasser, *Angew. Chem.* **1976**, *88*, 542.

[53] M. Alcarazo in *Structure and bonding* (Ed.: V. H. Gessner), Springer International Publishing, Cham, **2018**, pp. 25–50.

[54] a) J. C. Clardy, D. S. Milbrath, J. G. Verkade, *J. Am. Chem. Soc.* **1977**, *99*, 631; b) J. C. Clardy, D. S. Milbrath, J. P. Springer, J. G. Verkade, *J. Am. Chem. Soc.* **1976**, *98*, 623.

[55] D. S. Milbrath, J. G. Verkade, *J. Am. Chem. Soc.* **1977**, *99*, 6607.

[56] a) C. Lensink, S. K. Xi, L. M. Daniels, J. G. Verkade, *J. Am. Chem. Soc.* **1989**, *111*, 3478; b) M. A. H. Laramay, J. G. Verkade, *J. Am. Chem. Soc.* **1990**, *112*, 9421.

[57] J. G. Verkade in *Topics in current chemistry*, *Vol. 223* (Eds.: A. de Meijere, H. Kessler, S. V. Ley, J. Thiem, F. Vögtle, K. N. Houk, J.-M. Lehn, S. L. Schreiber, B. M. Trost, H. Yamamoto et al.), Springer Berlin Heidelberg, Berlin, Heidelberg, **2003**, pp. 1–44.

[58] T. L. Windus, M. W. Schmidt, M. S. Gordon, *J. Am. Chem. Soc.* **1994**, *116*, 11449.

[59] H. Schmidt, C. Lensink, S. K. Xi, J. G. Verkade, *Z. Anorg. Allg. Chem.* **1989**, *578*, 75.

[60] a) J.-S. Tang, J. G. Verkade, *Tetrahedron Lett.* **1993**, *34*, 2903; b) A. E. Wróblewski, J. Pinkas, J. G. Verkade, *Main Group Chemistry* **1995**, *1*, 69.

[61] M. A. H. Laramay, J. G. Verkade, *Z. Anorg. Allg. Chem.* **1991**, *605*, 163.

[62] P. B. Kisanga, J. G. Verkade, R. Schwesinger, *J. Org. Chem.* **2000**, *65*, 5431.

[63] R. Schwesinger, H. Schlemper, C. Hasenfratz, J. Willaredt, T. Dambacher, T. Breuer, C. Ottaway, M. Fletschinger, J. Boele, H. Fritz et al., *Liebigs Ann.* **1996**, *1996*, 1055.

[64] A. de Meijere, H. Kessler, S. V. Ley, J. Thiem, F. Vögtle, K. N. Houk, J.-M. Lehn, S. L. Schreiber, B. M. Trost, H. Yamamoto et al. (Eds.) *Topics in current chemistry*, *Vol. 223*, Springer Berlin Heidelberg, Berlin, Heidelberg, **2003**.

[65] J.-S. Tang, J. G. Verkade, *Angew. Chem. Int. Ed. Engl.* **1993**, *32*, 896.

[66] J.-S. Tang, J. G. Verkade, *Angew. Chem.* **1993**, *105*, 934.

[67] J. Tang, J. G. Verkade, *J. Org. Chem.* **1994**, *59*, 7793.

[68] S. Arumugam, D. McLeod, J. G. Verkade, *J. Org. Chem.* **1998**, *63*, 3677.

[69] T. Mohan, S. Arumugam, T. Wang, R. A. Jacobson, J. G. Verkade, *Heteroatom Chem.* **1996**, *7*, 455.

[70] S. Arumugam, J. G. Verkade, *J. Org. Chem.* **1997**, *62*, 4827.

[71] P. B. Kisanga, P. Ilankumaran, B. M. Fetterly, J. G. Verkade, *J. Org. Chem.* **2002**, *67*, 3555.

[72] P. B. Kisanga, J. G. Verkade, *J. Org. Chem.* **2002**, *67*, 426.

[73] R. Schwesinger, M. Mißfeldt, K. Peters, H. G. von Schnering, *Angew. Chem.* **1987**, *99*, 1210.

[74] R. Schwesinger, *Angew. Chem. Int. Ed. Engl.* **1987**, *26*, 1164.

[75] R. W. Alder, *Chem. Rev.* **1989**, *89*, 1215.

[76] R. Schwesinger, M. Mißfeldt, K. Peters, H. G. von Schnering, *Angew. Chem. Int. Ed. Engl.* **1987**, *26*, 1165.

[77] R. Schwesinger, *Angew. Chem.* **1987**, *99*, 1209.

[78] a) R. Schwesinger, *Nachr. Chem. Tech. Lab.* **1990**, *38*, 1214; b) R. Schwesinger, C. Hasenfratz, H. Schlemper, L. Walz, E.-M. Peters, K. Peters, H.-G. von Schnering, *Angew. Chem. Int. Ed. Engl.* **1993**, *32*, 1361; c) R. Schwesinger, C. Hasenfratz, H. Schlemper, L. Walz, E.-M. Peters, K. Peters, H. G. von Schnering, *Angew. Chem.* **1993**, *105*, 1420.

[79] R. Schwesinger, J. Willaredt, H. Schlemper, M. Keller, D. Schmitt, H. Fritz, *Chem. Ber.* **1994**, *127*, 2435.

[80] R. Schwesinger, R. Link, P. Wenzl, S. Kossek, M. Keller, *Chem. Eur. J.* **2005**, *12*, 429.

[81] a) C. T. Womble, J. Kang, K. M. Hugar, G. W. Coates, S. Bernhard, K. J. T. Noonan, *Organometallics* **2017**, *36*, 4038; b) R. Schwesinger, R. Link, P. Wenzl, S. Kossek, M. Keller, *Chem. Eur. J.* **2006**, *12*, 429.

[82] R. Schwesinger, R. Link, P. Wenzl, S. Kossek, *Chem. Eur. J.* **2006**, *12*, 438.

[83] C. Palomo, M. Oiarbide, R. López, E. Gómez-Bengoa, *Chem. Commun.* **1998**, 2091.

[84] a) T. Pietzonka, D. Seebach, *Chem. Ber.* **1991**, *124*, 1837; b) M.-A. Courtemanche, M.-A. Légaré, É. Rochette, F.-G. Fontaine, *Chem. Commun.* **2015**, *51*, 6858.

[85] J. Tang, J. Dopke, J. G. Verkade, *J. Am. Chem. Soc.* **1993**, *115*, 5015.

[86] a) S. K. Xi, H. Schmidt, C. Lensink, S. Kim, D. Wintergrass, L. M. Daniels, R. A. Jacobson, J. G. Verkade, *Inorg. Chem.* **1990**, *29*, 2214; b) J. S. Tang, M. A. H. Laramay, V. Young, S. Ringrose, R. A. Jacobson, J. G. Verkade, *J. Am. Chem. Soc.* **1992**, *114*, 3129; c) J. C. Clardy, D. S. Milbrath, J. G. Verkade, *Inorg. Chem.* **1977**, *16*, 2135; d) J. S. Tang, J. G. Verkade, *J. Am. Chem. Soc.* **1993**, *115*, 1660.

[87] a) R. Schwesinger, R. Link, G. Thiele, H. Rotter, D. Honert, H.-H. Limbach, F. Männle, *Angew. Chem. Int. Ed. Engl.* **1991**, *30*, 1372; b) R. Schwesinger, R. Link, G. Thiele, H. Rotter, D. Honert, H.-H. Limbach, F. Männle, *Angew. Chem.* **1991**, *103*, 1376.

[88] a) J. Braun, C. Hasenfratz, R. Schwesinger, H.-H. Limbach, *Angew. Chem. Int. Ed. Engl.* **1994**, *33*, 2215; b) J. Braun, C. Hasenfratz, R. Schwesinger, H.-H. Limbach, *Angew. Chem.* **1994**, *106*, 2302.

[89] a) J.-E. Siewert, A. Schumann, M. Fischer, C. Schmidt, T. Taeufer, C. Hering-Junghans, *Dalton Trans.* **2020**, *49*, 12354; b) D. H. Valentine Jr., J. H. Hillhouse, *Synthesis* **2003**, *2003*, 2437; c) A. M. Spokoyny, C. D. Lewis, G. Teverovskiy, S. L. Buchwald, *Organometallics* **2012**, *31*, 8478; d) M. Kaaz, R. J. C. Locke, L. Merz, M. Benedikter, S. König, J. Bender, S. H. Schlindwein, M. Nieger, D. Gudat, *Eur. J. Inorg. Chem.* **2019**, *2019*, 1586; e) L. Chen, P. Ren, B. P. Carrow, *J. Am. Chem. Soc.* **2016**, *138*, 6392; f) D. A. Hoic, W. M. Davis, G. C. Fu, *J. Am. Chem. Soc.* **1996**, *118*, 8176.

[90] D. J. Durand, N. Fey, *Chem. Rev.* **2019**, *119*, 6561.

[91] P. Mehlmann, C. Mück-Lichtenfeld, T. T. Y. Tan, F. Dielmann, *Chem. Eur. J.* **2017**, *23*, 5929.

[92] F. Buß, P. Mehlmann, C. Mück-Lichtenfeld, K. Bergander, F. Dielmann, *J. Am. Chem. Soc.* **2016**, *138*, 1840.

[93] T. Witteler, H. Darmandeh, P. Mehlmann, F. Dielmann, *Organometallics* **2018**, *37*, 3064.

[94] F. Dielmann, O. Back, M. Henry-Ellinger, P. Jerabek, G. Frenking, G. Bertrand, *Science* **2012**, *337*, 1526.

[95] F. Dielmann, C. E. Moore, A. L. Rheingold, G. Bertrand, *J. Am. Chem. Soc.* **2013**, *135*, 14071.

[96] M. Tamm, S. Beer, E. Herdtweck, *Z. Naturforsch., B: Chem. Sci.* **2004**, *59*, 1497.

[97] M. Tamm, D. Petrovic, S. Randoll, S. Beer, T. Bannenberg, P. G. Jones, J. Grunenberg, *Org. Biomol. Chem.* **2007**, *5*, 523.

[98] P. Mehlmann, F. Dielmann, *Chem. Eur. J.* **2019**, *25*, 2352.

[99] L. F.B. Wilm, P. Mehlmann, F. Buß, F. Dielmann, *J. Organomet. Chem.* **2020**, *909*, 121097.

[100] F. Buß, C. Mück-Lichtenfeld, P. Mehlmann, F. Dielmann, *Angew. Chem.* **2018**, *130*, 5045.

[101] F. Buß, C. Mück-Lichtenfeld, P. Mehlmann, F. Dielmann, *Angew. Chem. Int. Ed. Engl.* **2018**, *57*, 4951.

[102] F. Buß, P. Rotering, C. Mück-Lichtenfeld, F. Dielmann, *Dalton Trans.* **2018**, *47*, 10420.

[103] Y. Bai, J. He, Y. Zhang, *Angew. Chem. Int. Ed. Engl.* **2018**, *57*, 17230.

[104] P. Mehlmann, T. Witteler, L. F. B. Wilm, F. Dielmann, *Nature chemistry* **2019**, *11*, 1139.

[105] E. E. Nifantyev, V. V. Negrebetsky, M. K. Gratchev, G. I. Kurochkina, A. R. Bekker, L. K. Vasyanina, S. G. Sakharov, *Phosphorus, Sulfur Silicon Relat. Elem.* **1992**, *66*, 261.

[106] P. Rotering, L. F. B. Wilm, J. A. Werra, F. Dielmann, *Chem. Eur. J.* **2020**, *26*, 406.

[107] N. L. S. Yue, D. W. Stephan, *Organometallics* **2001**, *20*, 2303.

[108] S. Ullrich, B. Kovačević, X. Xie, J. Sundermeyer, *Angew. Chem. Int. Ed. Engl.* **2019**, *58*, 10335.

[109] S. Ullrich, B. Kovačević, X. Xie, J. Sundermeyer, *Angew. Chem.* **2019**, *131*, 10443.

[110] J. F. Kögel, S. Ullrich, B. Kovačević, S. Wagner, J. Sundermeyer, *Z. Anorg. Allg. Chem.* **2020**, *110*, 1055.

[111] J. A. Werra, M. A. Wünsche, P. Rathmann, P. Mehlmann, P. Löwe, F. Dielmann, *Z. Anorg. Allg. Chem.* **2020**, *253*, 1.

[112] V. H. Gessner (Ed.) *Structure and bonding*, Springer International Publishing, Cham, **2018**.

[113] a) T. Scherpf, R. Wirth, S. Molitor, K.-S. Feichtner, V. H. Gessner, *Angew. Chem.* **2015**, *127*, 8662; b) J. Tappen, I. Rodstein, K. McGuire, A. Großjohann, J. Löffler, T. Scherpf, V. H. Gessner, *Chem. Eur. J.* **2020**, *26*, 4281; c) T. Scherpf, H. Steinert, A. Großjohann, K. Dilchert, J. Tappen, I. Rodstein, V. H. Gessner, *Angew. Chem. Int. Ed. Engl.* **2020**, *59*, 20596; d) L. T. Scharf, I. Rodstein, M. Schmidt, T. Scherpf, V. H. Gessner, *ACS Catal.* **2020**, *10*, 999; e) C. Schwarz, T. Scherpf, I. Rodstein, J. Weismann, K.-S. Feichtner, V. H. Gessner, *ChemistryOpen* **2019**, *8*, 621; f) T. Scherpf, R. Wirth, S. Molitor, K.-S. Feichtner, V. H. Gessner, *Angew. Chem. Int. Ed. Engl.* **2015**, *54*, 8542; g) T. Scherpf, H. Steinert, A. Großjohann, K. Dilchert, J. Tappen, I. Rodstein, V. H. Gessner, *Angew. Chem.* **2020**, *132*, 20777.

[114] C. Schwarz, J. Handelmann, D. M. Baier, A. Ouissa, V. H. Gessner, *Catal. Sci. Technol.* **2019**, *9*, 6808.

[115] T. Scherpf, I. Rodstein, M. Paaßen, V. H. Gessner, *Inorg. Chem.* **2019**, *58*, 8151.

[116] T. Scherpf, C. Schwarz, L. T. Scharf, J.-A. Zur, A. Helbig, V. H. Gessner, *Angew. Chem.* **2018**, *130*, 13041.

[117] X.-Q. Hu, D. Lichte, I. Rodstein, P. Weber, A.-K. Seitz, T. Scherpf, V. H. Gessner, L. J. Gooßen, *Org. Lett.* **2019**, *21*, 7558.

[118] P. Weber, T. Scherpf, I. Rodstein, D. Lichte, L. T. Scharf, L. J. Gooßen, V. H. Gessner, *Angew. Chem. Int. Ed. Engl.* **2019**, *58*, 3203.

[119] T. Scherpf, C. Schwarz, L. T. Scharf, J.-A. Zur, A. Helbig, V. H. Gessner, *Angew. Chem. Int. Ed. Engl.* **2018**, *57*, 12859.

[120] P. Weber, T. Scherpf, I. Rodstein, D. Lichte, L. T. Scharf, L. J. Gooßen, V. H. Gessner, *Angew. Chem.* **2019**, *131*, 3235.

[121] A. Sarbajna, V. S. V. S. N. Swamy, V. H. Gessner, *Chem. Sci.* **2020**.

[122] S. Ullrich, D. Barić, X. Xie, B. Kovačević, J. Sundermeyer, *Org. Lett.* **2019**, *21*, 9142.

[123] R. W. Alder, P. S. Bowman, W. R. S. Steele, D. R. Winterman, *Chem. Commun.* **1968**, 723.

[124] V. Raab, E. Gauchenova, A. Merkoulov, K. Harms, J. Sundermeyer, B. Kovacević, Z. B. Maksić, *J. Am. Chem. Soc.* **2005**, *127*, 15738.

[125] J. F. Kögel, B. Oelkers, B. Kovačević, J. Sundermeyer, *J. Am. Chem. Soc.* **2013**, *135*, 17768.

[126] J. F. Kögel, N. C. Abacılar, F. Weber, B. Oelkers, K. Harms, B. Kovačević, J. Sundermeyer, *Chem. Eur. J.* **2014**, *20*, 5994.

[127] J. F. Kögel, N.-J. Kneusels, J. Sundermeyer, *Chem. Commun.* **2014**, *50*, 4319.

[128] J. F. Kögel, X. Xie, E. Baal, D. Gesevičius, B. Oelkers, B. Kovačević, J. Sundermeyer, *Chem. Eur. J.* **2014**, *20*, 7670.

[129] V. Raab, J. Kipke, R. M. Gschwind, J. Sundermeyer, *Chem. Eur. J.* **2002**, *8*, 1682.

[130] D. Uraguchi, S. Sakaki, T. Ooi, *J. Am. Chem. Soc.* **2007**, *129*, 12392.

[131] Y. - H. Wang, Z. - Y. Cao, Q. - H. Li, G. - Q. Lin, J. Zhou, P. Tian, *Angew. Chem.* **2020**, *132*, 8080.

[132] Y.-H. Wang, Z.-Y. Cao, Q.-H. Li, G.-Q. Lin, J. Zhou, P. Tian, *Angew. Chem. Int. Ed. Engl.* **2020**, *59*, 8004.

[133] J. M. Brunel, O. Legrand, S. Reymond, G. Buono, *J. Am. Chem. Soc.* **1999**, *121*, 5807.

[134] A. J. M. Farley, C. Sandford, D. J. Dixon, *J. Am. Chem. Soc.* **2015**, *137*, 15992.

[135] Q. Hu, A. Kondoh, M. Terada, *Chem. Sci.* **2018**, *9*, 4348.

[136] A. Kondoh, S. Akahira, M. Oishi, M. Terada, *Angew. Chem. Int. Ed. Engl.* **2018**, *57*, 6299.

[137] A. Kondoh, S. Akahira, M. Oishi, M. Terada, *Angew. Chem.* **2018**, *130*, 6407.

[138] S. Das, Q. Hu, A. Kondoh, M. Terada, *Angew. Chem. Int. Ed. Engl.* **2021**, *60*, 1417.

[139] S. Das, Q. Hu, A. Kondoh, M. Terada, *Angew. Chem.* **2021**, *133*, 1437.

[140] M. Formica, D. Rozsar, G. Su, A. J. M. Farley, D. J. Dixon, *Acc. Chem. Res.* **2020**, *53*, 2235.

[141] A. M. Goldys, M. G. Núñez, D. J. Dixon, *Org. Lett.* **2014**, *16*, 6294.

[142] M. G. Núñez, A. J. M. Farley, D. J. Dixon, *J. Am. Chem. Soc.* **2013**, *135*, 16348.

[143] a) J. Yang, A. J. M. Farley, D. J. Dixon, *Chem. Sci.* **2017**, *8*, 606; b) M. Formica, G. Sorin, A. J. M. Farley, J. Díaz, R. S. Paton, D. J. Dixon, *Chem. Sci.* **2018**, *9*, 6969.

[144] a) D. Uraguchi, Y. Ueki, A. Sugiyama, T. Ooi, *Chem. Sci.* **2013**, *4*, 1308; b) D. Uraguchi, K. Yamada, T. Ooi, *Angew. Chem. Int. Ed. Engl.* **2015**, *54*, 9954; c) D. Uraguchi, K. Yoshioka, Y. Ueki, T. Ooi, *J. Am. Chem. Soc.* **2012**, *134*, 19370; d) K. Yoshioka, K. Yamada, D. Uraguchi, T. Ooi, *Chem. Commun.* **2017**, *53*, 5495; e) L. Simón, R. S. Paton, *J. Org. Chem.* **2017**, *82*, 3855; f) D. Uraguchi, R. Tsutsumi, T. Ooi, *J. Am. Chem. Soc.* **2013**, *135*, 8161; g) D. Uraguchi, K. Yamada, M. Sato, T. Ooi, *J. Am. Chem. Soc.* **2018**, *140*, 5110; h) D. Uraguchi, K. Yamada, T. Ooi, *Angew. Chem.* **2015**, *127*, 10092.

[145] T. Takeda, M. Terada, *J. Am. Chem. Soc.* **2013**, *135*, 15306.

[146] A. Kondoh, M. Oishi, H. Tezuka, M. Terada, *Angew. Chem. Int. Ed. Engl.* **2020**, *59*, 7472.

[147] a) T. Takeda, A. Kondoh, M. Terada, *Angew. Chem. Int. Ed. Engl.* **2016**, *55*, 4734; b) A. Kondoh, M. Oishi, T. Takeda, M. Terada, *Angew. Chem. Int. Ed. Engl.* **2015**, *54*, 15836; c) T. Takeda, A. Kondoh, M. Terada, *Angew. Chem.* **2016**, *128*, 4812; d) A. Kondoh, M. Oishi, T. Takeda, M. Terada, *Angew. Chem.* **2015**, *127*, 16062.

[148] A. Kondoh, M. Oishi, H. Tezuka, M. Terada, *Angew. Chem.* **2020**, *132*, 7542.

[149] H. Krawczyk, M. Dzięgielewski, D. Deredas, A. Albrecht, Ł. Albrecht, *Chem. Eur. J.* **2015**, *21*, 10268.

[150] M. Priede, E. Priede, J. Saame, I. Leito, E. Suna, *Chem. Heterocycl. Comp.* **2016**, *52*, 541.

[151] U. Köhn, M. Schulz, A. Schramm, W. Günther, H. Görls, S. Schenk, E. Anders, *Eur. J. Org. Chem.* **2006**, 4128.

[152] J. F. Kögel, B. Kovačević, S. Ullrich, X. Xie, J. Sundermeyer, *Chem. Eur. J.* **2017**, *23*, 2591.

[153] A. Kroll, H. Steinert, L. T. Scharf, T. Scherpf, B. Mallick, V. H. Gessner, *Chem. Commun.* **2020**, *56*, 8051.

[154] J. F. Kögel, D. Margetić, X. Xie, L. H. Finger, J. Sundermeyer, *Angew. Chem. Int. Ed. Engl.* **2017**, *56*, 3090.

[155] J. F. Kögel, D. Margetić, X. Xie, L. H. Finger, J. Sundermeyer, *Angew. Chem.* **2017**, *129*, 3136.

[156] S. Ullrich, B. Kovačević, B. Koch, K. Harms, J. Sundermeyer, *Chem. Sci.* **2019**, *10*, 9483.

[157] R. F. Weitkamp, B. Neumann, H.-G. Stammler, B. Hoge, *Angew. Chem. Int. Ed. Engl.* **2019**, *58*, 14633.

[158] a) H. Kawai, Z. Yuan, E. Tokunaga, N. Shibata, *Org. Biomol. Chem.* **2013**, *11*, 1446; b) S. Okusu, K. Hirano, E. Tokunaga, N. Shibata, *Chemistry Open* **2015**, *4*, 581.

[159] R. F. Weitkamp, B. Neumann, H. - G. Stammler, B. Hoge, *Angew. Chem.* **2019**, *131*, 14775.

[160] S. Boileau, N. Illy, *Prog. Polym. Sci.* **2011**, *36*, 1132.

[161] a) M. Hong, E. Y.-X. Chen, *Angew. Chem. Int. Ed. Engl.* **2016**, *55*, 4188; b) N. Zhao, C. Ren, H. Li, Y. Li, S. Liu, Z. Li, *Angew. Chem. Int. Ed. Engl.* **2017**, *56*, 12987; c) M. Hong, E. Y.-X. Chen, *Angew. Chem.* **2016**, *128*, 4260; d) N. Zhao, C. Ren, H. Li, Y. Li, S. Liu, Z. Li, *Angew. Chem.* **2017**, *129*, 13167.

[162] a) T. Pietzonka, D. Seebach, *Angew. Chem. Int. Ed. Engl.* **1993**, *32*, 716; b) T. Pietzonka, D. Seebach, *Angew. Chem.* **1993**, *105*, 741.

[163] a) A. Grzelka, J. Chojnowski, W. Fortuniak, R. G. Taylor, P. C. Hupfield, *J. Inorg. Organomet. Polym.* **2004**, *14*, 85; b) A. Molenberg, M. Möller, *Macromol. Rapid Commun.* **1995**, *16*, 449.

[164] P. C. Hupfield, R. G. Taylor, *J. Inorg. Organomet. Polym.* **1999**, *9*, 17.

[165] a) D. Zhang, S. K. Boopathi, N. Hadjichristidis, Y. Gnanou, X. Feng, *J. Am. Chem. Soc.* **2016**, *138*, 11117; b) T. Nobori, T. Hayashi, A. Shibahara, T. Saeki, S. Yamasaki, K. Ohkubo, *Catal Surv Asia* **2010**, *14*, 164.

[166] *CCDC 2055273 contains the supplementary crystallographic data for this paper. These data can be obtained free of charge from The Cambridge Crystallographic Data Centre via www.ccdc.cam.ac.uk/conts/retrieving.html.*

[167] R. F. Weitkamp, B. Neumann, H.-G. Stammler, B. Hoge, *Angew. Chem. Int. Ed. Engl.* **2020**, *59*, 5494.

[168] R. F. Weitkamp, B. Neumann, H. - G. Stammler, B. Hoge, *Angew. Chem.* **2020**, *132*, 5536.

[169] R. F. Weitkamp, B. Neumann, H.-G. Stammler, B. Hoge, *Chem. Eur. J.* **2020**.

[170] R. F. Weitkamp, B. Neumann, H.-G. Stammler, B. Hoge, *Chem. Eur. J.* **2020**.

[171] a) K. C. Gross, P. G. Seybold, *Int. J. Quantum Chem.* **2001**, *85*, 569; b) A. Albert, E. P. Serjeant, *Ionization Constants of Acids and Bases*, Methuen, London, **1962**.

[172] a) L. L. Williams, R. D. Webster, *J. Am. Chem. Soc.* **2004**, *126*, 12441; b) P. Hapiot, J. Pinson, N. Yousfi, *New J. Chem.* **1992**, *16*, 877.

Entry for the Table of Contents

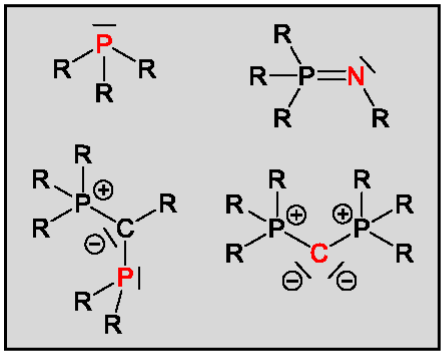

The hunt for the most powerful neutral superbase is still ongoing. The steadily growing scope of applications has resulted in a renaissance of strongly electron rich phosphorus containing Lewis and Brønsted bases. The recently published variation possibilities of strongly π-donating substituents at the basicity center to increase proton affinity and σ-donation ability are highlighted in this mini review especially focusing the past five years.

Institute and/or researcher Twitter usernames: ((optional))

ORCID: Robin Felix Weitkamp, https://orcid.org/0000-0002-0424-6943